THE BEHAVIOUR OF PLATE ANCHORS IN SAND

by

M.O. FADL, B.Sc.

A thesis submitted for the degree of

Doctor of Philosophy

Department of Civil Engineering

University of Glasgow

April, 1981

SUMMARY

The work presented in this thesis describes an investigation into the behaviour of plate anchors embedded in dry sand.

Previous theoretical, laboratory and field scale experimental work is reported. From the review of this work apparent discrepancies were found between the results, and these were attributed to the fact that certain properties of the soil had not been considered in the previous theories.

These parameters have been considered by the author in the development of an approximate method for the determination of anchor ultimate loads.

Extensive experimental model testing programme was carried out in uniformly deposited sand using air activated sand spreader and raining devices. In a main series of tests anchors with diameters up to 75 mm were embedded at depth upon diameter ratios up to 25 in dense, medium dense and loose sand and subjected to vertical and inclined loading. Anchor loads and displacements and surface deformations were recorded. Photographic tests were carried out to determine the failure surfaces within the sand mass.

From the analysis of the results it is shown that the behaviour of a plate anchor in sand is a function of a large number of factors. These factors include depth of embedment, anchor width, sand density, relative density and angle of internal friction.

A finite element method of analysis was used for predicting the anchor load-displacement relationship and the distribution of stresses within the sand mass.

The previous theories are shown to be of limited use when applied to the present test results and those of others. The approximate method developed is checked against the present experimental results and satisfactory agreement is obtained. The method is checked against previous model and field test results for shallow, deep, vertical and inclined cases and good agreement is found.

Conclusions are drawn and it is suggested by the author that in the absence of an exact method the approximate method can be used to predict ultimate uplift capacity of plate anchors. For the sand used in this investigation design curves for calculation of anchor ultimate loads are presented. Suggestions are made for future experimental and analytical work.

ACKNOWLEDGEMENTS

The author gratefully acknowledges the help received from his supervisor, Prof. Hugh B. Sutherland, Cormack Professor of Civil Engineering, University of Glasgow, without whose assistance this work could not have been carried out to its conclusion.

Considerable thanks are due to Mr. T.W. Finlay, Senior Lecturer in the Department of Civil Engineering, Glasgow University for his valuable assistance, continual guidance and interest shown during the research program.

The author is grateful to Dr. D.K. Brown of the Department of Mechanical Engineering, Glasgow University, for allowing the use of his program and his comments.

The author wishes to thank the laboratory staff in the Department of Civil Engineering at Glasgow University, especially Mr. Willie Henderson who took a keen interest in making and assembling the various parts of the test apparatus. The author also extends his thanks to Mr. I. Todd who arranged the electronic equipment.

The author thanks deeply his wife Aafaf, his daughter Sahar and his relatives for their boundless patience and continual encouragement.

Finally thanks are due to Mrs. Strachan for her neat typing of this thesis.

CONTENTS

NOTATION

The following notations have been used to represent the quantities described in this thesis. Symbols in general and those peculiar to a single author in Chapters 2 and 3 have been defined in the text.

A	area
b	anchor plate thickness
B	anchor plate width or diameter
B_o	anchor shaft diameter
c	cohesion of soil
C_u	uniformity coefficient
D	embedment depth of anchor
D_r	relative density
D_{50}	sand grain mean diameter
e	void ratio
E	Young's modulus
h	distance from defined origin
H	limited extent of failure surface above deep anchor plate
K	coefficient of earth pressure
K_o	coefficient of earth pressure at rest
L	distance from defined origin
n	porosity
p	average pressure on anchor plate
p_u	ultimate average pressure on anchor plate
R	ultimate uplift resistance
T	resultant force normal to a plane sliding surface
V	volume of soil within the failure surface
W	weight of sliding wedge at failure
x,y,z	distances from defined origins

α	inclination of linearly assumed failure surface to the vertical
γ	density of soil
γ_g	unit weight of soil
δ_a	anchor displacement
$\delta_{a90\%}$	anchor displacement at 90% of ultimate load
δ_{au}	anchor displacement at ultimate load
δ_c	surface displacement at anchor axis at ultimate load
δ_n	nodal displacement in the finite element mesh
δ_s	surface heave
ν	Poisson's ratio
σ	direct stress
σ_1, σ_2, σ_3	major, intermediate and minor principal stresses respectively
τ	shear stress
ϕ	angle of internal friction of soil
ψ	anchor axis inclination from the vertical

CHAPTER 1

INTRODUCTION TO ANCHORS

CHAPTER 1

INTRODUCTION TO ANCHORS

1.1 GENERAL INTRODUCTION:-

In this chapter a general introduction to different types of anchors and their applications in practice is presented. It is followed by discussion of the anchor problem and the most important factors influencing the anchor behaviour when embedded in soil. Some considerations of design and construction are then discussed and finally the purpose and scope of the present work are presented.

Anchors are used to support foundations subjected to tensile forces or overturning moments in both onshore and offshore conditions. Anchors can be defined as structural members which transmit tensile forces from the main structure to the surrounding medium. They are attached to the structure with suitable anchor tendons, shafts or mooring lines.

In the past uplift forces in structures were resisted by dead weight anchors in the form of mass concrete blocks, whose design consisted simply of equating the uplift forces to the necessary dead weight. More recently, structures have been built which involve uplift forces so great that dead weight anchors are not feasible, and it has become necessary to develop anchors embedded in the ground to utilize the strength of the overlying soil mass. The design of these embedded anchors requires a knowledge of soil properties and anchor behaviour within the soil and is therefore more complex than the relatively straightforward dead-weight anchor design.

1.2. TYPES OF ANCHORS:-

Several types of anchors have been used according to their application. Generally anchors can be classified into the following categories.

(i) Ground anchors

(ii) Rock anchors

(iii) Marine anchors

1.2.1. GROUND ANCHORS:-

Ground anchors are used in soils ranging in grain size from soft silts to gravels. The anchors are either steel cables, steel reinforcing cages with grout or concrete surroundings. Ground anchors can be described under the following headings.

1.2.1.1. GRAVITY TYPE:-

This is the simplest form of anchors used onshore and off-shore. Fig(1.1a)shows this type of anchor which depends on its self weight to resist the uplift forces. As the need for higher resisting loads grew, these massive concrete foundations were not justified economically.

1.2.1.2. PLATE OR SLAB TYPE:-

Fig(1.1b)shows a more economic design which can be achieved by placing a slab of concrete and steel in the base of an excavation, attaching a rod or cable, and then backfilling above the slab to the original ground surface. Connection of the structure to the rod or cable allows the uplift load to be transferred to the slab and resisted by the soil above. Considerable compaction of the backfill is necessary in order to restore part or whole of the original soil strength.

1.2.1.3. BORED OR UNDERREAMED TYPE:-

This anchor uses the natural strength of the soil by casting reinforced concrete members in bored holes. Underreaming can take place at the bottom of the hole to produce an underreamed footing as shown in Fig(1.1c)or at different positions along it to increase the uplift resistance of the anchor. This type of anchor can be constructed in place without disturbing the soil by use of an expandable reaming device. In more sandy ground the shaft is cased and sometimes stabilized by chemical grouting before reaming (Baker and Kondner, 1966). This casing is withdrawn as the concrete is placed.

1.2.1.4. GROUTED TYPE:-

This type is normally considered where it is required to support large tensile loads in poor ground or to transmit these loads into stronger soil or rock found at greater depths below the structure as illustrated in Fig (1.1d). Factory prepared steel tendons or multistrand cables spaced in the centre of a boring are grouted under pressure using a patented process.

1.2.2. ROCK ANCHORS:-

Rock anchors are usually tendons or cables held in position by grouting or some other suitable means and placed in holes in the rock. Rock anchors include rawlplug, grouted type, slot and wedge types as shown in Fig (1.2).

1.2.3. MARINE ANCHORS:-

The expansion of the field of coastal and ocean engineering has resulted in a great increase in the application of marine anchors. Marine anchors of various types, capable of providing uplift resistance in shallow and deep waters are employed by boats, buoys and ships. Salvage operations and the increased activity in exploration and utilization of ocean resources has drawn closer attention to the problem of pullout resistance of marine anchors. Fig (1.3) shows some of the marine anchors used such as drag anchor, umbrella pile anchor, propellant-actuated and embedded suction anchors.

1.3. APPLICATION OF GROUND ANCHORS IN ENGINEERING PRACTICE:-

The number of applications of anchors in engineering practice is large and is still growing. The main applications will be discussed below.

a/ RESISTANCE TO OVERTURNING FORCES:-

This was one of the earliest uses of ground anchors. Transmission towers (Fig 1.4a), radio and television masts subjected to wind or surcharge loading must be effectively restrained if overturning is to be prevented.

b/ DAM STABILIZATION:-

An increase in height or improvement in safety of concrete dams can often be accomplished by the use of ground anchors in raising and strengthening of dams. The anchors can be used in restoring the water tightness of cracked dams by compressing the structure and closing the cracks as illustrated in Fig (1.4b).

c/ RESISTANCE TO BUOYANCY FORCES:-

Hollow shaped structures, in the unloaded state, when located in areas of high ground water are pushed up by the hydrostatic uplift forces. Ground anchors can be used to solve this problem instead of adding mass concrete and the cost of extra excavation and material. Examples are of dry docks (Fig 1.4c), effluent tanks and submerged tunnels.

d/ SUSPENSION BRIDGES:-

Ground anchors have been used successfully in anchoring the tensile forces of suspension bridges (Fig 1.4d), arch bridges, aeroplane hangers. The same principle was used in the construction of the Munich Olympic tent-type roof, where tensile loads of 200 to 700 tons had to be sustained (Von Soos, 1972).

e/ SLAB WALLS:-

Fig (1.4e) shows how vertical cuttings adjacent to highways, railways and canals can be rendered stable by wall slabs secured by horizontal ground anchors. The advantage of using anchors in this situation compared with a traditional retaining wall is that the amount of excavation at the base of the cutting is reduced. External bracing from retaining structures can be eliminated when anchors can support the tie-back forces required (Abu Taleb, 1974).

f/ SLOPE STABILITY:-

Anchors can in some cases, provide an economical means of stabilizing slopes as an alternative to other solutions such as building large gravity walls or cutting the slopes to a lesser angle to correspond with the mechanical properties of the soil, see Fig (1.5a).

g/ PILE AND PLATE LOADING TESTS:-

Anchors can be used to resist the reactive forces created during tests on compression piles. This can be attractive in remote sites, where access and space is limited for the heavy equipment required by conventional methods. Movement on soft ground, reduction of transport costs, quick instrumentation and improved safety by eliminating heavy balancing weights are points in favour of using anchors as shown in Fig (1.5b).

h/ STABILISATION OF UNDERGROUND EXCAVATIONS:-

In tunnel excavation in rock, the roofs can be stabilised using prestressed rock anchors as shown in Fig (1.5c). Costly bracing can be avoided using this technique with an increase in the speed of excavation.

i/ OFFSHORE APPLICATION:-

With the recent advent of offshore oil exploration in the North Sea, numerous uses for anchors have developed, e.g. in anchoring vessels for site investigations, buoys, single point moorings, submersibles and submerged pipe lines. Drilling for oil in deep waters can be done economically by using semi-submerged platforms instead of the existing gravity platforms.

Fig (1.5d) shows GASUB design of a cable-stayed submerged buoyant rig or platform consisting of a 50m diameter multi-cell buoyant chamber positioned at about 30m below sea level where water is relatively calm. This chamber supports a working deck mounted clear of the worst expected wave conditions. The platform is suspended by cables and anchors embedded in the sea bed, providing a structure which is claimed to be as stable under all conditions as a comparable gravity platform but with a reduced cost. The design is thought to be suitable for water depths of at least 400m but is also viable for the shallower water at present being exploited (New Civil Engineer, 21 Feb 1974).

j/ MISCELLANEOUS GROUND ANCHOR APPLICATIONS:-

Many other applications of anchor are possible. In a compressible soil where it is not practical to extend the foundation to a solid stratum, settlement can be induced prior to construction by preloading the foundation with ground anchors. Heave due to excavation can be tackled in the same way. Ground anchors can be used to reduce or eliminate the settlement of structures adjacent to excavations by controlling and minimizing the retaining wall movements.

The present research being undertaken by the author aims at investigating the fundamental behaviour of simple disc anchors buried in cohesionless soil and obviously cannot attempt to cover all the aspects presented below. It is hoped that future research and use will lead to a better understanding, a wider and more economical use of anchors in civil engineering both on-shore and offshore.

1.4. INFLUENCE OF ANCHOR BEHAVIOUR:-

In this section the general effect of anchor, soil parameters and the loading characteristics on the anchor behaviour will be presented.

1.4.1. THE ANCHOR PROBLEM:-

Different factors are involved in the uplift resistance of anchors other than those encountered in the conventional bearing capacity of foundations. The calculation of the bearing capacity of soils and the prediction of associated deformations of foundations are well established. However research into the uplift resistance capacity of soils has been more limited.

Although it may be thought that an anchor being pulled upwards from within a soil mass is simply the reverse of the normal foundation problem, where a footing is being forced downwards into an infinite soil mass, this is not the case. The presence of the ground surface influences the anchor behaviour to a large extent, and the presence of that boundary does not allow a prediction of anchor holding capacity to be done in the same way as foundation bearing capacity. In addition, unlike the relatively undisturbed soil below a foundation, the soil above an anchor will have been disturbed by the method of placing the anchor and this disturbance must be taken into account in design.

1.4.2. THE SINGLE ANCHOR:-

In general the parameters influencing the behaviour of single anchors are the depth of embedment and the anchor dimensions which affect the shape and extent of the failure zone. Consequently the uplift resistance will be affected. The ratio of the depth of embedment D upon the anchor width B, i.e. $\frac{D}{B}$, has been found by many investigators to yield two different modes of failure. General shear failure reaching the soil surface is associated with low $\frac{D}{B}$ ratios and a localized type of failure with high $\frac{D}{B}$ ratios. As will be discussed in chapter 2 these correspond to shallow and deep anchor respectively.

1.4.3. SOIL PARAMETERS:-

Different types of soil ranging from clay to gravel have different effects on the uplift anchor problem. For the same type of soil, e.g. sands of different origins, gradings and texture will have an effect on the uplift resistance.

For sands the relative density and strength parameters play an important role where for dense sand a large failure zone occurs leading to high uplift resistance. The state of overconsolidation of a soil can influence the uplift capacity. The higher the overconsolidation, the higher will be the uplift capacity. An anchor embedded in a highly compressible soil will reach its maximum uplift resistance at a higher anchor displacement than if it were in a soil of low compressibility.

1.4.4. TYPE AND RATE OF LOADING:-

Different types of loading e.g. static or cyclic loading will affect the amount of uplift resistance and the deformation associated with it. However it has been found that the use of either load control or displacement control in static loading tests leads to the same load-displacement behaviour (Matsuo, 1967; Davie, 1973).

The rate of application of the load will affect the load-displacement curve in low permeability soils such as clay resulting in low ultimate values as the rate of load application decreases (Meyerhof and Adams, 1968). This effect decreases as the permeability increases and for sands the rate of load application is insignificant.

1.4.5. ANCHOR INCLINATION AND GROUP:-

Most of the anchors installed are located at an inclination from the vertical. Consequently the study of the behaviour of inclined anchors along with vertical anchors is important.

Anchor groups of different sizes and spacings between the individual anchors are used. Stressed anchorage zones of closely spaced anchors interact (Yilmaz, 1971; Abu Taleb, 1974; McMullan, 1974).

Additional parameters influencing the group of anchors can be summarized as group shape, size, spacing and stiffness of the capping slab (Hanna, Sparks, Yilmaz, 1972).

1.4.6. ANCHOR SHAPE:-

The effect of the anchor shape is considerable e.g. plate shape, helical, fluke, cylindrical or spherical anchors. Different shapes of anchors mobilize the resistance to uplift movement according to their configuration, e.g. end bearing, shaft resistance or a combination of both.

1.4.7. ANCHOR PRESTRESSING:-

Prestressing the anchor reduces the subsequent soil or structure deformations and improves the soil properties generally. The prestressing occurs by jacking the buried plate anchor against a surface bearing plate to introduce tension in the tie rod connecting them.

1.5. DESIGN AND CONSTRUCTION CONSIDERATIONS:-

Several types of anchors have been developed for use in different soils. Steel screw plate anchors have been used in Canada and the U.S.S.R. and fluke anchors have been used in marine applications in U.S.A. Grouted anchors are generally used in Western Europe. The types of anchors commercially available in the U.K. include boreholes filled with grout, boreholes enlarged by a controlled injected pressure grout and boreholes mechanically enlarged at one position or multistage grout as illustrated in Fig (1.6) (Hanna, 1976).

Anchor construction requires proper site investigation. Adequate safety factors are included to satisfy the design assumptions. The method of construction will include drilling, grouting and proper corrosion protection. Proof loading tests are carried out on each production anchor. Monitoring of the behaviour of some anchors during service is very important (Littlejohn and Bruce, 1975; Hanna, 1976).

1.6. PURPOSE AND SCOPE OF THE PRESENT INVESTIGATION:-

The importance and increasing application of anchors in civil engineering practice is reflected by the literature, symposiums and conferences held on the subject, the most recent of which were an ICE Conference in 1975, a seminar in 1976 on diaphragm walls and anchorages, a symposium on anchoring of offshore structures in September 1980 and a seminar on seabed anchorages for floating offshore structures in February 1981.

The parameters involved in the uplift problem of anchors are numerous and a study of them under field conditions would obviously be expensive. Model testing on the other hand allows the various parameters to be studied in detail to ascertain their relative importance. This thesis attempts, as outlined below, to cover certain aspects of the problem in association with theoretical analysis.

In the present programme the study has been mainly on circular plate anchors of different diameters embedded at various depths in cohesionless soil with a range of densities. Depth to diameter $\frac{D}{B}$ ratios from 1 to 25 have been covered to include both shallow and deep anchors, and vertical and inclined anchors have been studied.

A review of previous theoretical and experimental work in the uplift resistance problem in cohesionless soils is presented. The theories are discussed and compared in addition to previous laboratory and field tests. As a result an approximate method is proposed to predict the ultimate uplift resistance of shallow and deep anchors embedded in cohesionless soils. The approximate method is generalized to take into consideration the effect of inclination from the vertical and the most important soil parameters affecting the uplift resistance problem. A dimensional analysis is used to examine the factors relevant to the experimental tests proposed in the laboratory.

Extensive model scale tests were carried out covering shallow, deep, vertical and inclined anchors. Different soil conditions, loose, medium dense and dense states were tested. In addition the failure surfaces developed in the soil medium were observed and photographed in the three dimensional case. An investigation was necessary into methods of depositing uniform sand beds at the required relative density for the model tests.

An extensive series of model tests was carried out to examine the effect of the parameters such as density of the sand and depth upon width ratio of the anchor $\frac{D}{B}$ and the anchor inclination from the vertical on the load-displacement and failure mode of the anchor.

The complex nature of the stress and deformation is analysed using a finite element analysis. By varying the parameters of the laboratory tests, stresses and deformations were predicted at the elastic and plastic stages of loading.

Finally the results from the model tests, the approximate method and the finite element were discussed and compared and conclusions and suggestions for future work have been presented.

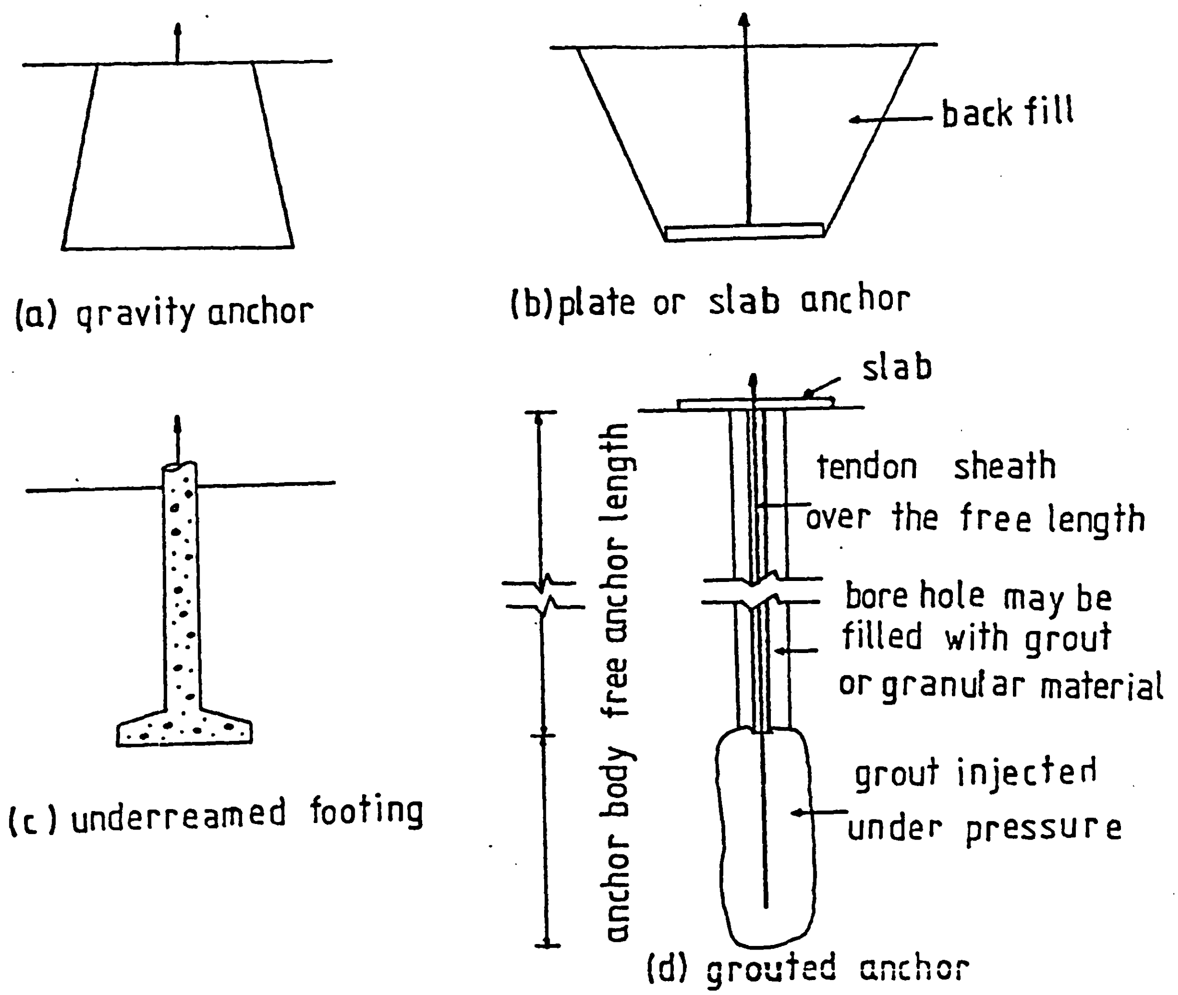

FIG.1.1 EXAMPLES OF GROUND ANCHORS

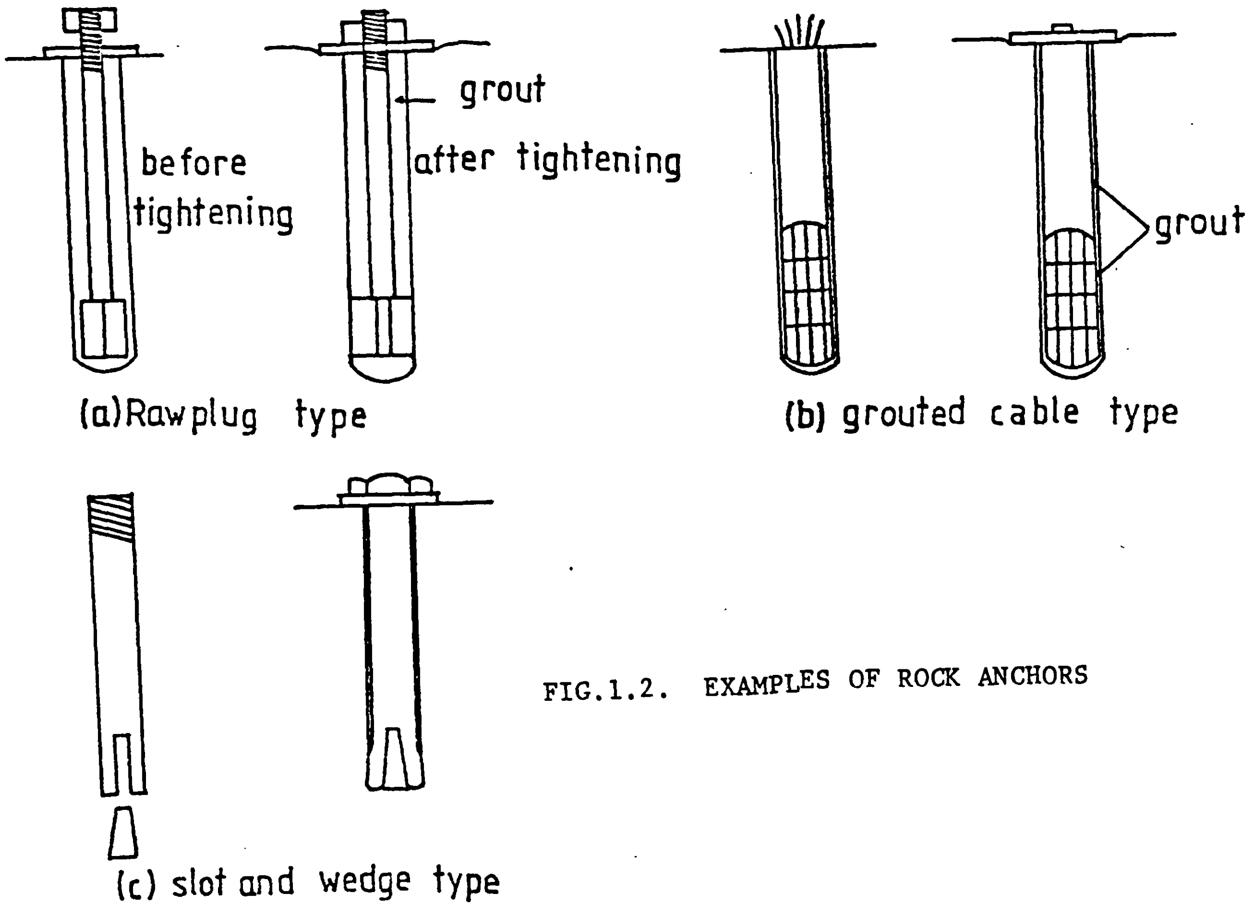

FIG.1.2. EXAMPLES OF ROCK ANCHORS

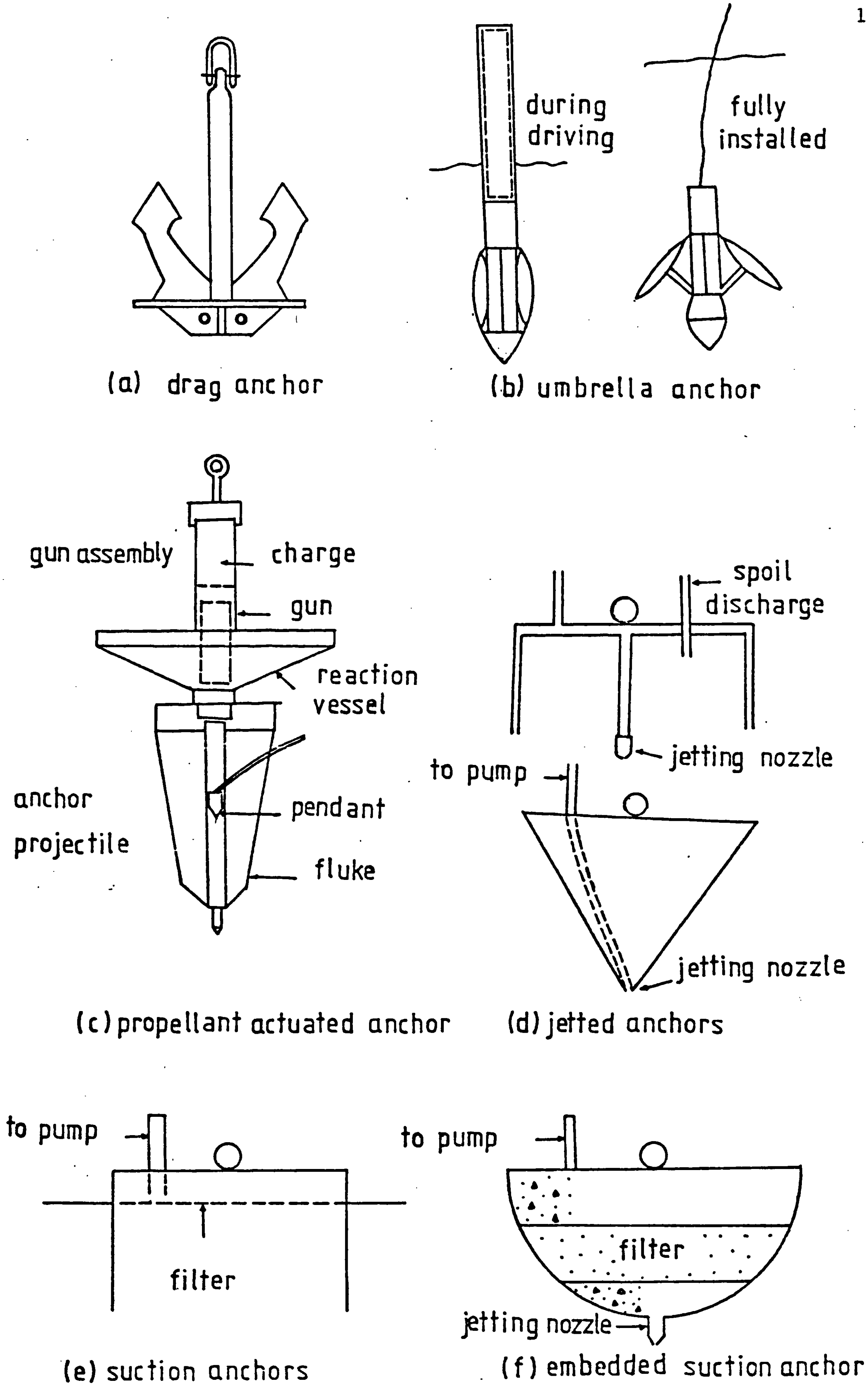

FIG.1.3. EXAMPLES OF MARINE ANCHORS

SAHOTA (1979)

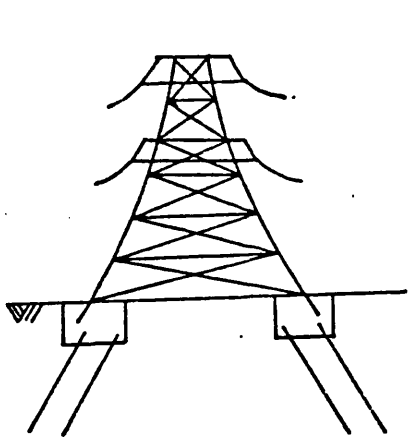

(a) trsmission towers

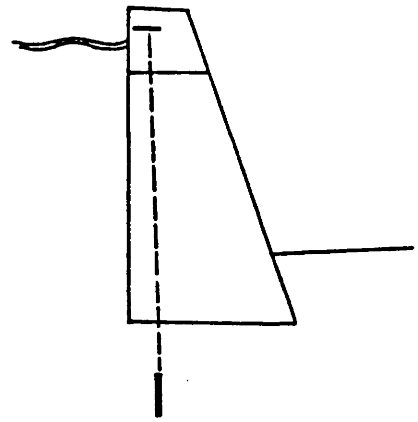

(b) heightening or stabilizing dams by stressing into rock

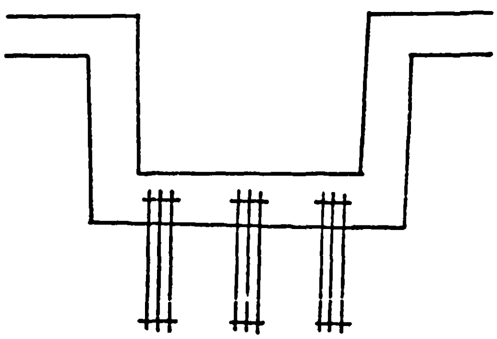

(c) resisting uplift forces in dry docks

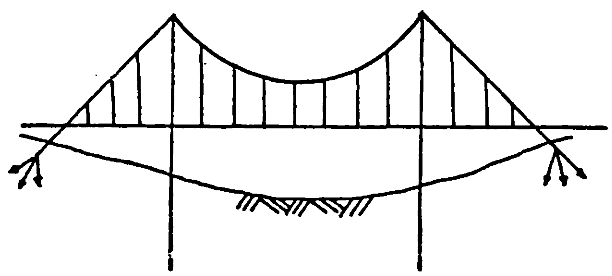

(d) cable suspension bridge

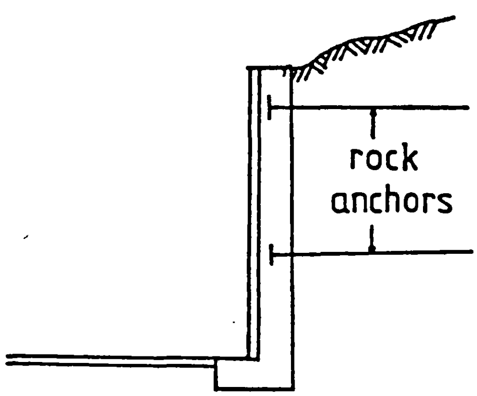

(e) revetment of rock with anchored retaining walls

FIG.1.4 SOME USES OF ANCHORS

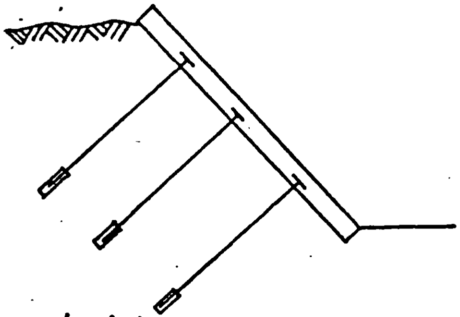

(a) restraining side slopes in road cuttings or other excavations

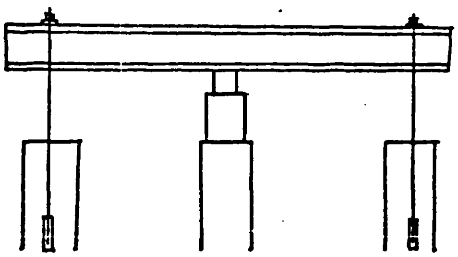

(b) providing anchorage for pile tests

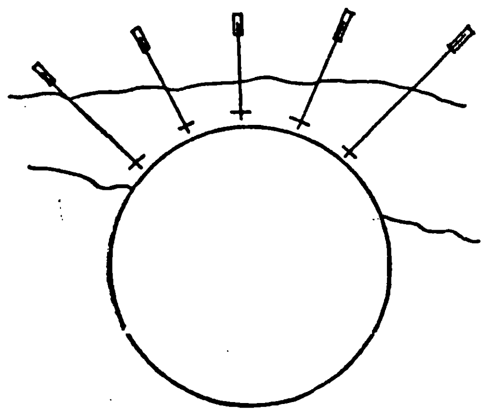

(c) tying in tunnel roofs in fissured rock

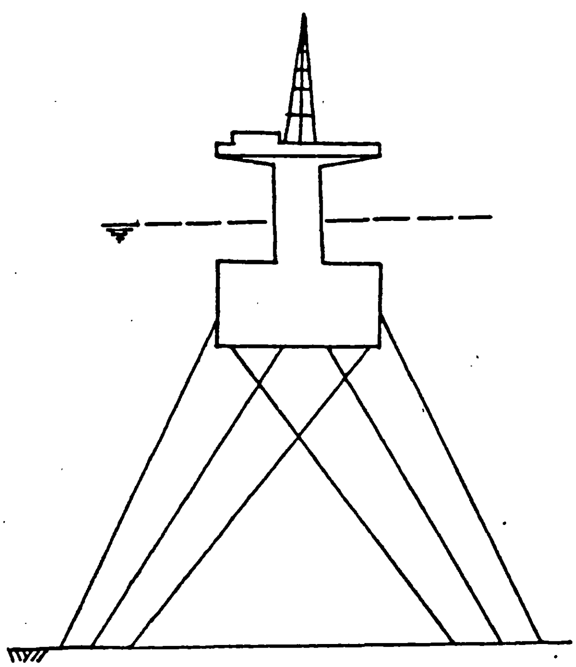

(d) model of a cable-stayed submerged buoyant rig

FIG.1.5 SOME FURTHER USES OF ANCHORS

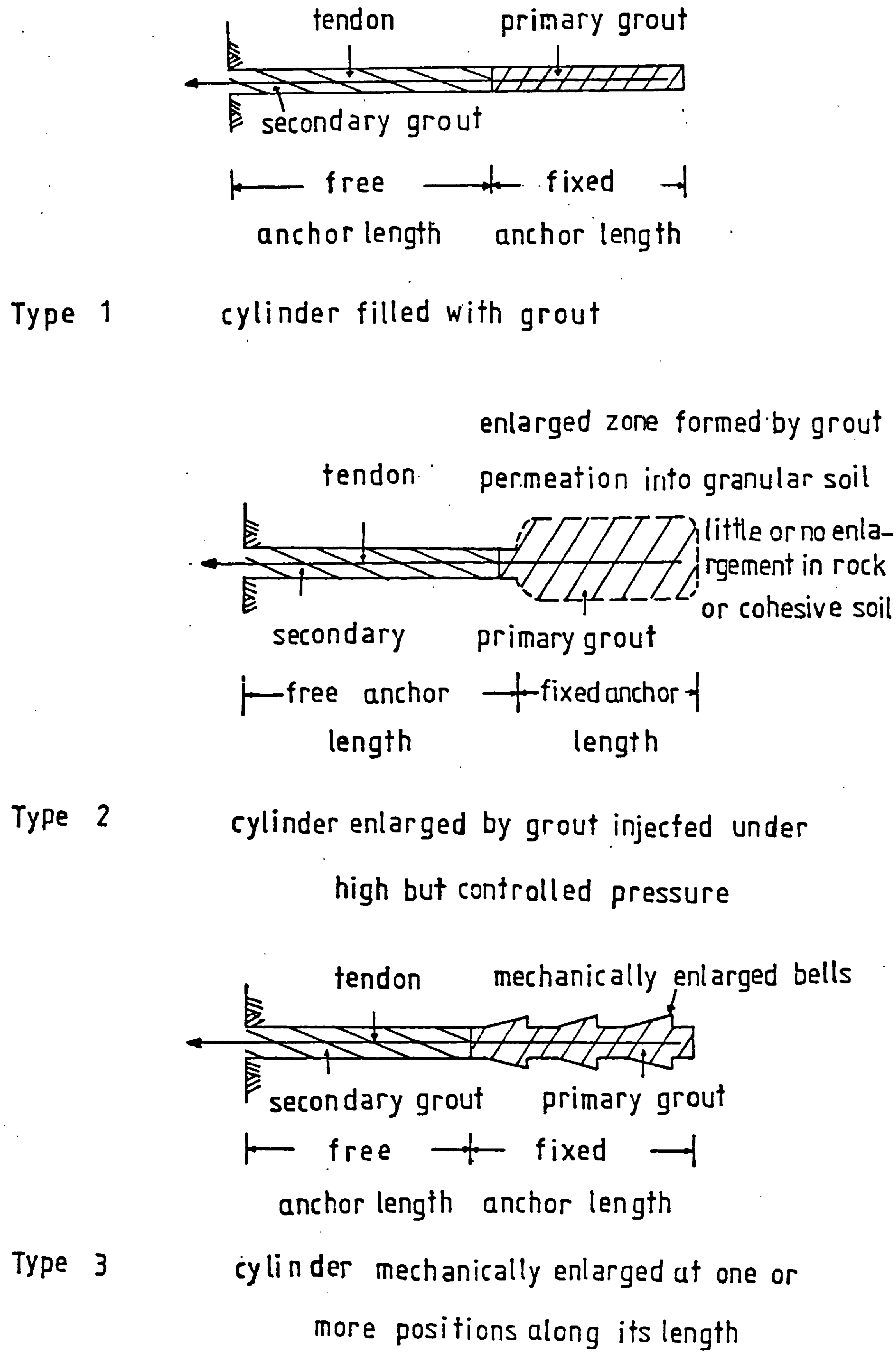

FIG.1.6 ILLUSTRATION OF MAIN ANCHOR GROUPS AVAILABLE IN THE U.K.

(HANNA ,1976)

CHAPTER 2

REVIEW OF PREVIOUS THEORETICAL AND EXPERIMENTAL WORK

CHAPTER 2

REVIEW OF PREVIOUS THEORETICAL AND EXPERIMENTAL WORK

2.1. INTRODUCTION:-

This chapter reviews the theoretical and experimental work carried out to investigate the behaviour of vertical and inclined circular plate anchors embedded in cohesionless soils. Discussion and comparison of these procedures will be presented.

An early solution to the problem of resisting uplift force was the dead weight anchor, which become impractical as the need arose for larger holding capacities. An alternative, the buried anchor, called for a more fundamental approach in predicting uplift resistance and many investigators have presented theoretical solutions to this anchoring problem. Most of the theories are based on model-scale study for different types of soils. Shallow, deep, vertical and inclined anchors have been considered, and various sizes and shapes of anchors, single or in groups have been investigated to develop a relationship between anchor resistance, geometry and soil parameters.

Two main types of behaviour have been observed for plate anchors subjected to uplift forces. For an anchor installed close to the surface of the soil, the failure surface in the soil mass extends from the top of the anchor and reaches the soil surface at an ultimate load. Up to this burial depth the anchor is called a shallow anchor. Footings subjected to uplift loads such as electricity pylon foundations can display this type of shallow anchor behaviour. As the burial depth increases the behaviour of the anchor changes. The maximum load is developed in the anchor without any deformation at the soil surface. The anchor can continue to displace upwards and the anchor load remain close to the maximum value resulting in a local shear failure around the anchor. The transition between the two types of behaviour is termed the critical depth ratio.

The most common methods of predicting anchor resistance are the limiting equilibrium analysis, finite element and dimensional analysis technique. In sections 2.2 to 2.5 a summary of the theories which have been proposed for shallow, deep and inclined anchors, dimensional, finite element and elastic analysis is presented. This is followed in section 2.6 by discussion and comparison of these methods.

2.2. VERTICAL SHALLOW ANCHOR THEORIES:-

In the limiting equilibrium methods a failure surface whose form is based on observations in laboratory or field tests is usually adopted and the force systems that are assumed to exist at failure are analysed.

Traditional methods incorporating elementary soil mechanics principles were used to calculate the uplift resistance of shallow anchor footings. The more recent methods reflect the growing understanding of soil mechanics principles to obtain the solution of the uplift problem.

2.2.1. TRADITIONAL METHODS:- (Matsuo, 1967)

2.2.1.1. Earth core method:-

The ultimate uplift resistance is assumed to be equal to the sum of the dead weight of the anchor and the weight of an inverted truncated cone of soil formed at failure between the top of the anchor plate and the soil surface as shown in Fig (2.1a). The ultimate uplift resistance R is given by:

$$R = G_o + \gamma_g(V_1 - V_o) \qquad (2.1)$$

where G_o is the dead weight of the anchor, γ_g is the soil unit weight, V_1 is the volume of the truncated cone and V_o is the anchor volume under the soil surface. Considering a circular plate anchor

$$V_1 = \frac{\pi D}{4}\left(B^2 + 2BD\tan\alpha + \frac{4}{3}D^2\tan^2\alpha\right) \qquad (2.2)$$

where D and B are the depth of embedment and diameter of the plate anchor respectively. The angle α is a function of the type of soil.

2.2.1.2. Earth pressure theory:-

In this method the failure surface is assumed to extend vertically above the plate and the ultimate load is resisted by the weight of the anchor, the weight of the soil in the vertical cylinder above the anchor and the frictional or cohesive forces developed at failure along the surface of the cylinder at the condition of earth pressure at rest as shown in Fig (2.1b)

$$R = G_o + \gamma_g(V_2 - V_o) + \frac{\pi}{2}(k_o\gamma_g BD^2\tan\delta) \qquad (2.3)$$

where V_2 is the cylindrical volume of the soil and δ and k_o are the frictional angle and the coefficient of earth pressure at rest respectively.

2.2.1.3. Shearing method:-

The ultimate uplift capacity is equal to the dead weight of the anchor, the weight of the soil inside the vertical cylinder plus the shearing force acting on this surface as shown in Fig (2.1b)

$$R = G_o + \gamma_g(V_2 - V_o) + (\pi cBD + \frac{\pi}{2}k\gamma_g BD^2\tan\phi) \qquad (2.4)$$

where c is the cohesion and ϕ is the angle of shearing resistance of the soil.

2.2.2. BALLA THEORY (1961)

Balla concentrated on mushroom foundations which are special types of pylon foundations. From laboratory investigations Balla approximated the observed slip failure surface to the arc of a circle starting with a vertical tangent to the edge of the anchor plate and intersecting the ground surface at an angle ($\frac{\pi}{4} - \frac{\phi}{2}$) as shown in Fig (2.2). The maximum load was assumed to be resisted by the weight of the anchor, the weight of the soil in the solid of revolution above the anchor that is generated by the failure surface, and the vertical components of the shear forces along the circular failure surface. Assuming a plane stress condition and applying Kotter's equation, Balla computed the vertical components of the forces acting on the failure surface. The theoretical pullout capacity R was shown to be proportional to the third power of the depth of embedment

$$R = G_1 + G_2 + T_v \tag{2.5}$$

where G_1 is the weight of the breaking-out solid of revolution (including the anchor shaft taken as soil)

$$G_1 = (D - t)^3 \gamma_g F_1 \tag{2.6}$$

where F_1 is a factor depending on ϕ and $\frac{D}{B}$.

G_2 is the difference in weight between the anchor material and the soil for the volume of the anchor shaft.

$$T_v = (D-t)^3 \gamma_g \left(\left(\frac{C}{\gamma (D-t)} \right) F_2 + F_3 \right) \tag{2.7}$$

where F_2 and F_3 are factors depending on ϕ and $\frac{D}{B}$.

2.2.3 VESIC'S THEORY (1963, 1965, 1971):-

A different analytical approach was proposed by Vesic in which the expanding sphere theory was adapted. An explosive charge placed in an earth medium at moderate depth from the surface of the soil is considered. At a limiting pressure, when the cavity expands a slip failure surface forms above the cavity causing yielding as shown in Fig (2.3). In a similar manner to Balla, he adopted a plane stress system for the three dimensional axially-symmetric problem and the failure surface was assumed to be a circular arc tangent to the expanding cavity and meeting the soil surface at an angle ($\frac{\pi}{4} - \frac{\phi}{2}$). The ultimate pullout resistance was equated to the limiting cavity pressure and is given by

$$R = G_3 + G_4 + T \cos \alpha - N \sin \alpha \qquad (2.8)$$

where T and N are functions of ϕ and α, which is illustrated in Fig (2.3). The limiting cavity pressure q_o was determined from the vertical equilibrium of the entire ruptured mass above the cavity, and the ultimate resistance R is expressed as

$$R = \frac{\pi B^2}{4} q_o = \frac{\pi B^2}{4} (c\ F_c + \gamma_g\ D\ F_q) \qquad (2.9)$$

F_c and F_q are the cavity breakthrough factors which depend on the shape and relative depth of the anchor and the angle of shearing resistance of the soil.

Esquivel-Diaz (1967) applied the analysis to the case of a plate anchor which was assumed to be at the horizontal mid-plane of the cavity. Esquivel-Diaz assumed the volume of the hemispherical cavity above the plate anchor to be filled with soil, a volume which had originally been neglected or treated as part of the cavity by Vesic. The additional pressure exerted on the anchor plate is $\frac{\pi B^3 \gamma g}{12} / \frac{\pi B^2}{4} = \frac{\gamma g B}{3}$, and the ultimate uplift resistance is given by

$$R = \frac{\pi B^2}{4} \ (c\ F_c + \gamma_g D\ F_q + \gamma_g \frac{B}{3}) \qquad (2.10)$$

2.2.4. MARIUPOLSKII (1965):-

Mariupolskii offered an explanation for the behaviour of the anchor which assumed that failure occurs as a separation of the soil mass in the form of a solid of revolution with a curvilinear generatrix as shown in Fig (2.4). If separation occurs, the limiting load corresponds to the formation of a continuous crack along the surface of separation after which the raised earth cannot resist the arising bending moments and breaks down into individual parts or disintegrates.

The shape of the failure surface and the state of stress in the wedge of the soil above the anchor plate were determined using the following assumptions

(i) The maximum shear stress is mobilized in every vertical cylindrical surface around the anchor axis.

(ii) The failure occurs in tension at different points along the line of separation whenever the vertical shear stresses exceed the shearing strength along the vertical cylindrical surface over which it is to be transmitted. Mariupolskii considered the ultimate uplift resistance to be equal to the weight of anchor, the weight of the cylinder of soil above the anchor plate G_5, the weight of the conical part of the entrained earth $\gamma_g V_3$ and the resistance force along the lateral surface of the separation cone Q, then

$$R = G_o + G_5 + \gamma_g V_3 + Q \tag{2.11}$$

where $$Q = \pi B \left(cD + \tan\phi \left(K\gamma_g \frac{D^2}{2} + \int_o^D \sigma_r \, dz \right) \right) - \gamma_g V_3 \tag{2.12}$$

and σ_r is the additional radial stress created by pressing the anchor slab on the overlying earth column in a cylindrical section of diameter B and it is determined from equilibrium equations

$$R = G_o + \frac{\pi}{4}(B^2 - B_o^2) \left(\frac{\gamma_g D \left(1 - \left(\frac{B_o}{B}\right)^2 + 2K_o \frac{D}{B} \tan\phi\right) + 4c \frac{D}{B}}{1 - \left(\frac{B_o}{B}\right)^2 - 2n \frac{D}{B}} \right) \tag{2.13}$$

B_o is the diameter of the anchor shaft and n is a certain dimensionless function of ϕ and is determined from experimental data.

2.2.5. MATSUO THEORY (1967):-

Matsuo assumed that a surface failure could be determined at the meridian section of the footing by means of a similar procedure to that in a two dimensional problem. As shown in Fig (2.5) the lower part of the curve is a logarithmic spiral with the equation

$$\int = \int_o^{\theta \tan \phi} \qquad (2.14)$$

which is tangential to a plane slip failure surface meeting the ground surface at an angle $(\frac{\pi}{4} - \frac{\phi}{2})$.

The critical slip surface is the one which results in a minimum pressure on the anchor and can be found by taking moments about O_1

$$R = G_o + \gamma_g V_4 + T_v' \qquad (2.15)$$

where V_4 = volume of soil in the breakingout solid of revolution.

T_v' is the vertical component of the resultant shearing resistance acting on the slip failure surface.

Matsuo derived a differential equation equivalent to Kotter's, but with a different coordinate system to find the vertical resultant shearing resistance which is a resultant of the shearing and normal forces on the failure surface. The uplift resistance is given by

$$R = G_o + \gamma_g (B_2^3 K_1 - V_5) + c_u B_2 K_2 \qquad (2.16)$$

where $K_1 = (a-1)(a^2 F_1 + aF_2 + abF_3 + bF_4 + F_5) + b \qquad (2.17)$

$$K_2 = \pi\{(a-1)(aF_6 + F_7) + b(b \tan\alpha + 2)\} \qquad (2.18)$$

$$a = \frac{x_o}{B_2} \quad (2.19) \quad \text{and} \quad b = \frac{D_2}{B_2} \qquad (2.20)$$

F_{1-7} are factors depending on θ, x_o, ϕ, B_2 and D_2 and V_5 is the volume of foundation below the ground surface. The other symbols are shown in Fig (2.5).

In a second paper Matsuo (1968) assumed an average value of $\theta_o = 60^o$ for sands which is found from his experimental tests. This simplified the calculations involved in the uplift resistance equations presented in his first paper in 1967.

2.2.6. MEYERHOF AND ADAMS THEORY (1968):-

Meyerhof and Adams proposed an approximate general theory of uplift resistance for plate anchors based on theoretical considerations and experimental results. From experiments they obtained a curved failure surface.

Meyerhof and Adams modified their basic analysis which was for a strip footing to give a method suitable for an axisymmetric circular anchor. However no rigorous solution existed for the stresses on the curved failure surface and they assumed that these stresses would be approximately equal to the stresses developed along the cylindrical surface extending vertically above the perimeter of the anchor for simplification as illustrated in Fig (2.6). The frictional stresses were calculated by using passive earth pressure coefficients. The frictional forces along the cylindrical surface were obtained by using an empirically derived shape factor to transform the plane stress system to the axisymmetric case, then

$$R = G_o + G_6 + \pi cBD + \frac{\pi}{2} S\gamma_g BD^2 K_u \tan\phi \qquad (2.21)$$

where G_6 is the weight of the soil in the cylinder above the anchor.

S = shape factor governing the passive earth pressure on a convex cylindrical wall.

$$K_u = K_{pv} \tan\phi \qquad (2.22)$$

K_{pv} is the vertical component of the coefficient of passive earth pressure K_p.

$$K_{pv} = K_p \tan\delta \qquad (2.23)$$

and δ was approximated as

$$\delta = \frac{2}{3}\phi \qquad (2.24)$$

and $$S = 1 + m\frac{D}{B} \qquad (2.25)$$

where m is a coefficient depending on ϕ.

2.3. VERTICAL DEEP ANCHOR THEORIES:-

Several methods of predicting the maximum uplift load which a deep vertical plate anchor can resist have been proposed. Methods based on energy considerations, pressures required to expand cavities within the soil and plastic equilibrium will be described. Local shear failure, leading to a failure surface which does not reach the soil surface, is assumed in all these methods.

2.3.1. MARIUPOLSKII'S THEORY (1965):-

Mariupolskii assumed that when deep anchors reach the limiting uplift resistance load, a conical wedge, which has been formed immediately above the anchor, forces the soil above it apart and to the sides, allowing the anchor to move upwards under constant load as shown in Fig (2.7). Mariupolskii, from his tests, adopted an apex angle of approximately 90° for the cone of the soil formed on top of the anchor plate. The solution is based on the assumption that the work done by the anchor during vertical displacement should be equal to the work needed to expand a cylindrical cavity of height S' from its original diameter B_o to B. He takes into account the work expended to overcome friction between the surface of the conical wedge and the soil surrounding it and obtains

$$R = G_o + P_p \qquad (2.26)$$

$$P_p = \frac{\sigma_r \, \pi (B^2 - B_o^2)}{4(1-0.5 \tan \phi)} \qquad (2.27)$$

where P_p = ultimate load transmitted to the soil by the anchor slab and σ_r is the radial pressure.

Mariupolskii assumes that the soil is in plastic equilibrium within a radius outwith which the mass of soil is assumed to behave elastically. The radius of the elasto-plastic boundary and the radial stresses on the boundary were found in terms of the soil properties represented by a coefficient of soil compressibility, a coefficient of earth pressure, the initial void ratio of the soil, the soil cohesion, the angle of shearing resistance and the unit weight of the soil.

Mariupolskii provided design curves for the calculation of anchor ultimate uplift resistance.

2.3.2. VESIC'S THEORY (1963, 1965, 1972):-

Vesic considers the expansion of a small cavity in an infinite homogenous, isotropic mass of soil. He assumes that the pressure in the cavity will increase until an expansion takes place and an equilibrium condition is reached at which the cavity will have an enlarged radius r_u sustained by an internal pressure P_u as depicted in Fig (2.8). This cavity will be surrounded by a zone of soil in a plastic state which in turn compresses and displaces the elastic zone outside the plastic zone such that the volume increase at the limit of the plastic zone is equal to the volume increase of the original cavity. The radial stress at any point in the plastic zone is obtained by solving the differential equation of equilibrium and the equations for the conditions of rupture to obtain the radial stress σ_r at any given radius in terms of r, r_u, c, ϕ and the ultimate cavity pressure P_{uc}. The volume change of the cavity is equated to the volume change of the elastic plus plastic zone in an expression involving U_p, the radial movement at the elastic plastic boundary. This expression is combined with the equation for radial stress at the boundary of the plastic zone, giving a relationship between the expanded cavity radius r_u and the radius of the plastic zone r_p. The behaviour of the plastic zone is defined in terms of the MohrCoulomb shear strength parameters c and ϕ and the average volumetric strain Δ, which relates the state of stress in the soil to the volume change of the soil mass. The behaviour of the soil in the elastic zone is defined by the modulus of elasticity E, and Poisson's ratio ν. The analysis yields an expression for the final cavity pressure

$$P_{uc} = c\bar{F}_c + \gamma_g D\bar{F}_q \qquad (2.28)$$

$\bar{F}_c$ and $\bar{F}_q$ represent spherical cavity expansion factors.

Vesic (1972) provided tables of the factors $\bar{F}_c$ and $\bar{F}_q$ for both the expansion of a spherical cavity (axisymmetric case) and the expansion of a cylindrical cavity (plane strain case).

2.3.3. MEYERHOF AND ADAMS THEORY (1968):-

Meyerhof and Adams suggested that a failure surface would be developed by a deep anchor with the same form as that adopted by them for the general shear failure of shallow anchor, but they believed that the compressibility and deformation of the soil mass above the deep anchor prevented the failure surface from reaching the ground surface as illustrated in Fig (2.6b). The extent of this local failure is limited to the height H, which is determined empirically and tabulated as a function of ϕ and B. The soil above the level of the failure surface is utilized as a surcharge pressure. Meyerhof and Adams assumed that the resultant frictional and cohesive forces acting on the curved surface would be approximately equal to the resultants of the passive earth pressure and the cohesion acting on that part of the cylindrical surface above the anchor plate perimeter which lay within the curvilinear failure surface, then the ultimate load R is given by

$$R = G_o + G_7 + \pi cBH + \frac{\pi}{2} S\gamma_g B(2D-H)HK_u \tan\phi \qquad (2.29)$$

G_7 is the weight of the soil inside the cylinder above the anchor.

They argue that at a certain depth there will be a limiting value of R which is equal to that given by the bearing capacity of the footing under downward load.

$$R = G_o + G_7 + \frac{\pi}{4}B^2(CN_c + \gamma_g DN_q) + A_s f_s \qquad (2.30)$$

where A_s is the surface area of the shaft

f_s is the average unit skin friction between soil and shaft.

N_c and N_q are bearing capacity factors for a footing under downward load (Meyerhof, 1951).

2.4. INCLINED ANCHOR THEORIES:-

Vertical anchors are a special case of the inclined anchors. In practice most of the anchors used are inclined from the vertical direction.

Due to the importance of inclined anchors a brief summary of the inclined anchor theories will be presented.

2.4.1. MEYERHOF THEORY (1973):-

Meyerhof extended the theory of vertical uplift capacity to inclined strip anchors under axial loads. The analysis was compared with the results of model and field tests on anchors in sand and clay.

Meyerhof assumed that when an inclined anchor is loaded to failure a mass of roughly truncated cone of pyramidal shape is lifted up as shown in Fig (2.9a). For shallow anchors the failure surface reaches the ground surface (i.e. general shear failure), while for greater depths, local shear failure occurs near the anchor. As for vertical uplift resistance the ultimate load of shallow anchors may be expressed by

$$R = (G_o + G_8)\cos\psi + (cK_c \frac{D_o}{\bar{B}} + \gamma_g D_o^2 \frac{K_b}{2\bar{B}})\,A \qquad (2.31)$$

where A is the area of anchor plate. $\bar{B}$ and D_o are the width and maximum depth of the anchor base respectively. K_b and K_c are uplift coefficients. G_8 is the weight of the soil mass vertically above the anchor base and ψ is the load inclination from the vertical direction.

For deep anchors, uplift coefficients N_{cu} and N_{qu} for strip anchors may be evaluated at footing level to estimate the anchor base resistance (ignoring anchor shaft friction), then the ultimate uplift resistance of an anchor inclined at ψ^o from the vertical R_ψ, see Fig (2.9b), is given by

$$R_\psi = G_o \cos \psi + A\,(cN_{cu} + \gamma_g DN_{qu}) \qquad (2.32)$$

where D is the average depth of the anchor base. N_{qu} is a function of ϕ and ψ

$$N_{cu} = (N_{qu} - 1) \cot \phi \qquad (2.33)$$

Although the analysis is presented for strip and square anchor plates, for circular plate anchors the ultimate load is considered by Meyerhof as that of a square plate anchor of equal area. He introduced an inclination factor by which the uplift capacity R_ψ of an inclined anchor can be estimated from the resistance $R_{\psi=o}$ of an anchor under vertical uplift i.e.

$$R_\psi = R_{\psi=o}\,\left(1 + \left(\frac{\psi}{90^o}\right)^2\right) \qquad (2.34)$$

2.4.2. HARVEY AND BURLEY (1973):-

Harvey and Burley considered shallow anchors embedded in soil with both friction and cohesive properties. The inclined pullout load is applied in the centre of a circular plate anchor at right angles to the plane of the plate.

As shown in Fig (2.10) they assumed the failure surface to be a circular arc perpendicular to the anchor plate and meeting the ground surface at an angle $\left(\frac{\pi}{4} - \frac{\phi}{2}\right)$ corresponding to the passive Rankine state of soil. They simplified the circular arc failure surface to a straight line and considering the state of earth pressure at rest, the forces acting on vertical slices of the failure surface were summed around the anchor shaft. It was stated that the ultimate uplift resistances of inclined and vertical anchors embedded at the same depth are approximately the same for non-cohesive soils.

Tran Von Nhiem (1971) represented the ultimate uplift resistance of an inclined anchor more simply by assuming that for small inclinations i.e. $0 < \psi < 30$ the inclined uplift capacity of an anchor has a trigonometric relation to the vertical capacity i.e.

$$R_{\psi} = R_{\psi=o} \frac{1}{\cos\psi} \qquad (2.35)$$

Hanna (1973) in a simplified analysis of inclined anchors embedded in clay pointed out that although ground anchors are very often inclined, the most convenient inclination for test anchor is usually vertical. Due to the frequent existence of anisotropic conditions, the pullout capacity at different inclinations for the same effective depth is not the same. Hanna produced expressions for the ultimate pullout load of inclined anchors.

2.5. DIMENSIONAL, FINITE ELEMENT AND ELASTIC ANALYSIS:-

2.5.1. DIMENSIONAL ANALYSIS:-

Dimensional analysis techniques have been applied by Baker and Kondner (1966) and Sutherland (1965) to the results of model tests to determine the relationship that governs the development of the maximum load resisted by anchors. More details of this technique and the relationships developed for the present study will be presented in section 3.7.

Baker and Kondner (1966) from laboratory pullout load tests on plate anchors in dense sand made a distinction between shallow and deep anchors at a $\frac{D}{B}$ ratio of 6, and produced empirical relationships for each case. For a shallow anchor the relationship is given by

$$\frac{R}{DB^2\gamma} = 3.0 + 0.67\left(\frac{D}{B}\right)^2 \qquad (2.36)$$

For a deep anchor

$$\left(\frac{R}{B^3\gamma_g} - 170\right)\frac{D}{b} = -2800 + 470\,\frac{D}{B} \qquad (2.37)$$

where b is the anchor plate thickness.

Sutherland (1965) applied dimensional analysis techniques to investigate the problem of raising a vertical closed ended shaft from a tunnel through sand to the sea bed at Sizewell Nuclear Power Station. He obtained the functional relationship

$$\frac{P_u}{\gamma_g D} = f\left(\frac{D}{B}, \phi\right)$$

where P_u is the ultimate anchor pressure.

From his model test results in beds of dry and submerged sand in both dense ($\phi = 45^o$) and loose ($\phi = 31^o$) states the plotting of $\frac{P_u}{\gamma_g D}$ against $\frac{D}{B}$ gave two distinct curves, one for each density. The agreement of the data from several different anchor diameters tested was good.

Sutherland used these relationships to predict the maximum jacking load required to push out the shaft. When these field test results were plotted on the same graph of model tests, they gave consistent results corresponding to angles of internal friction ϕ of the sand of 42^o and 35^o for dense and loose sands respectively.

2.5.2. FINITE ELEMENT ANALYSIS:-

Limiting equilibrium methods are concerned only with the estimation of the maximum load the anchor can resist and do not consider the deflections of the anchor required to develop loads up to the maximum. Finite element analysis can provide the load-deflection curve in both the elastic and plastic ranges. All of the existing finite element programs studied by the author have been restricted to vertical anchors only.

Ashbee (1969) proposed a finite element analysis of the soil anchor system in which a uniaxial model is adopted, where all movements and forces in the soil are in a direction parallel to the vertical axis of the footing (i.e. there are no radial movement or forces in the soil). The effect of lateral forces due to dilation or Poisson's ratio effects in the soils possessing friction results in an increase in shear strength in the vertical plane where there is an increase in radial pressure. Therefore, the uniaxial method can not be correctly applied to soils possessing friction and to problems where non-vertical plastic flow of material is involved. A linear elastic non-strain hardening plastic soil stress-strain relationship was adopted by Ashbee using different elastic moduli in tension and compression and assuming the degradation of the shear strength to its residual value after the maximum shear strength has been reached. Ashbee examined the load-deflection relationship for an anchor pulled out of the soil and found that various parts of the soil yielded or sheared at different anchor load levels indicating a progressive failure.

McMullan (1974) attempted to predict the behaviour of a vertical deep plate anchor in dry sand using both plane strain and axisymmetric analysis on triangular elements, with different stress-strain relationships for the soil. Due to the poor agreement with his model tests McMullan carried out a plane strain analysis in which the soil behaviour was specified as a linear elastic medium in compression but would display little resistance to tensile stresses.

2.5.3. ELASTIC ANALYSIS:-

Khadilkar and Gogate (1970) considered the general case of a plate anchor inclined to the vertical embedded in a semi-infinite elastic mass of soil. The load applied to the anchor shaft is assumed to be distributed uniformly across the plate anchor. They reported that the displacements are more sensitive to changes in the value of modulus of elasticity than to changes in Poisson's ratio.

Hunter and Gamblen (1974) analysed the problem of an anchor shaft with rigid circular disc in a semi-infinite linearly elastic soil mass. Load-displacement relationships were presented for two cases. The first case was where the soil adheres to the underside of the plate and the other where the soil would break away from the underside of the plate. The load displacement behaviour is dependent on the soil density, the shear modulus and Poisson's ratio, the geometry and depth of embedment of the anchor.

2.6. DISCUSSION OF ANCHOR THEORIES:-

2.6.1. SHALLOW VERTICAL ANCHOR THEORIES:-

Concerning the traditional methods, in the earth cone theory only the weight of the soil inside the truncated cone is taken neglecting the effect of cohesion and internal friction. However, although the important phenomenon of shear failure in the body is neglected, this method overestimates the ultimate load of anchors at high $\frac{D}{B}$ ratios.

The earth pressure method ignores cohesion, although it is based on the earth pressure theory.

In the shearing method the uplift resistance includes both cohesion and internal friction. The disadvantage of this method is the simplifying assumption of a vertical slip failure surface for those soils which possess internal friction.

Balla was the first to suggest a rational method for solving uplift problems by selecting a curved slip failure surface and analysing the shear stresses developed over it. He applied Kotter's equation to determine the distribution of stresses which is in a plane stress condition and assumed it to be the same as in the axially symmetrical case. Balla used the vertical component of the shearing stress only and no account was taken of the normal stresses which act on the slip failure surface.

Sutherland (1965) performed work on model and field tests and concluded that Balla's theory yields values of uplift resistance for loose sands approximately 90% of that of dense sand for the same depth to diameter ratio. This would lead to underestimation of loads mobilized in dense cohesionless soils and consequently to an unsafe error on shaft raising problems and an error on the safe side for pylon foundations. On the other hand the theoretical loads would be overestimated for loose cohesionless soils leading to safe errors for shaft raising and unsafe errors for a pylon foundation. It will be shown in chapter 7 that the same trend appears with the present experimental results.

The author found that some of the numerical values of the factors F2 and F3 plotted in Balla's paper did not agree with the corresponding values obtained from the equations reported. Doubts regarding some values in Balla's paper have also been expressed by Howat (1969) and Vesic (1971).

Mariupolskii (1965) proposed a new approach for the solution of the uplift problem. He argued that, as the anchor moves upwards and compresses the soil, the frictional forces in the vertical cylinders of soil around the anchor increase and failure occurs in tension over the surface below this soil. However the concept of a separation cone at failure is not widely accepted and is difficult to justify.

Vesic and others have pointed out that the assumptions made by Mariupolskii in his initial reasoning on the failure mechanism of shallow anchors are arbitrary and not in agreement with the elementary theory of earth pressure.

The parameter n in Mariupolskii's equation is determined from experimental results which reduces the theoretical value of his procedure.

Vesic (1965) considered in his theory the effect of both normal and shear components on the surface failure, but ignored the weight of the soil in the hemispherical cavity above the anchor plate. The adaptation of the theory by Squivel and Diaz (1967) by adding the pressure due to the soil originally ignored by Vesic restricts the application of the theory for depth to diameter ratio more than 0.5 only.

Matsuo (1967) like Vesic considered the effect of normal and shear stresses on the failure surface. As with Balla and Vesic, Matsuo applied the derived plane strain system of stress to the three dimensional axially symmetric case due to the non-existence of a method exactly representing the three dimensional stress condition. From experiments on sand Matsuo found the angle θ_0 (Fig 2.5) to vary between 55^o and 65^o but he adapted only 60^o for all the sand types and conditions. Matsuo obtained good correlation between his field test results and his approximate theory.

Meyerhof and Adams (1968) initially assumed a curved failure surface. Recognizing the difficulty found by previous authors of analysing stress on a curved surface in three dimensions, they finally assumed the slip failure surface to be a cylinder with diameter equal to that of the anchor. Certain factors derived from experimental observations were introduced into the calculation. The expression for ultimate uplift resistance is therefore partly theoretical and partly empirical.

2.6.2. DEEP VERTICAL ANCHOR THEORIES:-

Mariupolskii (1965) assumed the work done in moving the anchor plate over a certain height could be equated to the work done in expanding a cylindrical cavity of that height from a diameter equal to the shaft diameter to that of the plate. His assumption of equilibrium and continuity of the elastic and plastic states on the elastic plastic boundary enabled him to derive expressions for the radial stress on that boundary from which the ultimate uplift resistance could be calculated. The method of obtaining these expressions is not clearly demonstrated and the ultimate pressure was obtained by trial and error from a lengthy operation. Mariupolskii introduced many parameters without explaining their derivation (e.g. the volume compressibility of the soil). The slightly convex generatrix of the cone wedge was approximated to be rectilinear. Although Mariupolskii assumed the problem to be elastoplastic there is no mention of modulus of elasticity and Poisson's ratio.

Vesic (1972) considered the analogy of spherical cavity to apply to deep anchors. When the ultimate cavity pressure P_{uc} is reached a plastic zone around the sphere is formed and a volume change takes place in this zone and the surrounding elastic region to allow the anchor movement. The radius of the anchor becomes the ultimate cavity radius.

Meyerhof and Adams (1968) included certain factors for ultimate uplift resistance from experimental observations. They also assumed an infinite mass of soil when using Meyerhof's equation for bearing capacity at great depth to reach a limiting value of ultimate uplift resistance.

2.6.3. INCLINED ANCHOR THEORIES:-

Meyerhof (1973) observed that the influence of inclination on the uplift resistance varied with the shape and average depth to width ratio of the anchors and the shear strength parameters of the soil. His theory and test results indicated that the uplift coefficients, which must be found from earth pressure theory, generally increase with the inclination of the load and he also noted the decreasing influence of inclination as the depth of anchor increases. The shape of the failure surface in both shallow and deep cases is not clearly defined by Meyerhof. The analysis is presented for strip and square anchor plates. When considering circular plate anchors the ultimate load is taken by Meyerhof as that of a square plate anchor of equal area. The introduction of inclination factors is acceptable only for very small angles of inclinations.

Harvey and Burley (1973) first assumed a curved failure surface but due to the difficulties involved, they simplified it to be straight line. Although the theory gives reasonable agreement with laboratory experiments for shallow anchors, it overestimates the uplift capacity for deep anchors. They concluded that the values of ultimate uplift resistance for vertical and inclined anchors of the same depth and diameter are approximately the same although only one density of the sand was tested.

The work published is at variance as to whether inclined anchors have a greater uplift capacity than vertical anchors, for the same depth/diameter ratio. Trofimenkov and Mariuposkii (1965), Khadilkar and Gogate (1970), and Harvey and Burley (1973) all reported that there is very little difference in the respective values and that these differences decrease as $\frac{D}{B}$ increases.

On the other hand Kananyan (1966), Tran Von Nhiem (1971) and Larnach (1972, 1973) and McMullan (1974) all reported that inclined anchors have a greater capacity than vertical ones. Kananyan found that for an anchor inclined at an angle $\psi = 45^{o}$ from the vertical, the load was 50% greater while Larnach reported that the peak of the ultimate loads occurred at $\psi = 20^{o}$ in two sands of different ϕ values. McMullan also found that the peak of the ultimate loads occurred at $\psi = 18^{o}$.

2.6.4. DIMENSIONAL AND FINITE ELEMENT ANALYSIS:-

Sutherland (1965) used the relationship established from his model tests to predict the force required to raise a shaft upwards through a bed of saturated sand. The ϕ values of the saturated sand were not quoted but the estimates based on model tests in dense sand agreed with the maximum loads developed in the field.

Baker and Kondner (1966) included both the relative density and the void ratio in their analysis although they are interdependent.

Dimensional analysis technique might be applied to test results in the field if an adequate knowledge of the conditions of the tests was available. Although dimensional analysis can be useful in providing estimates of the maximum load, it can not provide information on the deformation behaviour of the soil anchor system.

Ashbee's finite element analysis predicted a general shear failure for both shallow and deep anchor cases. The prediction is suitable for the former case where the failure surface reaches the soil surface. However it contradicts the local type of failure associated with the latter case. The assumption of a uniaxial model where the nodes of the elements are constrained to move parallel to the central axis and the assumption that horizontal stress variations and displacements have a negligible effect on the footing will reduce the validity of the results. For soils with friction and cohesion the analysis shows that the peak stresses at various points in the soil mass are not reached simultaneously. This is a valid observation which was not considered by any of the previous theories.

McMullan (1974) explained that the disagreement of his finite element analysis with his model test results was due to the incorrect assumption of the distribution of the load in the anchor plate and shaft. When he used the program where no tension developed in the sand the displacements predicted were even greater than when he used a simple linear elastic soil. The difficulty of the finite element method is to select elastic soil properties which adequately reflect the behaviour of the soil under compressive and tensile loading.

2.7. PREVIOUS LABORATORY AND FIELD TESTS:-

Previous laboratory and field tests will be described in Section 2.7, followed by comparison of the theoretical and experimental work in Section 2.8.

A general summary of the previous experimental work is given in Tables 2.1, 2.2, 2.3.

2.7.1. LABORATORY MODEL TESTS FOR SHALLOW ANCHORS:-

Two basic types of model investigation have been carried out to provide information on the behaviour of anchors. The first type is to define the form of failure surfaces associated with the development of maximum load. These surfaces have been observed directly in half section or plane strain models using sand tanks with transparent walls and indirectly in axisymmetric models using mechanical displacement gauges and penetrometers to deduce the position of the failure surface or by using coloured layers in the sand bed and excavating the footing after failure.

The second type of test has used axisymmetric models to investigate what effects, changes in the geometry of the anchors, the properties of the sand and the type of loading, have on the load-displacement behaviour of the anchor.

2.7.1.1. FORM OF FAILURE SURFACE :-

(a) Balla (1961), Meyerhof and Adams (1968), and Khadilkar and Paradkar and Golait (1971), have used half section models of anchors in sand to observe the failure surface. Balla approximated the failure surface to an arc of a circle with a vertical tangent to the footing and curving outwards to intersect the sand surface at approximately ($\frac{\pi}{4} - \frac{\phi}{2}$), while Khadilkar and Paradkar and Golait described it as a logarithmic spiral curve and produced theoretical expressions for the ultimate load. Meyerhof and Adams observed the failure surface to extend outwards in a shallow arc from the anchor perimeter to the sand surface. In loose sands it extended almost vertically.

Baker and Kondner (1966), Carr (1970) and Yilmaz (1971) used plane strain models to determine the form of the failure surface.

(b) Matsuo (1967) and Carr (1970) investigated the form of failure surface on axisymmetric models. Matsuo found that the failure surface consists of a logarithmic spiral curve and a straight line tangent to it. Carr used mechanical displacement gauges to monitor the displacement within the sand. From the variation of density within the sand bed after failure an outwardly curved failure surface extending from the anchor to the sand surface was obtained in dense sand.

2.7.1.2. EFFECT OF DIFFERENT PARAMETERS ON THE BEHAVIOUR OF THE ANCHOR:-

Axisymmetric models of anchor have been carried out by many researchers to investigate the effects of anchor geometry, sand properties and type of loading on the behaviour of anchors. Many of the tests have been concerned with establishing the maximum load that can be developed by a particular anchor in a sand bed with particular properties. Some of the tests have been presented in sections 2.2, 2.3, 2.4 and a summary of some of them is given in Table 2.1. McDonald (1963), Heikkila and Laine(1964) derived empirical relationships from the results of a large number of tests in guyed anchor plates. Hanna (1976) showed the importance of sand stress history on the pull-out load capacity of anchor plates and warned against the indiscriminate use of uplift theories which neglect the stress history of the sand deposit.

2.7.2. FIELD SCALE TESTS FOR SHALLOW ANCHORS:-

Sutherland (1965), Trofimenkov and Mariupolskii (1965) carried out field tests for vertical shallow anchors in different densities.

Kananyan (1966) carried out tests on vertical and inclined plate anchors, from which he pointed out that maximum load increased with an increase in plate diameter but the average stress on the plates at failure decreased with an increase in plate diameter. Matsuo (1967) found that an increase in the density of the sand resulted in a substantial increase in the maximum load resisted by the footing. A summary is given in Table 2.1.

2.7.3. LABORATORY MODEL TESTS FOR DEEP ANCHORS:-

Many half section models in transparent sided tanks have been used to monitor the soil displacements.

Meyerhof and Adams (1968), Khadilkar and Gogate (1970) and Kupferman (1974) conducted half-section model tests. The outer boundary of the blurring in the time exposure photographs presented by Meyerhof and Adams is considered as a failure surface. This does not represent accurately the relative displacements within the mass of sand that has displaced and the outer boundary of the movement is not necessarily the surface of sliding. Khadilkar and Gogate (1970) using coloured layers reported that the sand immediately above the anchor was compressed and that the anchor moved upwards without the development of any general shear failure surface and the formation of cylindrical cavity below the anchor.

Carr (1970) used time exposure photography and observed that the maximum load coincided approximately with the first signs of sand moving downwards around the anchor.

McMullan (1974) used a stereophotogrammetric technique for deep anchors and showed that a zone of sand extending several diameters above the anchor suffers displacements of varying magnitude. The zone immediately around the anchor plate suffers displacements which appear to be due to the flow of sand around the anchor into the cavity below. By using the stereophotogrammetric technique it was only possible to build up the information on displacements in the sand bed rather than defining exactly the failure surface.

Many axisymmetric model tests have been carried out to determine the load-displacement behaviour of plate anchors failing in the deep mode.

Baker and Kondner (1966), Carr (1970), Harvey and Burley (1973), Abu Taleb (1974) and McMullan (1974) carried out model tests for deep anchors. Different investigators defined the critical depth to diameter ratio differentiating between shallow and deep anchors. This ratio depends on the type and condition of the sand used.

Carr (1970) used surcharge devices to over-consolidate the sand bed around the anchor to study its effects on the anchor behaviour. Carr concluded that the higher values of maximum load obtained for overconsolidated sand compared to normally consolidated sand are due to the higher stresses introduced in the bed by the overconsolidation. Abu Taleb (1974) found that elastic loads amount to 40% of the maximum load and that 50% of the anchor displacement at maximum load occurred during the application of the final 20% of the maximum load. McMullan (1974) found that for anchors inclined from the vertical at an angle ψ, the ultimate uplift resistance increases for $0^{o} < \psi < 18^{o}$ reaching a peak at 18^{o}, then decreases again for $\psi > 18^{o}$.

Generally it has been noted that in displacement controlled tests there is little or no decrease in the loading of the anchor as it is pulled through the soil until it is near the surface. The displacements of the anchor at maximum load for deep anchors are larger than those of shallow anchors.

2.7.4. FIELD SCALE TESTS FOR DEEP ANCHORS:-

Luga et al (1961) reported that the maximum load is developed at displacements of the anchor equal to 15% of the anchor diameter and observed that the appex angle of the cone above the anchor is $(90^{o} + \phi^{o})$.

Mariupolskii (1965) reported the formation of a cavity below the anchor plate on loading the anchor. The soil flowed into this cavity in unstable saturated soils or dry loose sands while the cavity remained intact for soils possessing some cohesion. The development of the maximum load and the subsequent displacement of the anchor through the overlying soil is associated with the formation of a cone of soil with an appex angle approximately 90^{o}.

Trofimenkov and Mariupolskii (1965) compared the performance of a screw plate anchor when subjected to uplift loading with its performance when it was loaded in compression as a pile. The anchor acting as a pile resisted 1.4 to 1.5 times the maximum uplift load that it could resist. These differences were due to the fact that under pile loading the plate bears on undisturbed soil whose strength increases with increasing distance below the plate and the reduction of the active area of the plate in the former case because of the existence of the anchor shaft above the plate.

Dzhioev (1970) carried out tests on plate anchors in sandy loams. He considered that once the maximum load had been developed this load would be maintained during the upward displacement of the anchor until it approached the soil surface. When the general shear failure developed the anchor pulled out and the load reduced.

2.8. COMPARISON OF THEORIES AND EXPERIMENTS:-

The author has compared the results of many of the previous theories proposed for the estimation of the ultimate uplift capacity of circular plate anchors, embedded in cohesionless soils. The results are given in a non-dimensional form using dimensional analysis. The ultimate anchor pressure over the soil over-burden pressure ratio $\frac{P_u}{\gamma_g D}$ is plotted versus the depth over diameter ratio $\frac{D}{B}$ of the shallow anchors as shown in Fig (2.11).

The comparisons are carried out for a range of $\frac{D}{B}$, angles of shearing resistance and densities of sand representing dense and loose states.

The maximum loads predicted by various methods are not in good agreement with each other, although different authors compared their theoretical prediction with their results from laboratory and field tests for particular conditions of the tests and obtained reasonable agreement. The theories reviewed depend on the assumption of the shape of the failure surface and the behaviour of the soil within the failure surface which is dependent on the relative density and the angle of shearing. A wide variety of assumptions made by different authors have led to these disagreements.

Referring to Fig (2.11) it is shown that ultimate loads for loose sand in Balla's theory are higher than those values for dense sand predicted by Vesic and similar trends exist between some of the other theories. Generally Balla's theory is found to be insensitive to changes in the values of ϕ.

Fig (2.12) shows the comparison between the best fitting curves of the experimental results conducted by El-Rayes (1965), and Fig (2.13) shows the results obtained by Baker and Kondnor (1966), Adams and Hayes (1967), Carr (1970) and Harvey and Burley (1973) in different types of sands. From El-Rayes's results in Fig (2.12) it was found that $\frac{P_u}{\gamma D_g}$ values for Leighton Buzzard sand ($\phi = 33^o$, $D_r = 62.1\%$) are higher than that of Sizewell sand ($\phi = 38^o$, $D_r = 4.5\%$). Similar trends are shown in Fig (2.13) between Baker and Kondner results ($\phi = 42^o$) and that of Harvey and Burley ($\phi = 40^o$) and between Adams and Hayes results ($\phi = 34^o$) and Carr test results ($\phi = 37^o$).

The use of γ and ϕ only to define the failure surface and the shear behaviour of the soil along it is a simplification and does not cover all the types and states of sand. Using different states and types of sands, the relative density is an important parameter which should be included in the analysis and it explains the anomaly of the results shown in Figs (2.12) and (2.13). A sand with high value of ϕ and comparatively low relative density will yield lower values of uplift resistance than those of moderate value of ϕ and high relative density. The behaviour of a soil anchor system is likely to be affected by the compressibility of the soil and the stress history which might include overconsolidation or compaction by vibration.

None of the methods appear to give a comprehensive solution to the behaviour of anchors at failure for a wide range of soil types and conditions.

2.9. COMMENTS AND CONCLUSIONS:-

2.9.1. SHALLOW VERTICAL ANCHORS:-

(1) Shallow anchors are those which develop a general shear failure at or near the development of the maximum load. It is associated with the uplift of the soil above the anchor and the development of failure surfaces extending from the perimeter of the anchor to the sand surface.

(2) Curvilinear failure surfaces are observed to have developed in the field and laboratory model tests and are related to the properties of the soil.

(3) The behaviour of the anchor depends on the anchor geometry, the depth of embedment, the soil properties such as the angle of shearing resistance, the relative density and the stress history of the soil.

(4) The theories developed do not yield good results except for the conditions under which they were established. This is due to the different assumptions of failure surfaces, representation of the stresses at failure and neglect of some soil parameters.

2.9.2. DEEP VERTICAL ANCHORS:-

(1) The deep anchor is one in which the maximum load is developed without disturbance of the ground surface. Experimental evidence shows

that the behaviour of a deep anchor is associated with local shear failure around the anchor plate and the formation of a cone of soil on top of the anchor.

(2) A cavity formed below the anchor plate is not sustained for dry or saturated cohesionless soils but it can be sustained with moist sands or soils possessing some cohesion.

(3) The maximum load developed is dependent on the anchor geometry and the soil properties e.g. angle of shearing resistance, relative density, stress history and the compressibility of the sand.

(4) There is no difference between the load-displacement curves obtained from displacement or load controlled tests, and the rate of loading does not affect the maximum load in cohesionless soils.

2.9.3. INCLINED ANCHORS:-

(1) The same concept of shallow and deep anchors resisting general and local shear failure also appears and occurs with inclined anchors.

(2) Failure surfaces observed are of a complex nature in three dimensions and most of the investigators who experimentally observed curvilinear failure surfaces eventually assumed straight lines in their theoretical analysis for simplification.

(3) The additional parameter affecting the ultimate uplift capacity of inclined anchors as compared with vertical anchors is the magnitude of the inclination of the anchor from the vertical.

(4) From the previous experimental work there is a difference of opinion as to whether the ultimate load of an inclined anchor is greater than the vertical anchor under similar conditions.

2.9.4. CONCLUSIONS:-

From the foregoing review it has been established that no theoretical method satisfactory for all types and conditions of cohesionless soil has been developed for assessing the ultimate uplift resistance of anchors. The experimental work conducted by each investigator did not cover the full range of effective parameters.

It was decided by the author to try and develop an approximate method for shallow, deep, vertical and inclined anchors embedded in different types and conditions of cohesionless soils. This method was to be checked by an extensive experimental program to cover shallow, deep, vertical and inclined anchors embedded in different densities of sand. The method of analysis is described in chapter 3.

The development of a finite element technique could be useful provided an adequate stress-strain curve for the soil can be obtained. With this in mind a finite element program has been used to analyse the problem and is presented in chapter 6 of this thesis.

Type of Test	Investigator	Type	Dia(cm)	Density	ϕ^o	m.c. %	Method of placing	Loading
VERTICAL MODEL TESTS	Balla (1961)	under ream	6-12	Dense	36^o - 38^o	Dry and 10-12	Layers	Load cont
	ElRayes (1965)	plate	2.5 - 5.7	loose med.dense dense	24^o 38^o	Dry	Raining	Displ. cont.
				loose dense	28.5^o 47.5^o	Dry & submerged		
				loose dense	38^o 50^o	Dry		
	Sutherland (1965)	plate	3.8 - 15	loose dense	31^o 45^o	Dry and submerged		load cont.
	Matsuo (1967)	plate under ream	18 - 40	loose dense	37.5^o 42.5^o	Dry and submerged	compacted in layers	load cont. displ.cont.
	Howat (1969)	spherical	3.8 - 11.2	dense	28^o	5	vibrated in layers	disp. cont.
	Khadilkar & Gogate (1970)	under ream	5-10	dense	35^o	10-12	compacted in layers	load cont.
	Kupferman (1974)	Fluke	7.5 - 15	loose dense		saturated	poured thr.water and vibrated under water	Disp. cont.
VERTICAL FIELD TESTS	Fielitz (1953)	under ream	110 - 140	loose med.dense	30^o			
	Jyoev (1956)	under ream	20-50	dense	23^o			
	Brown-Boweri (1959)	under ream	190	dense	36^o			
	Mariupolskii(1965)	screw piles	500	dense	27^o	dry		
	Sutherland (1965)	shaft	239	loose dense	35^o 42^o	saturated		

Table 2.1 Details of previous tests on vertical shallow anchors.

Type of Test	Investigator	anchor type	sand			Critical $\frac{D}{B}$ ratio
			Density	ϕ	m.c.%	
Vertical Model Tests	Baker and Kondner (1966)	plate	dense	42°	Dry	6
	Meyerhof and Adams (1968)	strip footing	loose dense	25° 45°	Dry	3 9
	Howat (1969)	spherical	dense		5	10
	Carr (1970)	plate	dense		Dry	10
	Vesic (1971)	plate	loose dense		Dry	3 10
Vertical Field Tests	Luga *et al* (1961)	screw plate		15° 34°		4 6.5
	Baker and Kondner (1966)	plate	dense	37°	Dry	

Table 2.2 Details of previous tests on vertical deep anchors.

<table>
<tr><th rowspan="2">Type of Test</th><th rowspan="2">State of Anchor</th><th rowspan="2">Investigator</th><th rowspan="2">Anchor type</th><th colspan="3">sand</th><th rowspan="2">Critical $\frac{D}{B}$ ratio</th></tr>
<tr><th>Density</th><th>ϕ</th><th>m.c. %</th></tr>
<tr><td rowspan="4">Inclined model tests</td><td rowspan="2">shallow</td><td>Gillon (1970)</td><td>strip footing</td><td>med. dense</td><td>37^{o}</td><td>Dry</td><td></td></tr>
<tr><td>Meyerhof (1973)</td><td>strip footing</td><td>dense</td><td>43^{o}</td><td>Dry</td><td></td></tr>
<tr><td>shallow and deep</td><td>Harvey and Burley (1973)</td><td>plate</td><td>dense</td><td>40^{o}</td><td>Dry</td><td>6</td></tr>
<tr><td></td><td>McMullan (1974)</td><td>plate</td><td>med. dense</td><td>33^{o}</td><td>Dry</td><td>4.67</td></tr>
<tr><td rowspan="2">Inclined field tests</td><td>shallow</td><td>Kananyan (1966)</td><td>plate</td><td>dense</td><td>32^{o}
34^{o}</td><td>Dry</td><td></td></tr>
<tr><td>deep</td><td>Trofimenkov and Mariupolskii (1965)</td><td>screw plate</td><td>loose
med. dense</td><td>30^{o}
34^{o}</td><td>saturated</td><td>5
6</td></tr>
</table>

Table 2.3 Details of previous tests on inclined anchors

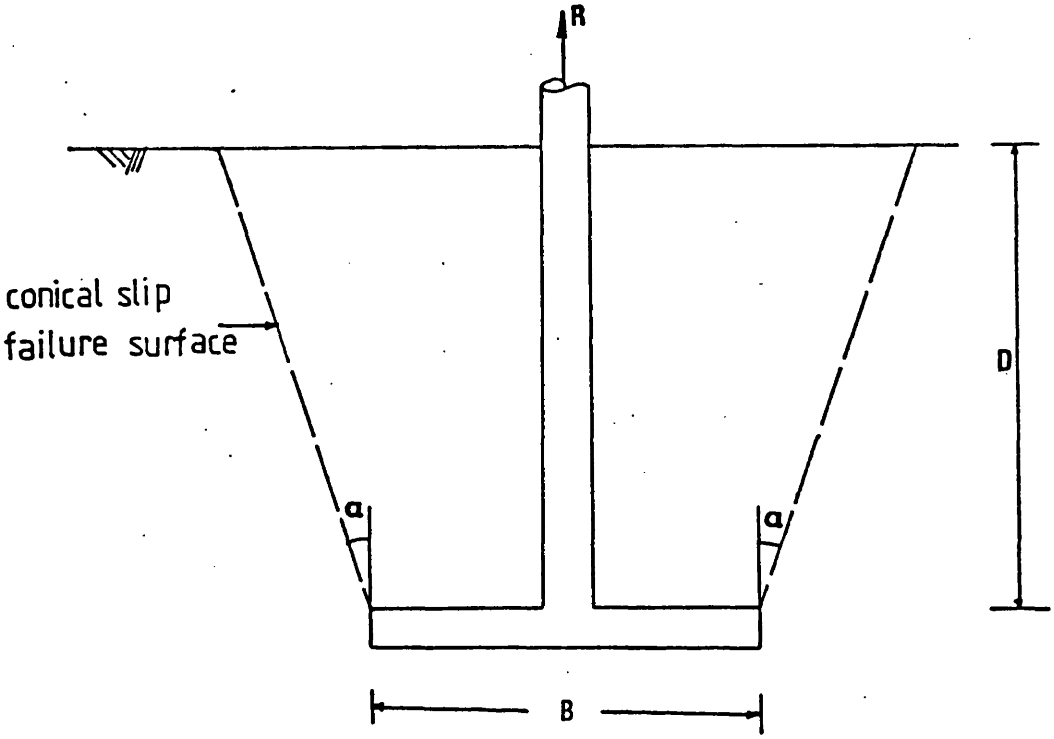

FIG.2.1a EARTH CONE THEORY

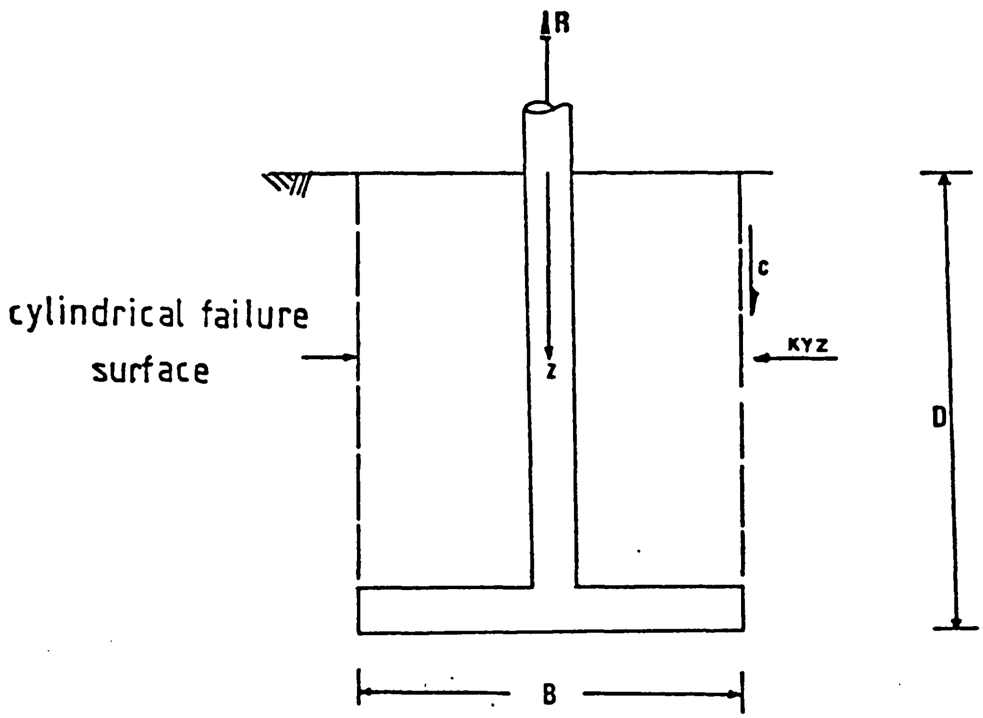

FIG.2.1b. EARTH PRESSURE AND SHEARING THEORIES

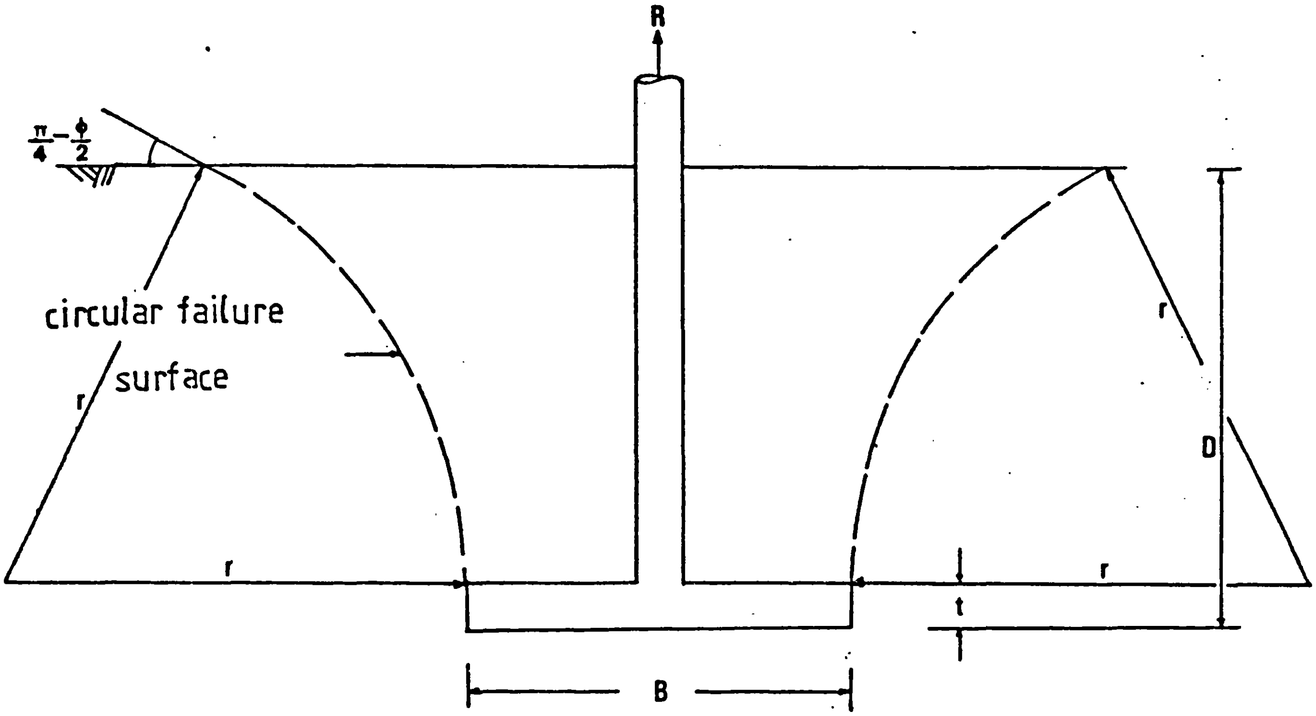

FIG.2.2. BALLA'S THEORY

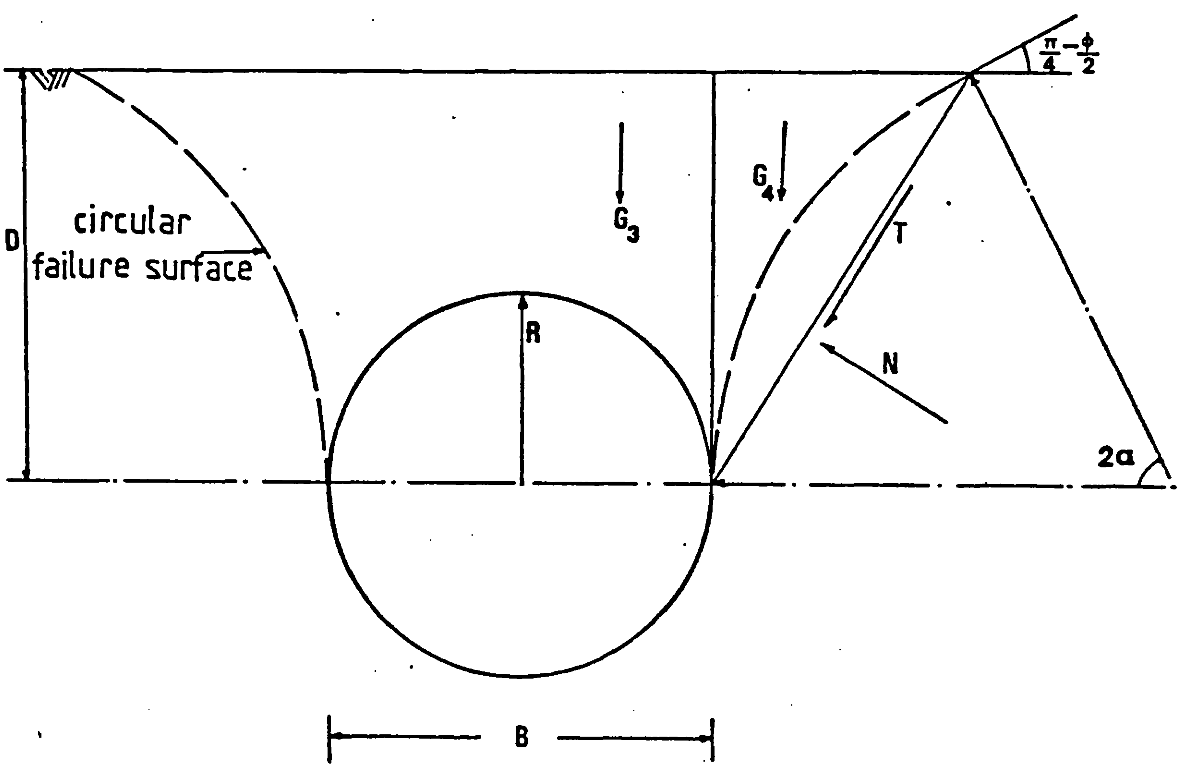

FIG.2.3. VESIC'S THEORY

(EXPANSION OF SPHERICAL CAVITY CLOSE TO GROUND SURFACE)

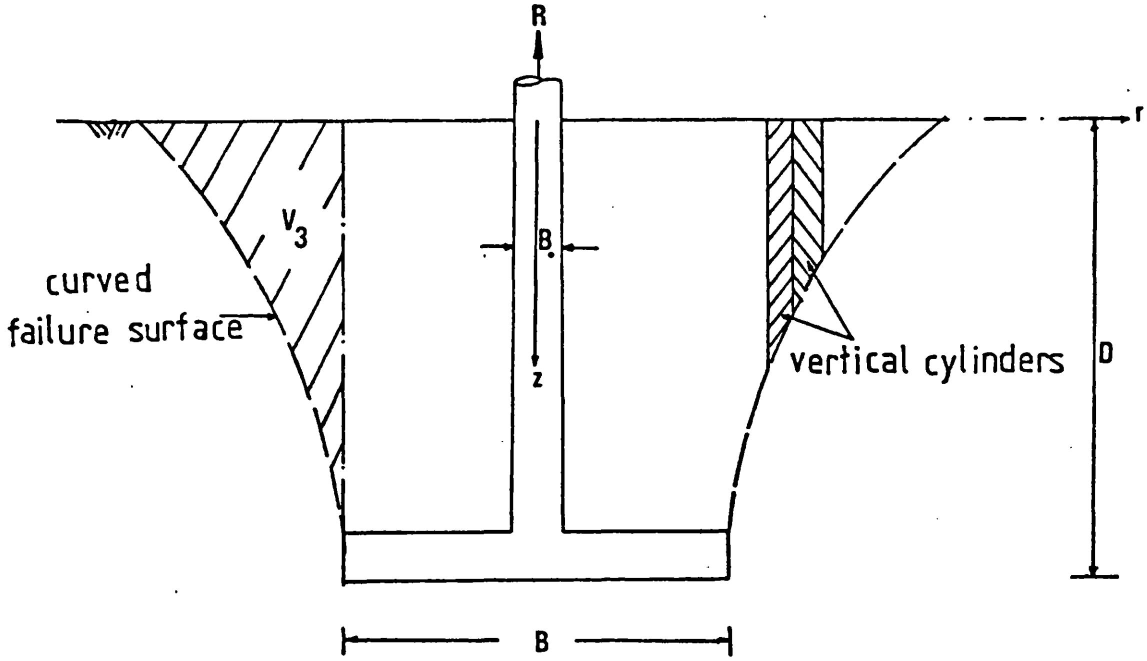

FIG.2.4. MARIUPOLSKII THEORY

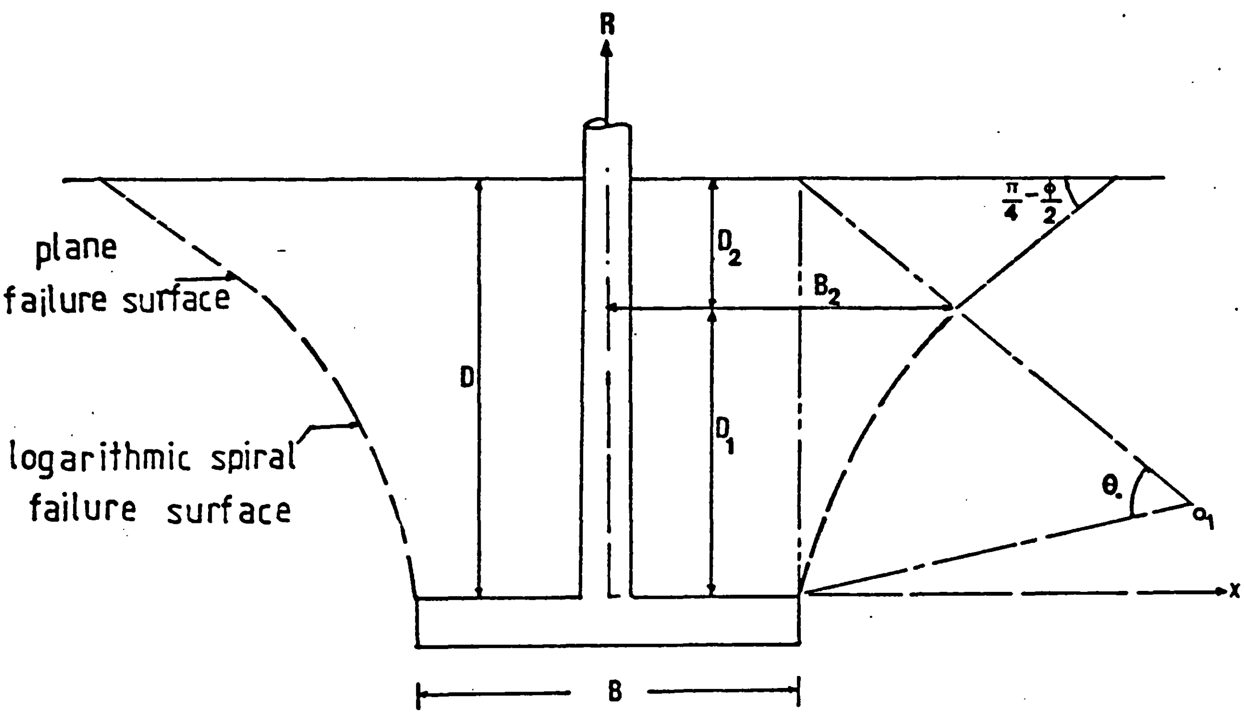

FIG.2.5. MATSUO THEORY

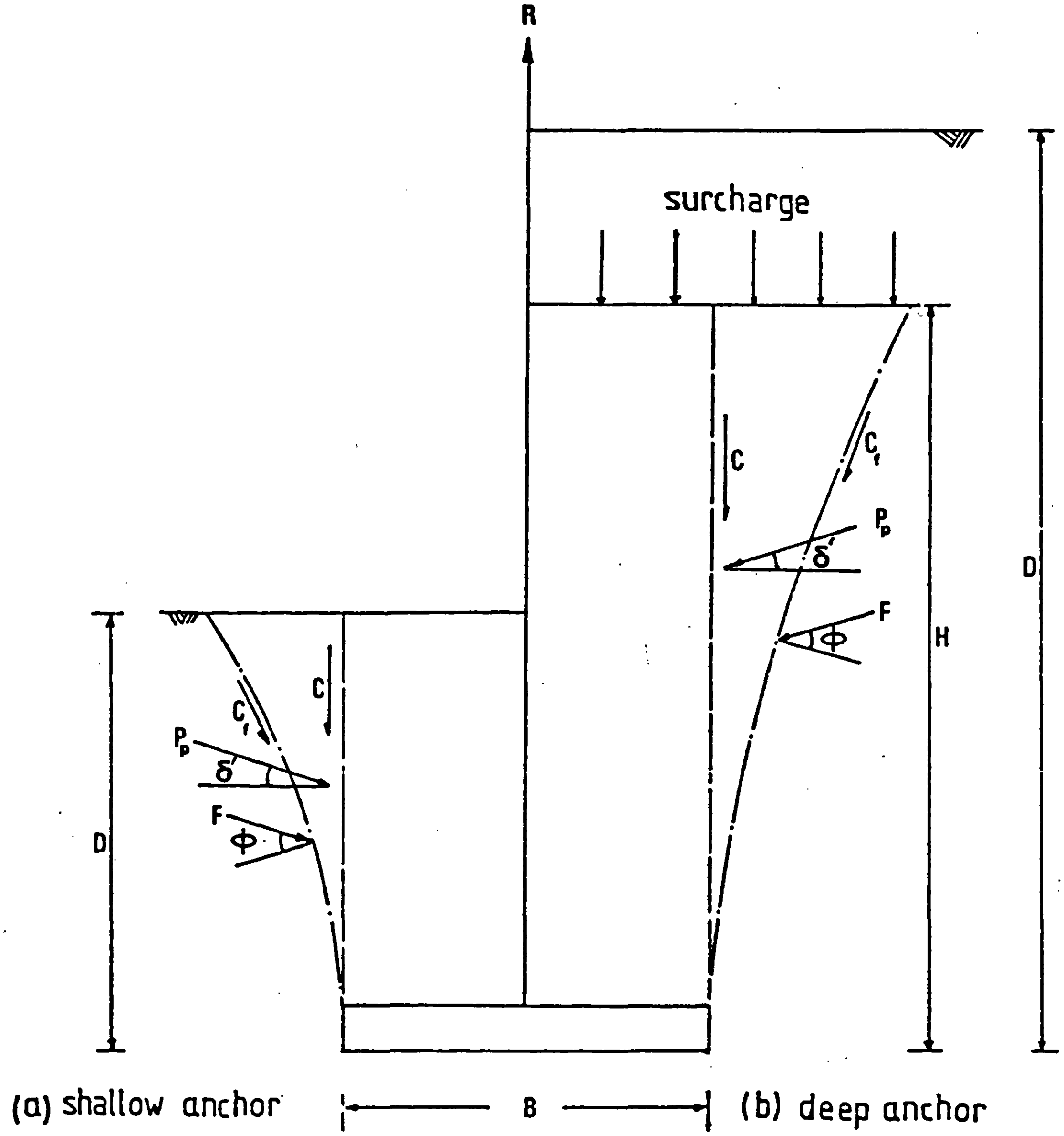

FIG.2.6. MEYERHOF AND ADAMS THEORY FOR SHALLOW AND DEEP ANCHORS

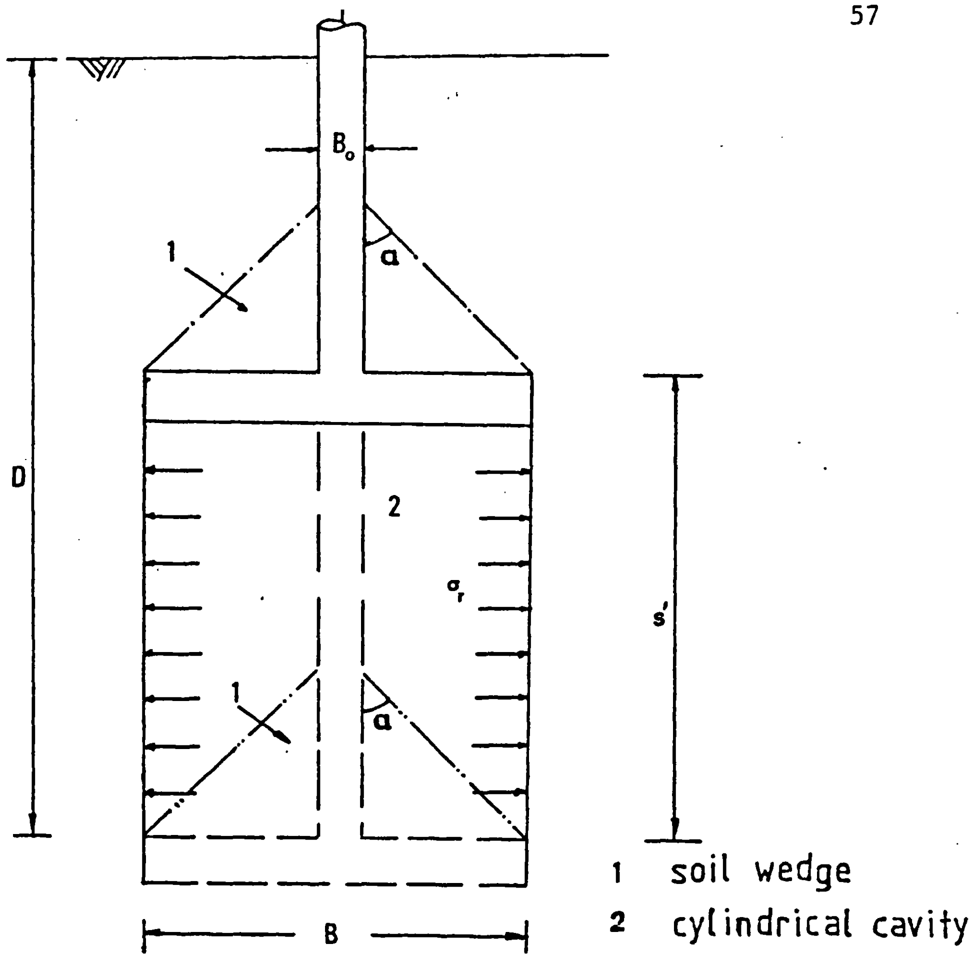

FIG.2.7. MARIUPOLSKII THEORY (DEEP ANCHOR)

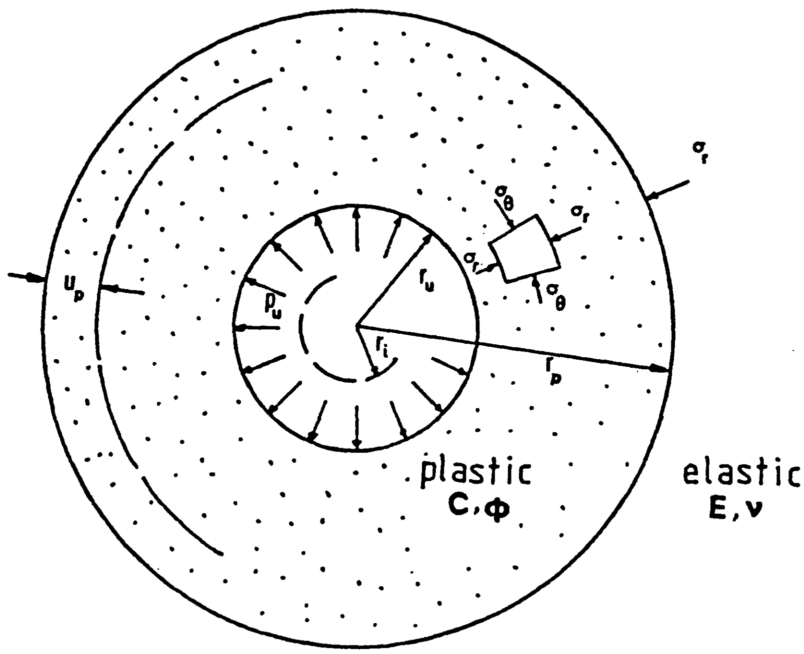

FIG.2.8. VESIC THEORY (EXPANSION OF A DEEP SPHERICAL CAVITY)

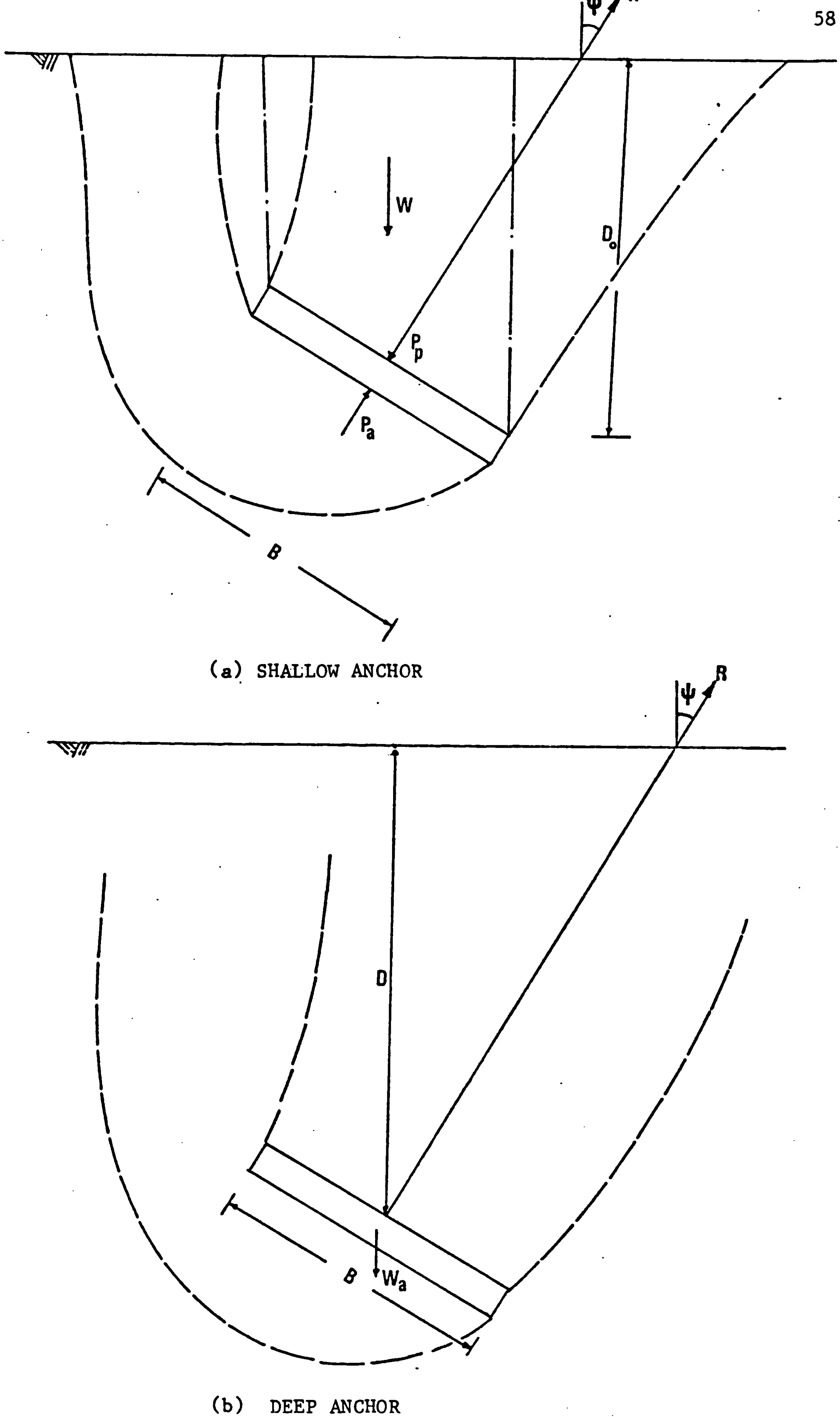

FIG.2.9. MEYERHOF INCLINED ANCHOR THEORY

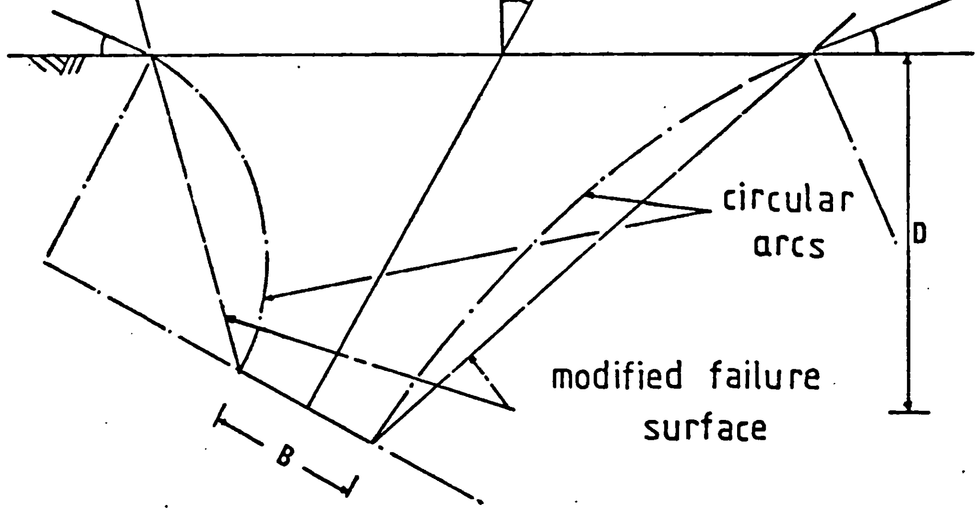

FIG.2.10. HARVEY AND BURLEY INCLINED ANCHOR THEORY

(VERTICAL SECTION THROUGH FAILURE ZONE)

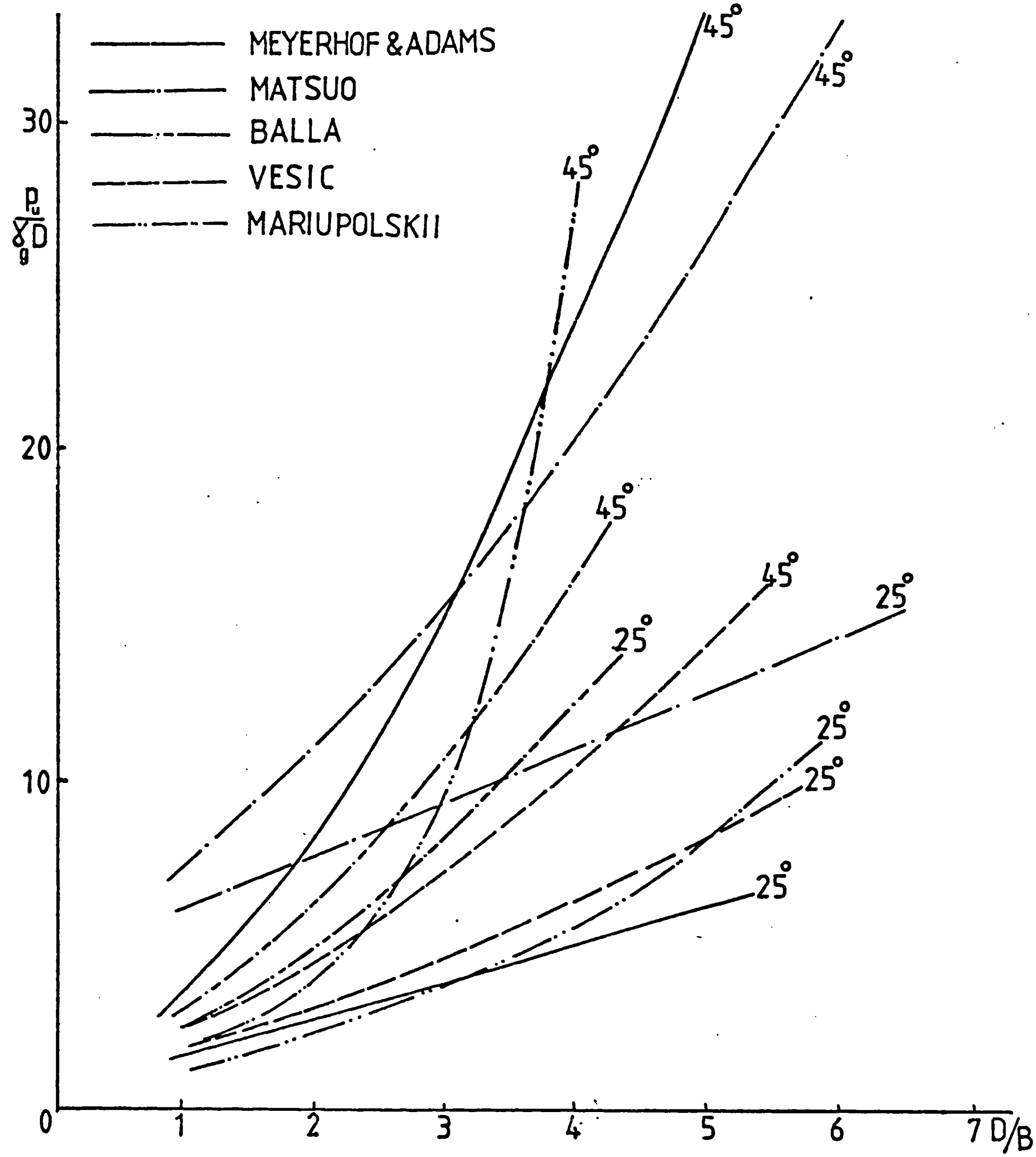

FIG.2.11. COMPARISON OF DIFFERENT THEORIES

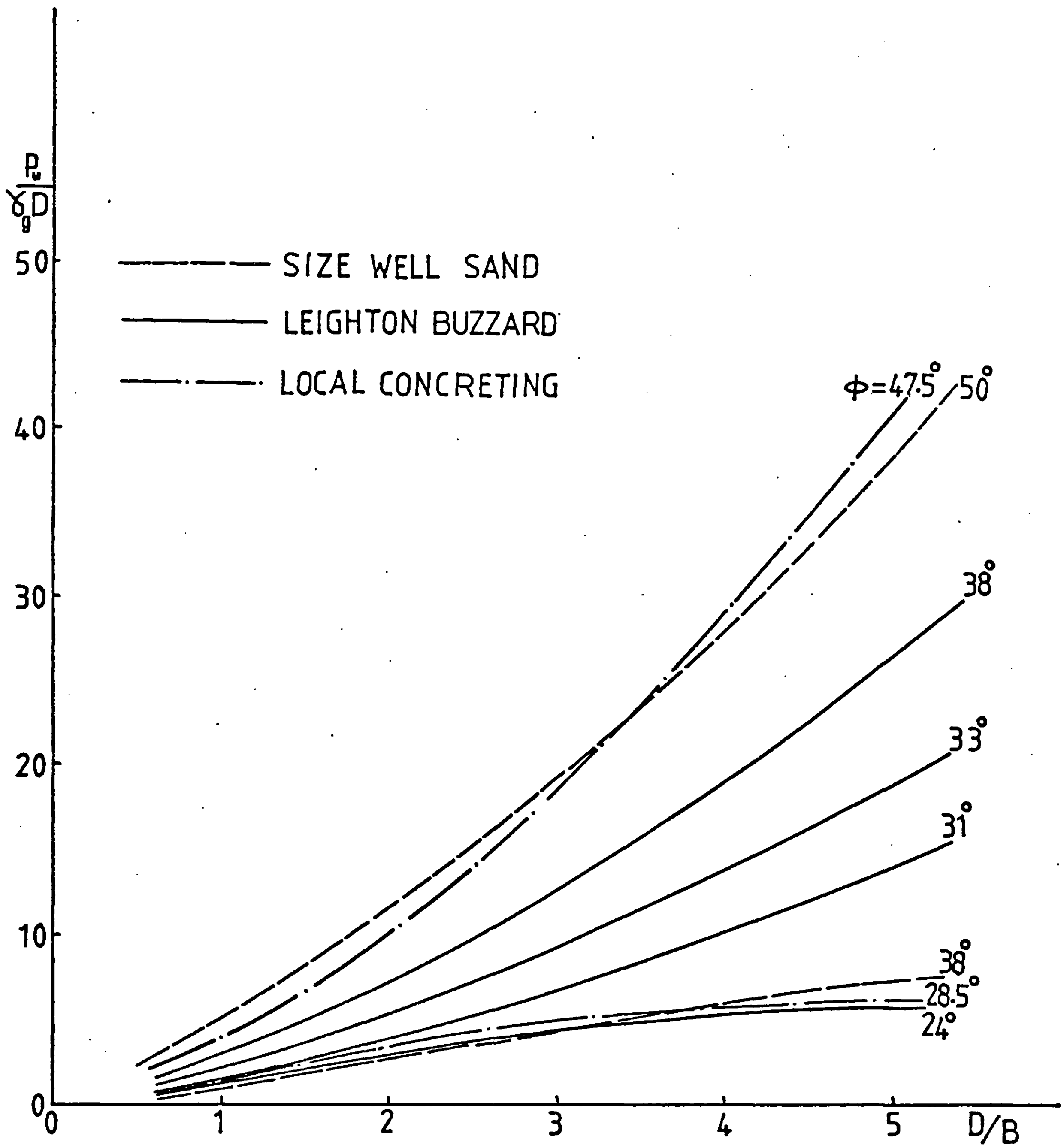

FIG.2.12. COMPARISON OF EL-RAYES EXPERIMENTAL RESULTS

(SHALLOW VERTICAL ANCHORS)

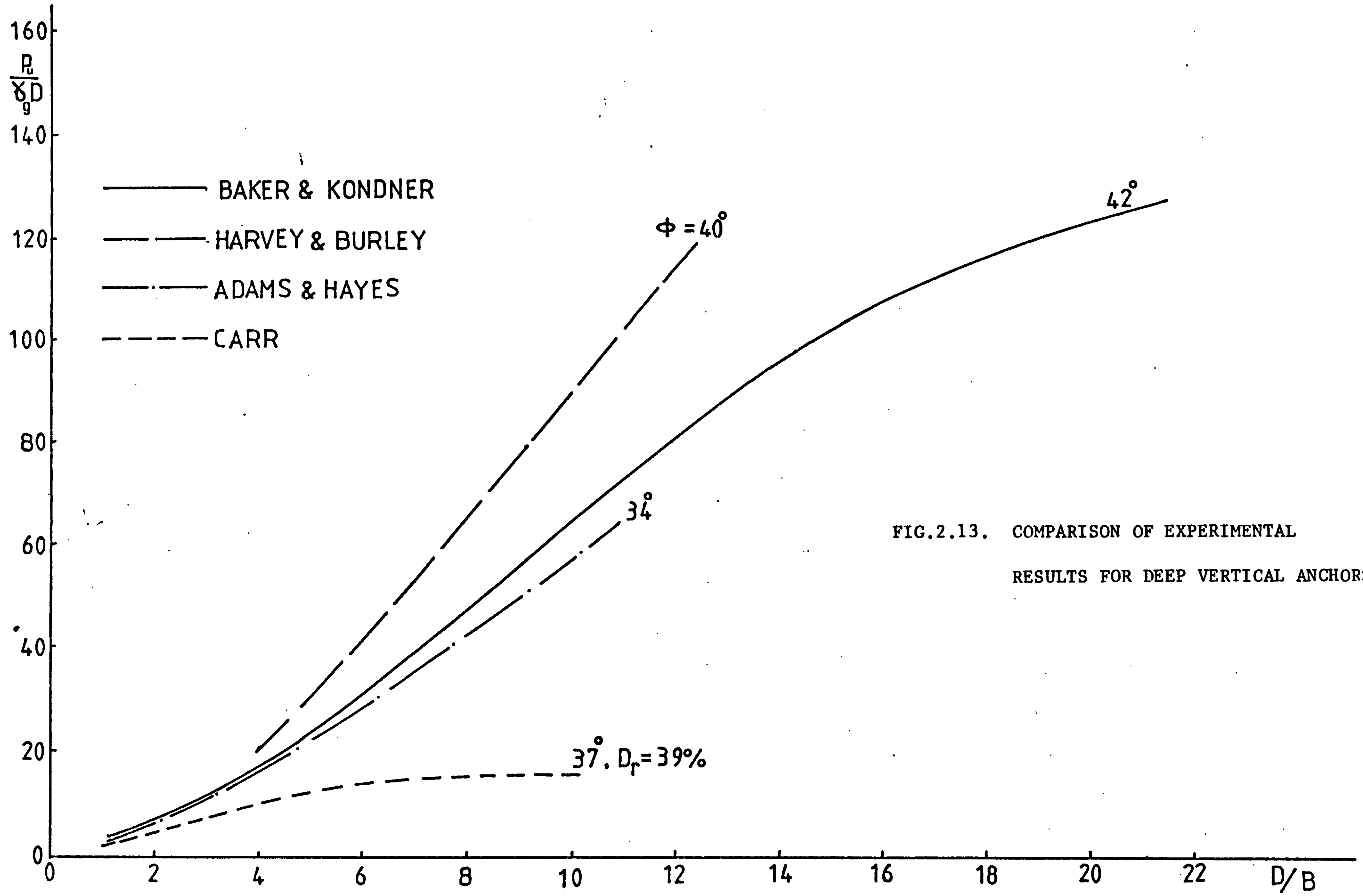

FIG.2.13. COMPARISON OF EXPERIMENTAL RESULTS FOR DEEP VERTICAL ANCHORS

CHAPTER 3

APPROXIMATE METHOD FOR DETERMINATION OF ULTIMATE UPLIFT RESISTANCE OF PLATE ANCHOR AND DIMENSIONAL ANALYSIS

CHAPTER 3

APPROXIMATE METHOD FOR DETERMINATION OF ULTIMATE UPLIFT RESISTANCE OF PLATE ANCHOR AND DIMENSIONAL ANALYSIS

3.1. INTRODUCTION:-

The theories and methods dealing with the uplift resistance of anchors have been reviewed in Chapter 2. It was shown that some theories contradict each other and that none of the theories is valid for all types of sand, at different densities and different inclinations of the anchor axis from the vertical direction. Extensive experimental work carried out by the author and reported in Chapters 4 and 5 has indicated the pertinent factors e.g. shape of failure surface and the influence of the angle of internal friction, density, relative density and compressibility of the sand. From a consideration of the simplified assumptions made, and of their importance, it was therefore decided to develop another method which attempts to take into account all the important parameters, some of which were not included in the previous methods.

A new approximate method was first developed for shallow vertical circular plate anchors, then extended to include deep vertical anchors. To take into account the inclination of the anchor from the vertical direction general equations for the inclined shallow and deep anchors are presented.

At the end of this chapter the method of dimensional analysis is applied in order to convert the parameters affecting the ultimate uplift resistance into non-dimensional products. By so doing model tests can be planned to give similarity between the models and the prototypes.

3.2. ASSUMPTIONS:-

In the proposed approximate method, the shape of failure surface has been simplified to allow easier application to inclined as well as vertical anchors, and several factors, not taken into account by other investigators, have been included. Since rigorous solutions of most of the problems in soil mechanics are very complicated the need for simplified procedures is necessary (Terzaghi, 1956).

As shown in Figs (3.1) and (3.4), the assumptions made in developing the approximate method are as follows:-

a/ The soil is homogeneous, isotropic and cohesionless.

b/ Full frictional resistance is developed along the failure surface.

c/ For a shallow anchor as shown in Fig (3.1) the failure surface near the ground surface is a truncated cone with an apex angle 2α. The type of the failure is taken as a general shear failure and the angle α is a function of the angle of internal friction and the relative density of the sand.

d/ For deep anchors as shown in Fig (3.4) the failure surface is limited at a distance below the ground surface (i.e. local shear failure) and the effect of the overlying soil is taken into consideration.

3.3. EVALUATION OF ULTIMATE UPLIFT RESISTANCE OF SHALLOW VERTICAL ANCHORS:-

3.3.1. GENERAL

For specified anchor dimensions the self weight of the anchor is known, so it could be added to the other two components (i.e.)

a/ The weight of the soil inside the failure wedge.

b/ The resultant shear resistance developed along the failure surface in the direction of loading i.e. the axis of the anchor.

3.3.2. SHAPE OF THE FAILURE SURFACE:-

The anchor consists of a circular plate pushed or pulled upwards vertically. The earth mass above the anchor is loaded and shear failure develops along the peripheries of the plate anchor in the above and outwards direction. From the experiments it was found that the meridian section is slightly curved. As indicated earlier this is approximated by a straight line as shown in Fig (3.1).

The components of the ultimate uplift resistance R are as follows

$$R_1 = G_o + V\gamma_g + T \tag{3.1}$$

where G_o = weight of the anchor body

V = volume of the truncated cone of failure

γ_g = unit weight of soil

T = vertical resultant shear force along the failure surface of the truncated cone.

3.3.3. SOIL WEIGHT:-

For the calculation of the soil weight inside the failure cone, the volume is found by revolving the straight sliding surface FG around the anchor axis EH as shown in Fig (3.2). Alternatively it could be found from the geometry of the figure as a difference between the volumes of the large cone MGI and the small cone MFJ.

$$V_1 = \int_o^{D\tan\alpha} \pi \left(\frac{B}{2} + x \right)^2 dh \tag{3.2}$$

where D is the depth of top surface of the plate anchor

B is the diameter of the anchor

and h is any depth from the surface of the soil

and $dh = \frac{dx}{\tan\alpha}$ where α is the inclination of the failure surface from the vertical direction.

Integrating and rearranging

$$V_1 = \frac{\pi D}{12} \left(4\, D^2 \tan^2\alpha + 6\, BD\tan\alpha + 3B^2\right) \qquad (3.3)$$

The weight of this volume of soil is W_1 and is given by

$$W_1 = \frac{\pi D \gamma g}{12} \left(4\, D^2 \tan^2\alpha + 6\, BD\tan\alpha + 3B^2\right) \qquad (3.4)$$

3.3.4. VERTICAL RESULTANT SHEARING RESISTANCE ALONG THE SLIDING SURFACE:-

From the previous literature Matsuo (1967) presented a relationship similar to Kotter's equation in a rectangular coordinate system, which describes the variation of the resultant shear stress on a rupture line or failure surface. This differential equation represents the plane stress condition for the failure surface within the soil mass which is assumed by Matsuo to be in a state of plastic equilibrium. Although the problem of uplift resistance of a circular plate anchor is an axisymmetric stress condition in three dimensions the assumed plane stress condition for the sliding surface was calculated on the three dimensional sliding surface. This is due to the absence of a method which can exactly represent the three dimensional stress condition. Matsuo (1967) presented the differential equation

$$\frac{\partial p}{\partial S} + 2p \tan\phi \frac{\partial \theta}{\partial S} = \gamma \sin\theta \qquad (3.5)$$

where p is the resultant shearing resistance acting on the sliding surface.

For the straight line FG in Fig (3.3), the term $\frac{\partial \theta}{\partial S}$ is equal to zero. Taking the component of the resultant shear force in the direction of loading p_1 i.e. in the vertical direction (Matsuo, 1967)

$$p_1 = \gamma g(y - D) \sin\alpha \qquad (3.6)$$

and y is given in Fig (3.3). See P. 79a.

The total vertical component of the resultant shearing resistance T_1 acting on the sliding surface which is formed by the revolution of line FG in Fig (3.3) around the axis of the anchor is obtained by the author by integrating over the whole failure surface

$$T_1 = \int_0^{D\tan\alpha} \int_0^{2\pi} p_1 \left(\frac{B}{2} + x \right) dS\, d\beta \qquad (3.7)$$

Taking $h = D - y = \dfrac{D\tan\alpha - x}{\tan\alpha}$ and $ds = \dfrac{dx}{\sin\alpha}$ and since T_1 is acting downwards

$$T_1 = 2\pi\sin\alpha \int_0^{D\tan\alpha} \left(\frac{B}{2} + x \right) \gamma g h \frac{dx}{\sin\alpha} \qquad (3.8)$$

integrating and rearranging

$$T_1 = \frac{\pi D^2 \gamma g}{6} \tan\alpha (3B + 2D\tan\alpha) \qquad (3.9)$$

The total vertical uplift resistance R_1 is found to be

$$R_1 = G_o + \frac{\pi D \gamma g}{12} (4D^2\tan^2\alpha + 6DB\tan\alpha + 3B^2) + \frac{\pi D^2 \gamma g}{6} \tan\alpha (3B + 2D\tan\alpha) \qquad (3.10)$$

3.4. ULTIMATE UPLIFT RESISTANCE OF DEEP VERTICAL ANCHORS:-

3.4.1. GENERAL:-

The method proposed for shallow anchors is based on the assumption of a general shear failure, where the failure surface extends from the anchor to the surface of the soil. This is proved to be true from the previous and present experimental work. It was also found that in the case of deep anchors local shear failure occurs where the failure surface does not extend to the surface of the soil.

In dealing with deep anchor as shown in Fig (3.4) the vertical resultant shear force develops along the failure surface and the weight of the soil inside the failure cone is calculated.

The additional forces taken into consideration will be the weight of the overburden soil directly over the truncated cone and the effect of the resistance of the soil around IN and GO in Fig (3.4).

3.4.2. SOIL WEIGHT INSIDE THE TRUNCATED CONE:-

As shown in Fig (3.4) the weight of the soil inside the truncated cone FGIJ can be found as in section 3.3.3 and was found to be

$$W_2 = \frac{\pi H \gamma g}{12} \left(4H^2 \tan^2\alpha + 6\ HB\ \tan\alpha + 3B^2\right) \qquad (3.11)$$

where H is the limiting height of the failed truncated cone and the critical ratio $\frac{H}{B}$ is a function of the soil properties ϕ and D_r.

3.4.3. WEIGHT OF OVERBURDEN SOIL:-

In addition to the soil weight inside the truncated cone the weight of soil above it is considered to affect the ultimate uplift resistance. As shown in Fig (3.4) the weight of the cylinder of diameter IG and height IN is calculated as

$$W_3 = \frac{\pi(D-H)\gamma g}{4} \left(B^2 + 4\ BH\ \tan\alpha + 4H^2 \tan^2\alpha \right) \qquad (3.12)$$

3.4.4. RESULTANT VERTICAL SHEARING RESISTANCE ACTING ALONG THE SLIDING SURFACE:-

Using the same procedure as in Section 3.3.4 the vertical resultant shearing resistance acting all over the surface area of the truncated cone is calculated (Fig. 3.4)

$$T_2 = \int_0^{H\tan\alpha} \int_0^{2\pi} \left(\frac{B}{2} + x\right)(D - H + h)\gamma g \tan\alpha \, d\beta \, \frac{dx}{\sin\alpha} \qquad (3.13)$$

Integrating and rearranging

$$T_2 = \frac{\pi H \gamma g}{6} \tan\alpha\left(3B(2D - H) + 2H(3D - 2H) \tan\alpha\right) \qquad (3.14)$$

3.4.5. RESISTANCE OF SOIL SURROUNDING THE CYLINDER (GONI):-

As shown in Fig (3.4) the effect of the soil above level IG is not just the weight of the soil inside the cylinder GONI, but also some resistance is offered by the surrounding soil as the failed soil inside the cone FGIJ pushes up. It is assumed that this resistance could be simulated by a partial shear friction around the cylinder GONI.

The horizontal pressure acting on the surface of the cylinder at depth Z is the earth pressure at rest $K_o \gamma_g Z$. K_o is the ratio between horizontal and vertical pressure. Its value depends on the type of soil, on the geological origin of the soil, and on the temporary loads which have acted on the surface of the soil (Terzaghi, 1956). It is assumed that the value of K_o is independent of the depth of the soil below the surface and is equal to the theoretical formula $(1 - \sin\phi)$ where ϕ is the angle of internal friction (i.e. Jaky's formula). The partial shear resistance can be obtained by multiplying the normal horizontal stress on the surface of the cylinder GONI by $\tan \bar{C}\phi$, where $\bar{C}$ is a parameter depending on ϕ and D_r. The normal horizontal force acting on the cylindrical surface area is calculated as

$$N = \int_0^{D-H} \int_0^{2\pi} \left(\frac{B + 2H\tan\alpha}{2}\right) K_o \gamma Z \, d\beta \, dz \qquad (3.15)$$

from which the vertical shear resistance T_3 acting on this cylindrical surface area is

$$T_3 = N \tan \bar{C}\phi = \frac{\pi K_o}{2} (D-H)^2 \gamma g \tan\bar{C}\phi \, (B + 2H\tan\alpha) \qquad (3.16)$$

The total ultimate uplift resistance R_2 for a deep vertical anchor is

R_2 = soil weight inside the truncated cone + weight of overburden soil + resultant shearing resistance along the failure surface of the truncated cone + resistance of the surrounding soil + anchor body weight.

$$\text{i.e. } R_2 = W_2 + W_3 + T_2 + T_3 + G_o \qquad (3.17)$$

$$\text{and } R_2 = \frac{\pi\gamma g}{12} \Big(4H^3\tan^2\alpha + 6H^2B\tan\alpha + 3B^2D + 12H\tan\alpha\,(D-H)(B+H\tan\alpha) + 2H\tan\alpha\,(3B(2D-H) + 2H(3D-2H)\tan\alpha) + 6K_o \tan\bar{C}\phi(B+2H\tan\alpha)(d - H)^2\Big) + G_o \qquad (3.18)$$

3.5. GENERALIZATION OF THE METHOD FOR INCLINED ANCHORS:-

3.5.1. GENERAL:-

The present investigation is also concerned with inclined anchors and the approximate method has been extended to cover this case.

Few investigators have dealt with shallow inclined anchors and this is the case with deep inclined anchors.

3.5.2. SHALLOW INCLINED ANCHORS:-

3.5.2.1. SOIL WEIGHT:-

Fig (3.5) shows a cross section along the centre line of the plane of inclination ψ to the vertical and also shows the assumed shape of the failure surface. From the geometry of Fig (3.5) the volume bounded by FGIJ is calculated. The weight of the soil is obtained and its component in the direction of loading i.e. the anchor axis is presented.

In Fig (3.5) to find the distances a_1 and a_2 can be found from the two triangles GHN and HIK.

$$\frac{\frac{B}{2} + L \tan\alpha}{\sin(\frac{\pi}{2} - (\psi+\alpha))} = \frac{a_1}{\sin(\frac{\pi}{2} + \alpha)} \qquad (3.19)$$

$$\frac{\frac{B}{2} + L \tan\alpha}{\sin(\frac{\pi}{2} - (\psi-\alpha))} = \frac{a_2}{\sin(\frac{\pi}{2} - \alpha)} \qquad (3.20)$$

where L is the perpendicular distance of the centre of the anchor face to the surface.

$$a_1 = \frac{B + 2\ L \tan\alpha}{2} \quad \frac{\cos\alpha}{\cos(\psi+\alpha)} \qquad (3.21)$$

$$a_2 = \frac{B + 2\ L \tan\alpha}{2} \quad \frac{\cos\alpha}{\cos(\psi-\alpha)} \qquad (3.22)$$

The shape of the failure created at the soil surface is an ellipse with the major axis $2a = a_1 + a_2$

$$\therefore\ 2a = \frac{B + 2\ L \tan\alpha}{2} \left(\frac{\cos\alpha \cos(\psi-\alpha) + \cos\alpha \cos(\psi+\alpha)}{\cos(\psi+\alpha) \cos(\psi-\alpha)} \right) \qquad (3.23)$$

and the minor axis

$$2b = B + 2\ L \tan\alpha \qquad (3.24)$$

The shape of any cross section parallel to FJ in Fig (3.5) will be a circle with its centre on the axis . The height of the cone MGI is

$$MO = (L + \frac{B}{2\ \tan\alpha})\cos\ \psi \tag{3.25}$$

and the height of the cone MFJ is

$$MP = \frac{B\ \cos\psi}{2\ \tan\alpha} \tag{3.26}$$

The volume of the truncated cone FGIJ = volume of cone MGI - volume cone MFJ = V_2 where

$$V_2 = \frac{\pi}{24}((B + 2L\tan\alpha)^2(\cos\alpha\frac{(\cos(\psi-\alpha)+\cos(\psi+\alpha))}{\cos(\psi-\alpha)\cos(\psi+\alpha)})(L+\frac{B}{2\tan\alpha})\cos\psi - \frac{B^3}{\tan\alpha}) \tag{3.27}$$

The component of the soil weight in the direction of loading is W_4 where

$$W_4 = \frac{\pi\gamma g\cos\psi}{24}((B+2D\frac{\tan\alpha}{\cos\psi})^2(\cos\alpha\frac{(\cos(\psi-\alpha)+\cos(\psi+\alpha))}{\cos(\psi-\alpha)\cos(\psi+\alpha)})(D + \frac{B\cos\psi}{2\tan\alpha}) - \frac{B^3}{\tan\alpha}) \tag{3.28}$$

3.5.2.2. RESULTANT SHEAR RESISTANCE IN THE DIRECTION OF LOADING:-

As can be seen in Fig (3.6) the inclination of the anchor produces unsymmetrical distributions of the resultant shear stress on the failure surfaces (IJO, FPG). To simplify the calculations an equivalent stress distribution symmetrical to the axis of the anchor is assumed, namely KJQ and NFM. Then the resultant shearing force on an infinitesimal element is integrated along the assumed symmetrical shape FNKJ in the direction of the anchor axis to obtain T_4 where

$$T_4 = \int_0^{L\tan\alpha}\int_0^{2\pi}(\frac{B}{2} + x)\gamma\ \ell\ \tan\alpha\ \cos\psi\ d\beta\ \frac{dx}{\sin\alpha} \tag{3.29}$$

where ℓ is any distance from point H to E and is equal to

$\frac{L\tan\alpha - x}{\tan\alpha}$ at a corresponding point x. Substituting and integrating

$$T_4 = \frac{\pi D^2\gamma g}{6\cos^2\psi}\tan\alpha(3B\cos\psi + 2D\tan\alpha) \tag{3.30}$$

The total ultimate uplift resistance R_3 in the direction of the anchor axis is equal to the soil weight, the resultant shear resistance and the anchor body weight, all in the direction of anchor axis.

$$R_3 = W_4 + T_4 + G_o\cos\psi \tag{3.31}$$

$$R_3 = \frac{\pi\gamma g}{24\cos^2\psi} \left(\cos^3\psi\left(\left(B+2D\frac{\tan\alpha}{\cos\psi}\right)^2\left(\cos\alpha\frac{\cos(\psi-\alpha)+\cos(\psi+\alpha)}{\cos(\psi-\alpha)\cos(\psi+\alpha)}\right)\left(D+\frac{B\cos\psi}{2\tan\alpha}\right) - \frac{B^3}{\tan\alpha}\right) + 4D^2\tan\alpha\,(3B\cos\psi + 2D\tan\alpha)\right) + G_o\cos\psi \qquad (3.32)$$

3.5.3. DEEP INCLINED ANCHORS:-

3.5.3.1 SOIL WEIGHT:-

From Fig (3.7) the weight of the soil inside the failed truncated cone FGIJ in the direction of the anchor axis is found as described in section 3.5.2.1.

$$W_5 = \frac{\pi\gamma g\cos\psi}{24} \left(\left(B+2H\frac{\tan\alpha}{\cos\psi}\right)^2\left(\cos\alpha\frac{\cos(\psi-\alpha)+\cos(\psi+\alpha)}{\cos(\psi-\alpha)\cos(\psi+\alpha)}\right)\left(H+\frac{B\cos\psi}{2\tan\alpha}\right) - \frac{B^3}{\tan\alpha}\right) \qquad (3.33)$$

3.5.3.2. WEIGHT OF OVERBURDEN SOIL:-

From Fig (3.7) the volume of the soil inside the elliptical prism GINO can be obtained. The weight of the soil in the anchor axis direction is then found to be W_6 where

$$W_6 = \pi\gamma gab\,(D-H)\cos\psi \qquad (3.34)$$

$$\therefore W_6 = \frac{\pi\gamma g}{8}\left(B+2H\frac{\tan\alpha}{\cos\psi}\right)^2\left(\cos\alpha\frac{(\cos(\psi-\alpha)+\cos(\psi+\alpha))}{\cos(\psi-\alpha)\cos(\psi+\alpha)}\right)(D-H)\cos\psi \qquad (3.35)$$

3.5.3.3. RESULTANT SHEAR RESISTANCE ALONG THE SLIDING SURFACE:-

From Fig (3.8) the distribution of the resultant shearing stress will take the form of the trapezoids FGTP and IJOU. For simplicity an equivalent symmetrical distribution is assumed i.e. FNRM and KJQS.

$$T_5 = \int_0^{L\tan\alpha}\int_0^{2\pi}\left(\frac{B}{2}+x\right)(D-H+l\cos\psi)\gamma g\tan\alpha\,d\beta\,\frac{dx}{\sin\alpha} \qquad (3.36)$$

Integrating and rearranging the terms

$$T_5 = \frac{\pi H\gamma g}{6\cos^2\psi}\tan\alpha\,(B\cos\psi(6D-3H) + H\tan\alpha\,(6D-4H)) \qquad (3.37)$$

3.5.3.4. RESISTANCE OF SOIL SURROUNDING THE ELLIPTICAL PRISM (GIVW):-

From Fig (3.8) and using the same method as in section 3.4.5, the normal horizontal load on the elliptical prism (GIVW) can be obtained. Then the effect of the surrounding soil as a partial shear resistance can be calculated.

To find the surface area of the elliptical prism, the circumference of the ellipse with semiaxes a and b is

$$C_1 = \pi (a+b)\left(1 + \frac{m^2}{4} + \frac{m^4}{64} + \frac{m^6}{256} + \cdots \right) \quad (3.38)$$

where $m = \frac{a-b}{a+b}$ or

$$C_{1_{approx.}} = \pi\left(1.5(a + b) - \sqrt{ab}\right) \quad (3.39)$$

The vertical partial shear resistance created by the surrounding soil is evaluated as

$$T_6 = \frac{\gamma g K_o}{2} \tan \bar{C}\phi (D-H)^2 \left(\pi\left(1.5 \left(\frac{B+2L\tan\alpha}{2}\right)\left(1+\cos\alpha\left(\frac{\cos(\psi-\alpha)+\cos(\psi+\alpha)}{2\cos(\psi-\alpha)\cos(\psi+\alpha)}\right)\right)\right.\right.$$
$$\left.\left. -\sqrt{\left(\frac{B+2L\tan\alpha}{2}\right)^2 \cos\alpha \frac{(\cos(\psi-\alpha)+\cos(\psi+\alpha))}{2\cos(\psi-\alpha)\cos(\psi+\alpha)}}\right)\right) \quad (3.40)$$

The component of the resistance of the surrounding soil in the direction of the anchor axis

$$T_7 = \frac{\pi\gamma g K_o}{2} \tan \bar{C}\phi\ (D-H)^2 \left((B\cos\psi + 2H\tan\alpha) \left(3 + \frac{3}{2} \cos\alpha\frac{(\cos(\psi-\alpha)+\cos(\psi+\alpha))}{\cos(\psi-\alpha)\cos(\psi+\alpha)}\right.\right.$$
$$\left.\left. -2 \sqrt{\cos\alpha\frac{(\cos(\psi-\alpha)+ \cos(\psi+\alpha))}{2\cos(\psi-\alpha)\cos(\psi+\alpha)}}\right)\right) \quad (3.41)$$

The total ultimate uplift resistance of the deep inclined anchor is R_4 where

$$R_4 = W_5 + W_6 + T_5 + T_7 + G_o \cos\psi \quad (3.42)$$

$$R_4 = \frac{\pi\gamma g\cos\psi}{24} \left(\left(B+2H\frac{\tan\alpha}{\cos\psi}\right)^2\left(\cos\alpha\frac{(\cos(\psi-\alpha)+\cos(\psi+\alpha))}{\cos(\psi-\alpha)\cos(\psi+\alpha)}\right) \left(H + \frac{B\cos\psi}{2\tan\alpha}\right) - \frac{B^3}{\tan\alpha}\right)$$

$$+ \frac{\pi\gamma g}{8} \left(B+2H \frac{\tan\alpha}{\cos\psi} \right)^2 \cos\alpha\frac{(\cos(\psi-\alpha)+\cos(\psi+\alpha))}{\cos(\psi-\alpha)\cos(\psi+\alpha)} (D - H) \cos\psi$$

$$+ \frac{\pi H \gamma g}{6\cos^2\psi} \tan\alpha \quad (B \cos\psi \; (6D-3H) + H \tan\alpha \quad (6D-4H))$$

$$+ \frac{\pi\gamma g}{2} K_o \tan \bar{C}\phi \; (D-H)^2 \quad ((B \cos\psi + 2H \tan\alpha) \left(3 + \frac{3}{2} \cos\alpha \frac{(\cos(\psi-\alpha)+\cos(\psi+\alpha))}{\cos(\psi-\alpha)\cos(\psi+\alpha)} \right.$$

$$\left. -2 \sqrt{\cos\alpha \frac{(\cos(\psi-\alpha) + \cos(\psi+\alpha))}{2\cos(\psi-\alpha)\cos(\psi+\alpha)}} \right)) + \quad G_o \cos\psi \qquad (3.43)$$

3.6. SUMMARY OF THE EQUATIONS:-

The following equations for predicting the ultimate uplift resistance are applicable to circular plate anchor embedded in cohesionless soils according to the assumptions stated earlier.

a/ Shallow vertical anchor

$$R_1 = \frac{\pi D \gamma g}{12} \left((4D^2 \tan^2\alpha + 6DB\tan\alpha + 3B^2) \quad + 2D\tan\alpha(3B+2D\tan\alpha) \right) + G_o$$

b/ Deep vertical anchor

$$R_2 = \frac{\pi\gamma g}{12} \quad (4H^3\tan^2\alpha + 6H^2B\tan\alpha + 3B^2D + 12 \; H \tan\alpha \; (D-H)(B+H\tan\alpha)$$

$$+ 2 \; H \tan\alpha \; (3B(2D - H) + 2H \; (3D - 2H) \; \tan\alpha)$$

$$+ 6K_o \tan \bar{C}\phi \quad (B + 2H \tan\alpha) \; (D - H)^2) \qquad + G_o$$

c/ Shallow inclined anchor

$$\text{Taking } Q = \cos\alpha \quad \frac{\cos(\psi-\alpha) + \cos(\psi+\alpha)}{\cos(\psi-\alpha)\cos(\psi+\alpha)}$$

$$R_3 = \frac{\pi\gamma g}{24\cos^2\psi} \quad \left(\cos^3\psi \; \left((B+2D \frac{\tan\alpha}{\cos\psi}\right)^2 \quad Q \quad \left(D + \frac{B\cos\psi}{2\tan\alpha} \right) - \frac{B^3}{\tan\alpha}\right) + 4D^2\tan\alpha$$

$$(3B\cos\Psi+2D\tan\alpha)) + G_o\cos\Psi$$

d/ Deep inclined anchor

$$R_4 = \frac{\pi\gamma g}{24} \; \left(\cos\psi \; \left((B+2H \frac{\tan\alpha}{\cos\psi} \right)^2 Q \; \left(H+ \frac{B\cos\psi}{2\tan\alpha}\right)- \frac{B^3}{\tan\alpha}\right) + 3\left(B+2H\frac{\tan\alpha}{\cos\psi}\right)^2 Q(D-H)\cos\psi$$

$$+ \frac{4H\tan\alpha}{\cos^2\psi} \; (B\cos\psi(6D-3H)+H\tan\alpha(6D-4H)) + 12K_o \tan \bar{C}\phi(D-H)^2(\; (B\cos\psi+ 2H\tan\alpha)$$

$$(3 + \frac{3Q}{2} - \sqrt{2Q}) \;) + G_o\cos\psi$$

The equations were first evaluated for the vertical anchors then generalized to the inclined case. The equations of the general inclined anchors can be reduced to obtain the equations for the vertical case when the angle of inclination ψ is zero.

3.7. DIMENSIONAL ANALYSIS:-

3.7.1. INTRODUCTION:-

One of the methods used in establishing similitude between model and prototype, apart from the laws of structural theory, is dimensional analysis. It is used when the mathematical laws are not known but the factors affecting the phenomena are. It is also used to investigate the nature of the solution of physical problems and greatly reduces the number of the functionally related quantities to less than the number of physical quantities. This method is of great help as a basis for planning and organizing experiments and to obtain the maximum useful information from them. Finally it can help to give a partial solution for complex problems (Jasiewicz, 1963).

Geometric and dynamic similarity between prototype and model is essential in order to apply the results of the model to the prototype. Where there is dissimilarity the effects of the factors causing it must be estimated.

The π theorem presented by Buckingham (1914) forms the basis of dimensional analysis. The theorem states that a physical phenomenon which is a function of n physical quantities involving m fundamental units can be described in the functional form (Baker & Kondner, 1966)

$$f(\pi_1, \pi_2, \pi_3, \ldots \pi_{n-m}) = o \qquad (3.44)$$

where the π terms are the (n-m) independent non-dimensional products of the n physical quantities.

3.7.2. FACTORS AFFECTING THE UPLIFT RESISTANCE:-

In the present investigation dimensional analysis was carried out to examine the uplift resistance problem with respect to the soil properties and anchor dimensions.

3.7.2.1. SOIL PARAMETERS:-

The basic parameters involved in the problem are the soil particle size distribution, shape, specific gravity and hardness of the soil particles. Other parameters which describe the behaviour of the soil are the bulk density of the soil γ, angle of internal friction ϕ and relative density D_r. Additional secondary parameters are compressibility and permeability.

Since only cohesionless soil will be used in this investigation the most pertinent parameters will be taken. Since the weight of the soil above the anchor is part of the uplift resistance the bulk density is considered. Parameters affecting the limiting material strength are important, so the angle of internal friction and the relative density are taken. The permeability will be neglected since sand will be used in the laboratory model tests.

The anchor material is rigid enough to undergo negligible deformation compared to that of the soil during the tests. The weight of the anchor footing in both model and prototype is known so it is omitted from the dimensional analysis.

3.7.2.2. PHYSICAL DIMENSIONS AND ORIENTATION OF THE ANCHOR:-

The most important parameters are the diameter of the anchor plate B, and the initial depth of embedment D, so both are included in the analysis. The width of the container in the model tests is large enough compared to the plate anchor diameter to result in negligible or zero boundary effects, accordingly it is neglected. The effects of the anchor plate thickness and the anchor shaft are small so both are neglected. Part of the tests carried out were inclined from the vertical direction, so the angle of inclination ψ will be considered.

3.7.3. APPLICATION OF DIMENSIONAL ANALYSIS TO ANCHOR PROBLEM:-

For the uplift resistance problem the primary physical quantities influencing the ultimate uplift resistance R are shown below. The fundamental units chosen are the force, length and time.

$$R = f_1\,(\gamma_g,\ D,\ B,\ \phi,\ D_r,\ \psi) \qquad (3.45)$$

Utilizing Buckingham π method the physical quantities yield the functional relationship

$$\frac{R}{\frac{\pi}{4}B^2D\gamma_g} = f_2\,\left(\frac{D}{B},\ \phi,\ D_r,\ \psi\right) \qquad (3.46)$$

Using algebraic transformations the following alternative independent π terms can be obtained (Baker & Kondner, 1966)

$$\frac{R}{DB^2\gamma g} = f_3\,\left(\frac{D^2}{B^2},\ \phi,\ D_r,\ \psi\right) \qquad (3.47)$$

$$\frac{R}{B^3\gamma g} = f_4\,\left(\frac{D}{B},\ \phi,\ D_r,\ \psi\right) \qquad (3.48)$$

The conclusions which can be drawn from (e.g. equation 3.46) are that for a given circular anchor plate embedded in cohesionless soil with known ϕ, D_r, ψ:-

a/ $\frac{R}{\frac{\pi}{4}B^2D\gamma g}$ depends only on $\frac{D}{B}$

b/ For a given ratio of $\frac{D}{B}$, $\frac{R}{\frac{\pi}{4}B^2D\gamma g}$ is constant and the value determined in a model test is applicable to the prototype problem.

c/ For a constant angle of inclination ψ, $\frac{R}{\frac{\pi}{4}B^2D\gamma g}$ plotted against $\frac{D}{B}$, the complete solution is a family of curves each corresponding to particular ϕ and D_r values.

From the information provided by the dimensional analysis the transformation of the ultimate uplift resistance equations (3.10, 3.18, 3.32, 3.43) to non-dimensional products is possible and will be presented in chapter 7. This method will help in the planning of the laboratory model tests. In the following section the reason for performing these tests will be stated.

3.8. NECESSITY FOR MODEL TESTS:-

3.8.1. JUSTIFICATION OF MODEL TESTS:-

Due to the complex nature of the behaviour of soil experimental analysis is important. It is used either to examine the validity of the assumptions of a theoretical solution or to provide experimentally the answers to problems to which no satisfactory theoretical solution exists.

Full scale or field tests are the most representative of the actual conditions in the field due to the existence of all the variable parameters. Full scale tests are costly and time consuming, so the laboratory model tests are justified for use in experimental soil mechanics.

3.8.2. CLASSIFICATION OF THE PHYSICAL MODEL TESTS:-

According to the purpose of model tests, scale models used in soil mechanics can be classified into three types (Roscoe, 1968; James, 1970).

a/ Type 1

To examine, on a small scale, the intrinsic assumptions and factors on which the proposed theoretical solution of the prototype is based. Another objective is to confirm that soil properties established from fundamental testing apparatus, relevant to the stress condition in the model, can be used to predict the performance of the model (James, 1970).

b/ Type 2

To predict directly the behaviour, under conditions of similarity, of a specific full scale prototype structure. For similarity, all the physical quantities that are relevant to the problem should be defined. Although knowledge of the mechanical behaviour of the prototype material is of great importance for establishing conditions of similarity, especially when a different material is used in the model, there is still some uncertainty regarding the fundamental stress-strain laws of soils.

c/ Type 3

To serve theoretical purposes when it is desired to study in detail the behaviour of a soil mass under various specified boundary stresses or strains. It is not necessary to conform with any possible prototype problem. This would lead to improvement in new methods of analysis which in turn would lead eventually to better design rules for complicated boundary value problems or soil-structure interaction problems.

3.9. SUMMARY:-

In this chapter the necessity for a new method of calculating the uplift resistance of circular plate anchors embedded in cohesionless soils is demonstrated. A new method and a statement of the assumptions involved and an evaluation of the ultimate loads for different conditions is then presented. Dimensional analysis is used to convert the physical quantities involved in the uplift resistance problem to non-dimensional products for similarity and comparison purposes.

The present model tests intended fall into the second type of model tests (section 3.8.2). Few attempts have been directed towards the study of the condition of similitude for soil mechanics models of the second type (Rocha, 1957; Sutherland, 1965; Roscoe, 1968).

Following from the above information a program of laboratory experiments based on model testing is intended. Cohesionless soils will be used. The properties of the soil and its behaviour during deposition will be discussed in chapter 4 for the preparation of the laboratory model tests.

It should be noted in Matsuo's work that α is a function of ϕ (i.e. $\alpha = \frac{\pi}{4} + \frac{\phi}{2}$). In the present work α is a function of both ϕ and the relative density and the value of α is given by equation 7.4.

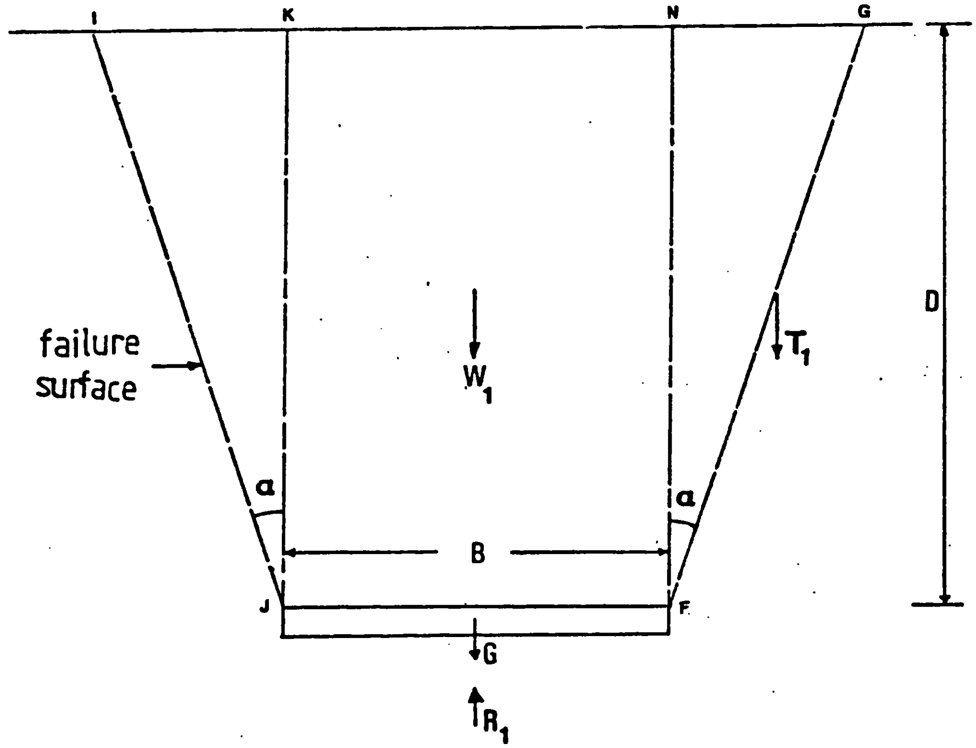

FIG.3.1. FAILURE SURFACE OF VERTICAL SHALLOW ANCHOR

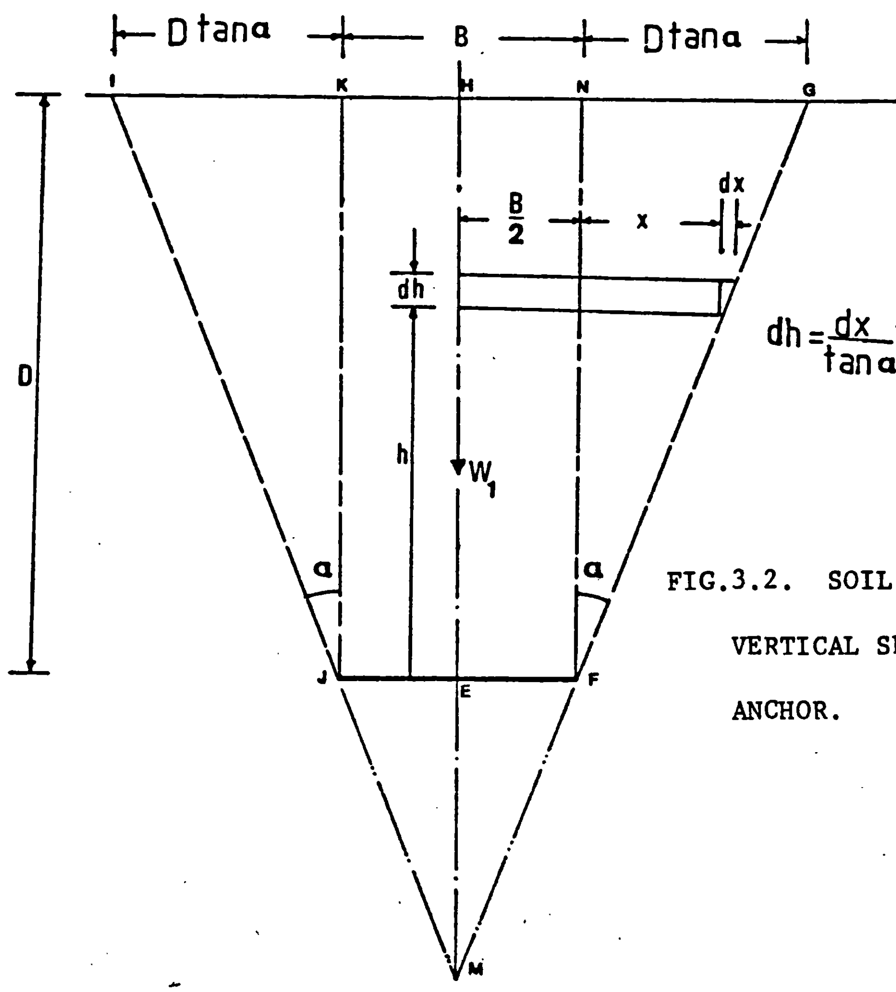

FIG.3.2. SOIL WEIGHT OF VERTICAL SHALLOW ANCHOR.

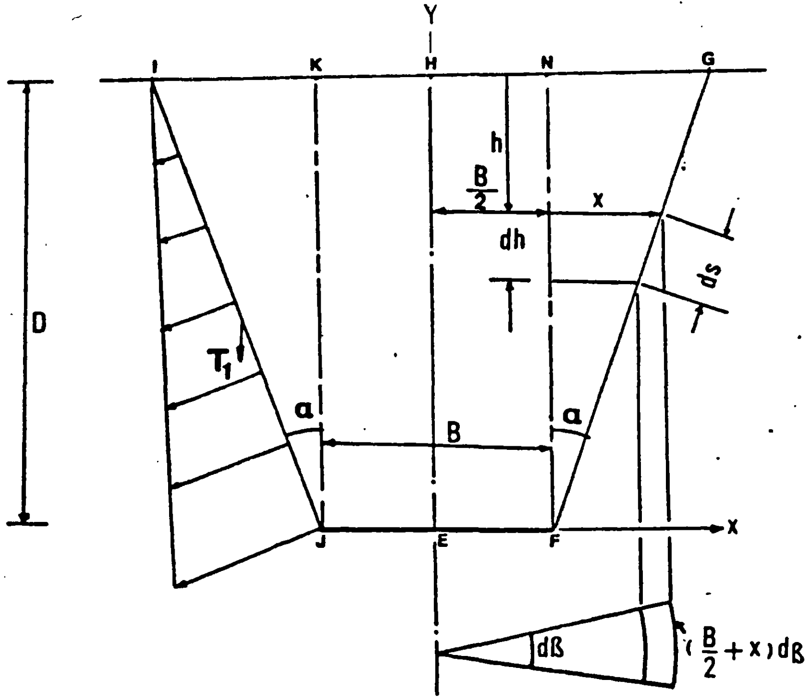

FIG.3.3 DISTRIBUTION OF VERTICAL RESULTANT SHEAR RESISTANCE (VERTICAL SHALLOW ANCHOR)

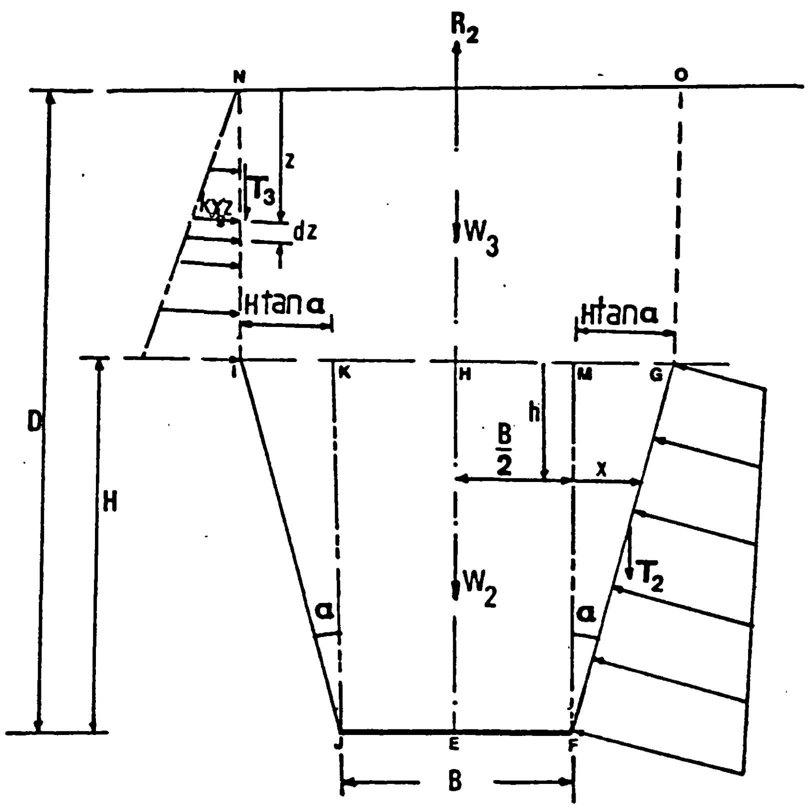

FIG.3.4 DISTRIBUTION OF FORCES FOR VERTICAL DEEP ANCHOR

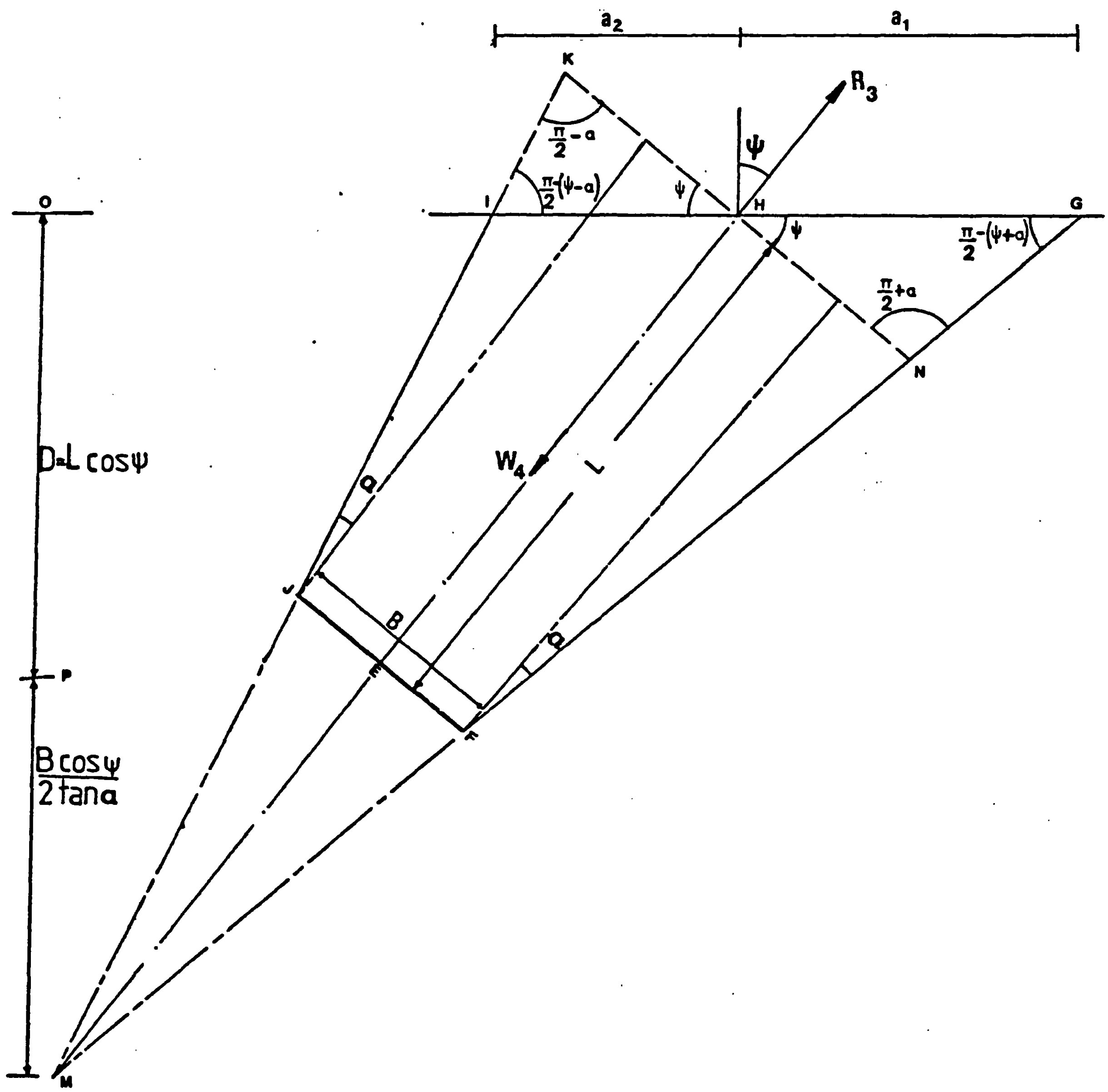

FIG.3.5 SOIL WEIGHT OF INCLINED SHALLOW ANCHOR

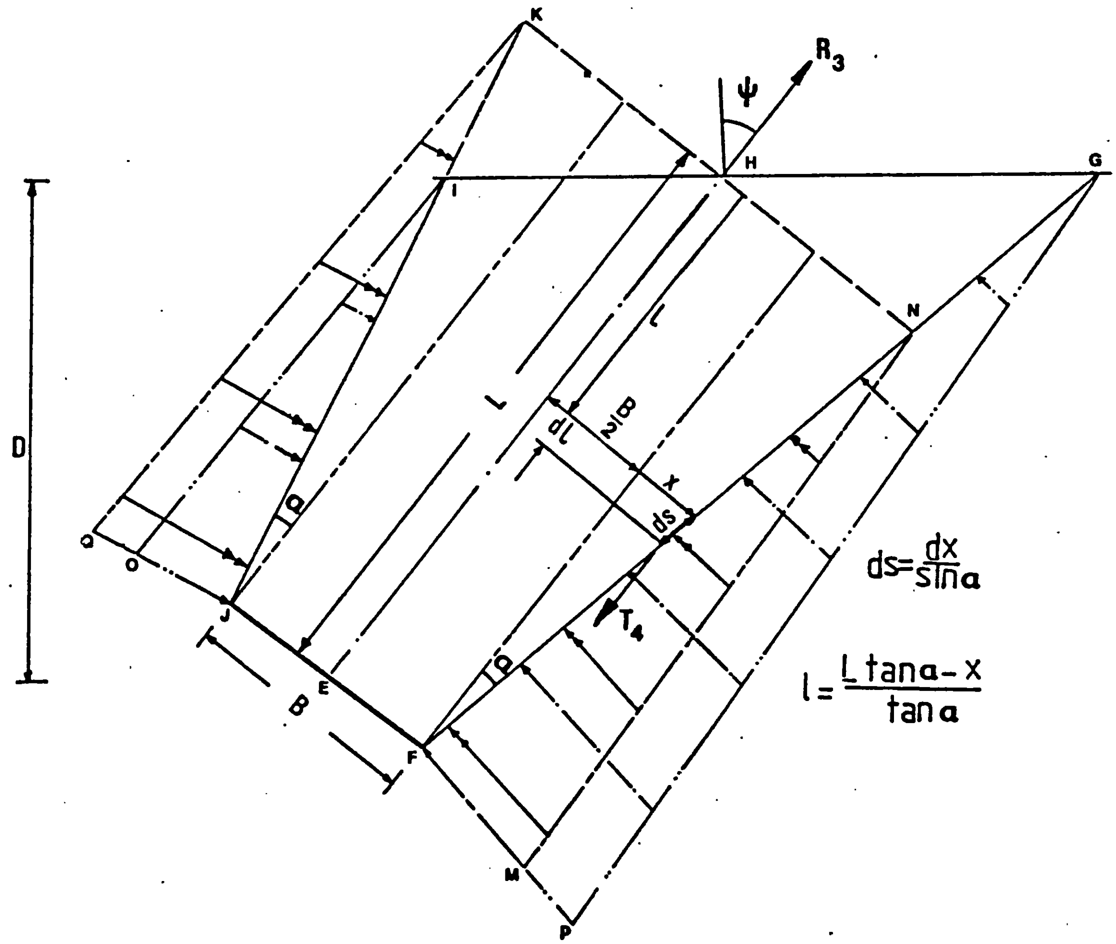

FIG.3.6 DISTRIBUTION OF RESULTANT SHEAR RESISTANCE IN THE DIRECTION OF LOADING (INCLINED SHALLOW ANCHOR)

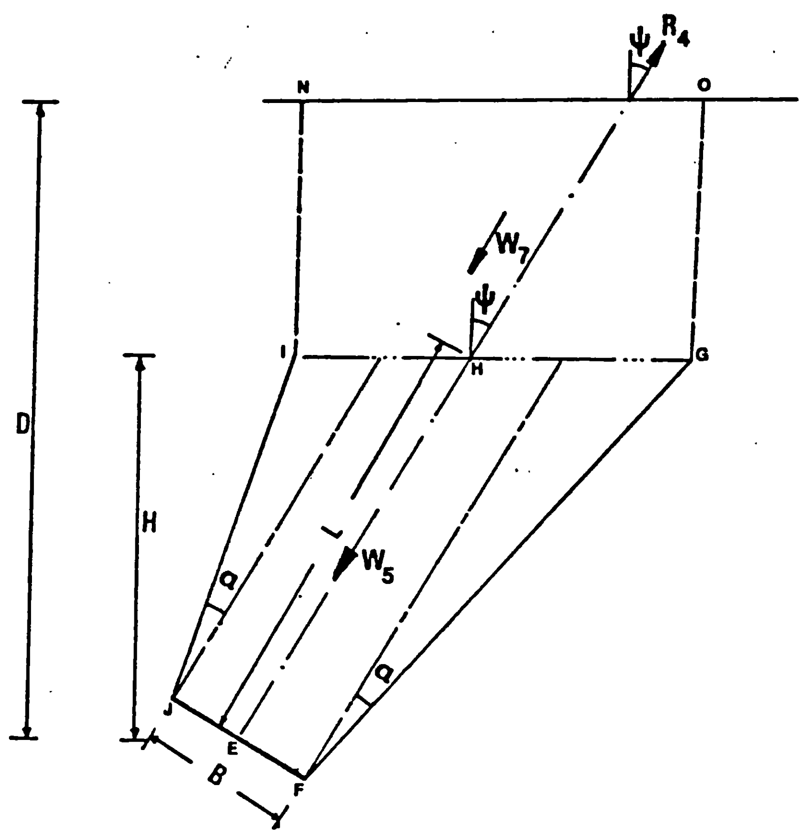

FIG.3.7 SOIL WEIGHT OF INCLINED DEEP ANCHORS

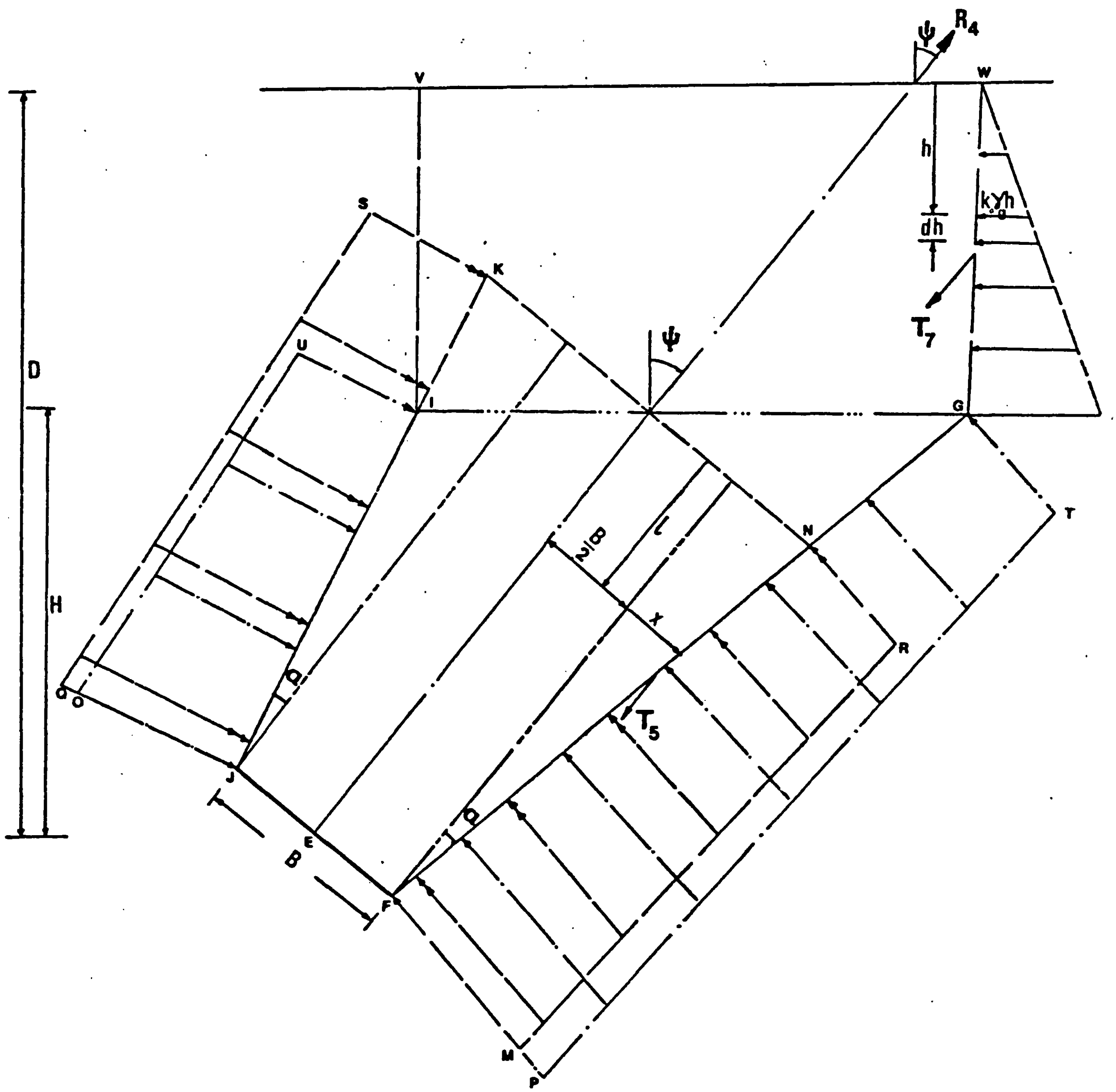

FIG.3.8 DISTRIBUTION OF RESULTANT SHEAR RESISTANCE IN THE DIRECTION OF LOADING (INCLINED DEEP ANCHOR)

CHAPTER 4

PROPERTIES OF THE SAND USED AND ITS BEHAVIOUR DURING DEPOSITION

CHAPTER 4

PROPERTIES OF THE SAND USED AND ITS BEHAVIOUR DURING DEPOSITION

4.1. INTRODUCTION:-

In this chapter, the type of sand chosen for the laboratory model testing is described.

Creation of uniform beds of sand for model tests is very important. In order to achieve this uniformity, the factors controlling the porosity of the sand are discussed. The existing methods of deposition of sand are compared and suitable methods for the present investigation are chosen. The shortcomings of the existing methods are also discussed and the ways of reducing or eliminating them reported.

The apparatus used by the author for depositing the sand along with other equipment used and their calibration are reported in Chapter 5.

4.2. TYPE OF SOIL USED AND ITS PROPERTIES:-

For the laboratory model tests it was decided to use Leighton Buzzard sand. This type of sand was chosen because it is widely used in many research laboratories as a standard sand and so affords a basis of comparison between work in different laboratories.

4.2.1. PHYSICAL PROPERTIES:-

4.2.1.1. PARTICLE SIZE DISTRIBUTION:-

Using the standard method by wet sieving (B.S.1377), the sand used had a particle size range of 2.0-0.2 mm (B.S.S. 10-170). The particle size distribution is shown in Fig (4.1). The grading curve shows a uniform sand containing medium to coarse sand with a very small proportion of fine sand. The particle shape is subrounded, the uniformity coefficient $C_u = 1.75$ and the mean diameter $D_{50} = 0.75$ mm.

4.2.1.2. SPECIFIC GRAVITY:-

Following the test method for fine grained soil described in B.S.1377 the specific gravity was determined and found to be 2.65. The mineral composition of the sand is mainly quartzite.

4.2.1.3. POROSITY LIMITS:-

The maximum and minimum densities were determined using the methods suggested by Kolbuszewski (1948a). In the loosest sand condition the maximum porosity $n_{max} = 44.06\%$ and in the densest state $n_{min} = 32.74\%$. Close agreement was found between the results obtained and those reported by El-Rayes (1965).

4.2.2. MECHANICAL PROPERTIES:-

The shear strength of the sand was measured using 100 mm diameter, 200 mm high triaxial samples, tested in dry and saturated conditions. The tests were performed at different densities and the confining pressure ranged from 11-56 KN/m^2 which is relevant to the expected minor principal stress range in the model tests when loaded to failure.

Fig (4.2) shows the variation of the internal angle of friction with initial porosity obtained by the author by plotting a regression line through the experimental points.

4.3. DEPOSITION OF UNIFORM BEDS OF SAND:-

It is important in a series of model tests that the sand beds used are uniform and isotropic, since all theoretical work is based on idealised conditions. The sand beds should be reproducible and the method of deposition should not induce any lateral stress that gives rise to a coefficient of earth pressure at rest, K_o, that is higher than the coefficient for an undisturbed, unconsolidated sand bed.

Here it is intended to present a brief review of the common practice pursued to evaluate the uniformity of the sand mass, the factors controlling the porosity of deposited sands and previous methods used to form uniform sand beds in model studies. It is followed by a description of the method chosen to deposit a uniform sand mass for the current investigation.

4.3.1. POROSITY LIMITS AND MEASUREMENT OF UNIFORMITY OF DEPOSITED SAND BEDS:-

The uniformity of a particulate mass is commonly tested by measuring the porosity, or alternatively the density, at different locations within the mass.

As an example, consider the simple case of particles of equal spheres. There are six possible types of regular packings for the particulate medium formed of monosize spheres (Granton and Fraser, 1935). For each type the porosity at any part of the mass is equal to the overall porosity, and is independent of the diameter of the forming spheres. The maximum and minimum theoretical porosities among such arrangements are 47.64% and 25.95%.

If the discrete medium of monosize spheres is formed by a random process, then there will be variations in the local porosity values throughout the mass from the overall porosity value and the mass is said to be of non-uniform formation. One of the reasons for such variations is arching which may cause the protection of some openings within the mass leaving them unfilled. Sometimes the protected gaps may be larger than a whole sphere leading to a local porosity value even higher than the maximum theoretical one for regular packings (47.64%).

In a sand mass the particles are of different shape and size.

Yet similar to the ideal case of monosize spheres, there are two limiting overall porosities (minimum and maximum) for every type of sand (Kolbuszewski, 1961, 1963). The limiting porosities depend mainly on the shape, surface roughness and size distribution of the particles (Kolbuszewski, 1948a, 1948b).

The porosity values at different positions in the sand mass and their variation can be used as a measure of uniformity of the mass (Kolbuszewski, 1961). This uniformity of porosity in the sand mass depends on the method of deposition.

Due to the great influence of the shape, size, distribution and surface roughness on the value of porosity, the porosity alone does not indicate the state of packing. The maximum porosity of some sands can be even lower than the minimum porosity of some others (Alyanak, 1961).

The state of packing is best described, in terms of the maximum and minimum porosities which the sand can attain, by the relative porosity or alternatively by the relative density.

However the relative porosity does not describe the internal geometry of the packing.

The most common method of measuring the porosity of the sand at different parts of a model container (Butterfield and Andrawes, 1968) are

1/ Density pots:-

This is the most frequently used and is suitable for sand beds formed in large tanks. Cylindrical pots of known volume are placed at the desired points and their weight before and after deposition is measured. To prevent bouncing of the particles on the top edge, the pot should have a knife edge top. The diameter of each pot should not be less than 76 mm (3 in) since smaller diameter pots tend to give a higher porosity (Kolbuszewski, 1948a).

2/ Suction Method:-

A thin metal walled cylinder is driven into the sand to a certain depth. The sand in the cylinder is sucked up through a nozzle, collected and weighed. Knowing the corresponding volume, the porosity can be calculated (Ovesen, 1962).

3/ Penetration Method:-

The penetration resistance of a cylindrical rod inserted under specific condition is measured at different positions of the sand bed. It is considered to be an indication of the porosity and the uniformity of the sand (Feda, 1961).

4.3.2. FACTORS CONTROLLING POROSITY OF DEPOSITED SAND:-

Kolbuszewski found that for any sand, the porosity of a bedding formed by vertical deposition is mostly governed by the simultaneous effect of two factors during deposition:-

a/ Velocity of fall of the particle at the surface of deposited sand. The height of fall may be taken instead of velocity as a dependent factor.

b/ The intensity of deposition, which is defined by the weight deposited per unit area per unit time.

Generally porosity is directly proportional to intensity of deposition at constant velocity of fall, and inversely proportional to the velocity, or height of fall at constant intensity.

4.3.2.1. EFFECT OF THE VELOCITY (HEIGHT OF FALL) OF SAND GRAINS:-

Velocity is the only independent parameter in the energy expression for the falling particles measured at the surface of deposition. For a given intensity, the grains with high energy (velocity) tend to fill larger spaces in the available voids in order to settle into a position of minimum potential energy, which results in low porosity. A particle falling freely, due to forces of inertia, gravity and resistance, eventually reaches a constant velocity (the terminal velocity).

The relationship according to Kolbuszewski (1958) between the porosity and velocity of deposition or the height of fall, at a constant intensity of deposition is shown in Fig (4.3a).

4.3.2.2. EFFECT OF INTENSITY OF DEPOSITION:-

The energy alone is not enough to produce dense packing, but the grains must fall as individuals in order to have sufficient time to occupy the open gaps. For this condition the grains will take up positions of minimum potential energy. With increasing intensity of deposition the grains will be interlocked into positions of higher potential energy by the succeeding falling grains. This will result in higher porosity and looser packing. As in the case of velocity, there is a limiting value of the intensity, regardless of the velocity, beyond which no, or a very slight, increase in the porosity takes place. The relationship between the porosity and the intensity of deposition reported by Kolbuszewski (1958) is shown in Fig (4.3b).

4.3.3. METHODS OF FORMING UNIFORM SAND BEDS:-

According to the technique used for controlling the overall porosity of the sand bed, the methods can be divided into two major groups (Butterfield and Andrawes, 1970).

4.3.3.1. POROSITY CONTROLLED AFTER DEPOSITION:-

Porosity is controlled after placing the sand in the container by vibration, tamping, fluidization with air, or shearing with sieves.

Usually sand is poured in layers of equal thickness, then porosity is adjusted for each individual layer after its placement. Beds formed by these methods often exhibit inherent anisotropic properties and periodic porosity variations in the vertical direction (Feda, 1961; Hansen, 1961; James, 1967).

If the size of the container is not too large, the whole bed, rather than individual layers, can be vibrated. This method is suitable where a dense sand is required.

In this group of methods the reproducibility of any overall porosity is rather poor and in some cases they are manually performed (e.g. tamping method) and are therefore subject to high operator errors.

4.3.3.2. POROSITY CONTROLLED DURING DEPOSITION:-

The methods used to form sand beds at a predetermined porosity are all based on the work of Kolbuszewski (1948a, 1948b). The porosity is governed by the intensity and velocity of deposition and the methods vary these parameters to obtain a range of porosities within the minimum and maximum limits.

Two different techniques of deposition are commonly used:-

a/ Sand rain over the whole bed area:-

Kolbuszewski and Jones (1961) devised an apparatus which enabled them to control the intensity of the sand rain and the velocity of deposition. A rain of sand particles was allowed to fall at any required intensity over the whole bed area from a receptacle placed above the receiver tank. The base of the apparatus consisted of two perforated plates and a shutter plate which could open and close the apertures above. The top two plates could be fixed relative to each other so that the effective openings of the system of holes could be varied from fully open to nearly closed. The hopper containing the sand could be mounted at any height directly above the sand container.

The main parts of the apparatus are depicted diagrammatically in Fig (4.4). The jets of sand created by opening the apertures were dispersed into a uniform rain of sand by placing a sieve mesh between the plates and the receiving tank. Kolbuszewski and Jones formed sand beds by depositing several layers and their examinations of the uniformity of the beds using porosity pots showed very little variation throughout the beds. They also reported that at no setting of the perforated plates were the deposited samples perfectly level. Several investigators have used similar set-ups utilizing the sand rain technique e.g. (James, 1965; Sherif, 1975).

As the receptacle size becomes larger, the adjustment of the perforated plates and the sliding of the shutter plate will be difficult due to the frictional resistance developed and the crushing of the sand grains. It is also difficult to change the height of the receptacle to allow for a wide range of porosities.

b/ Sand curtain traversing bed area:-

In this technique the bed is built up of thin layers each of which is produced from falling curtain of sand, discharged from a slot in a hopper, during every traverse of the hopper over the receiver tank.

Various types of apparatus have been constructed based on this principle, and differing only in the method of controlling the intensity of deposition. The height of fall may or may not be kept constant.

Fig (4.5) shows details of the sand spreader devised by Walker and Whitaker (1967) to control the intensity of the sand curtain by means of a rotating longitudinal metal roller situated underneath the hopper's aperture. When the roller is stationary no sand flows out of the hopper. The spreader traverses backwards and forwards across the sand tank on rails and the rails and spreader are raised to maintain a constant height of fall to the surface of the sand bed. A wide range of porosities between the maximum and minimum porosity values of the sand can be reproduced by this spreader using different gap settings and roller speeds to control the intensity of deposition. Three motors were used to rotate the roller, raise the hopper with its rail track assembly and to traverse the hopper in the horizontal direction simultaneously. Walker and Whitaker reported that in a closed container the performance of the spreader could be affected by air currents, set up by the sand curtain, interfering with the falling sand. They suggested using a tank in which the walls could be built up in lifts and so minimise the reflection of these air currents.

Similar apparatus was used by James (1967), Uzuner (1975) and Vafaeian (1977).

Butterfield and Andrawes (1970) proposed a simpler apparatus called an "Air-activated sand spreader" in which air pressure was used to control the intensity of the sand curtain. As shown in Fig (4.6) the box is divided into two compartments connected through a horizontal narrow gap. A composite wire mesh is fixed in the horizontal gap across the full width of the spreader. The upper compartments, with its base sloping at 35° to the horizontal, is used for placing the sand. The lower compartment, which is airtight except for the discharge orifice along the width of the spreader, is used as a pressurized air reservoir when connected to an air pressure line. The pressurized air discharges through the wire mesh, up through a shallow bed of sand and out into the atmosphere via an adjustable discharge slot. The discharge slot is adjusted to give no sand discharge when there is no air flow. When air flows seepage forces disturb the equilibrium of the sand mass and a uniform sand curtain discharges from the slot at an intensity which is proportional to the air pressure inside the lower compartment. The spreader is kept at a constant level and hence the height of fall changes during deposition. To compensate for the decrease in height of fall, as the depth of the sand bed increases, the intensity of deposition of the sand is varied by reducing the air pressure in the spreader.

The uniformity and reproducibility of the porosity were within $\pm$ 0.23% and 0.13% respectively for Leighton Buzzard sand with particle size (0.3-0.85 mm).

The advantages of the air-activated sand spreader over the rotating cylinder method are:-

a/ Accurate continuous control over the rate of deposition leading to better reproducibility.

b/ Simple, compact and maintenance free apparatus in which only one motor is used to traverse the spreader across the sand box at constant speed and reverse the direction of travel.

c/ By using air pressure it is possible to eliminate the need to maintain a constant height of fall and hence the complicated assembly required to raise the traversing box.

The common shortcoming of all the sand laying methods using the sand curtain traversing technique is layering which was detected using X rays (James, 1965) as shown in Fig (4.7).

This happens because the intensity of flow from the orifice is considerably higher below the centre than the edges of the sand flow. The edges of the moving sand curtain will result in thin denser layers above and below the looser layer due to the bulk of the flow.

The stratification can be eliminated by placing a diffuser mesh between the sand curtain and the bed (James, 1967). It is also minimised if the intensity is very low (i.e. dense sand). In this case the thickness of the layer deposited is very thin, and in the case of coarse sand, it is reduced to a fraction of the mean diameter of the particles, giving no possibility of layering to take place. It was concluded by the writer that the sand curtain technique is more suitable than the other methods described for preparing dense sand beds of large size.

4.4. CHOICE OF A SAND LAYING METHOD:-

From the above review it was decided to take a design decision regarding the method to be used in depositing uniform beds of sand in which the model anchor would be embedded.

The methods of controlling porosity after deposition were avoided for the following reasons:-

a/ Presence of high locked up horizontal stresses causing anisotropic characteristics in the sand bed.

b/ Uniformity and reproducibility are not as accurate as the methods of controlling porosity during deposition.

c/ Disturbance of the anchors already embedded in the sand.

d/ Possibility of high operator errors.

A sand rain technique was excluded due to the following factors:-

a/ For the receptacle to cover the whole bed area, it becomes large, heavy and difficult to change its position.

b/ It is very difficult to keep the height of fall constant since the receptacle is heavy. Alternatively the aperture size requires to be changed to compensate for the reduction of the height of fall. This is also difficult with the receptacle full of sand. Moreover friction and sand grain crushing is developed when the bottom perforated plates are adjusted.

The traversing sand curtain technique was considered to be most suitable for use in the present study. Although there is the possible problem of stratification when using this method, it was believed that this could be minimized or even eliminated when using the technique to deposit dense samples. This can be done by using a diffuser mesh (James, 1967) or even without a diffuser mesh if the intensity is so low that the thickness of every deposited layer is less than the mean diameter of the sand particles.

A decision had to be taken between using the rotating cylinder method and the air activated sand spreader. The air activated sand spreader was finally chosen for the following reasons:-

a/ Compactness and low cost of the apparatus even when used to lay sand beds in large tanks.

b/ Reasonable reproducibility and uniformity of porosity can be produced.

c/ The spreader is kept at constant level, so there is no need to lift it up as deposition progresses.

d/ By changing the size and shape of the discharging slot various types of sand could be used.

4.5. DEPOSITION OF LOW AND INTERMEDIATE DENSITIES:-

After construction of the air activated sand spreader and its calibration it was found that a porosity higher than 37% at the maximum height of fall could not be obtained. The air-tight chamber of the air activated sand spreader was checked for leakage of air and found to be satisfactory. The volume of the air tight chamber was reduced to increase the air pressure inside. It was found that the porosity of the bed for sands falling through a large height is not very sensitive to changes in intensity of deposition. The reduction of the height of fall was found to be difficult for the experimental apparatus. The maximum air pressure supplied from an air compressor (10 bars) was utilized fully.

Due to the above-mentioned difficulties it was decided to use another simpler method for depositing loose and medium dense sand. A sand raining technique of small scale was chosen. A perforated plate fixed at the bottom of a metal box was used. The sand from a box, raining at a constant intensity, was kept at a constant height of fall in order to produce uniform porosity all over the sand bed.

The apparatus used by the author to deposit uniform beds of sand and its calibration are described in Chapter 5.

4.6. CONCLUSIONS:-

1/ A dry, intermediate to coarse, subrounded Leighton Buzzard sand graded between the 2.0 mm and 0.2 mm B.S. sieve sizes was chosen for the model tests.

2/ Sand beds created by adjusting porosity after deposition (tamping, vibration) are most likely to have excess horizontal stresses induced in them. The stress systems in the completed bed will be more like those in an over-consolidated bed than in a normally consolidated bed.

3/ Both sand rain and traversing sand curtain methods of depositing sand can be used to obtain uniform sand beds at a specified porosity. The use of meshes to further disperse the rain or curtain can improve the uniformity of the sand bed. Attempts should be made to minimize air currents that may be set up by the sand falling into closed, unventilated containers.

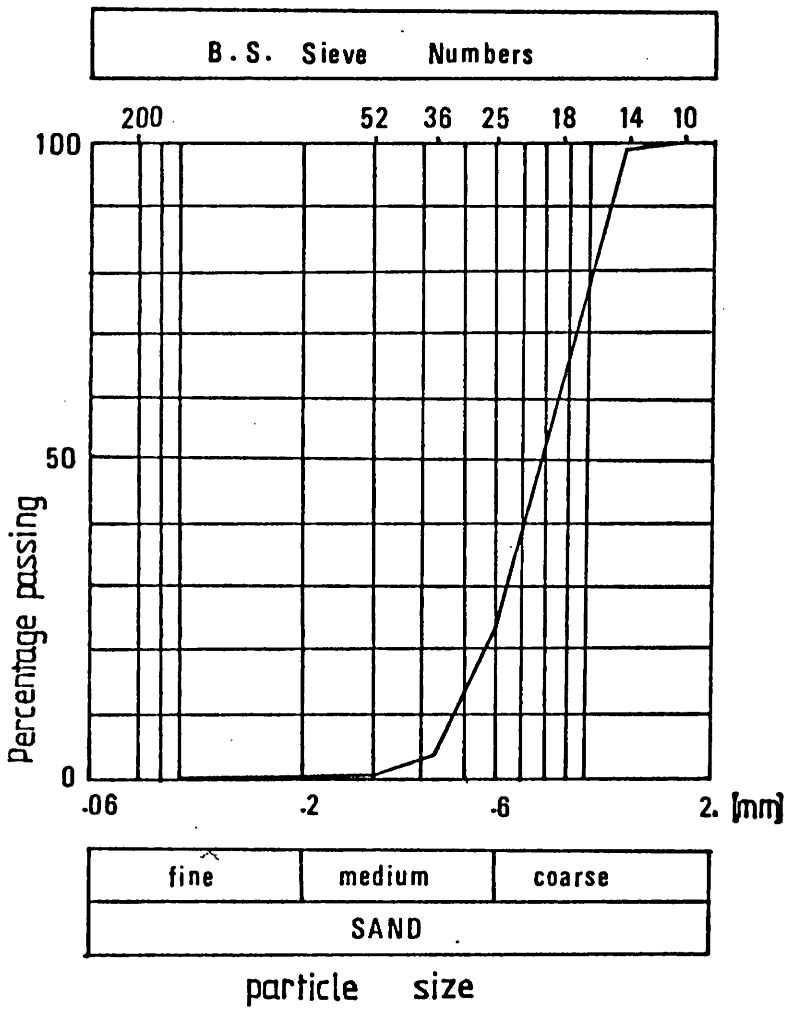

FIG.4.1 PARTICLE SIZE DISTRIBUTION OF THE LEIGHTON BUZZARD SAND

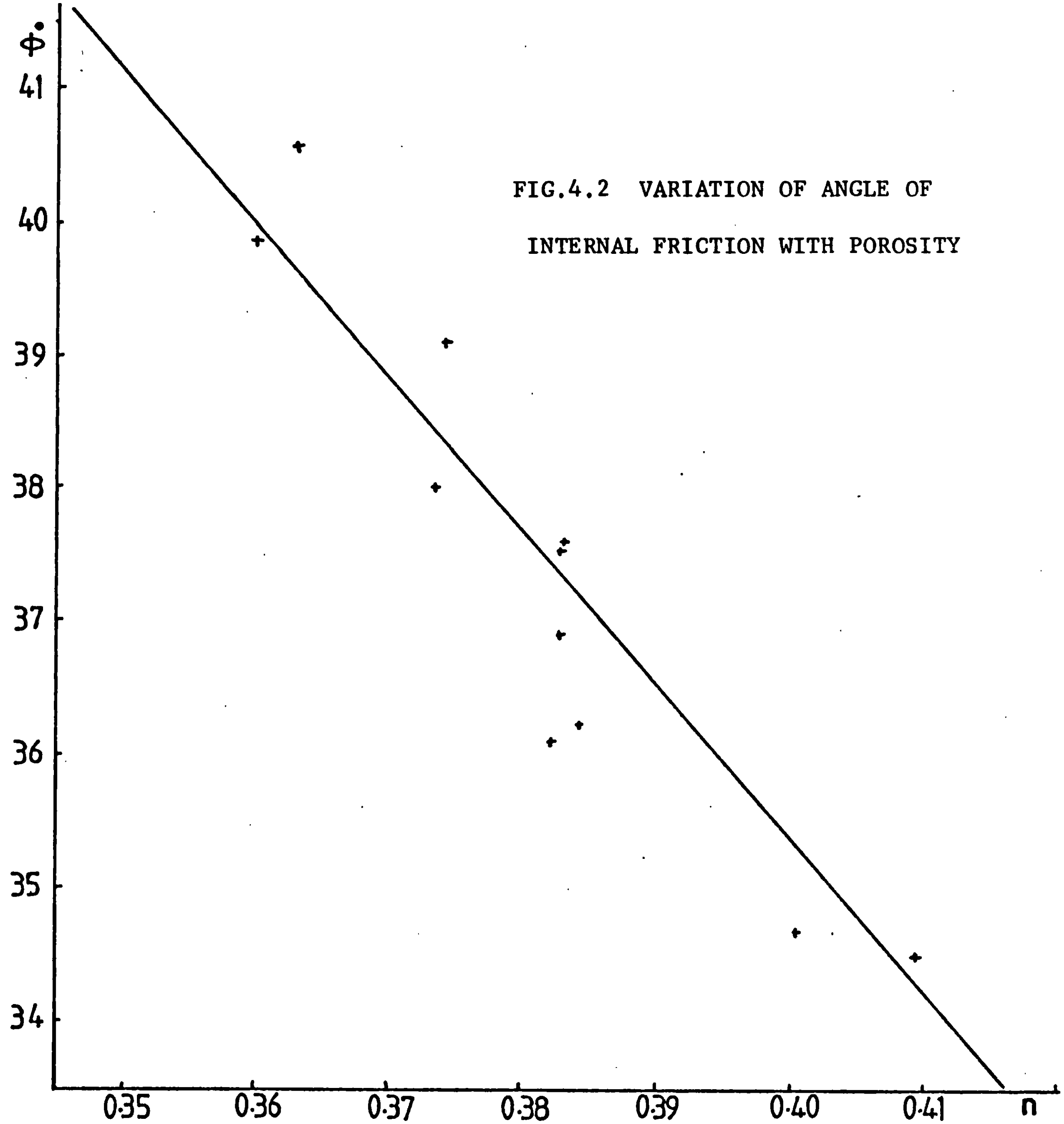

FIG.4.2 VARIATION OF ANGLE OF INTERNAL FRICTION WITH POROSITY

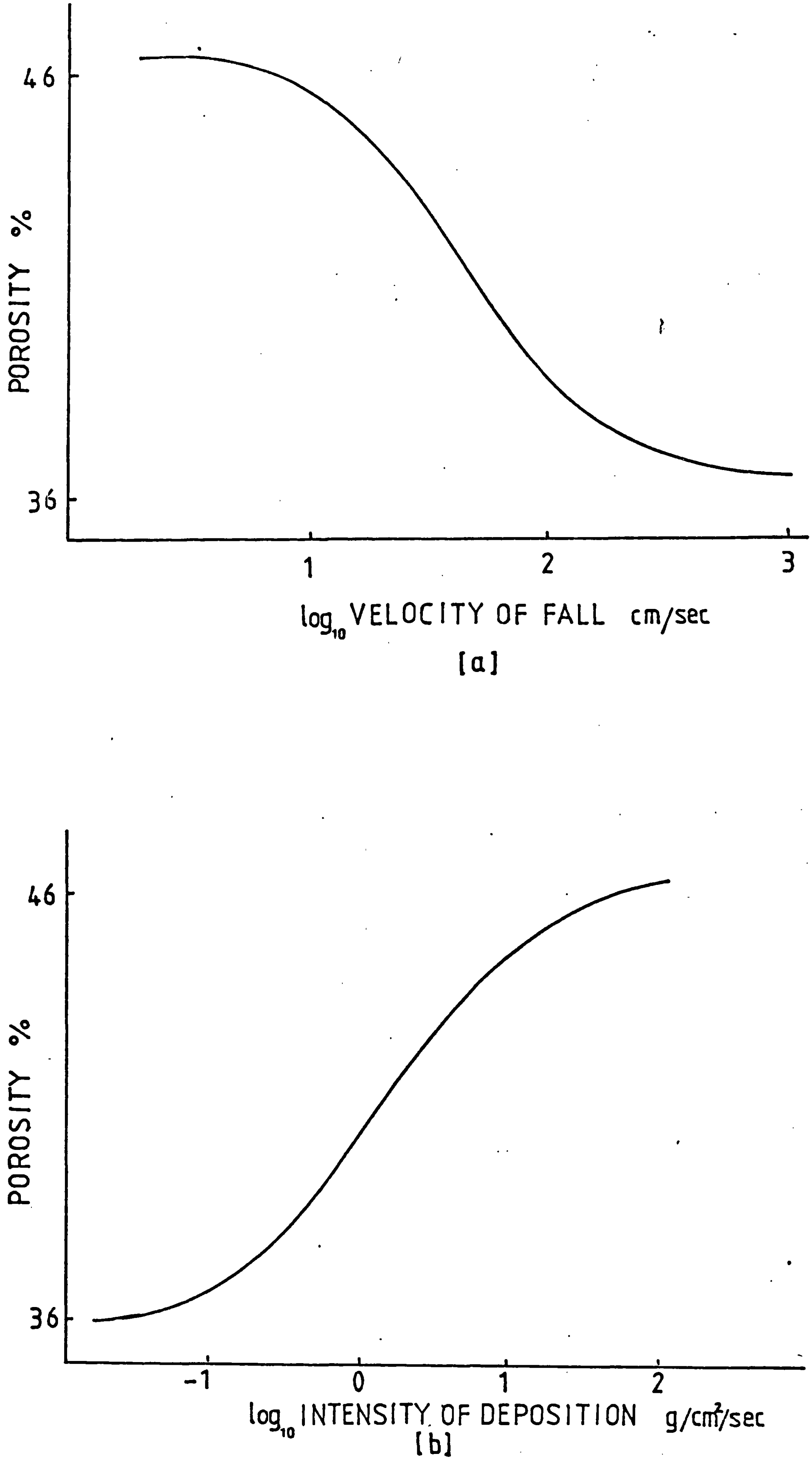

FIG.4.3 FUNDAMENTAL FACTORS CONTROLLING THE DEPOSITION OF SAND, KOLBUSZEWSKI (1958)

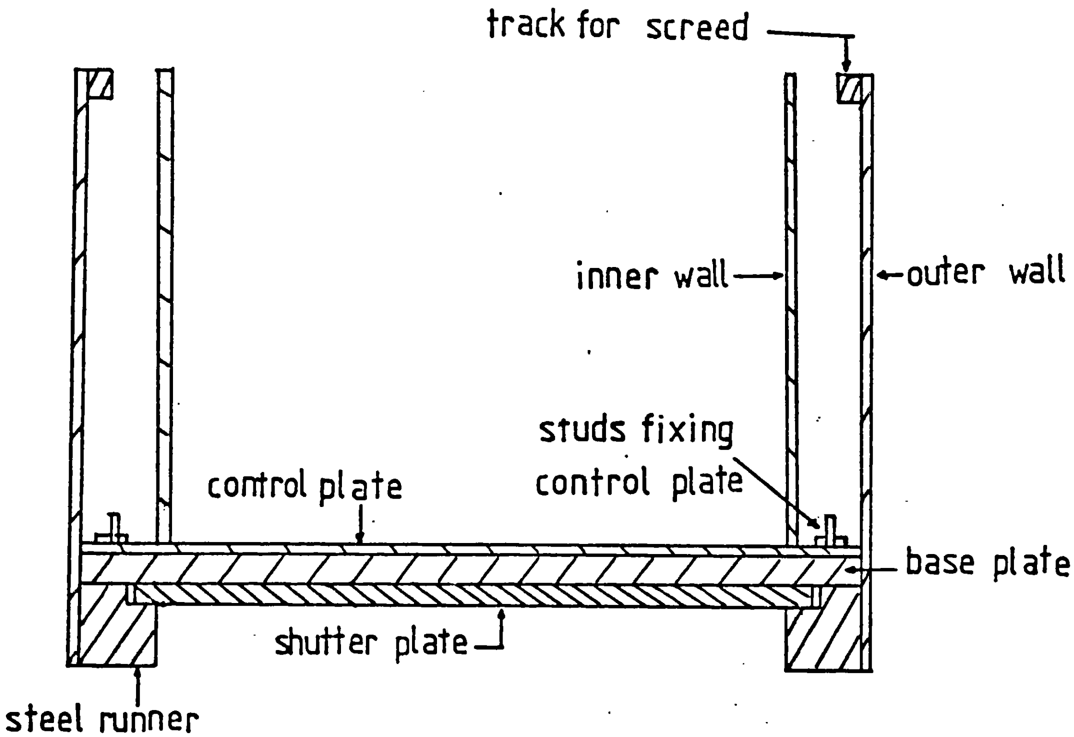

FIG.4.4 DIAGRAMMATIC SECTION THROUGH THE HOPPER, KOLBUSZEWSKII AND JONES (1961).

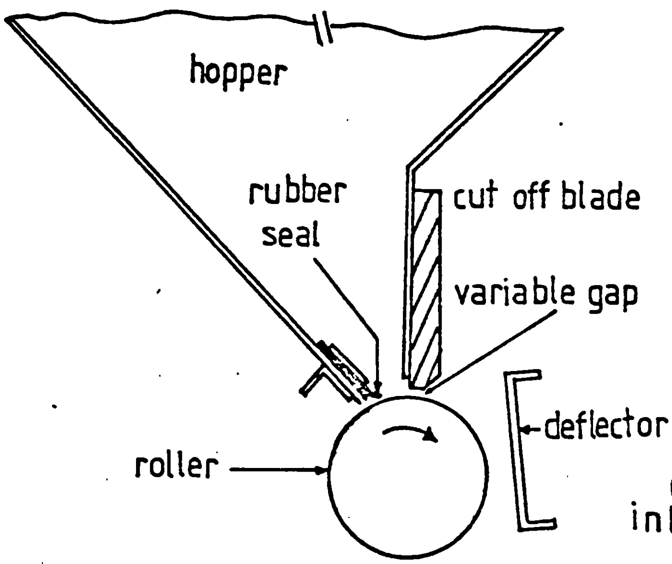

FIG.4.5

ROLLER ACTIVATED SAND SPREADER TO CREATE A UNIFORM CONTROLLED CURTAIN OF SAND (WALKER AND WHITAKER, 1967)

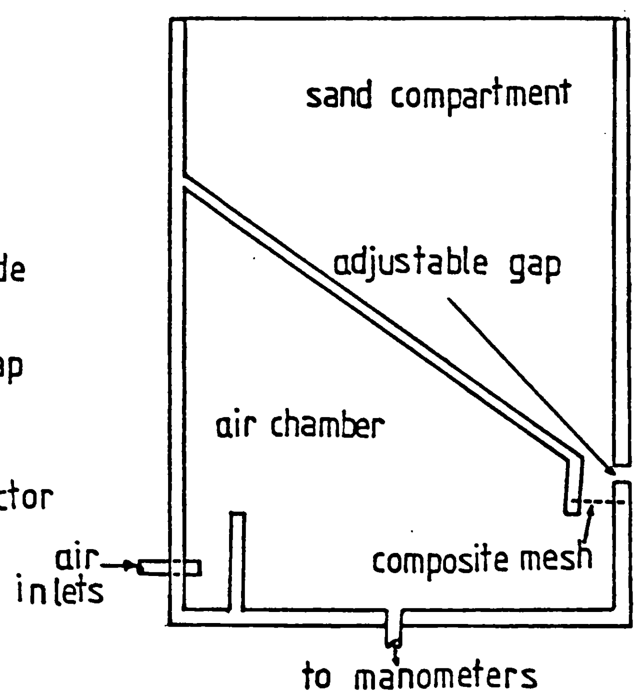

FIG.4.6

AIR ACTIVATED SAND SPREADER TO CREATE A UNIFORM CONTROLLED CURTAIN OF SAND (ANDRAWES, 1970)

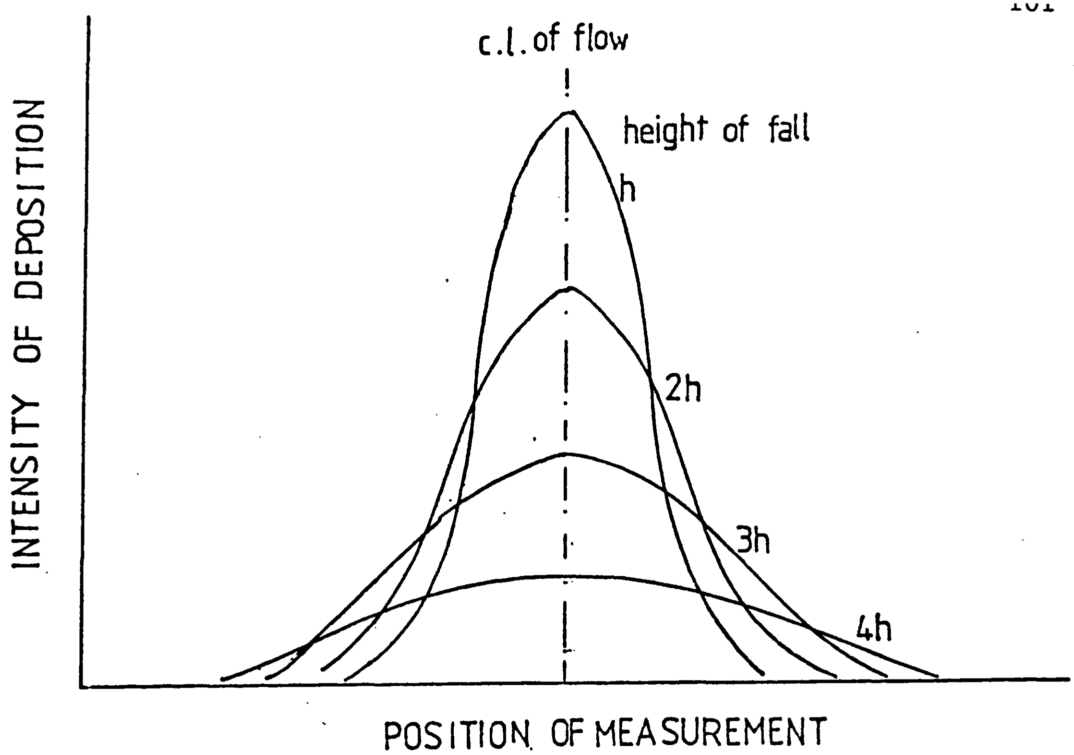

(a) change in the intensity below the orifice

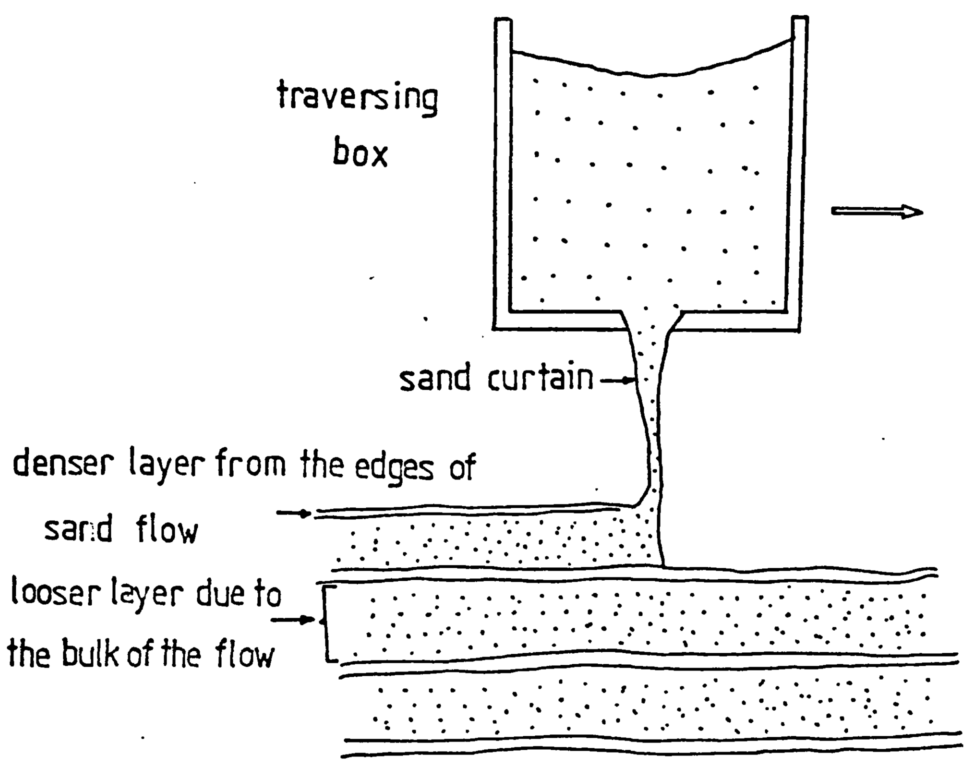

(b) stratification due to changes in the intensity

FIG.4.7 TRAVERSING SAND CURTAIN METHOD OF DEPOSITION

CHAPTER 5

APPARATUS AND TEST PROCEDURES

CHAPTER 5

APPARATUS AND TEST PROCEDURES

5.1. INTRODUCTION:-

In this chapter the apparatus used for load and photographic tests will be described. The appliances for measuring loads and displacements and the equipment designed to create uniform beds of sand and their calibrations are presented. This is followed by the testing procedures and the results obtained. The discussion of the results will be reported in Chapter 7.

The load tests were carried out in order to obtain experimental evidence concerning the following:-

a/ The load-displacement relationship up to and beyond the ultimate uplift resistance of the anchor.

b/ Measurement of the vertical deformation of the soil surface due to the anchor displacement for different types of tests.

c/ Determination of the shape and dimensions of the surface failure in shallow anchor tests.

The photographic tests were conducted to measure deformations within the sand mass due to anchor displacement from which the size and shape of the failure surface after failure of the anchor could be established. The technique of placing horizontal thin strips of cement between the layers of the sand was adopted where measurement of the internal deformation of the soil was required. Details of this technique are described in section (5.8.3) of this chapter. Burland and Roscoe (1969) have used X-ray techniques, by which displacements inside the soil during a test were measured. This was achieved by tracing the path of lead shot which was placed in the sample during preparation. Even using the most powerful X-ray equipment, a penetration of not more than 250 mm was considered to be the maximum possible. This limitation reduces the size of model which can be used and require most sophisticated equipment to measure the displacement of the lead shot. Moreover the danger of using X-rays will increase the precautions necessary in the laboratory. Another technique used by other investigators was the semi-spatial tests where only half section of the anchor is placed against a glass face. Coloured layers are deposited and their movement traced through the glass during and after the test. The disadvantage of this method is that the deformations and the shape of failure can be affected by the presence of the glass face boundary.

In the present study photographic tests were performed on a three-dimensional model to avoid the difficulties and disadvantages involved in the above-mentioned techniques.

In order to predict the magnitude and distribution of the radial and normal vertical stresses and shear stresses and the magnitude and direction of the principal stresses in the soil during the uplift resistance tests in the soil, a finite element analysis was employed. This is described in Chapter 6 .

5.2. APPARATUS FOR LOAD AND PHOTOGRAPHIC TESTS:-

The diagram of the apparatus used for performing load tests is shown in Fig (5.1). Figs (5.2, 5.3) show photographs of the apparatus used for load and photographic tests respectively. The main features are described below.

5.2.1. TANK, RIG AND PORTAL FRAME:-

Evidence shows that boundaries more than 8 times the diameter of the anchor from the anchor have little influence (Carr, 1970; Yilmaz, 1971). On this basis the dimensions of the tank base area (762 x 762 mm) were chosen. Moreover the depth of the tank (762 mm) was adopted to enable the performance of deep anchor tests with the ratio of depth upon diameter of anchor up to 25. Two holes were drilled in the base to accommodate vertical and inclined anchors. Below the tank base a rotating bush was fixed to reduce the friction forces on the anchor shaft during anchor displacement.

The tank was fixed on a rig made of steel angles. A portal frame was set up over the rig to support the device required for depositing high porosity sand beds.

For the performance of photographic tests a perspex tank of dimensions (500 x 500 x 500 mm) was used as shown in Fig (5.3).

5.2.2. THE LOADING SYSTEM (MOTOR, GEARBOX AND CONVERTOR):-

Fig (5.4) shows the arrangement whereby a reversible electric motor was connected to a gearbox and convertor which produced a vertical or inclined displacement of 2.24 mm per minute in the anchors.

The displacement in the photographic tests was produced using a 1 tonne loading frame.

5.2.3. ANCHOR UNITS:-

Brass discs with smooth faces and diameters ranging from 25.4 to 76.2 mm and 3 mm thickness were used. Anchor shafts 6 mm diameter were screwed into the brass discs to make the anchor unit. Using these anchors, depth upon diameter ratios ranging from 1 to 25 were obtained.

5.3. LOAD AND DISPLACEMENT MONITORING UNITS:-

To measure the anchor load, a load cell of capacity 2224 Newtons (500 lb) was connected above the convertor as shown in Fig (5.4). The load cell is connected to an amplifier and electronic equipment.

Six linear variable displacement transducers with a maximum output dependent on their sizes were used. The largest of these was connected to measure the anchor displacement while the other five were attached to a gantry above the tank to measure continuously during the test the vertical deformations at selected points along the centre line of the anchor. The transducers were connected to the electronic equipment.

5.4. THE ELECTRONIC EQUIPMENT:-

When loading the anchor at a constant rate of strain it was intended to observe not only the peak load, but also pre-peak and post-peak load behaviour. Besides the anchor loads and displacements, sand surface deformations at different stages of the test were also monitored. Accuracy of observation depends on how frequently the load and displacements are sampled. Manual recording is obviously too slow. It was decided to use a data logger with an electric mechanical printer output device as shown in Figs (5.1, 5.2).

Data is taken from the load cell and transducers to a twenty channel strain gauge bridge. Channel and sampling rate are selected using the scanning unit on the data logger. The sampling rate was dependent on the choice of output device accepting the digited information from the digital voltmeter. Ten channels could be sampled every twenty seconds by the printer.

5.5. TYPE OF TEST AND THE LOADING APPLIED:-

The general load test apparatus shown in Figs (5.1 & 5.2) could be simply adjusted for four combinations of testing and loading.

a/ Pushout test with displacement controlled loading.

b/ Pushout test with load controlled loading.

c/ Pullout test with displacement controlled loading.

d/ Pullout test with load controlled loading.

In the present investigation a pushout test was chosen rather than pullout test for the following reasons:-

a/ The pushout test is more convenient since there is no anchor shaft to create problems during sand deposition.

b/ The placement of the gantry carrying the deformation displacement transducers along the centre line above the anchor will be easy.

c/ It was found that the difference between the pushout test and the pullout test for the same dimensions of anchor and depth of sand is not significant (El Rayes, 1965).

The displacement-controlled test was preferred over the load controlled test for the following reasons:

a/ The displacement controlled test will enable the observation of the pre- and post-peak load behaviour.

b/ Greater degree of control could be exercised over the location of the anchor plate.

Vibrations induced in a mass of loose sand will result in a densifying of the sand. To prevent this from happening vibrations in the apparatus were minimized by positioning foam-rubber insulation beneath the three motors used for the loading mechanism, driving mechanism and the rotating bush. It was also placed under the two rigs and the print out apparatus.

5.6. APPARATUS TO CREATE UNIFORM SAND BEDS:-

An air activated sand spreader traversing the tank at a constant velocity and producing a uniform curtain of sand was used to produce a uniform bed of sand around the model anchors. The changing height of fall as the depth of the sand bed was built up could be compensated for by altering the air supply to the spreader to vary the intensity of deposition. Care was taken to maintain the uniformity of the sand bed by preventing the sand that fell outside the tank from bouncing into it.

The apparatus comprised a sand spreader box, air pressure controls and support and driving mechanism.

5.6.1. SAND SPREADER BOX:-

The design principles of the air activated sand spreader whose basic functions have been described in Chapter 4 section 4.3.3.2 were given by Butterfield and Andrawes (1970). Fig (5.5) shows the main features of the box. The plywood box was divided by a plywood sheet inclined at 35^{o} to the horizontal into two compartments diagramatically shown in Fig (5.6). The sand was placed in the upper compartment and moved down under its own weight. The front face of the spreader was strengthened by steel bars of rectangular section at the upper and lower edges to prevent the curvature of the face when the box is loaded with sand and ensure that the discharge slot would be uniform and straight edged. The upper plate could slide to adjust the slot height. The plate was locked in place to give a 11 mm slot height for the tests reported in this thesis and no sand flowed out of the spreader unless the air supply was turned on. The rest of the box was coated with araldite to ensure that there was no leakage.

The air, which is pressurised in the lower compartment, comes up through the composite mesh into the sand mass in the upper compartment. The sand mass is in a state of equilibrium. Due to the uplift drag forces caused by the flow of air, the sand particles lose stability and discharge in the form of a sand curtain.

The intensity of the discharging sand increases with increasing air pressure inside the lower compartment. The air supply was led into the spreader through two pipes in the rear wall. Two buffer plates were fixed within the lower compartment in order to reduce the air velocity and redistribute the pressure evenly. The intensity of deposition was controlled by varying the pressure within the spreader as monitored on a manometer connected to the air space in the spreader.

5.6.2. AIR PRESSURE CONTROLS:-

A photograph of the air pressure controls is shown in Fig (5.7). A regulator was used to control the air pressure produced by a compressor. The air pressure inside the pipe was measured by a pressure gauge. The air line pressure could be used in the same way as the water manometer reading to control the intensity of fall of the sand curtain. Thus more accurate control over the air pressure, and hence the intensity of fall, could be achieved. Two different on-off valves were used at different locations on the line to control the feeding and cutting of the supply. Friction head losses were reduced by using a large diameter service pipeline from the compressor. The water manometer provided an indication of the point at which the air began to discharge through the discharge slot and the sand in the spreader. This happened only when the spreader was nearly empty and during the filling of the sand compartment this condition was not allowed to be reached. The spreader was connected to the air supply by a flexi-hose which did not affect the air flow during the motion of the spreader.

5.6.3. SUPPORT AND DRIVING MECHANISM:-

Figs (5.2, 5.5, 5.7) show the support and driving mechanism of the sand spreader. The sand spreader is required to traverse the sand tank at a constant velocity and reverse the direction of motion at the end of the travel. The sand spreader is provided with two grooved wheels at each side running on two track rails fixed on top of the rig.

An electric motor connected through a system of chains, sprockets and gear system traverses the sand spreader along the tank in both directions.

The sand spreader rig was provided with foam-rubber insulation below the base and fixed to the floor in order to minimize vibration.

5.6.4. SAND RAINING DEVICES:-

The air activated sand spreader produced sand in only a dense range for the whole depth of the sand bed and the reasons were stated in Chapter 4 section 4.5. In order to achieve intermediate and low densities a sand raining box suspended over the sand bed was used. The dimensions of the box were 305 mm high with a 280 mm square base. The base of the box was removed and replaced by steel plate drilled on 20 mm grid line. For deposition of intermediate density the diameter of the holes drilled was 6.35 mm and for loose sand 12.7 mm.

The box was connected by a steel wire over the pulleys and fixed to the portal frame. The height of fall was initially 150 mm. The sand was poured into the raining box and deposited over the whole bed area. In order to keep the height of fall approximately constant while the sand bed built up, the box was raised at certain intervals and the steel wire fixed when the height of fall reached the initial value. The sand was built up over the anchor until the required depth was deposited. To deposit different densities the appropriate steel plate was used.

5.6.5. CUT OFF PLATES AND OVERSPILL:-

The width of the sand curtain falling from the spreader was designed to be slightly wider than the sand tank. Vertical deflector plates were fixed around the top edges of the sand tank so that they were flush with the inside face of the tank. The plates acted as knife edges and any sand falling outside the inner area of the tank was deflected away from the sand bed. The deflected sand was allowed to fall down a polythene sheet curtain and was funnelled into a collecting tray which had to be emptied into storage sand containers when it was filled.

5.7. CALIBRATION OF EQUIPMENT:-

In this section the calibration of the air activated sand spreader and the sand raining device are presented. It is followed by the calibration of the load and displacement monitoring units.

5.7.1. CALIBRATION OF THE SAND SPREADER AND RAINING DEVICES:-

The minimum intensity of deposition to produce a uniform curtain of sand corresponded to a pressure equivalent to a head of 6 mm of water in the manometer. The maximum intensity available corresponds to a head of 13 mm of water. At six different levels spaced throughout the height of the sand tank the porosity of the deposited sand was measured in different positions all over the area of deposition. This procedure was repeated for four different intensities of deposition between and including 6 and 13 mm head of water.

Porosity was determined by placing a number of density pots on a false floor installed at the required level in the tank. The dimensions of the pots were 76.2 mm in diameter, 50.8 mm high internally with knife edge upper rims to prevent the bouncing of sand grains into the pots. The factors affecting the choice of the dimensions of the density pots used have been discussed in Chapter 4, section 3.1.

To determine each porosity the air pressure was set to a particular value and the spreader traversed the tank until the pots were buried. The sand around the density pots was dug out carefully and the excess sand removed from the top of the pots by gentle scraping with a metal straight edge. The pots were weighed to the nearest 0.1 g. At each level and for each air pressure three tests were carried out. In each test twelve pots were arranged in three lines parallel to the direction of the spreader motion. The average value was used to calculate the density, void ratio and porosity of the sand layer. The calculated porosity was taken to be the porosity of the sand at the mid height of the measuring pot and the height of fall was considered to be from the mid point of the discharge slot to this level.

The results of this series of tests were plotted to show the relationship between the porosity and air pressure for the range of heights of fall from the bottom to the top of the sand tank, as shown in Fig (5.8). This figure shows that only porosities below 37% corresponding to relative density of 67% can be obtained throughout the height of the tank. This agrees with Kolbuszewski's finding that the intensity of deposition has less effect on the porosity for a large height of fall of the sand. Fig (5.9) which is derived from Fig (5.8) shows the variation of air pressure with change in the height of fall needed to produce a sand bed of the same porosity throughout the depth of the sand tank. During the laboratory investigations a porosity of 34.7% (D_r = 85.2%) was chosen for deposition of dense sand as illustrated in Fig (5.9). The tank was filled following this curve by reducing the air pressure when the sand in the tank had reached the appropriate level. The air pressure was adjusted with the spreader at one end of its traverse of the sand tank.

For the deposition of medium sands the sand raining box was suspended by the steel cable with an initial height of fall of 150 mm. The sand is poured in the box and rained uniformly all over the bed area. When the layer of deposited sand reached 30 mm, the box was raised by pulling the cable to bring the height of fall to the initial value of 150 mm. By repeating the same procedure the bed could be built up to the desired depth. To deposit loose sand it was necessary to fix the appropriate perforated plate then the same steps mentioned above were carried out. The porosities obtained for medium and loose sand after series of tests were found to be 38.99% (D_r = 50.2%) and 41.57% (D_r = 25.47%) respectively.

Uniformities and reproducibility of the sand bed were determined from the calibration tests. The uniformities of the produced beds for dense, intermediate and loose sand were found to be within $\pm$ 0.29%, $\pm$ 0.36% and $\pm$0.42% respectively and the reproducibility within $\pm$ 0.1%, $\pm$ 0.14% and $\pm$ 0.23% respectively.

One of the objectives of this study is to investigate the effect of different densities on the uplift resistance of the anchor. One density was chosen in each of the dense, medium and loose states. The densities corresponding to the chosen porosities were found to be 1730 $\pm$ 8, 1618 $\pm$ 9 and 1548 $\pm$ 11 kg/m^3 and their respective relative densities were 85.2, 50.2 and 25.4%.

5.7.2 CALIBRATION OF LOAD AND DISPLACEMENT MONITORING UNITS:-

It was decided in section 5.3 that the data obtained from the load tests would include anchor load and displacement and sand surface deformations at different points and at different stages of loading. The digitised output from the digital voltmeter would be converted from a voltage to loads and displacements.

An hour before the calibration started, the electronic equipment was switched on. This is to warm up the system and prevent any drift in the readings. In the laboratory the system was covered by a polythene sheet to exclude dust and reduce air currents around the electronics.

The load cell was calibrated against a compression testing machine and the calibration curve is shown in Fig (5.10).

The linear transducers were calibrated against a micrometer. The anchor displacement transducer had a range of 15 cm while the surface deformation transducers had a range of 5 cm. Figs (5.11, 5.12) show the calibration curves for the anchor displacement transducer and one of the surface deformation transducers.

5.8. EXPERIMENTAL PROCEDURES:-

The test procedure consisted of setting up the plate anchor model, loading the model and recording the loads, displacements and failure zones. Ten sets of tests were carried out. The first three sets were vertical load tests for the three different densities. The next six sets were conducted at two inclinations from the vertical direction at 22.5° and 45° and the different densities were covered and the last set comprised the photographic tests. All the tests were displacement controlled to study the behaviour of the anchor at pre- and post-peak loads. The displacement was applied at a constant rate until anchor failure was ensured. Table (5.1) shows the tests carried out to produce the results presented in this thesis.

5.8.1. SETTING UP THE ANCHOR MODEL:-

Figs (5.1& 5.2) show the diagram of the anchor model set up. At the start of the test the anchor shaft or the pushing rod was lubricated to reduce the friction along its surface. It was then screwed into the circular plate anchor which rested on the base of the sand tank. The end of the anchor shaft was connected to the load cell at the beginning of the loading. The deflector plates were fitted to the top of the tank. The curtains and the overspill collecting tray were then set up to make the tank ready for filling.

The tank was filled using the sand spreader, the spreader controls being adjusted to follow the calibration curve. When the sand bed reached the desired depth the air supply was shut off and the sand spreader stopped. The deflector plates were removed, and the displacement transducers were placed in their appropriate positions.

5.8.2. TESTING OF THE ANCHOR MODEL:-

The motor was switched on to raise the load cell until it touched the lower end of the anchor shaft. The motor was then switched off, and the load cell reading adjusted to zero. The readings of the six transducers were adjusted in the straight line of their corresponding calibration curves. The sampling rate of taking the readings was selected as the minimum period to record the load cell, displacement transducers readings and the time of sampling from eight channels. The scanning rate was found to be 20 seconds.

Preparations for the test having been completed, the teleprinter and the loading system were switched on simultaneously. The initial and subsequent readings were recorded by the teleprinter. The load was observed until failure of the anchor was ensured, either by the falling of load measurements from a maximum value or due to constant load value for increasing displacement. The surface of the sand was observed if there was any surface failure. Then the loading was stopped and the motion of the motor reversed. The dimensions of the surface failure were taken if there was any visible.

5.8.3. SETTING UP AND CHECKING PHOTOGRAPHIC TESTS:-

The primary purpose of this test was to provide a method for examining the failure pattern which existed within the sand mass after the completion of an uplift resistance test. The apparatus is illustrated in Fig (5.3).

The perspex box was fixed on the rig with the anchor unit in place. The sand was deposited as in the load test except that in this case a layerwise filling of the perspex box was done. Between the layers a very thin layer of cement powder was laid as a narrow strip above the anchor. The existence of the narrow and thin strips of cement was assumed not to affect the properties of the sand.

Loading of the anchor was carried out using a 1 tonne compression machine. The anchor was tested and after failure the loading system was stopped. Then the whole bed of sand was moistened to stabilize it, and to set the cement powder strips. The sand in one of the half sections of the perspex box passing through the centre of the circular plate anchor and parallel to the cement strips, was removed carefully. The vertical section was photographed and the points of discontinuity on the cement strips were considered to form the failure surface. The profile of failure was measured at this section for each test. For the preparation of another model test new sand was used.

5.9. VARIABLE PARAMETERS AND FAILURE LOAD:-

5.9.1. VARIABLE PARAMETERS:-

The parameters varied in the model tests were as follows:-

(i) Depth of embedment D = 76.2 to 635 mm.

(ii) Diameter of circular anchor B = 25.4 to 76.2 mm, accordingly a range of $\frac{D}{B}$ ratio of 1 to 25 could be obtained.

(iii) Angle of inclination from the vertical $\psi = 0^{o}, 22.5^{o}, 45^{o}$.

(iv) Density of the sand (dense, medium, loose corresponding to D_r = 85.2, 50.2, 25.4% respectively).

Tests were carried out to establish the reproducibility of the test results.

5.9.2. FAILURE LOAD:-

The full resistance of the soil was mobilized when the load measured reached a maximum value. Each test was given enough displacement to ensure that failure had occurred.

5.10. PRESENTATION OF TEST RESULTS:-

In this section the results of the model uplift resistance tests are presented. Comparison and discussion of the results will be presented in Chapter 7.

Summary of the result details of the model uplift resistance performed by the author are presented in Tables (5.2, 5.3, 5.4). These tables include the details of anchor and soil parameters for each test, i.e. the anchor plate diameter B, the depth of embedment D, the dry density of the sand γ_d and the angle of inclination ψ from the vertical. The loading parameters, i.e. the ultimate load R, the ultimate uplift resistance pressure on the plate anchor P_u and the dimensionless ratio $\frac{Pu}{\gamma gD}$ are also included. The anchor displacements at ultimate load δ_{au} and at intermediate stage corresponding to 90% of the ultimate load were presented. After failure of the anchor the dimensions of the clearly defined failure zone on the surface of the soil from the load tests are shown in Table (5.5.).

The results obtained from the laboratory model tests can be divided as follows:-

(i) Internal and surface deformations.

(ii) Relationship between anchor load and displacement.

(iii) Values of ultimate uplift resistance.

5.10.1. INTERNAL AND SURFACE DEFORMATIONS:-

5.10.1.1. INTERNAL DISPLACEMENTS:-

Figs (5.13, 5.14) are typical photographs of the displacement of the cement strips obtained from the photographic tests after failure had occurred. They were taken at a section through the centre of the anchor plate of diameters 77,135mm with $\frac{D}{B}$ = 2 and 3 respectively. From the measurements taken at these sections the pattern and shape of the failure surface could be obtained. The findings are used in the discussion of the approximate method in Chapter 7.

5.10.1.2. SURFACE DEFORMATIONS:-

In addition to the knowledge of the internal deformation, the measurement of the surface deformations at different stages of loading were measured and some of the results are shown and discussed in Chapter 7 section 7.2.5. From both load and photographic tests it was found that for shallow anchors where the failure surface reached the soil surface considerable surface deformations occur and the surface failure takes the form of a bulge.

The boundaries of the bulge form a circle in the case of vertical anchors and an ellipse with the major axis in the plane of inclination in the case of inclined anchors.

In the case of deep anchors only local shear failure occurred and no surface deformation was visible or monitored by the surface displacement transducers.

For vertical shallow anchors the diameters of the bulge B_s are shown in a dimensionless ratio $\frac{Bs}{B}$ plotted versus $\frac{D}{B}$ as illustrated in Fig (5.15a). The ratios of the major and minor axis of the ellipse in the case of inclined shallow anchors $\frac{Bsj}{B}$ and $\frac{Bsn}{B}$ were also plotted in Fig (5.15b,c) corresponding to $\psi = 22.5^{o}$ and 45^{o} respectively. These figures will be discussed in Chapter 7.

5.10.2. ANCHOR LOAD-DISPLACEMENT RELATIONSHIP:-

The figures reported in this section will be discussed in Chapter 7. Fig (5.16) shows the relationship between the uplift resistance pressure ratio $\frac{p}{\gamma g D}$ and the displacement dimensionless ratio $\frac{\delta_a}{B}$ where p and δ_a are the uplift resistance pressure and the displacement of the anchor at any stage of the loading. The $\frac{D}{B}$ parameter was taken as a variable. Two values of $\frac{D}{B}$ i.e. 4 and 15 were taken representing the shallow and deep anchor cases respectively and the different angles of inclinations were covered. In each case of Fig (5.16) the density and the angle of inclination were kept constant. Fig (5.17) shows the effect of varying the density of the sand, keeping $\frac{D}{B}$ and ψ constant and Fig (5.18) illustrates the effect of inclination while $\frac{D}{B}$ and γ are kept constant.

It was observed that the anchor displacement at different stages of the loading and at ultimate load is a function of $\frac{D}{B}$, γ, ψ. Fig (5.19) depicts the relation between $\frac{\delta au}{B}$ and $(\frac{D}{B})^2$ for all the tests, and empirical relationships can be established correlating the displacement ratio $\frac{\delta au}{B}$ to the anchor dimensions. Fig (5.20) shows the relation between $\frac{\delta a90\%}{B}$ and $\frac{D}{B}$ for all the tests, where $\delta_{a90\%}$ is the anchor displacement at 90% of the ultimate load. The rate of displacement taken as a ratio $\frac{\delta a90\%}{\delta au}$ is plotted versus $\frac{D}{B}$ as shown in Fig (5.21).

5.10.3. ULTIMATE UPLIFT RESISTANCE:-

The most important purpose of the present investigation was to find the ultimate uplift resistance of the anchor as a function of different parameters.

Some parameters taken into consideration as mentioned in Chapter 3 were $\frac{D}{B}$, the relative density and the angle of inclination. The dimensionless ratio $\frac{pu}{\gamma gD}$ was calculated for each test where p_u is the ultimate uplift resistance pressure. Fig (5.22) shows the relationship between $\frac{pu}{\gamma gD}$ and $\frac{D}{B}$ for three relative densities (25.4, 50.2, 85.2%), keeping $\psi = 0^o$ representing the vertical anchor. Figs (5.23, 5.24) illustrate the same relationship for the other two inclinations of 22.5^o and 45^o from the vertical direction.

In this chapter the design and calibration of the apparatus used in the model tests have been presented. The procedure of performing the tests and the results obtained from them followed. Discussion of the results and comparison with the previous theories and the approximate theory outlined in Chapter 3 will be presented in Chapter 7. In the following chapter a description of the finite element method for analysing the problem of the uplift resistance will be presented and the results obtained will be given.

Type of Test	Preliminary Tests	Load Tests			Photographic Tests
Angle of inclination	$\psi = 0^o$	$\psi = 0^o$	$\psi = 22.5^o$	$\psi = 45^o$	$\psi = 0^o$
Low density	2	33	11	11	2
Intermediate density	2	21	11	11	2
High density	2	17	11	11	3

Table 5.1. Details of model uplift displacement testing program.

TABLE 5.2. DETAILS AND RESULTS OF UPLIFT RESISTANCE TESTS IN LEIGHTON BUZZARD SAND (Dense, Intermediate, Loose Densities) ANGLE OF INCLINATION $\psi = 0^{o}$.

R = ultimate load
P_u = ultimate uplift resistance pressure

TEST NO.	SOIL DENSITY KG/m^3	ANCHOR DIMENSIONS			ANCHOR LOADING			ANCHOR DISPL.	
		D (mm)	B (mm)	$\frac{D}{B}$	R (N)	P_u KN/m^2	$\frac{P_u}{\gamma g D}$	δau (mm)?	$\delta a90\%$ (mm)?
1	1730	76.2	76.2	1	22.15	4.86	3.76	1.5	1.22
2		152.4	76.2	2	97.8	21.45	8.29	2.24	1.3
3		76.2	25.4	3	9.81	19.36	14.97	0.75	0.68
4		76.2	25.4	3	9.81	19.36	14.97	0.75	0.68
5		152.4	50.8	3	72.7	35.87	13.87	1.87	0.74
6		203.2	50.8	4	156.2	77.07	22.35	2.24	1.13
7		190.5	38.1	5	120.8	105.96	32.78	2.78	1.2
8		304.8	50.8	6	445.3	219.7	42.48	3.81	1.87
9		266.7	38.1	7	316.5	277.6	61.35	3.73	1.5
10		304.8	38.1	8	441.1	386.9	74.8	5.2	2.6
11		254	25.4	10	250	493.38	114.48	4.48	2.24
12		254	25.4	10	263	519.04	120.43	5	1.93
13		304.8	25.4	12	383.4	756.65	146.3	6	2.5
14		381	25.4	15	565.8	1116.62	172.73	17.92	1.87
15		431.8	25.4	17	757.1	1494.16	203.93	9.0	3.8
16		508	25.4	20	966.1	1906.62	221.2	20.2	8.5
17		635	25.4	25	1250.8	2468.49	229.1	41.4	11.2
18	1618	76.2	76.2	1	17.69	3.88	3.21	1.83	1.2
19		127	63.5	2	35.8	11.3	5.61	1.5	1.22
20		152.4	76.2	2	57.7	12.65	5.23	2.61	0.8
21		152.4	50.8	3	45	22.2	9.18	2.24	0.8
22		190.5	63.5	3	80.3	25.36	8.39	3.73	1.7
23		152.4	38.1	4	40.8	35.79	14.8	2.18	1.19
24		203.2	50.8	4	84.92	41.9	12.99	3.8	1.5
25		127	25.4	5	18.7	36.9	18.31	3.8	1.5
26		190.5	38.1	5	67.5	59.2	19.59	3.73	1.85
27		266.7	50.8	5.25	156.2	77.07	18.21	4.1	2.2
28		273	50.8	5.375	165.1	81.46	18.8	6.72	2.9

TABLE 5.2. CONTINUED

TEST NO.	SOIL DENSITY KG/m^3	ANCHOR DIMENSIONS D (mm)	B (mm)	$\frac{D}{B}$	ANCHOR LOADING R (N)	P_u KN/m^2	$\frac{P_u}{\gamma g D}$	ANCHOR DISPL. δau	$\delta a90\%$
29	1618	304.8	50.8	6	232	114.46	23.67	9.7	3.6
30		266.7	38.1	7	147.5	129.38	30.57	6.0	2.61
31		304.8	38.1	8	169.8	148.94	30.79	6.77	4.1
32		254	25.4	10	94.3	186.1	46.17	6.72	2.24
33		304.8	25.4	12	138.8	273.93	56.64	12.7	5.6
34		381	25.4	15	201.1	396.88	65.65	17.27	8.31
35		431.8	25.4	17	241.1	475.82	69.44	16.3	9.6
36		508	25.4	20	307.8	607.45	75.35	32.8	6
37		558	25.4	22	356.76	704.07	79.52	35.8	15.5
38		635	25.4	25	379	747.97	74.23	42.6	20.1
39	1548	76.2	76.2	1	13.24	2.9	2.5	0.75	0.68
40		127	63.5	2	22.5	7.1	3.68	3.8	1.9
41		127	63.5	2	27	8.53	4.42	2.24	1.25
42		152.4	76.2	2	39.9	8.75	3.78	2.24	1.52
43		114.3	38.1	3	9.65	8.46	4.87	0.82	0.5
44		152.4	50.8	3	27.2	13.42	5.8	2.5	1.0
45		190.5	63.5	3	53.6	16.92	3.85	6.72	2.98
46		228.6	76.2	3	84.4	18.51	5.33	8.3	3.8
47		152.4	38.1	4	23	20.17	8.71	2.24	1.7
48		203.2	50.8	4	49.5	24.42	7.91	6.46	3.97
49		127	25.4	5	9.81	19.36	10.04	0.81	0.5
50		127	25.4	5	9.81	19.36	10.04	0.75	0.5
51		190.5	38.1	5	31.9	27.98	9.67	7.4	4.8
52		254	50.8	5	80.6	39.77	10.3	10.5	4.8
53		317.5	63.5	5	151.5	47.84	9.92	14.5	7.1
54		381	76.2	5	231	50.65	8.75	10	6.67
55		304.8	50.8	6	98.4	48.55	10.49	6.7	4.4
56		266.7	38.1	7	54.13	47.48	11.72	6.72	3.8

TABLE 5.2 CONTINUED

TEST NO.	SOIL DENSITY KG/m^3	ANCHOR DIMENSIONS			ANCHOR LOADING			ANCHOR DISPL.	
		D (mm)	B (mm)	$\frac{D}{B}$	R (N)	P_u KN/m^2	$\frac{P_u}{\gamma g D}$	δau	$\delta a90\%$
57	1548	533.4	76.2	7	409	89.69	11.07	15	8.75
58		304.8	38.1	8	63	55.26	11.93	6.5	4.1
59		254	25.4	10	32	63.15	16.37	14.1	6.5
60		381	38.1	10	107.5	94.29	16.3	8.3	3.9
61		508	50.8	10	205.2	101.24	13.12	11.23	6.0
62		304.8	25.4	12	40.9	80.72	17.44	15	7.0
63		381	25.4	15	54.3	107.16	18.52	21.7	12.0
64		381	25.4	15	56	110.52	19.1	16	10.5
65		571.5	38.1	15	169.8	148.94	17.16	13.44	4.5
66		431.8	25.4	17	67.64	133.49	20.36	17.92	13
67		508	25.4	20	85.4	168.54	21.85	9.75	6.3
68		508	25.4	20	85.43	168.54	21.85	11.87	8.6
69		508	25.4	20	89.8	177.22	22.97	12.7	9
70		558	25.4	22	89.88	177.38	20.93	29.12	20
71		635	25.4	25	107.7	212.55	22.04	36.5	18.6

TABLE 5.3. DETAILS AND RESULTS OF UPLIFT RESISTANCE TESTS IN LEIGHTON BUZZARD SAND (Dense, Intermediate, Loose densities).
ANGLE OF INCLINATION $\psi = 22.5^{o}$.

TEST NO.	SOIL DENSITY KG/m^3	ANCHOR DIMENSIONS			ANCHOR LOADING			ANCHOR DISPL.	
		D (mm)	B (mm)	$\frac{D}{B}$	R_t (N)	P_u KN/m^2	$\frac{P_u}{\gamma g D}$	δau	$\delta a90\%$
72	1730	76.2	76.2	1	24.3	5.33	4.12	1.29	1.0
73		152.4	76.2	2	108.82	23.86	9.23	2.24	1.1
74		190.5	63.5	3	158.08	49.92	15.44	2.3	1.23
75		203.2	50.8	4	162.79	80.32	23.3	2.61	1.31
76		254	50.8	5	302.92	149.46	34.68	4.51	2.61
77		266.7	38.1	7	303.09	265.85	58.75	3.73	1.65
78		254	25.4	10	266	524.96	121.81	5.0	2.1
79		304.8	25.4	12	396.78	783.1	151.4	7	2.24
80		381	25.4	15	590.14	1164.66	180.16	17.25	3.0
81		431.8	25.4	17	761.5	1502.84	205.12	16.4	3.2
82		508	25.4	20	959.32	1893.2	219.64	18.8	8.6
83	1618	76.2	76.2	1	15.41	3.38	2.79	2.98	1.8
84		152.4	76.2	2	59.89	13.13	5.43	2.98	1.5
85		190.5	63.5	3	86.91	27.44	9.08	6.72	3.0
86		203.2	50.8	4	82.72	40.81	12.66	2.98	1.51
87		254	50.8	5	144.99	71.53	17.75	8.3	5.1
88		266.7	38.1	7	122.95	107.84	25.48	9.6	4
89		254	25.4	10	96.41	190.27	47.21	7.4	3.8
90		304.8	25.4	12	131.99	260.49	54	12.7	4.5
91		381	25.4	15	198.71	392.16	64.87	15	7.5
92		431.8	25.4	17	220.95	436.05	63.64	17.9	7.5
93		508	25.4	20	274.33	541.85	67.22	32.9	10.5
94	1548	76.2	76.2	1	11.9	2.61	2.26	2.24	1.35
95		152.4	76.2	2	37.65	8.26	3.56	10	4.5
96		190.5	63.5	3	51.93	16.4	5.67	3.74	2.24
97		203.2	50.8	4	42.69	21.06	6.82	3.74	2.6
98		254	50.8	5	78.27	38.62	9.98	9.7	3.9
99		266.7	38.1	7	60.67	53.22	13.14	5.77	5.0

TABLE 5.3. CONTINUED

TEST NO.	SOIL DENSITY KG/m^3	ANCHOR DIMENSIONS			ANCHOR LOADING			ANCHOR DISPL.	
		D (mm)	B (mm)	$\frac{D}{B}$	R (N)	P_u KN/m^2	$\frac{P_u}{\gamma g D}$	δau	$\delta a90\%$
100	1548	254	25.4	10	31.68	62.52	16.2	6.72	2.7
101		304.8	25.4	12	49.8	98.28	21.23	9.7	4.1
102		381	25.4	15	56.38	111.27	19.23	9.6	4.5
103		431.8	25.4	17	49.84	98.36	15.63	4.63	3.7
104		508	25.4	20	63.2	124.73	16.69	22.4	11

TABLE 5.4. DETAILS AND RESULTS OF UPLIFT RESISTANCE TESTS IN LEIGHTON BUZZARD SAND (Dense, Intermediate, Loose densities) ANGLE OF INCLINATION $\psi = 45^{\circ}$.

TEST NO.	SOIL DENSITY KG/m^3	ANCHOR DIMENSIONS			ANCHOR LOADING			ANCHOR DISPL.	
		D (mm)	B (mm)	$\frac{D}{B}$	R (N)	P_u KN/m^2	$\frac{P_u}{\gamma g D}$	δau	$\delta a90\%$
105	1730	76.2	76.2	1	43.8	9.6	7.43	1.5	0.9
106		152.4	76.2	2	186.7	40.94	15.83	3.35	2.1
107		190.5	63.5	3	253.4	80.01	24.75	4.48	2.59
108		203.2	50.8	4	240.7	118.76	34.44	4.58	3.91
109		254	50.8	5	449.8	221.92	51.49	6.72	3.7
110		266.7	38.1	7	423.3	371.29	82.05	5.53	2.98
111		254	25.4	10	303.3	598.57	138.89	13	3.5
112		304.8	25.4	12	459.1	906.05	175.19	14.7	4.14
113		381	25.4	15	667.01	1316.36	203.62	21.7	6.05
114		431.8	25.4	17	846	1669.6	227.88	26.2	6.3
115		508	25.4	20	1046.2	2064.7	239.54	39.8	11.8
116	1618	76.2	76.2	1	20	4.39	3.63	3.5	2.5
117		152.4	76.2	2	77	16.88	6.98	8	2.7
118		190.5	63.5	3	120.4	38.02	12.58	8.3	5.2
119		203.2	50.8	4	125	61.67	19.13	7	4.6
130		254	50.8	5	196.3	96.85	24.03	13	6.1
121		266.7	38.1	7	172.14	150.95	35.67	31.36	14.3
122		254	25.4	10	101.08	199.48	49.49	26.9	9
123		304.8	25.4	12	152.15	300.27	62.08	15.74	7.84
124		381	25.4	15	207	408.52	67.57	23	11.87
125		431.8	25.4	17	254.4	502.06	73.28	32.9	15.3
126		508	25.4	20	274.56	541.85	67.22	31.33	18.3
127	1548	76.2	76.2	1	26.5	5.81	5.02	2.98	1.53
128		152.4	76.2	2	51.95	11.39	4.67	8.96	4.48
129		190.5	63.5	3	80.3	25.36	8.76	12.75	7.31
130		203.2	50.8	4	64	31.58	10.73	17	10
131		254	50.8	5	107.3	52.94	13.72	14.3	8.9
132		266.7	38.1	7	85.26	74.78	18.46	17.9	9

TABLE 5.4. CONTINUED

TEST NO.	SOIL DENSITY KG/m^3	ANCHOR DIMENSIONS D (mm)	B (mm)	$\frac{D}{B}$	ANCHOR LOADING R (N)	P_u KN/m^2	$\frac{P_u}{\gamma g D}$	ANCHOR DISPL. δau	$\delta a90\%$
133	1548	254	25.4	10	30	59.2	15.35	8.0	6.0
134		254	25.4	10	32	63.15	16.37	8.3	6.2
135		381	25.4	15	56.6	111.7	19.3	8.96	5.4
136		431.8	25.4	17	65.5	129.27	19.72	13.42	6.61
137		508	25.4	20	94.3	186.1	24.14	25	12

TABLE 5.5. DETAILS OF THE SURFACE FAILURE DIMENSIONS FOR ALL DENSITIES AND ANGLES OF INCLINATION

TEST NO.	ANGLE OF INCLINATION ψ	SOIL DENSITY γ KG/m^3	ANCHOR DIMENSIONS			SURFACE DEFORMATION DIMENSIONS		SURFACE DEFORMATION RATIOS	
			D (mm)	B (mm)	$\frac{D}{B}$	B_{sj} (mm)	B_{sn} (mm)	$\frac{B_{sj}}{B}$	$\frac{B_{sn}}{B}$
5	0°	1730	152.4	50.8	3	216		4.25	
6			203.2	50.8	4	254		5	
8			304.8	50.8	6	343		6.75	
18		1618	76.2	76.2	1	140		1.83	
20			152.4	76.2	2	203		2.67	
22			190.5	63.5	3	203		3.2	
39		1548	76.2	76.2	1	89		1.17	
72	22.5°	1730	76.2	76.2	1	178	152	2.33	2
73			152.4	76.2	2	305	254	4	3.33
74			190.5	63.5	3	355	305	5.6	4.8
75			203.2	50.8	4	305	254	6	5
83		1618	76.2	76.2	1	165	127	2.17	1.67
84			152.4	76.2	2	216	191	2.83	2.5
94		1548	76.2	76.2	1	152	127	2	1.67
95			152.4	76.2	2	229	178	3	2.33
105	45°	1730	76.2	76.2	1	216	152	2.83	2
106			152.4	76.2	2	254	229	3.33	3
107			190.5	63.5	3	254	229	4	3.6
109			254	50.8	5	305	254	6	5
116		1618	76.2	76.2	1	229	178	3	2.33
117			152.4	76.2	2	203	178	2.67	2.33
118			190.5	63.5	3	305	203	4.8	3.2
127		1548	76.2	76.2	1	216	152	2.83	2
128			152.4	76.2	2	254	178	3.33	2.33

1 portal frame with pulleys
2 sand spreader rig
3 sand container rig
4 sand tank
5 sand spreader
6 anchor plate
7 motor, gear box and converter
8 load cell
9 anchor displacement transducer
10 rotating bush
11 motor and connecting rod
12 surface deformation transducers
13 deformation transducer gantry
14 power supplies voltmeter amplifier and data logger
15 printer & tape punch
16 aluminum plate

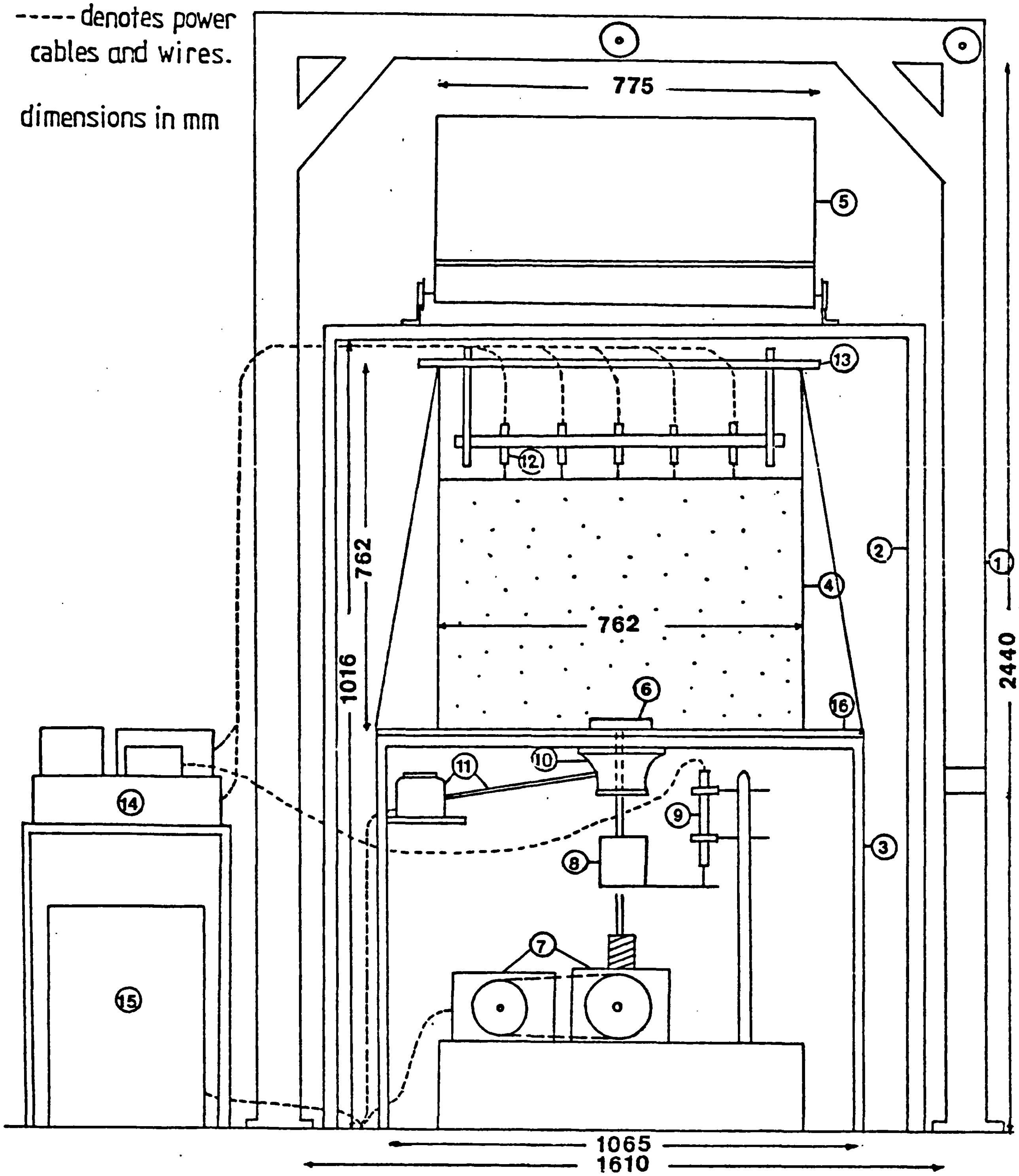

FIG. 5.1 ELEVATION VIEW OF GENERAL APPARATUS FITTED FOR PUSHOUT DISPLACEMENT-CONTROLLED LOADING.

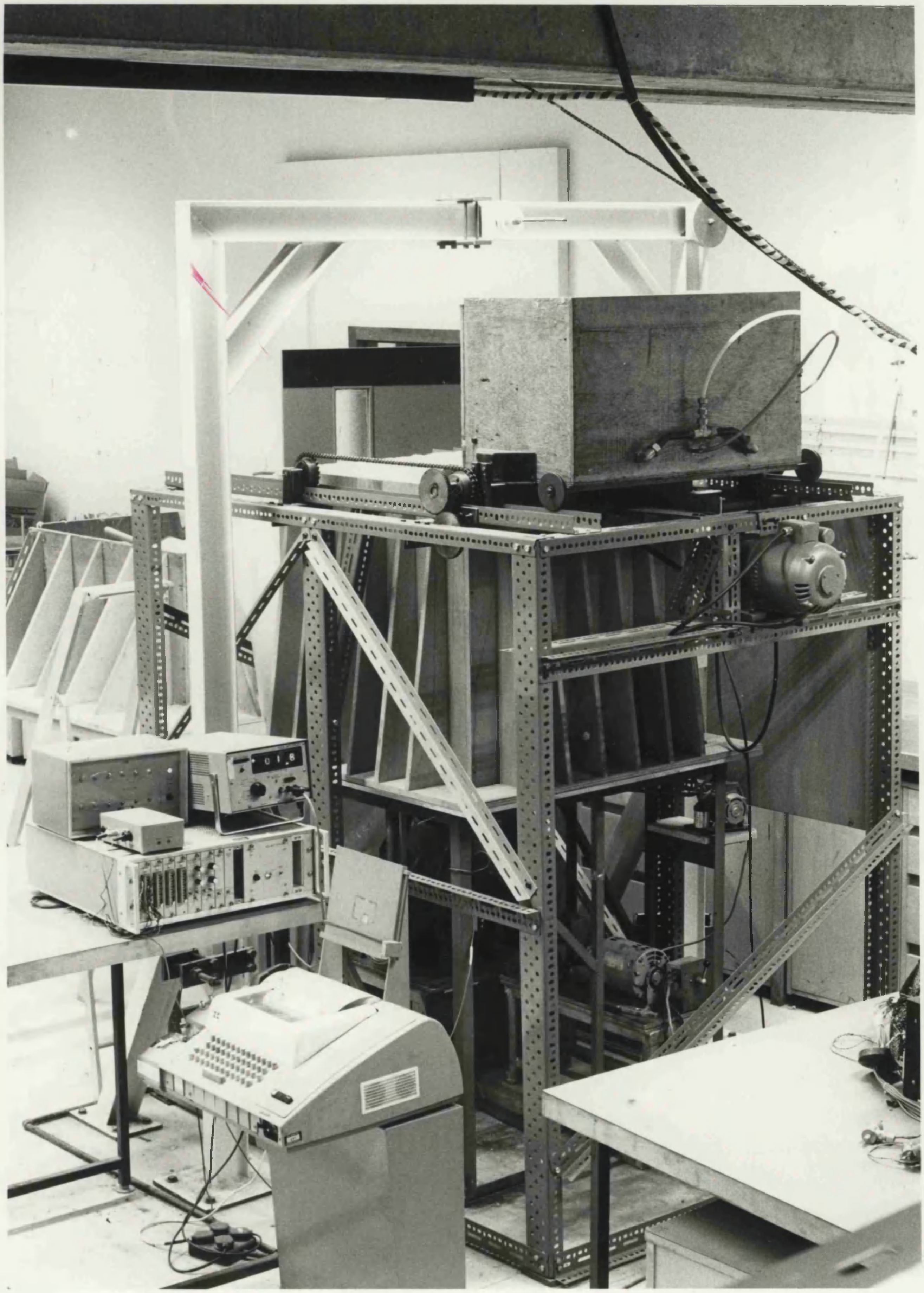

FIG. 5.2 LOAD TEST APPARATUS

FIG. 5.3 PHOTOGRAPHIC TEST APPARATUS

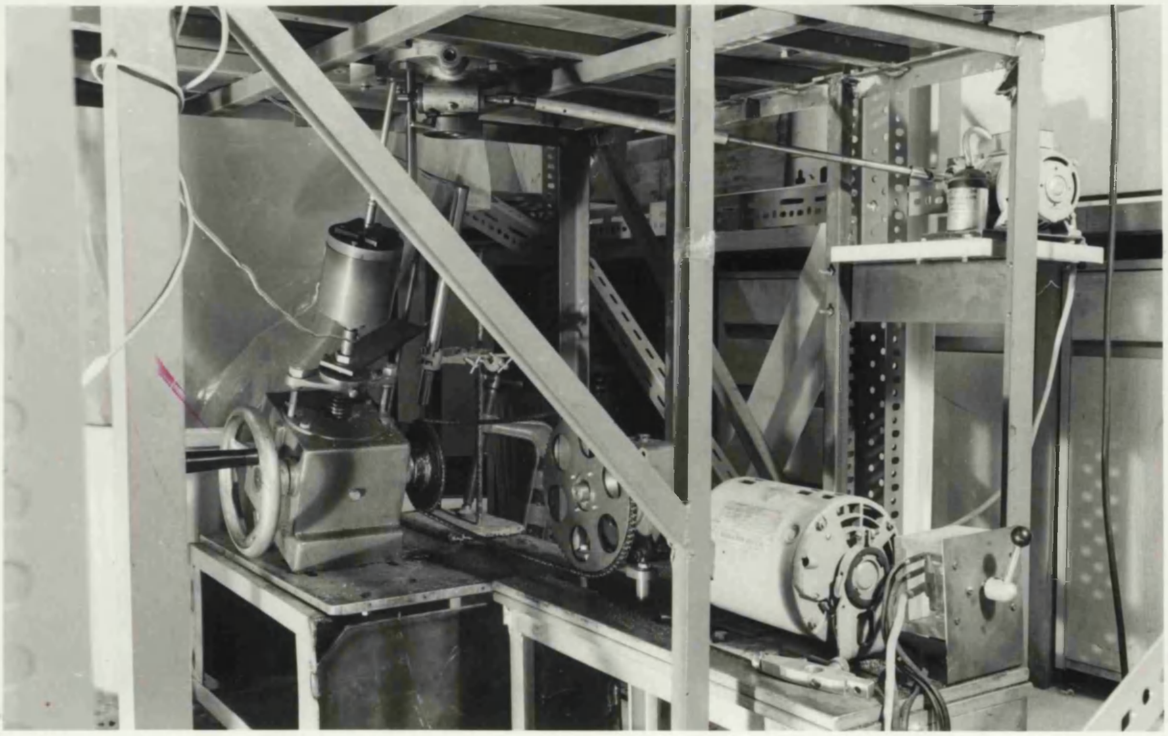

FIG. 5.4 ARRANGEMENT OF THE LOADING SYSTEM

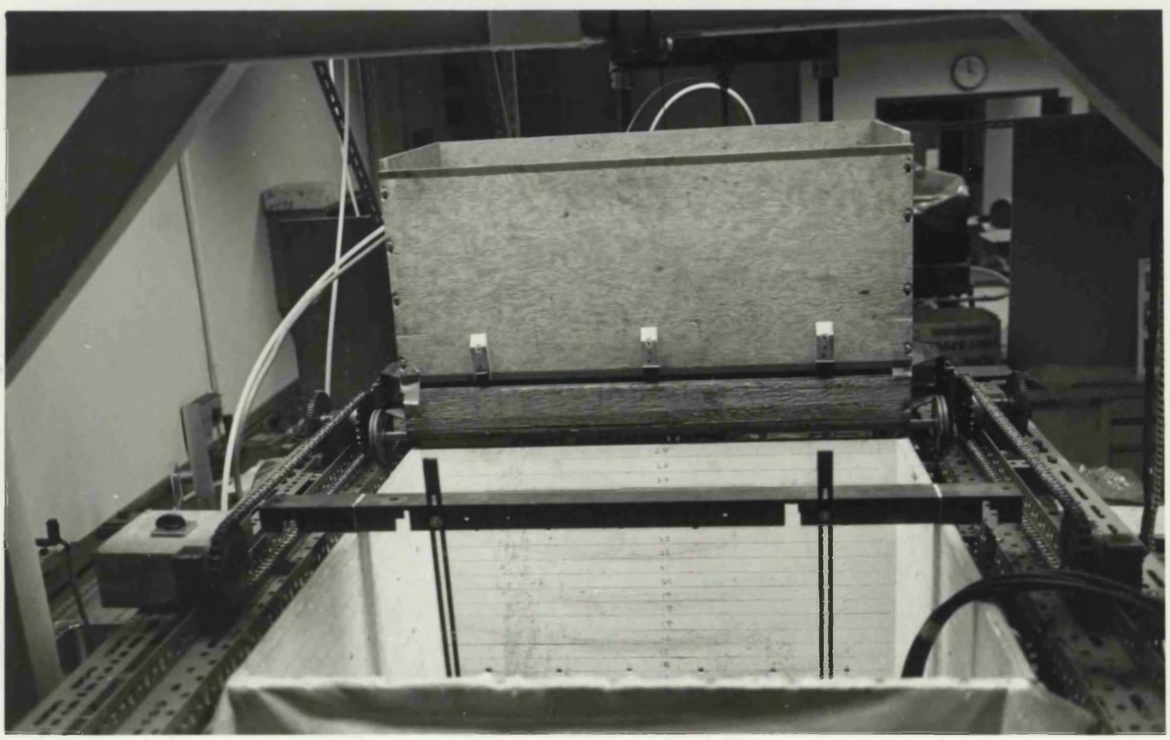

FIG. 5.5 AIR ACTIVATED SAND SPREADER

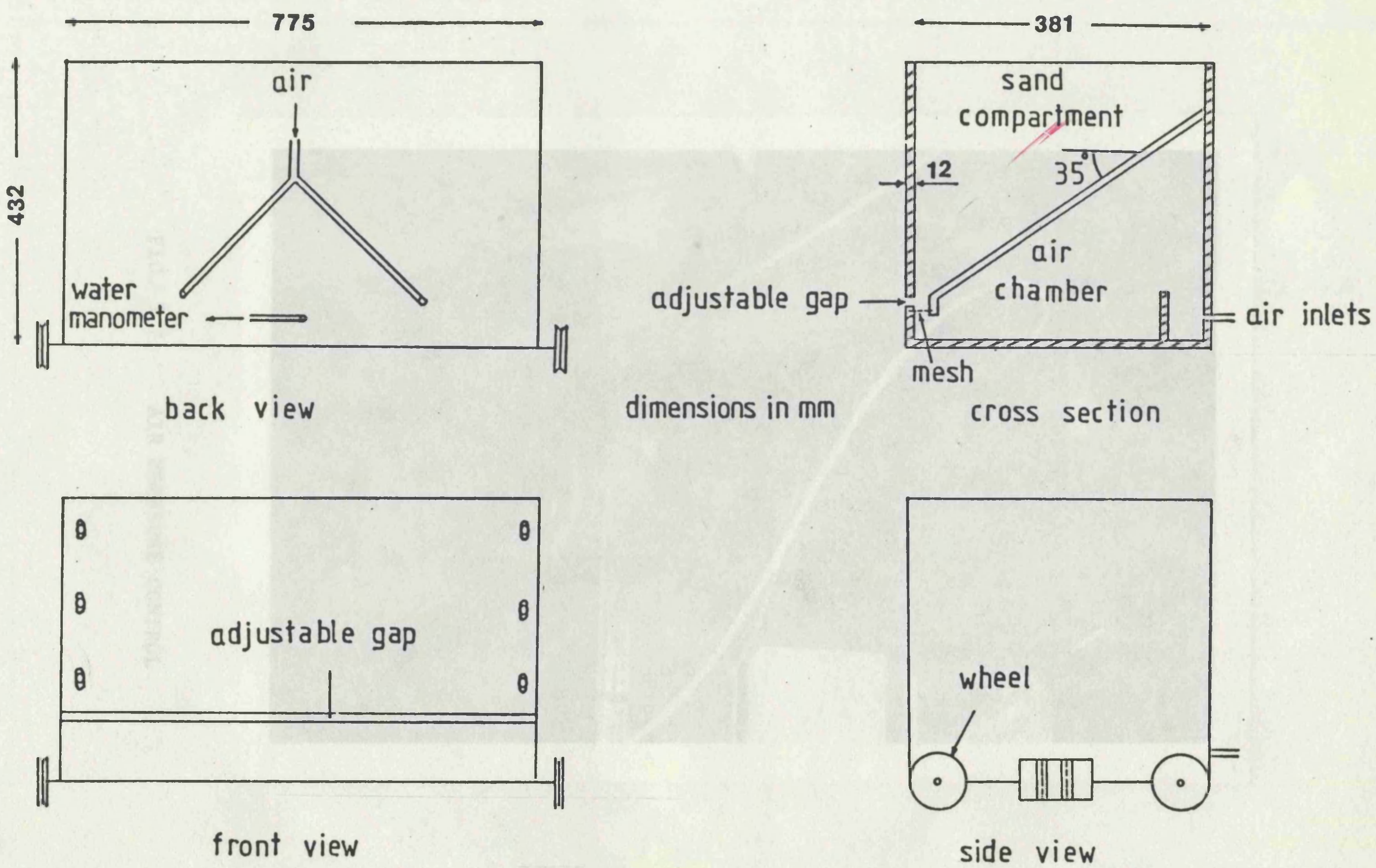

FIG. 5.6 DIAGRAM OF THE SAND SPREADER BOX.

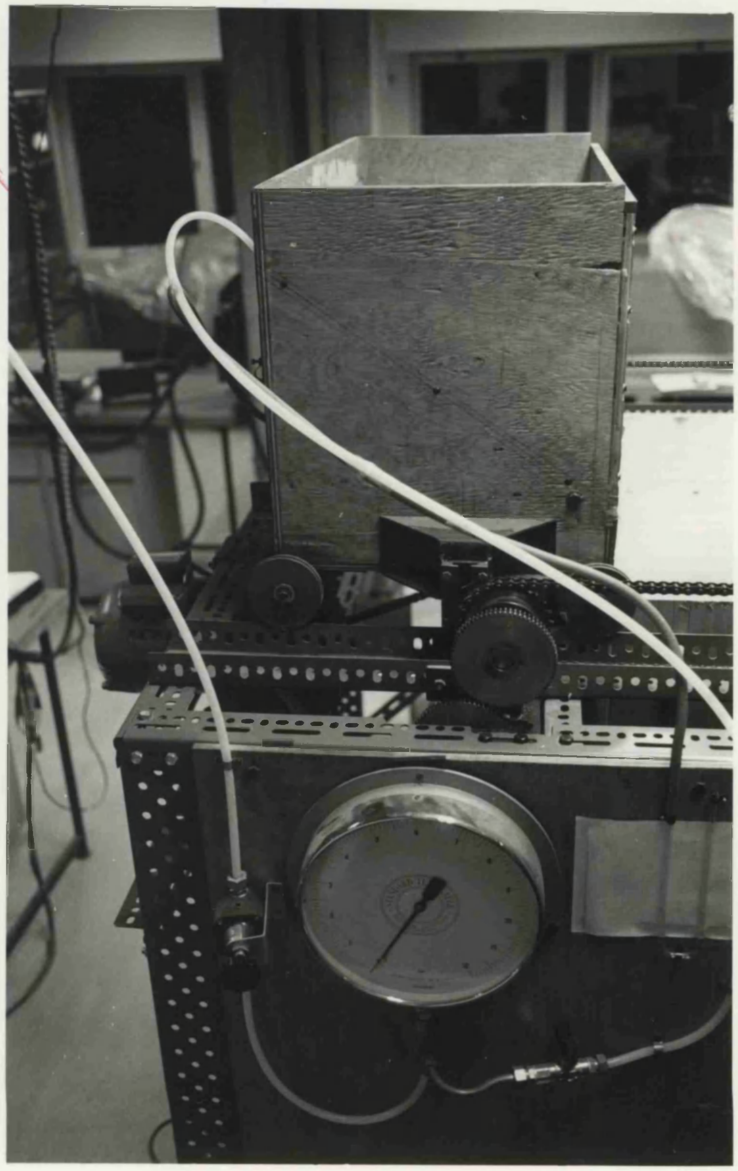

FIG. 5.7 AIR PRESSURE CONTROL

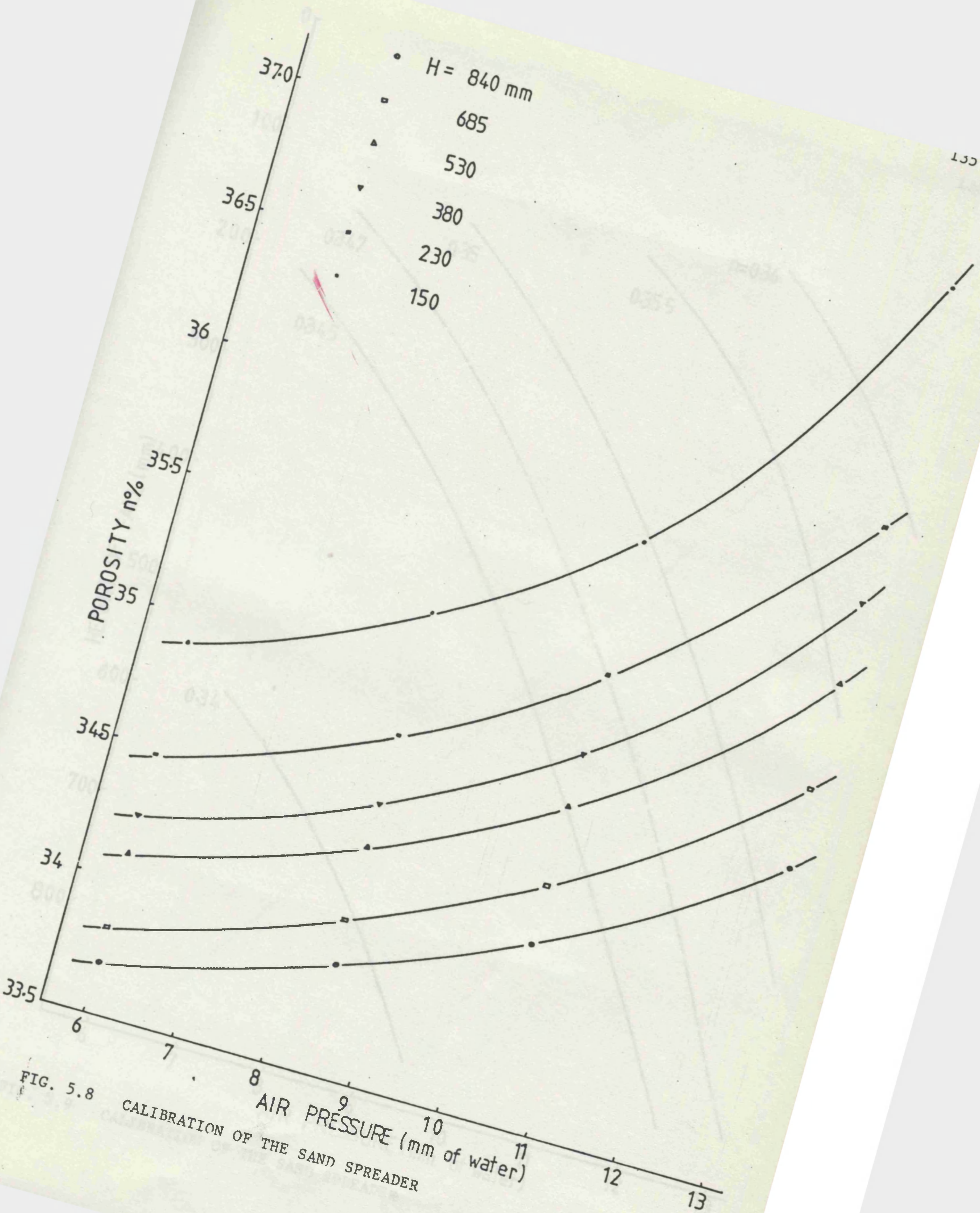

FIG. 5.8 CALIBRATION OF THE SAND SPREADER

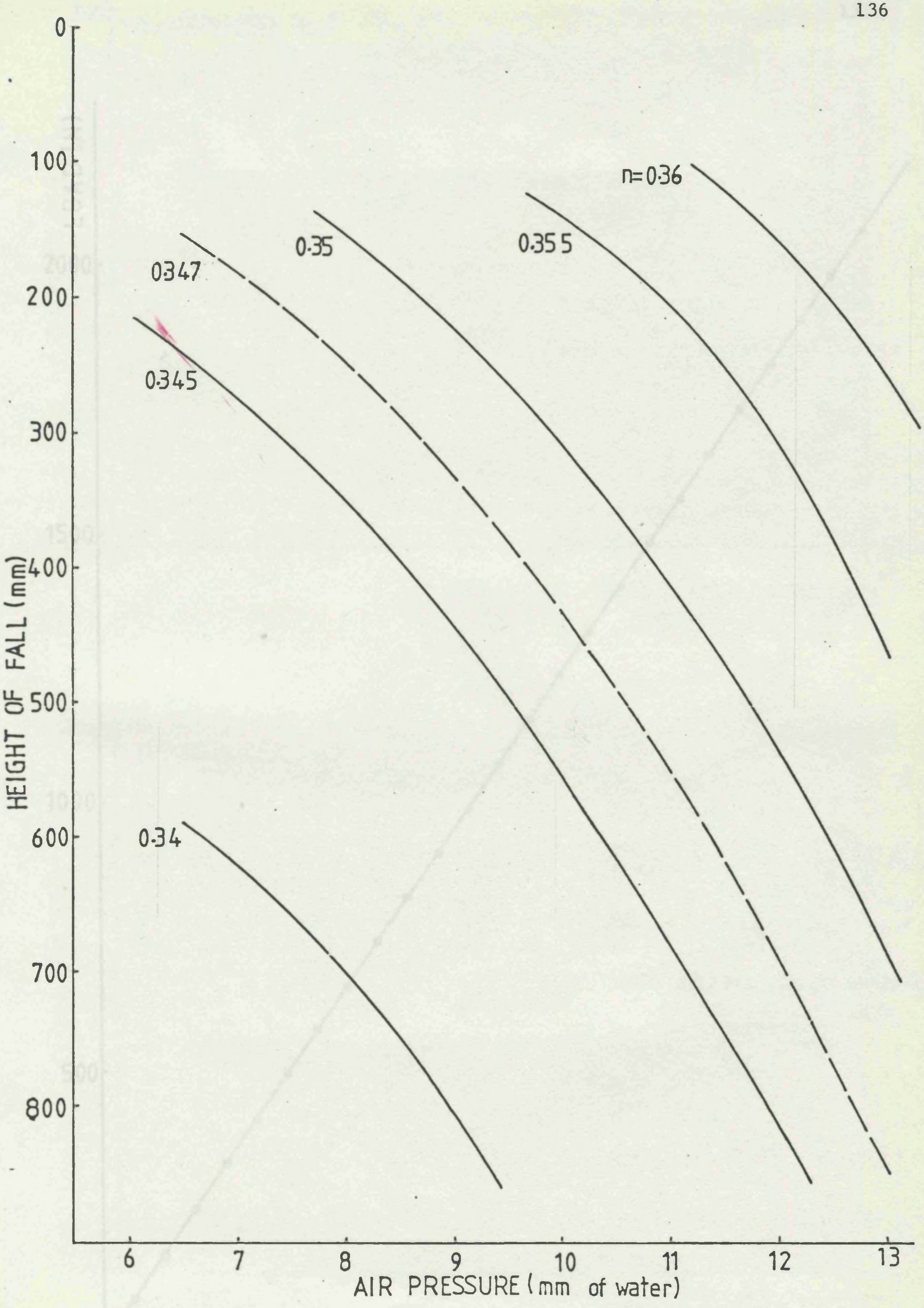

FIG. 5.9 CALIBRATION OF THE SAND SPREADER

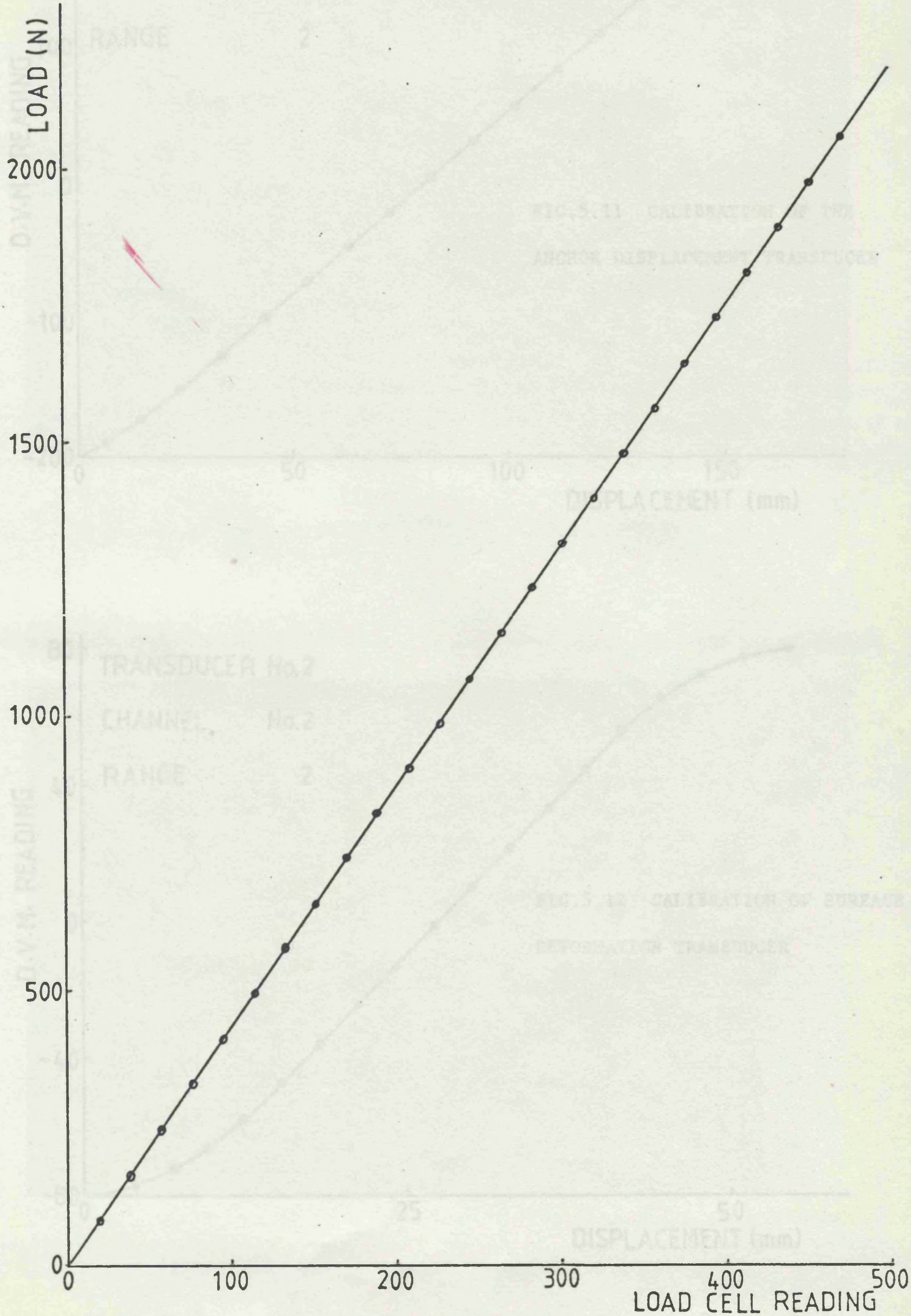

FIG. 5.10 CALIBRATION OF THE LOAD CELL

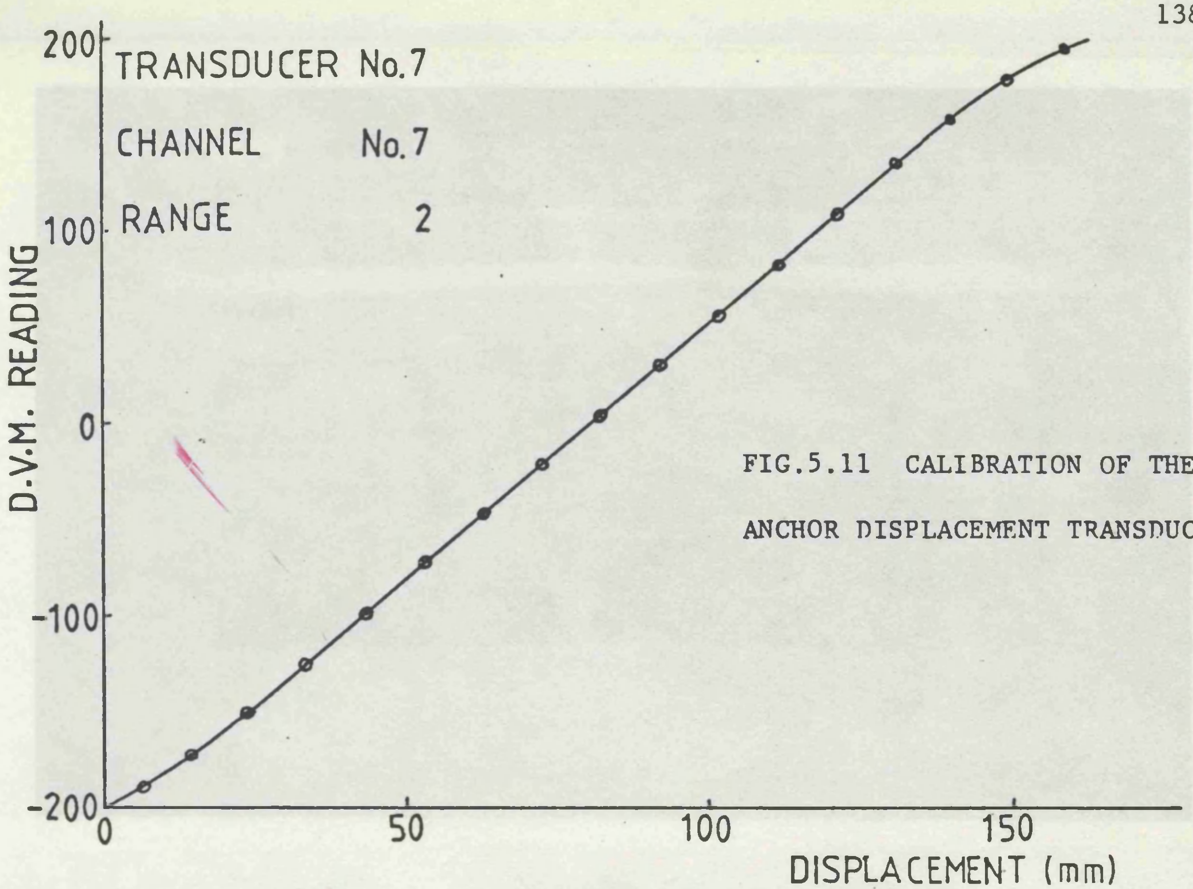

FIG.5.11 CALIBRATION OF THE ANCHOR DISPLACEMENT TRANSDUCER

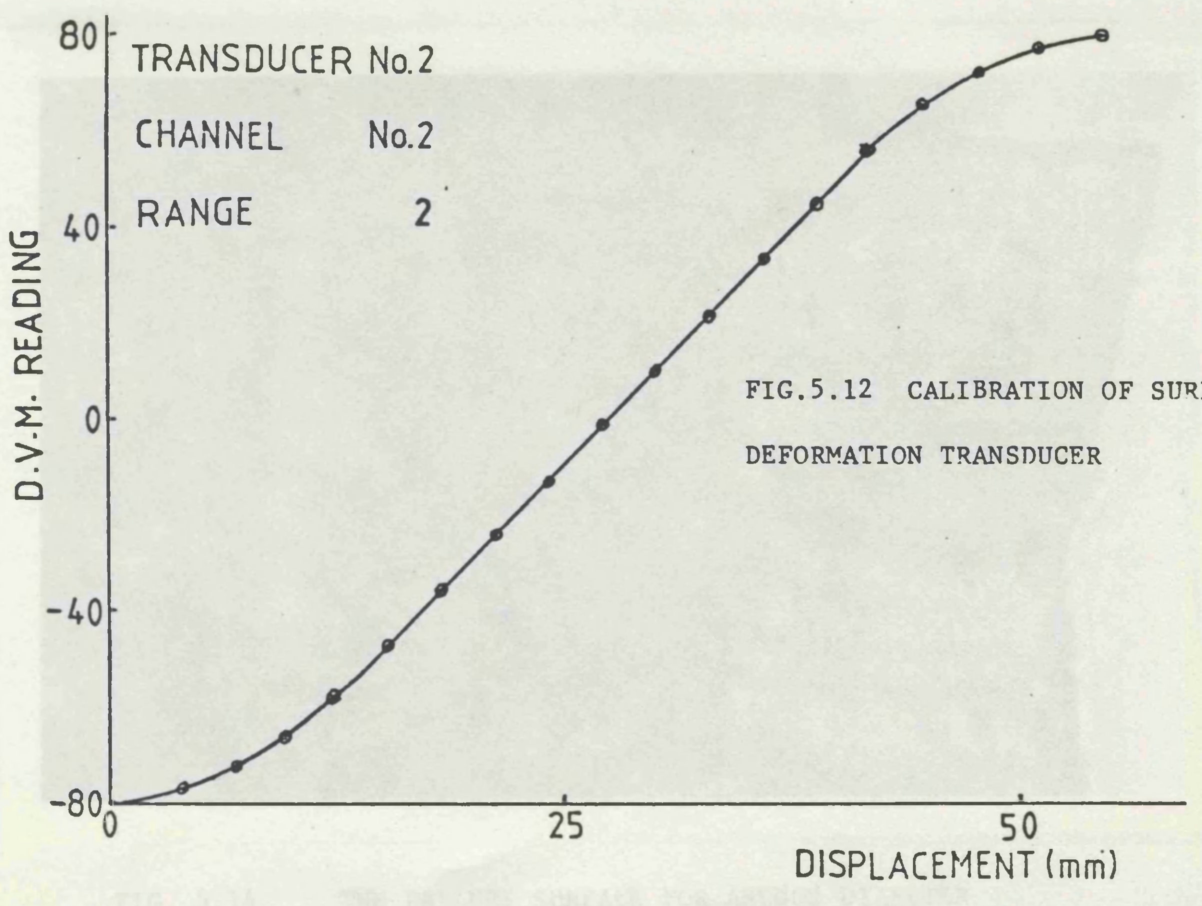

FIG.5.12 CALIBRATION OF SURFACE DEFORMATION TRANSDUCER

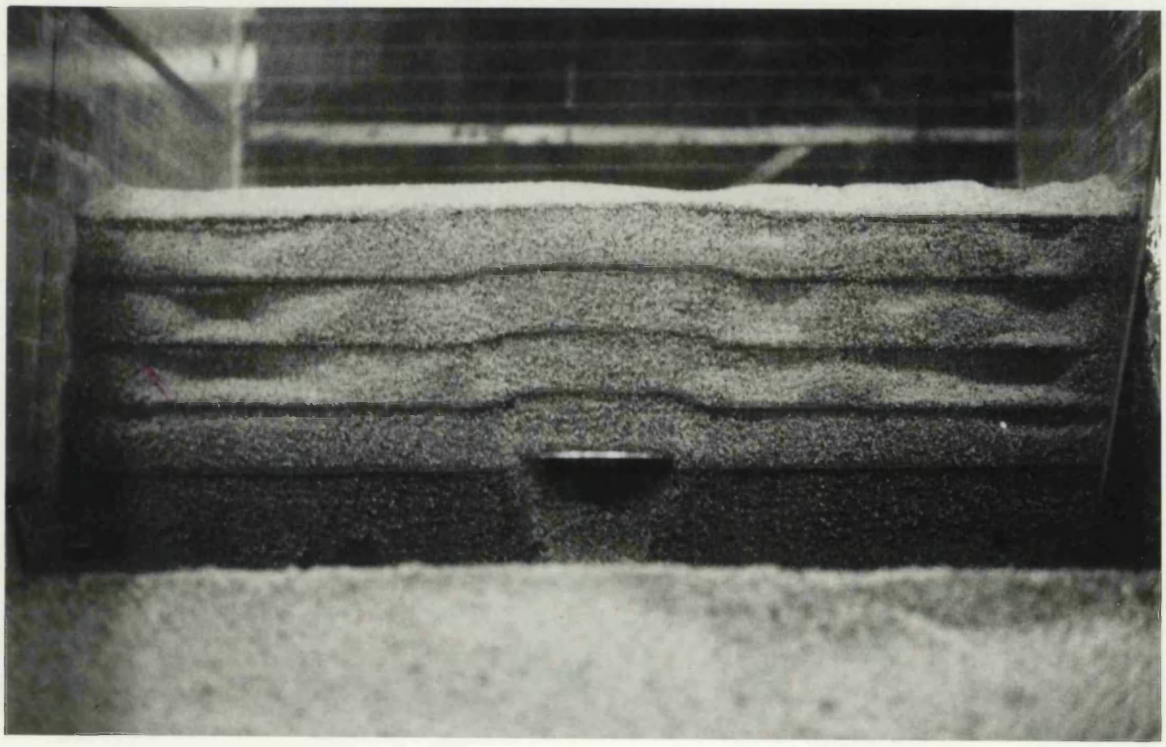

FIG. 5.13 THE FAILURE SURFACE FOR ANCHOR DIAMETER = 77 mm and $\frac{D}{B} = 2$.

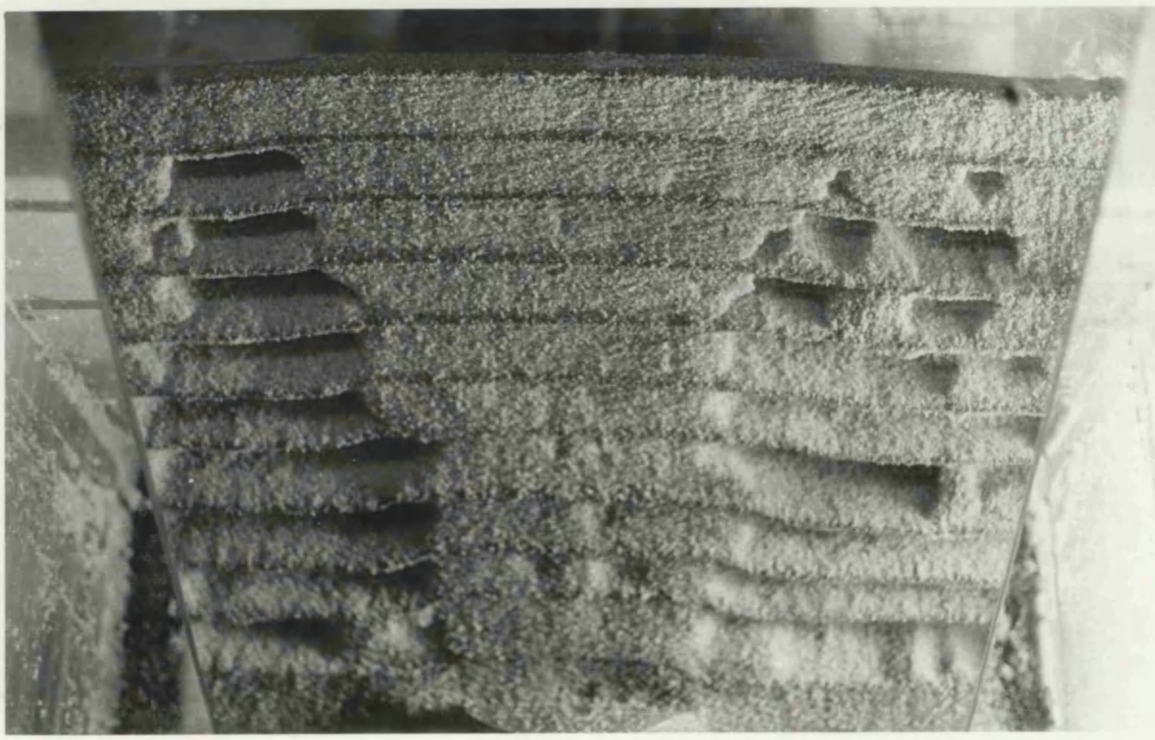

FIG. 5.14 THE FAILURE SURFACE FOR ANCHOR DIAMETER = 135 mm and $\frac{D}{B} = 3$.

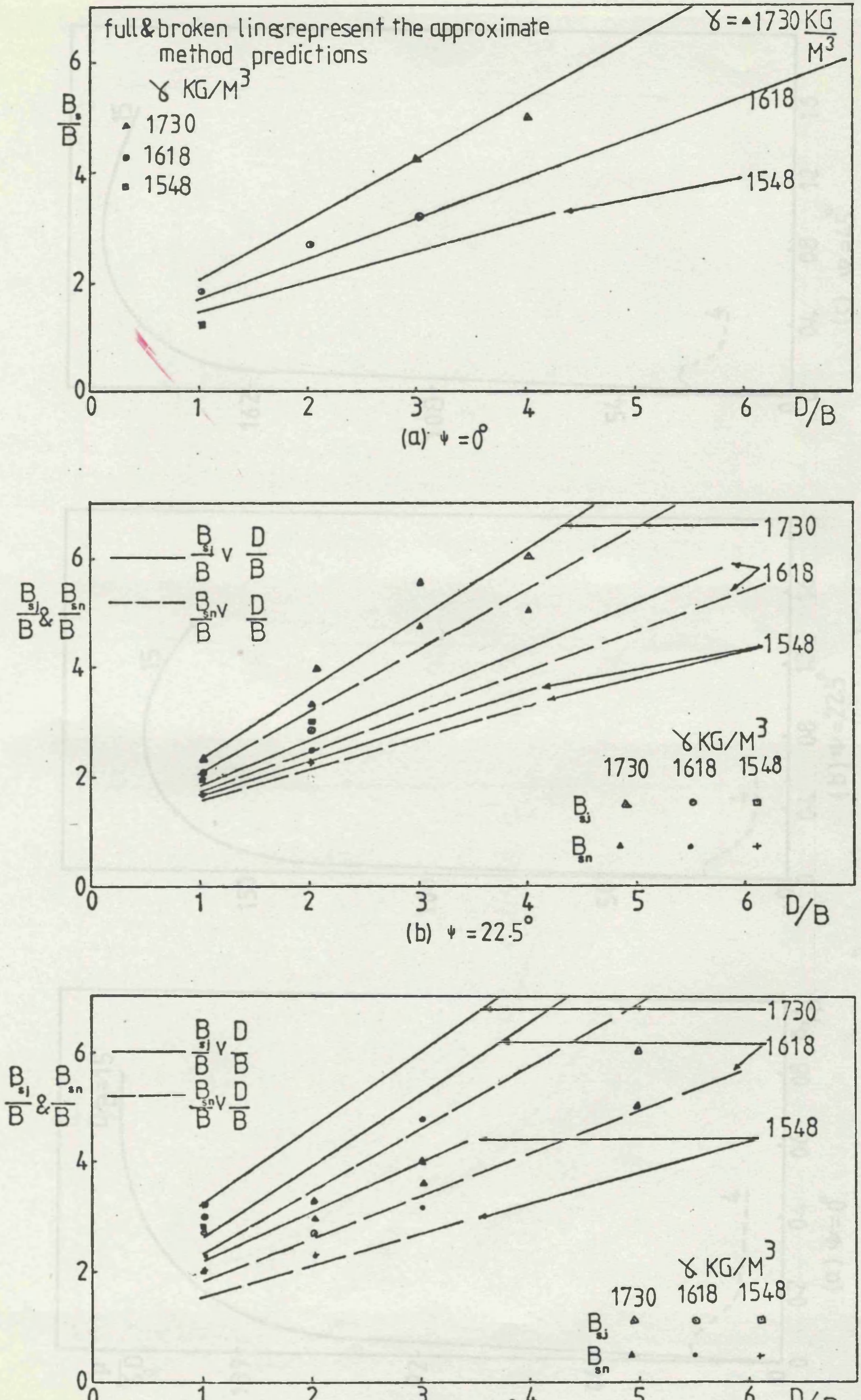

FIG.5.15 RATIO OF SURFACE FAILURE BULGE DIAMETERS TO ANCHOR DIAMETER VERSUS D/B

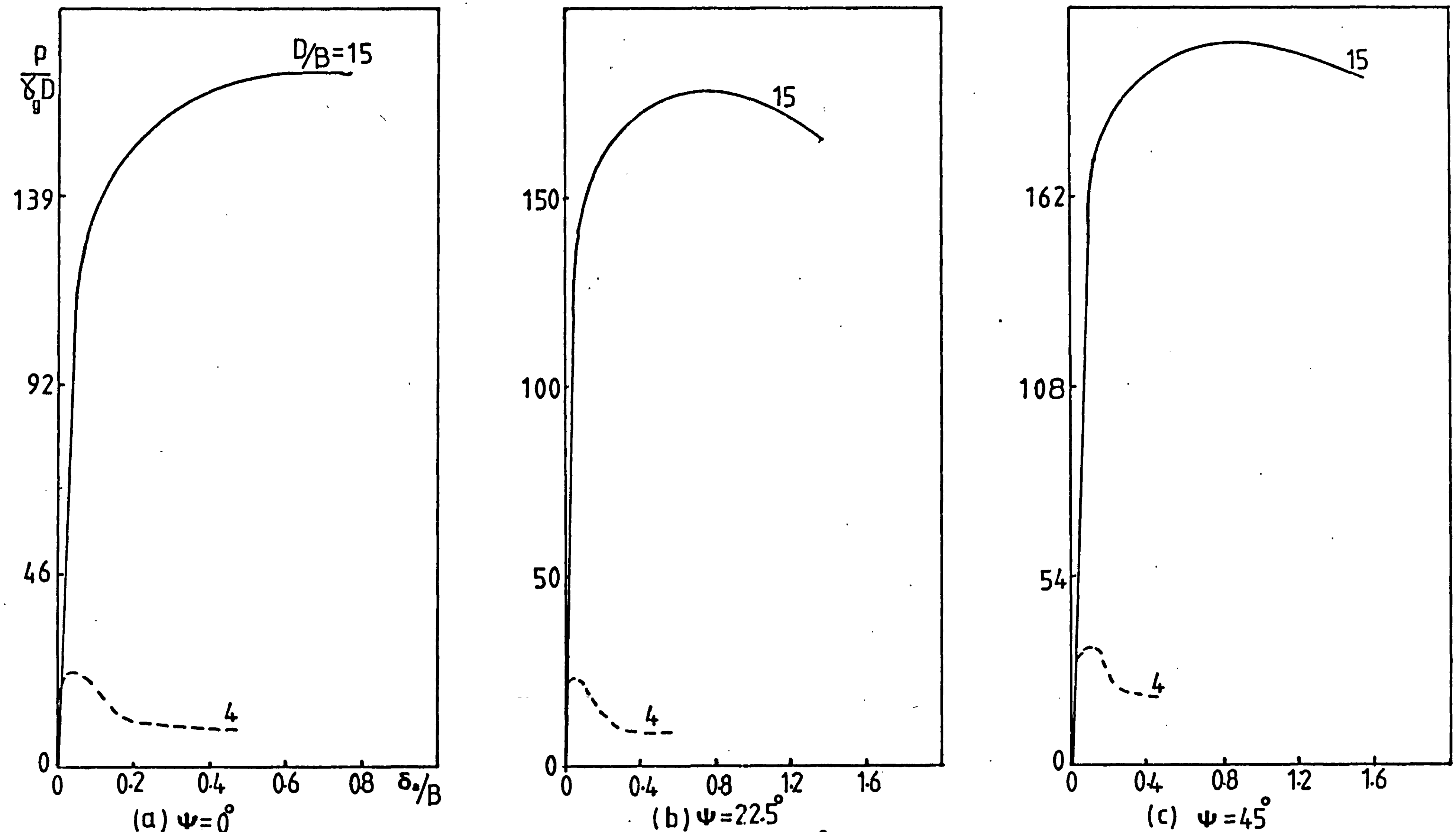

FIG.5.16 EFFECT OF VARIATION OF $\frac{D}{B}$ FOR CONSTANT γ = 1730 kg/M^3

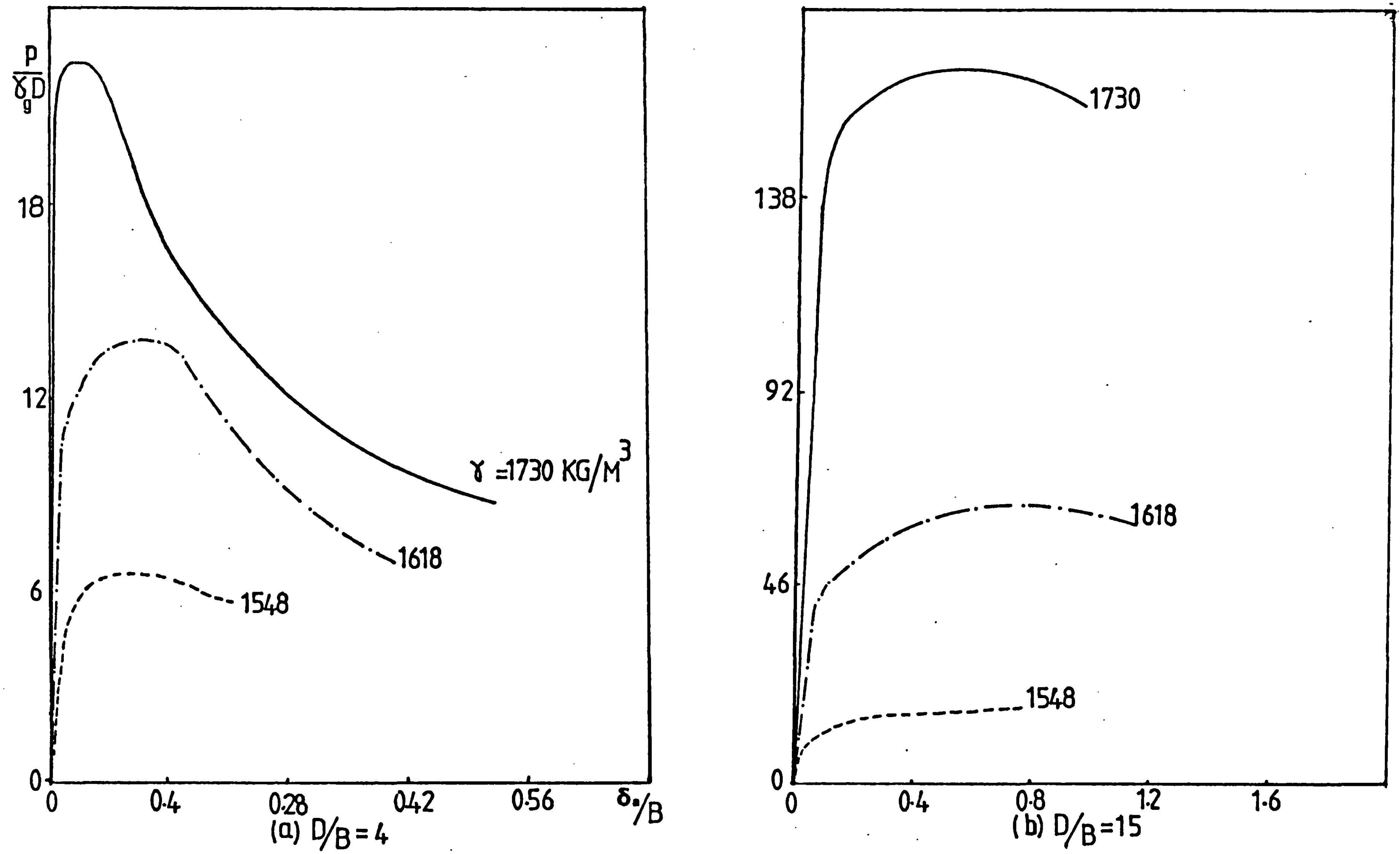

FIG.5.17 EFFECT OF VARIATION OF γ FOR CONSTANT $\psi = 0^{\circ}$

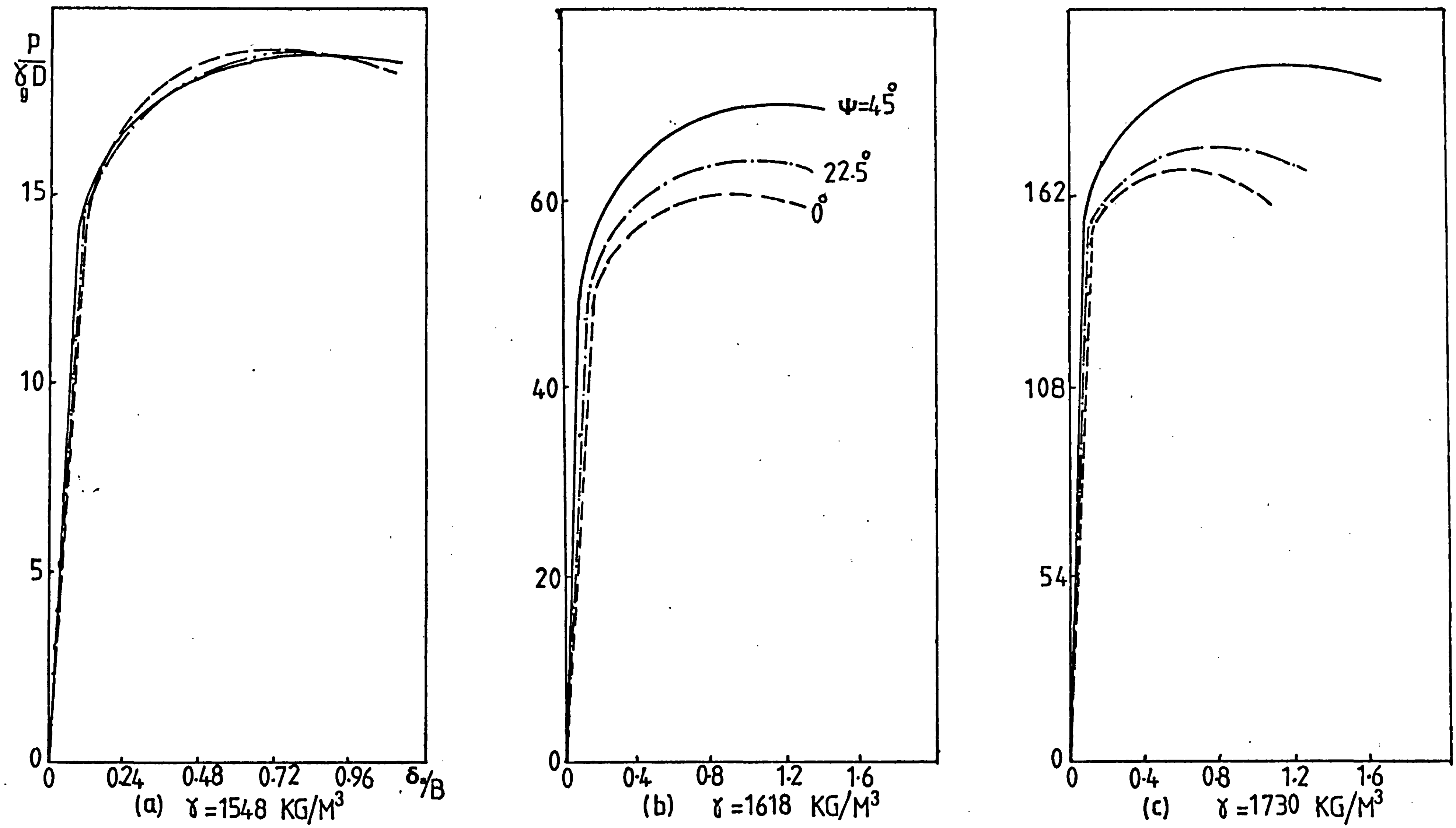

FIG.5.18 EFFECT OF VARIATION OF ψ FOR CONSTANT $\frac{D}{B}$ = 15

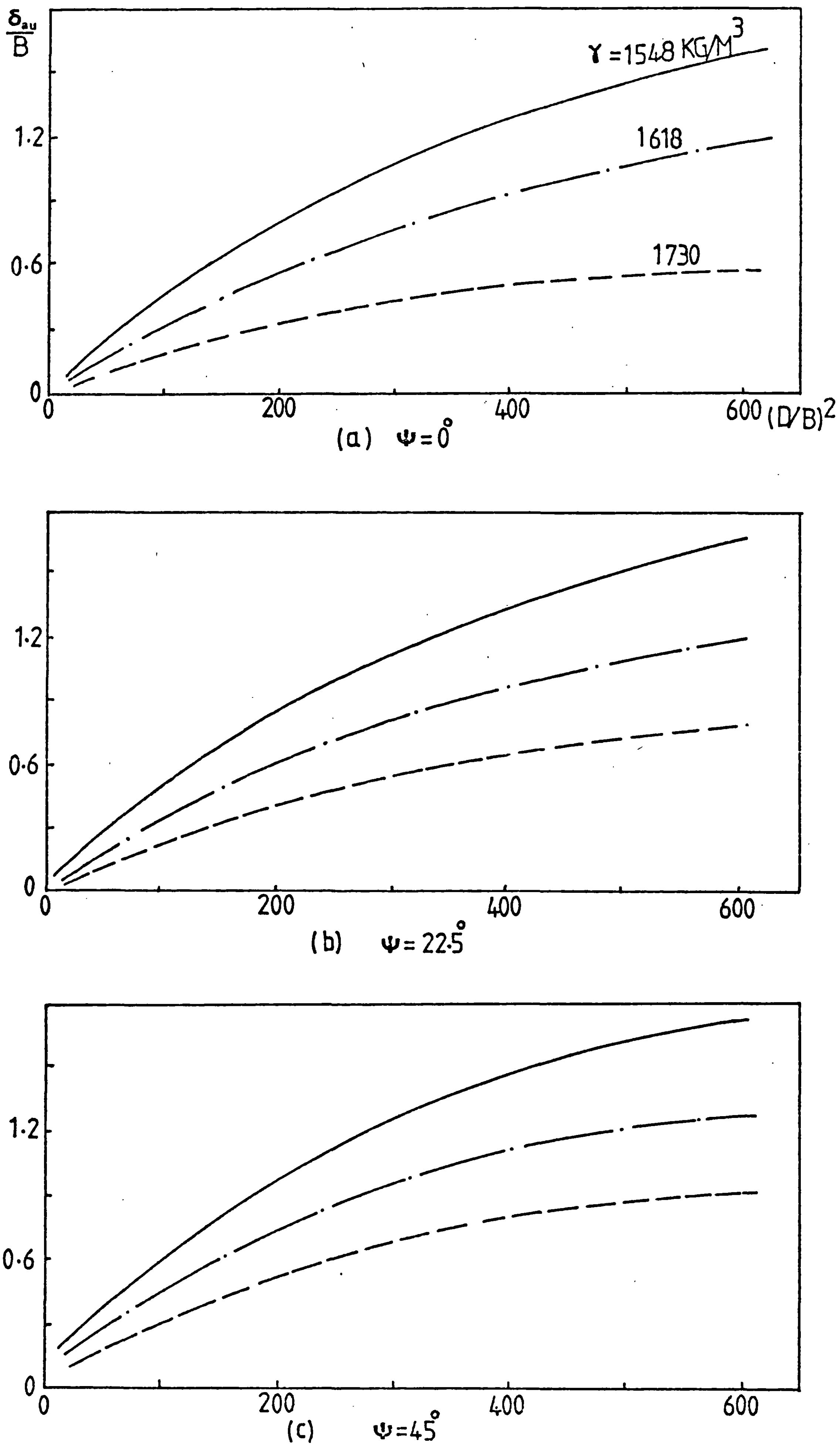

FIG.5.19 ANCHOR DISPLACEMENT RATIO AT ULTIMATE LOAD VERSUS $(\frac{D}{B})^2$

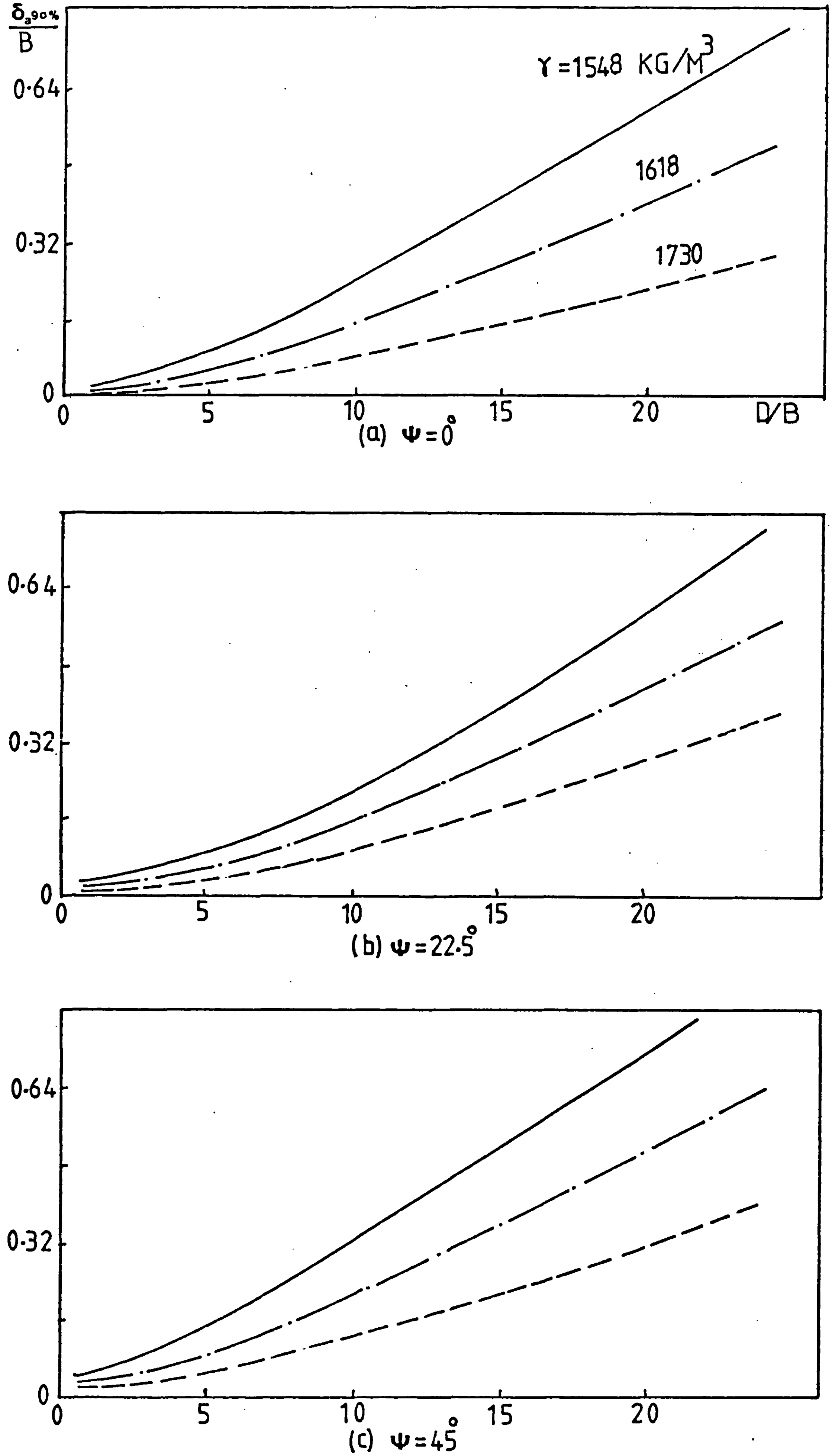

FIG.5.20 ANCHOR DISPLACEMENT RATIO AT 90% OF ULTIMATE LOAD VERSUS D/B.

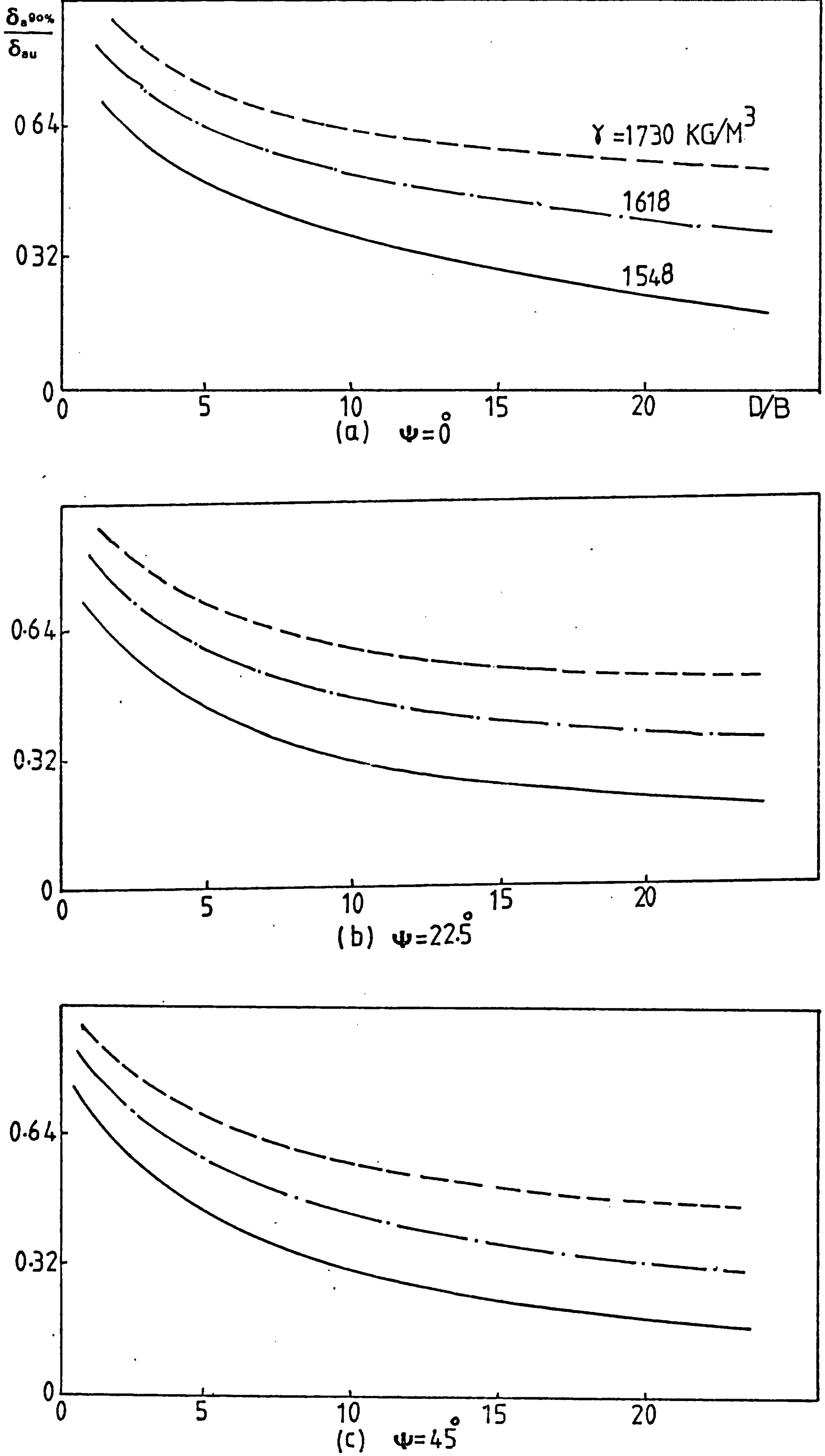

FIG.5.21 ANCHOR DISPLACEMENT RATIO AT 90% AND ULTIMATE LOAD VERSUS D/B.

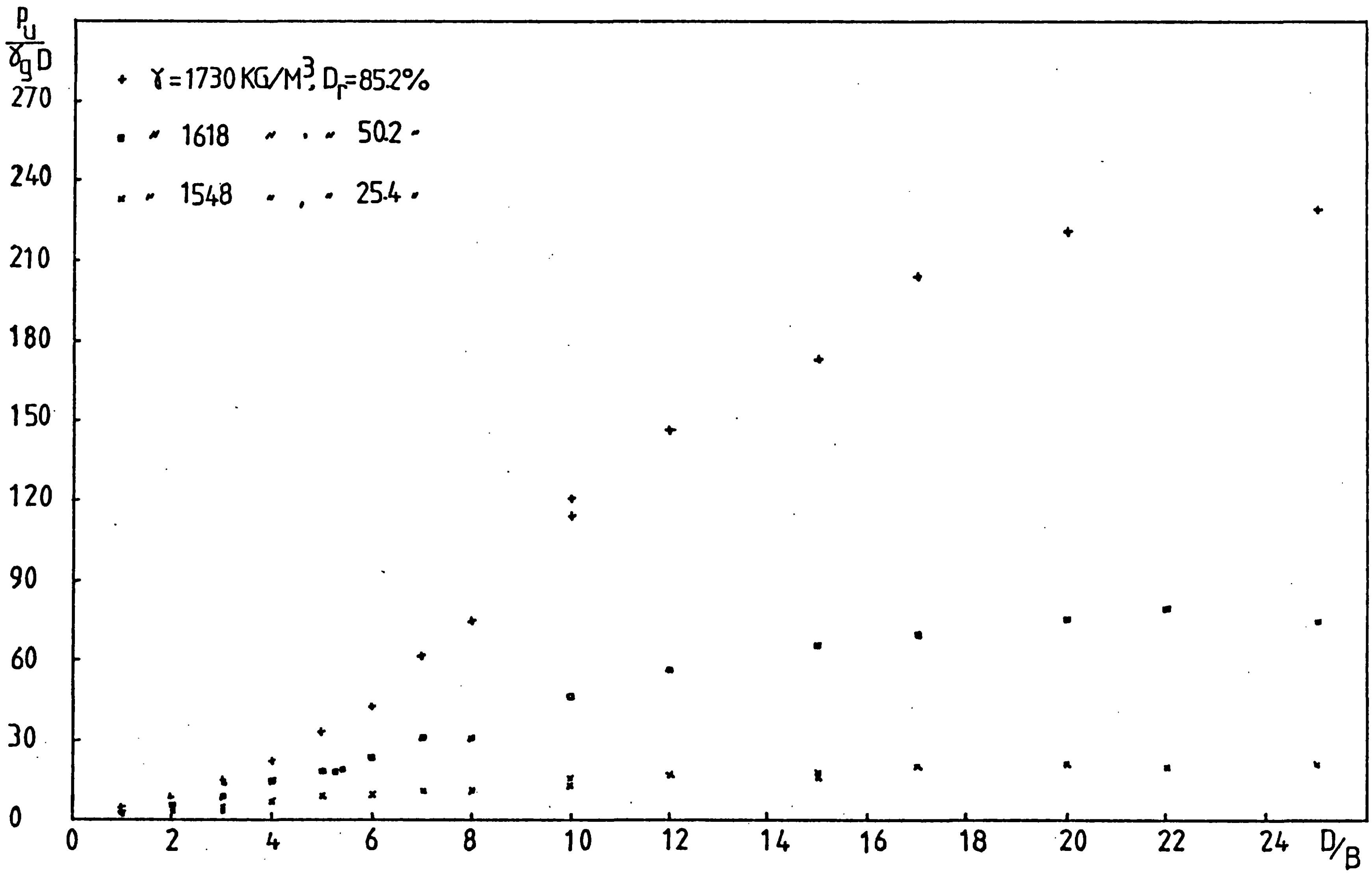

FIG.5.22 $\frac{pu}{\gamma gD}$ V $\frac{D}{B}$ FOR DIFFERENT DENSITIES IN SAND ($\psi = 0^o$)

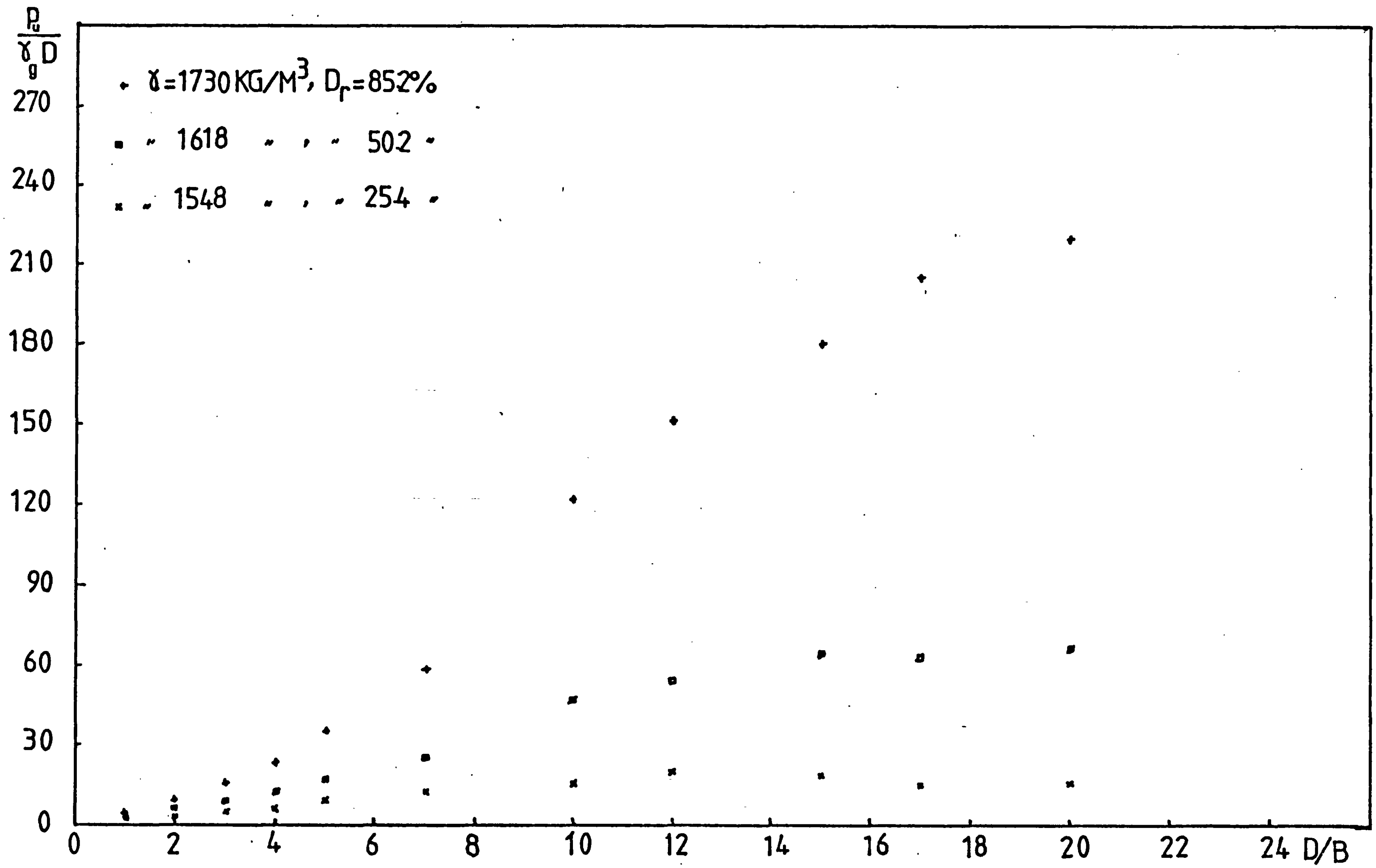

FIG.5.23 $\frac{pu}{\gamma gD}$ V $\frac{D}{B}$ FOR DIFFERENT DENSITIES IN SAND (ψ = 22.5°)

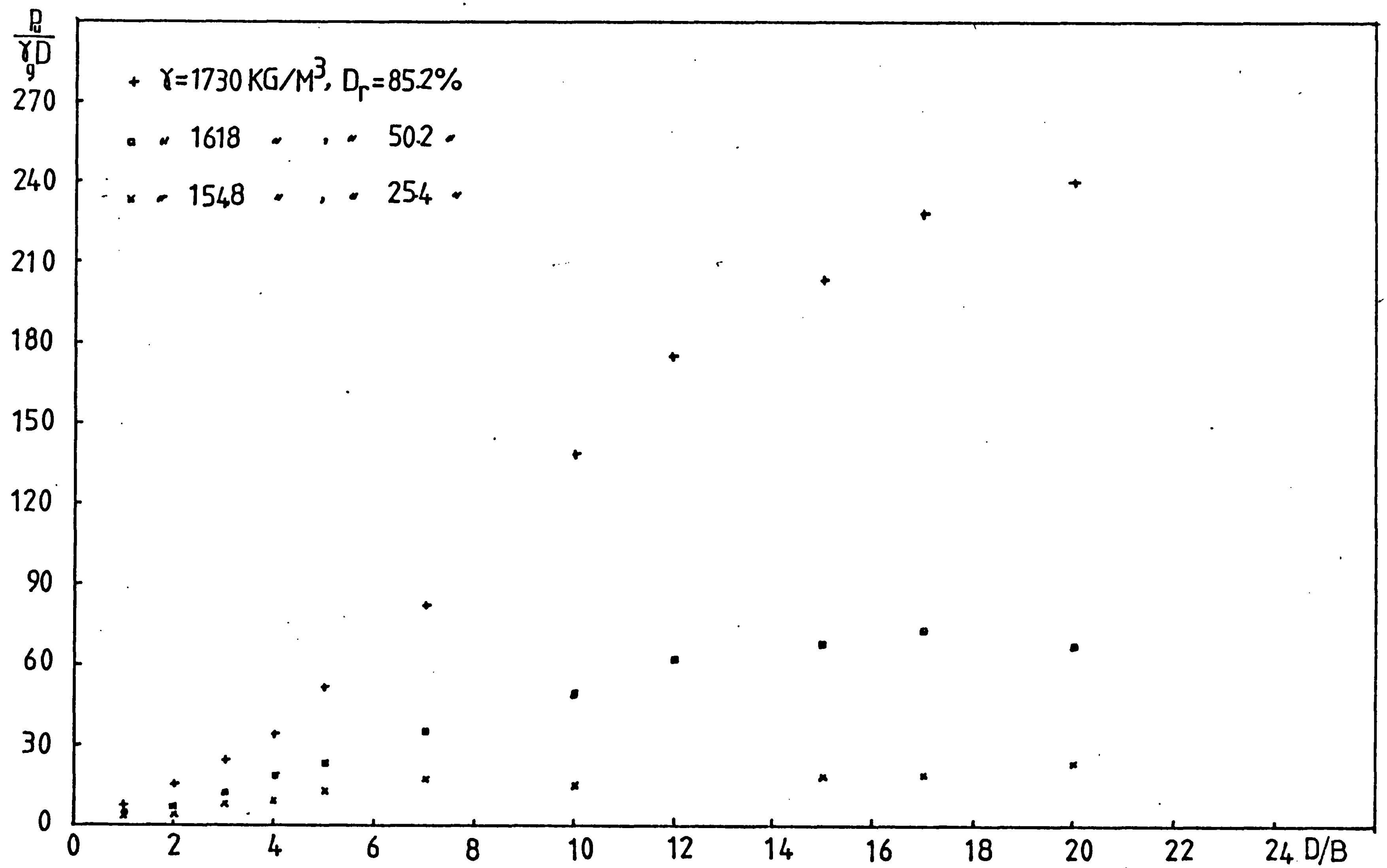

FIG.5.24 $\frac{pu}{\gamma gD}$ V $\frac{D}{B}$ FOR DIFFERENT DENSITIES IN SAND (ψ = 45^o)

CHAPTER 6

FINITE ELEMENT ANALYSIS

CHAPTER 6

FINITE ELEMENT ANALYSIS

6.1. INTRODUCTION:-

The results obtained from the laboratory model tests include load-displacement relationships of circular plate anchors embedded in cohesionless soils. The values of ultimate load, the surface deformation during the test and the internal deformations at failure were also examined.

Measurements of the magnitude and distribution of the stresses and displacements within the sand during the uplift resistance tests were not taken due to the difficulties involved. These stresses and displacements can be assessed however by developing a theoretical method of their prediction during the elastic and plastic stages of the tests. Various numerical methods are possible. Among these methods the finite element method has been chosen as it is a useful technique for tackling a wide variety of problems that have defied conventional and closed-form solutions encountered in soil mechanics.

This method is based on the principle of discretization in which a continuum constituting the system is discretized into smaller equivalent units. With the availability of large high-speed digital computers and efficient computer programs, a wide range of continuum mechanics problems can be analysed by the finite element method.

The advantages of finite element over other numerical methods is the ability to formulate solutions for individual elements before putting them together to represent the entire problem and the variety of ways in which the properties of the individual elements can be formulated. The finite element method can account for non-homogenity by assigning different properties to different elements and geometric representation. The advantage of changing the size of the elements as necessary allows for the most efficient approximation to the continuum.

On the other hand the accuracy of the results depends mainly on the accuracy of the data used. Unlike other engineering materials soils are multi-phase in nature, possess anisotropic and complex nonlinear material properties as well as consisting of discontinuities. The soil media is an infinite system and hence its representation as a finite model of limited extent requires careful consideration. The representation of the laboratory data to the actual field conditions of complex stress system is sometimes questionable. However the limitation of the accuracy is applicable to any form of analysis for prediction of soil behaviour in the field from laboratory data.

The processing of correct input data is necessary since some errors may go undetected, therefore experience and judgement are needed to construct a good finite element model and interpret the results.

When established programs are used, the advantages outweigh the disadvantages. In the following sections the main steps involved in the finite element method and the features of the program used in the present investigation will be described. The data used, the limitation of the program and the results obtained will then be dealt with.

6.2. BASIC STEPS:-

The description of the main steps involved in the finite element method is given as follows:-

a/ A continuum is discretized or divided into an equivalent system of smaller continua which are called the finite elements.

b/ Approximation functions are selected in which a pattern of solution for the unknown quantity such as displacement over each element is assumed. Polynomials are usually chosen and expressed in terms of some generalized displacement or displacements of the nodes of the element.

c/ One of the procedures available for the derivation of equations defining properties of a finite element such as the variational and residual method is used. Use of any of the formulation procedures leads to the development of the stiffness matrix of an arbitrary element, quadrilateral in the present investigation, with respect to a conventional local coordinate system. The stiffness matrix is then transformed by a transformation matrix to a generalized coordinate system.

d/ The final stiffness matrix for the entire assembly is generated by combining the matrix equations for each element to satisfy the compatibility conditions and incorporate boundary conditions.

e/ The resulting system of simultaneous equations is solved and in the present investigation the Gaussian elimination technique is used.

f/ From the computation of the nodal displacements as primary quantities, secondary quantities such as the stresses and strains can be obtained.

6.3. FEATURES OF THE MODIFIED MARC FINITE ELEMENT PROGRAM:-

The program is a version of the finite element program (MARC) which was originally written by B. Marcal and subsequently modified at Brown University, U.S.A. The present program was used by Dr. D. Brown of Glasgow University for application to the problem of the uplift resistance of vertical plate anchors embedded in cohesionless soils. Although in the more general case a finite element method should be able to cope with inclined anchors, the modification of the program to accommodate this is outwith the scope of this thesis.

The details of the program are given by Tracey (1973), Rice and Tracey (1973), but the general features are outlined as follows:

a/ It is a tangent stiffness program for geometrical and constitutive nonlinear plane strain and axisymmetric problems.

b/ It is an elastic plastic analysis using isoparametric quadrilateral elements having a uniform dilation enforced over each element (Nagtegaal, Park, Rice, 1974).

c/ The program can deal with large strains and rotations (McMeeking and Rice, 1973).

d/ Four types of element are available for use including a special crack tip element.

e/ The facility of tied nodes exists to allow easier concentration of elements in positions of high stress and strain gradients.

f/ Loading can be applied either by force or displacement, or both boundary conditions can be applied simultaneously.

g/ Numerical integration of Gaussian quadrature formula is used to calculate the element stiffness.

h/ Gaussian elimination procedure is used to obtain nodal displacements from the stiffness matrix and load vector.

i/ Displacements are increased by specified amounts to the anchor and in any element if the resultant stress state does not lie on the appropriate yield surface, an iterative procedure exists to make a more accurate evaluation.

j/ For the initial displacement, assuming an elastic stress strain curve, the values of the terms in the displacement vector can be proportionally increased or decreased by the program to obtain stresses in the critical element which will be assigned to a value fractionally less than the specified Von Mises yield stress for the material. Thus at the end of the first stage of loading all other elements lie on the elastic portion of the stress strain curve.

k/ The plate anchor is assumed to be rigid and this requires that all the nodes on the plate are displaced by the same amount.

The meshes selected consist essentially of seven squares as shown in Fig (6.1a) which are then divided into grids to form shallow and deep anchor cases as in Figs (6.2, 6.3) respectively. For a shallow anchor mesh the region above the anchor plate is later divided into finer meshes and certain modifications are added to the elements of the mesh at the outer edge of the anchor, as will be explained in section 6.6.

As illustrated in Figs (6.2, 6.3) meshes 1, 2 are half sections through the axis of the anchor system. Due to the axial symmetry of the problem each element is actually a toroid. To simulate the rigidity of the anchor the nodes at the top of the anchor plate are displaced vertically by equal amounts. To simulate the no suction condition below the anchor plate the elements e, f, g have separate nodes 6, 12, 18, 24 in both shallow and deep anchor meshes. This allows the elements above and below the anchor plate to separate freely when the nodes directly on the top of the plate are displaced vertically.

The nodes of the axis of symmetry of mesh are restricted in the radial direction for symmetry. Also the nodes at the bottom and side extremities of the mesh are restrained in the vertical and radial directions respectively. This simulates the rigid boundaries of the box in which the soil is tested. Due to the concentration of stresses near and above the anchor plate the mesh becomes finer as it approaches the anchor.

6.4. INPUT AND OUTPUT DATA:-

6.4.1. INPUT DATA:-

The input data required by the program concerning the mesh is as follows.

(i) Number of sides of elements, nodal coordinates and the number of degrees of freedom.

(ii) Total number of elements and their total number of nodes.

(iii) The restrained and loaded nodes.

(iv) The total number of degrees of freedom and the anchor plate position in the mesh.

The input data regarding the soil parameters is as follows.

(i) An idealised stress-strain curve as shown in Fig (6.4).

(ii) Poisson's ratio as given in Table 6.1.

Finally the loading mechanism input data is given as follows.

(i) The amount of vertical displacements applied to loaded nodes.

(ii) Number and amount of subsequent displacements.

(iii) The number of iterations in each increment.

6.4.2. OUTPUT FROM THE PROGRAM:-

The parameters affecting the uplift resistance can be varied to simulate both shallow and deep anchors by using various depth upon diameter ratios and by altering element sizes and numbers. Different densities of soil can be simulated using the appropriate stress-strain curve. Simulation of a complete rough anchor plate can be achieved by restraining the horizontal movements of the anchor nodes.

The following information can be obtained from the results of the program run.

a/ Vertical and radial displacements of all nodes. There is no circumferential displacement because it is an axisymmetric problem.

b/ The magnitude and direction of the principal stresses and the maximum shear in each element at any stage of loading.

c/ The distribution of vertical, radial and circumferential normal stresses and shear stresses at any stage. Due to the symmetry of the anchor no shear stresses exist in the circumferential plane.

d/ The order in which the elements yielded according to Von-Mises failure criterion.

e/ The load-displacement relationship of the anchor in the soil.

6.5. LIMITATIONS OF THE FINITE ELEMENT PROGRAM:-

In addition to the dependence of the accuracy of the results on the accuracy of the data employed in the program, the accuracy of the results will be affected by the following limitations of the program.

a/ A power law curved stress-strain relationship for the soil could have been used. In this particular case, to better match the experimental stress-strain curve, a multilinear stress-strain curve was used as shown in Fig (6.4) to reduce computer time. The values of yield strength are assumed to be equal in tension and compression which is not the case.

b/ The use of quadrilateral elements with two degrees of freedom per node assumed that all element sides remain straight during deformation which is different from the behaviour of real soils as shown in the deformed mesh at ultimate load in Figs (6.5, 6.6).

c/ The values of stresses obtained in each element were calculated at the centre of the element.

d/ The program can not handle the strain softening of the stress-strain curve and the post peak part of the curve is taken as the extrapolation of the last straight segments CE and DF in Fig (6.4).

e/ The constitutive non-linearity is restricted to either elastic-plastic behaviour of Von-Mises yield type (Prandtl-Reuss eqn) or deformation plasticity.

f/ The material is assumed to be weightless.

g/ An approximate value of anchor plate loading is obtained by integrating the stresses at the centre of the elements which are adjacent to and directly above the anchor over the total area.

6.6. DETAILS OF DATA USED:-

As explained in chapter 3 the parameters involved in this investigation were numerous. In the finite element analysis only vertical anchors were dealt with due to the symmetry of the problem. With the remaining parameters a large number of program runs would be required to analyse and compare the output from various combinations of these parameters. Accordingly it was decided to vary those parameters which the author considers to be most important.

The parameters which were varied were the depth to diameter ratios, $\frac{D}{B}$ of the anchor plate. Runs were made with two different meshes representing shallow and deep anchors (i.e. $\frac{D}{B} = 2$ and

9 respectively), and to make comparison with the laboratory model tests conducted as shown in Table 6.1.

A smooth anchor face was assumed in the runs where radial degrees of freedom of the anchor nodes were not restricted. This would result in shortening the anchor diameter very slightly. Variation of roughness of the anchor resulted in small differences in element stresses but without a consistent pattern in the differences (Davie, 1973). The author therefore considered smooth anchors to represent anchors used in the laboratory tests. The compressive stresses obtained directly above the anchor were integrated over the original and final anchor plate area to obtain the uplift resistance of the anchor at different stages. Insignificant differences were found between them and hence the anchor load calculated for the original area was adopted.

6.7. PRESENTATION OF RESULTS:-

The results obtained from the runs of shallow and deep anchors yielded a large amount of data, the most important of which in the author's opinion, are presented in the following sections.

6.6.1. Nodal displacements.

6.6.2. Load-displacement curve.

6.6.3. Values of stresses in the elements.

All the runs were based on the stress-strain curves representing shallow and deep anchors, as shown in Fig (6.4), obtained from triaxial tests carried out on sand by the author. The curve chosen for a particular case depends on the depth of the anchor and the appropriate confining cell pressure in the triaxial test to represent the state of stress around the anchor. Therefore confining pressure of $\sigma_3 = 36$ KN/m^2 was chosen for deep anchor and the lowest value of $\sigma_3 = 12.8$ KN/m^2 obtained from the triaxial tests was assigned for shallow anchor.

In the case of the shallow anchor the mesh shown in Fig (6.1b) was first adopted. Due to the difficulties encountered with the hatched critical element in Fig (6.1b) the mesh in Fig (6.1c) was used. Finally a modification was made to the critical element at the tip of the anchor. The original four noded element with two nodes at the same co-ordinate had the two coincident nodes separated as shown in Fig (6.2).

6.7.1. NODAL DISPLACEMENTS:-

The original meshes for both shallow and deep anchors deformed during loading are produced by displacing the anchor vertically. The deformed shapes were investigated at two stages on the stress strain curves represented by points A, E and B,F in Fig (6.4) corresponding to shallow and deep anchor cases. The first stage was when the critical element was just below the value of Von-Mises yield stress. The deformations at this stage were very small and the deformed mesh could not be differentiated from the original one. At this stage of loading all the elements remained in the elastic range but any increase of loading would have caused the critical element to yield.

The second stage is at failure represented by points E and F in Fig (6.4) for shallow and deep anchors respectively. The deformed mesh for the shallow anchor at ultimate load is shown in Fig (6.5), while that for the deep anchor is illustrated in Fig (6.6). For presentation purposes the deformations were enlarged by a factor of 3.

For more detailed information about the internal deformation, Fig (6.7) was drawn to show the relationship between $\frac{\delta n}{\delta a}$ to $\frac{Dn}{D}$ where $\frac{\delta n}{\delta a}$

is the ratio of the vertical displacement, δn, at failure of nodes on the anchor axis to the vertical displacement δa of the anchor. $\frac{Dn}{D}$ is the ratio of the depth, D_n, of the nodes below the surface to the depth, D, of the anchor. Both curves of shallow and deep anchors are presented. High values of displacement ratios are observed for the shallow anchor up to the soil surface. For deep anchors only nodes near the anchor plate showed large displacement ratios.

Concerning the soil surface displacements, Fig (6.8) shows the vertical deformations of the nodes at the soil surface. For the shallow anchors the profile of surface deformation were plotted for two stages of loading. In Fig (6.8) curves 1 and 2 represent the profiles at 38% and 100% of the ultimate load. Similarly for deep anchors curves 3 and 4 in Fig (6.8) are for 35% and 100% of the ultimate load. Higher values of surface deformations are observed for shallow anchors in comparison to that of deep anchor at both stages of loading.

Discussion and comparison of these results with those found from the laboratory model testing will be presented in chapter 7 where the possible mode of failure will be considered.

6.7.2. UPLIFT RESISTANCE AND ANCHOR DISPLACEMENT:-

Load-displacement relationships were obtained from the finite element analysis up to failure of the anchor. Fig (6.9) shows the curve plotted for the shallow anchor. The corresponding experimental ultimate load (D = 152.4, B = 76.2, $\frac{D}{B} = 2$) of 97.8 Newtons, Fig (6.9), is shown and does not compare well with the finite element value of 462 Newtons.

Fig (6.10) also represents the load-displacement relationship for the deep anchor. The ultimate experimental load is 1033 Newtons compared to the predicted value of 931 Newtons. These results will be discussed in chapter 7.

6.7.3. VALUES OF STRESSES IN THE ELEMENTS:-

6.7.3.1. ORDER OF YIELDING OF ELEMENTS:-

Unlike the physical models, where failure can be physically observed, a criterion is required in the finite element to indicate the onset of anchor failure. The criterion used to determine the anchor failure was that if the elements completely surrounding the anchor have all failed then the anchor was considered to have reached its ultimate load.

Figs (6.11, 6.12) show the order of yielding of the elements, according to the Von-Mises failure criterion in shallow and deep anchors respectively. These figures illustrate the progress of yielding at early stages which can give an idea about the progressive yielding surfaces and the mode and type of failure.

6.7.3.2. PRINCIPAL STRESSES:-

Due to the importance of principal stresses, according to which yielding of the material can be determined by the yield criterion, these have been calculated above the anchor for the elements surrounding the anchor axis. The major principal stress is taken as the greatest compressive or least tensile stress in each element. Intermediate principal stress in an axisymmetric problem is the same as the circumferential stress or σ_θ. Both major and minor principal stresses at failure were plotted for shallow anchor in Fig (6.13) and their directions also have been calculated. The same stresses were obtained for the deep anchor and are plotted in Fig (6.14).

6.7.3.3. MAGNITUDE AND DISTRIBUTION OF NORMAL AND SHEAR STRESSES:-

The subject of stress distribution in the soil above the anchor plate has attracted considerable interest. Some difficulties are involved in obtaining stresses and strains at these positions from experimental work, however using finite element this information can be obtained at any stage of loading more easily.

Variation of stress in the elements along the axis of the anchor have been plotted for various type of stresses. Fig (6.15) shows the distribution of vertical normal stress and radial normal stress for the shallow anchor. Fig (6.16) illustrates for the same mesh the distribution of shear stresses on the radial plane in the vertical direction. These shear stresses are identical to the complementary shear stresses on the vertical plane in the radial direction. On the same figure the distribution of the maximum shear stress is also illustrated.

Figs (6.17, 6.18) represent the distribution of the vertical, radial normal stresses and shear, maximum shear stresses respectively for the case of deep anchor. Similarly these stresses are at the stage of maximum load.

6.7.3.4 DISTRIBUTION OF VERTICAL NORMAL STRESSES ON THE PLATE ANCHOR:-

The distribution of the normal stresses on the plate anchor is considered by the author to be important. This is due to the fact that this distribution will indicate the mechanism of the transfer of loading at any stage to the plate from the anchor tendon.

Fig (6.19) shows the distribution of the normal stresses on the plate from the anchor axis to the edge of the plate for both shallow and deep anchors.

In chapters 5 and 6 details of the laboratory investigation and the finite element analysis performed by the author have been presented. The discussion and comparison of these results will be presented in chapter 7.

TABLE 6.1. DETAILS OF MAIN FINITE ELEMENT RUNS

RUN NO.	MESH NO.	NO. OF ELEMENTS	NO. OF NODES	VALUE OF $\frac{D}{B}$	VALUE OF $\frac{Bc}{B}$	NO. OF DISP. INCR.	POISSON'S RATIO ν
1	1	207	239	2	10	44	0.3
2	2	303	341	2	10	21	0.3
3	3	303	341	2	10	20	0.3
4	4	207	239	9	20	41	0.3

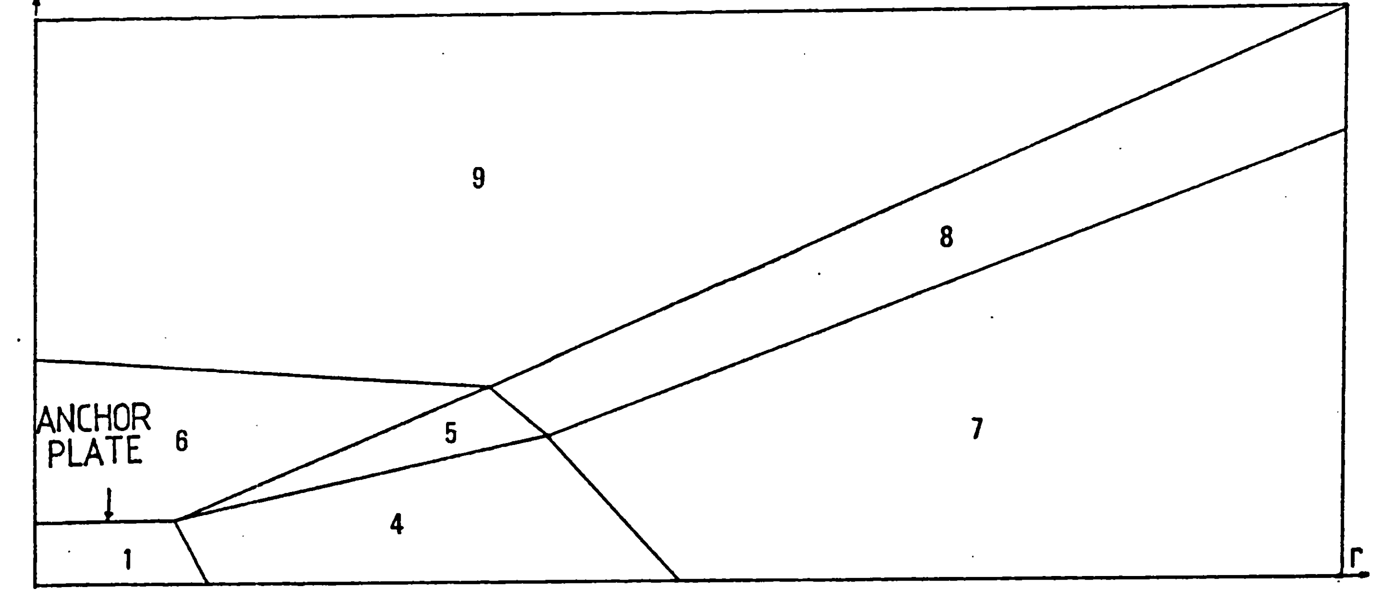

(a) Shaped squares before gridding

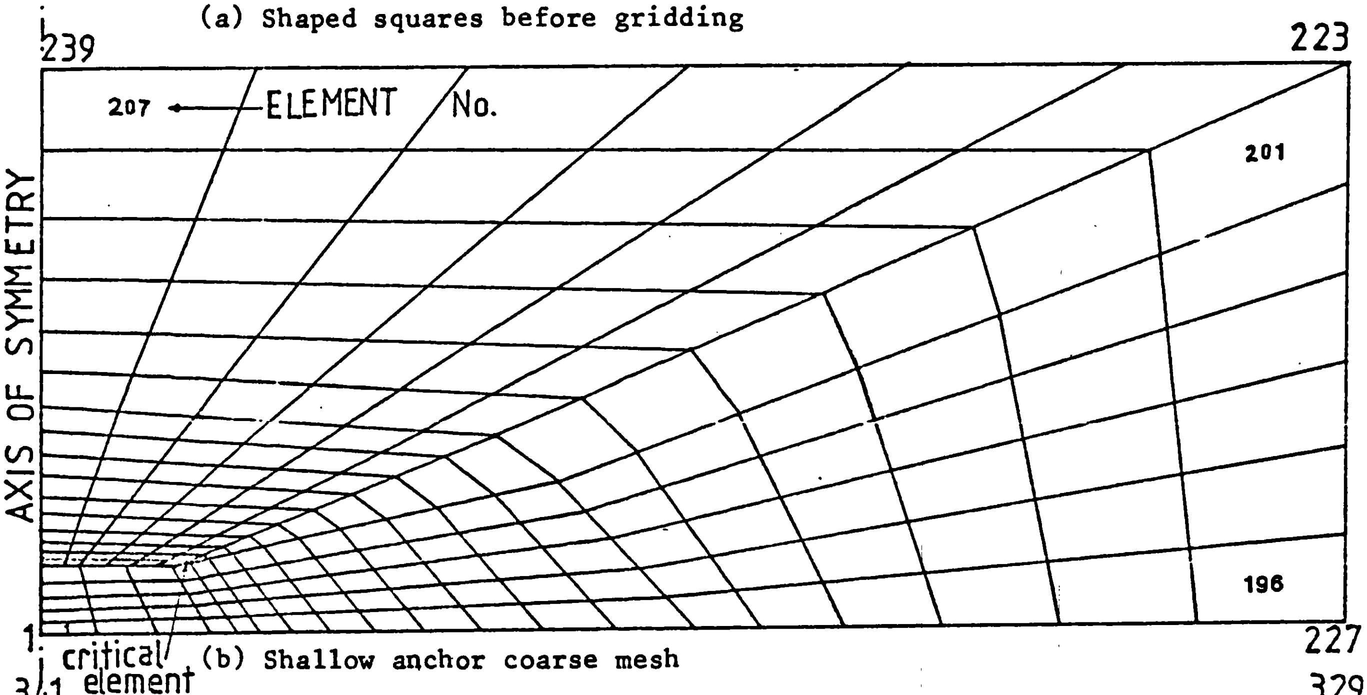

(b) Shallow anchor coarse mesh

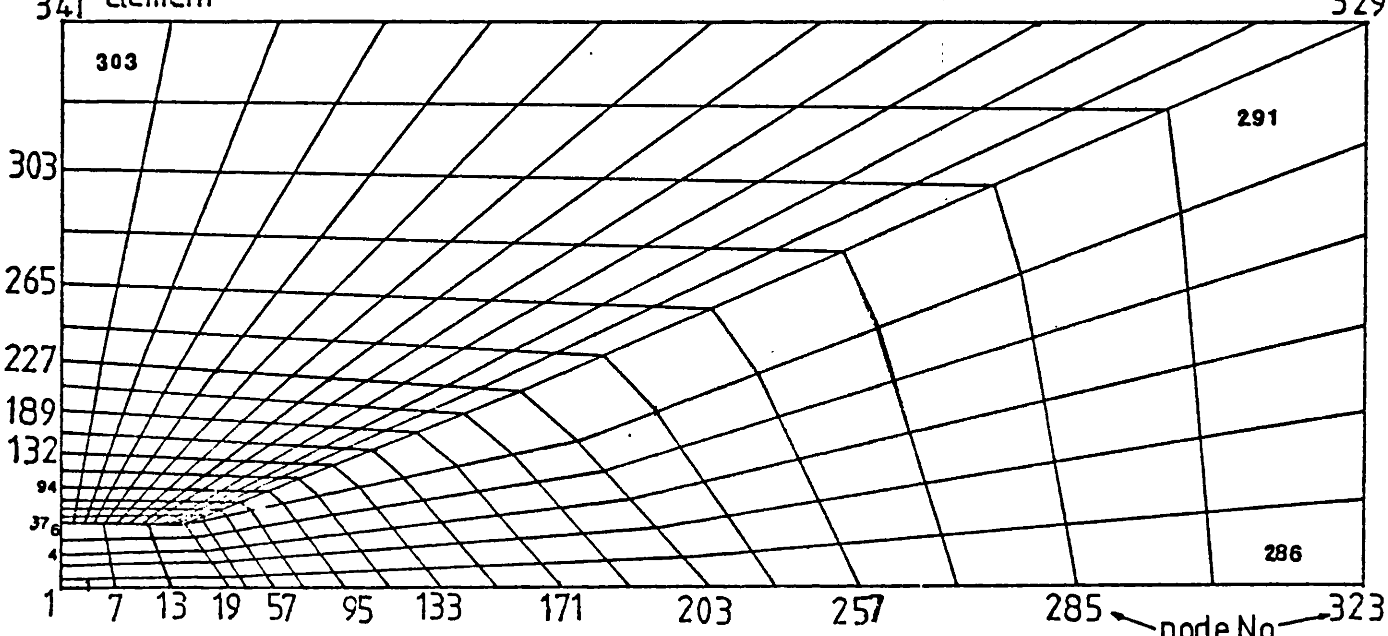

(c) Shallow anchor fine mesh

FIG.6.1 GENERAL ANCHOR MESH

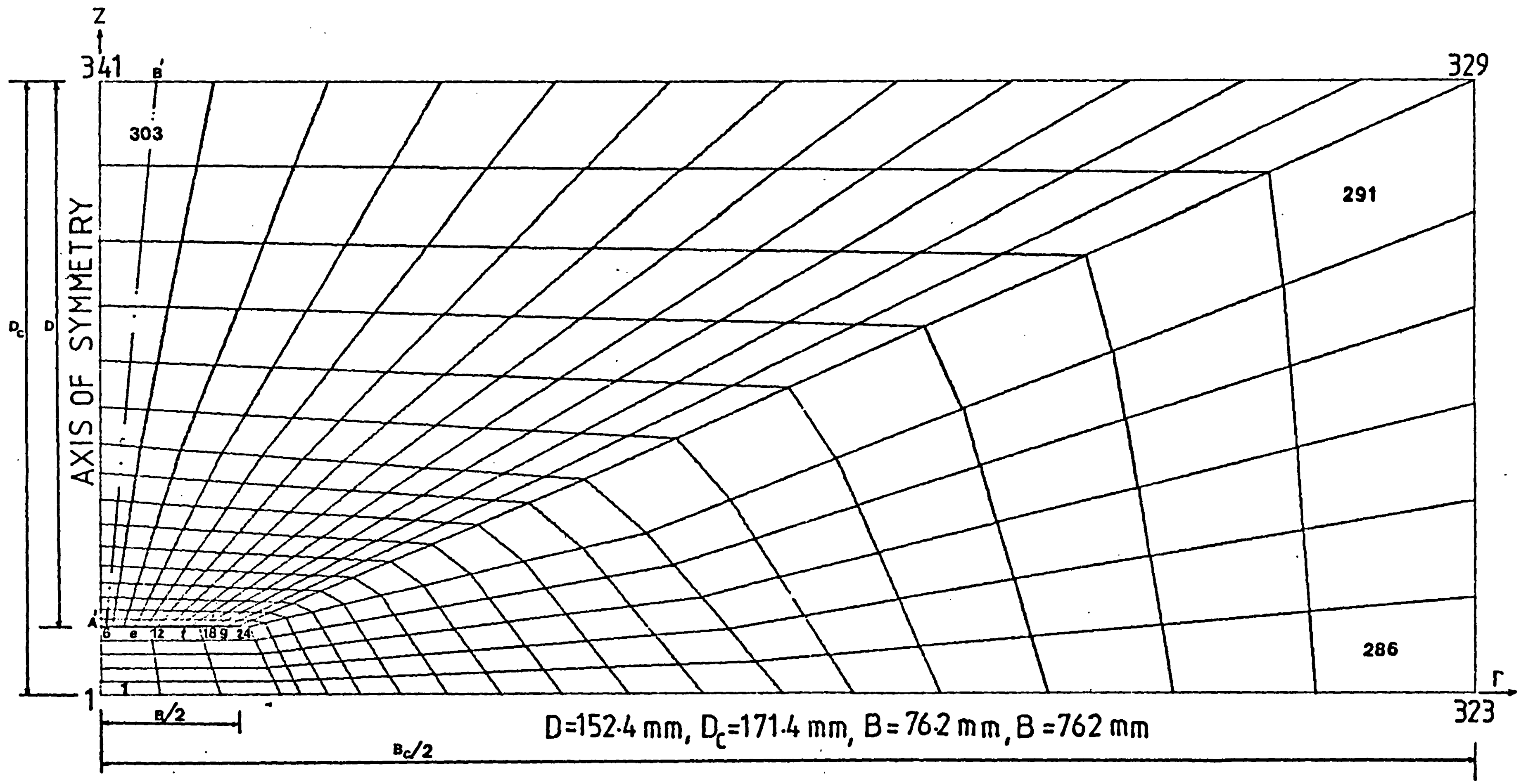

FIG.6.2 SHALLOW ANCHOR MODIFIED MESH

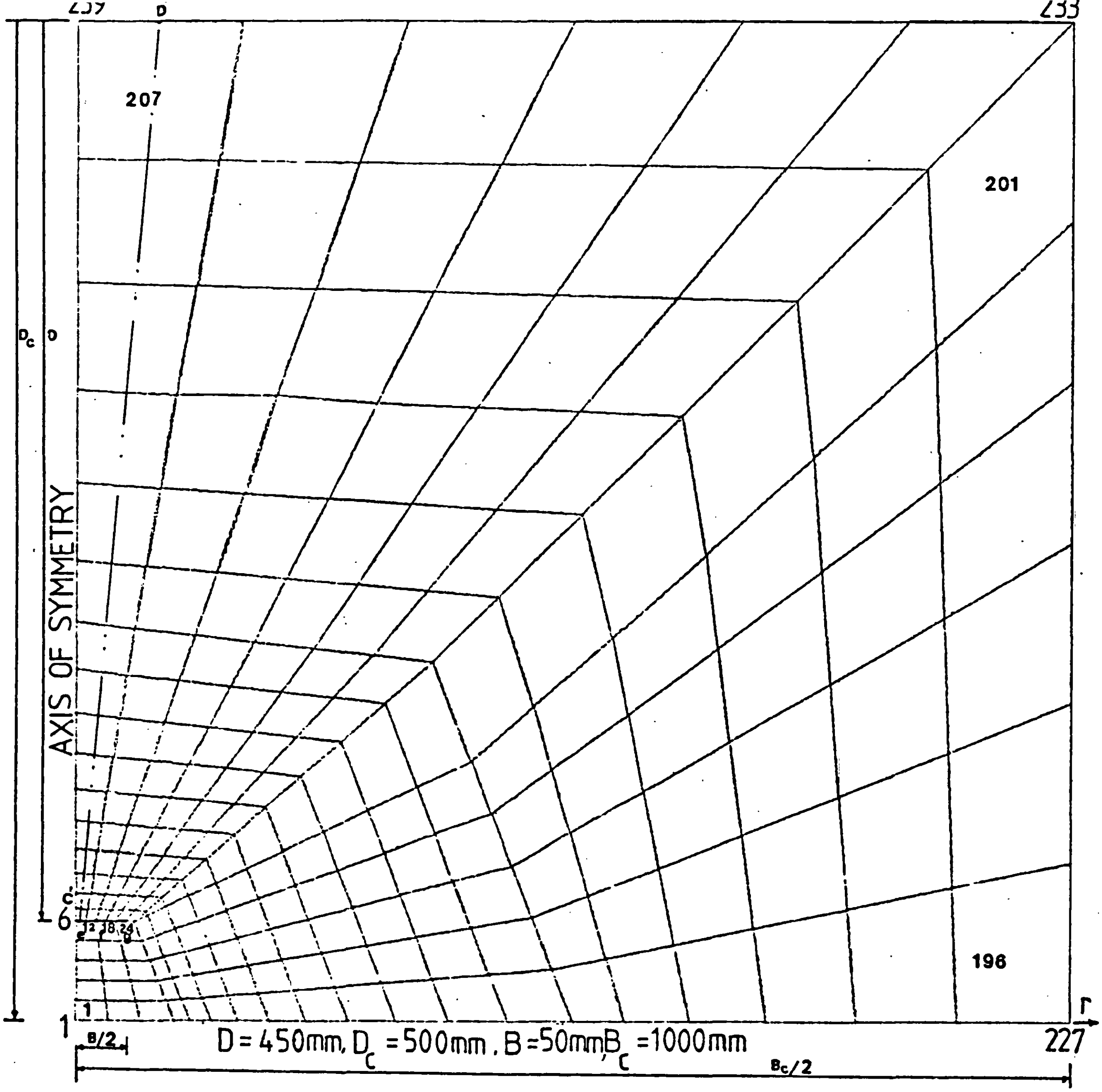

FIG.6.3 DEEP ANCHOR MESH

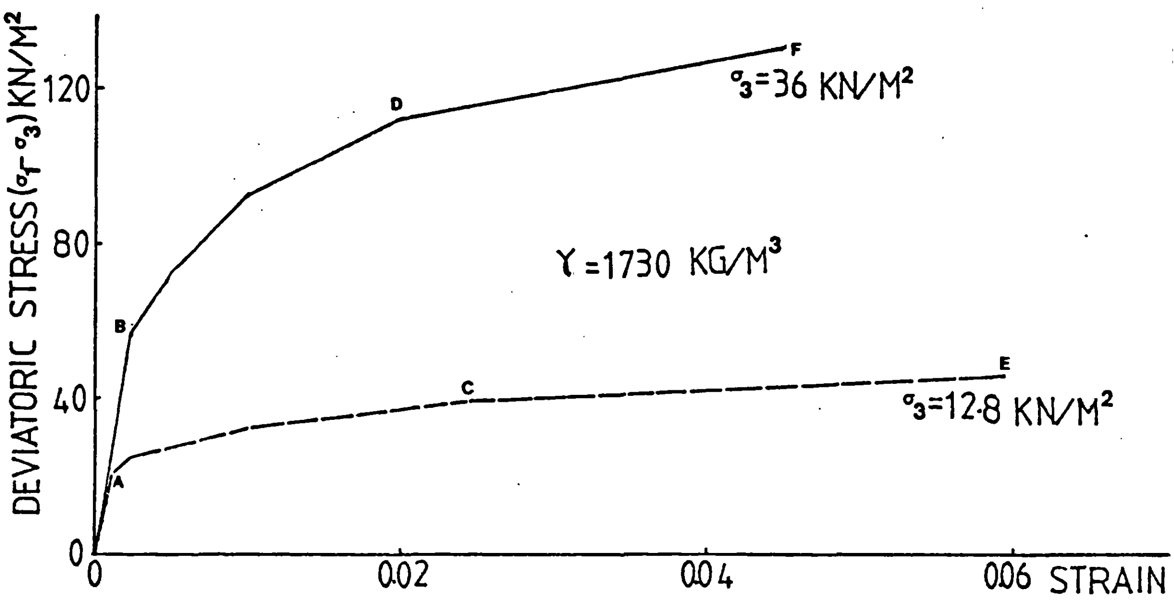

FIG.6.4 DEVIATORIC STRESS VERSUS STRAIN OF LEIGHTON BUZZARD SAND

(γ = 1730 kg/m^3)

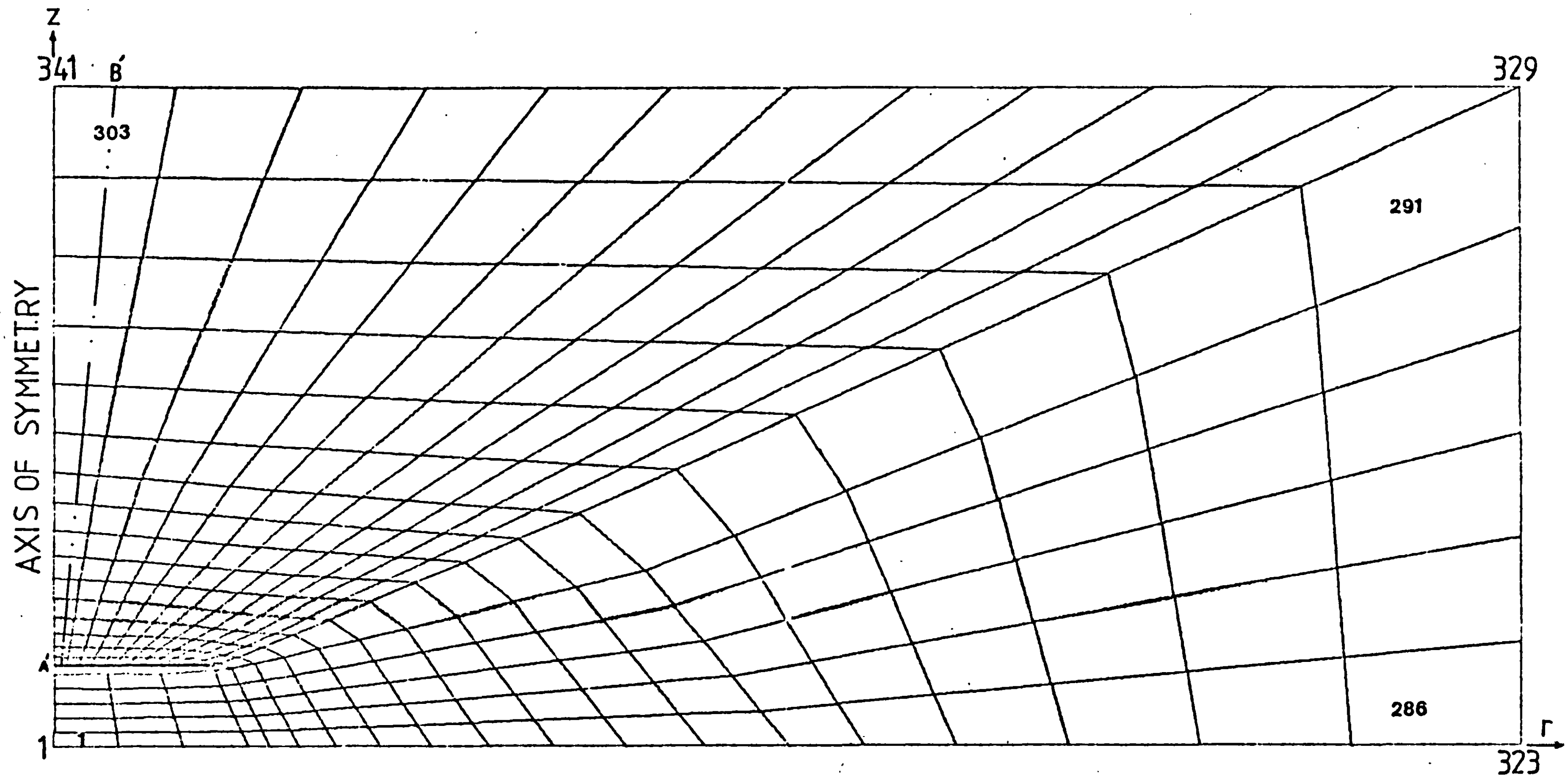

FIG.6.5 NODAL DISPLACEMENTS AT ULTIMATE LOAD (i.e. POINT E IN FIG 6.4)

SHALLOW ANCHOR, RUN NO. 3, $\frac{D}{B} = 2$, DISPLACEMENTS ENLARGED BY A FACTOR OF 3

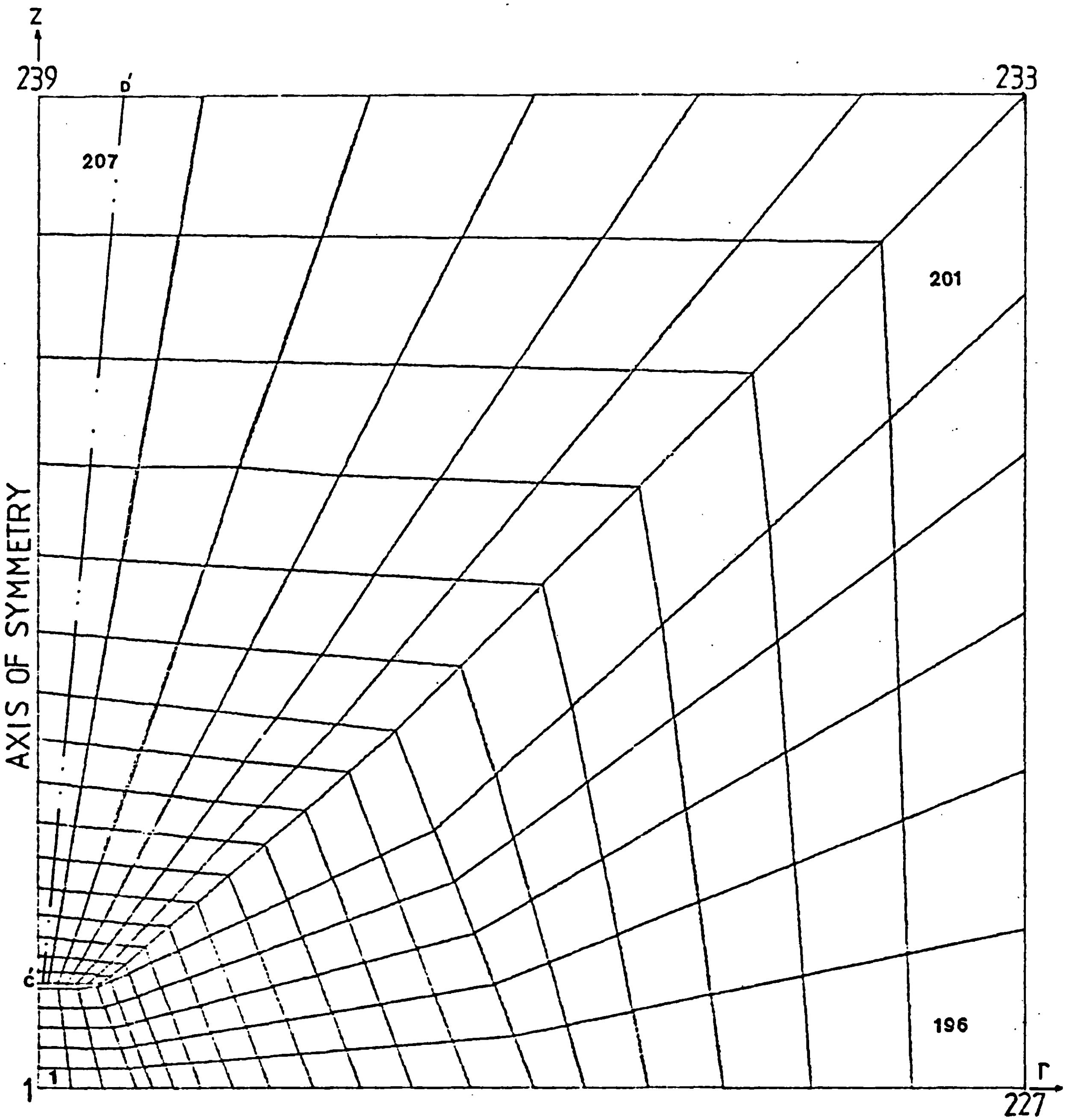

FIG.6.6. NODAL DISPLACEMENTS AT ULTIMATE LOAD (i.e. POINT F IN FIG.6.4) DEEP ANCHOR, RUN NO. 4, $\frac{D}{B}$ = 9, DISPLACEMENTS ENLARGED BY A FACTOR OF 3.

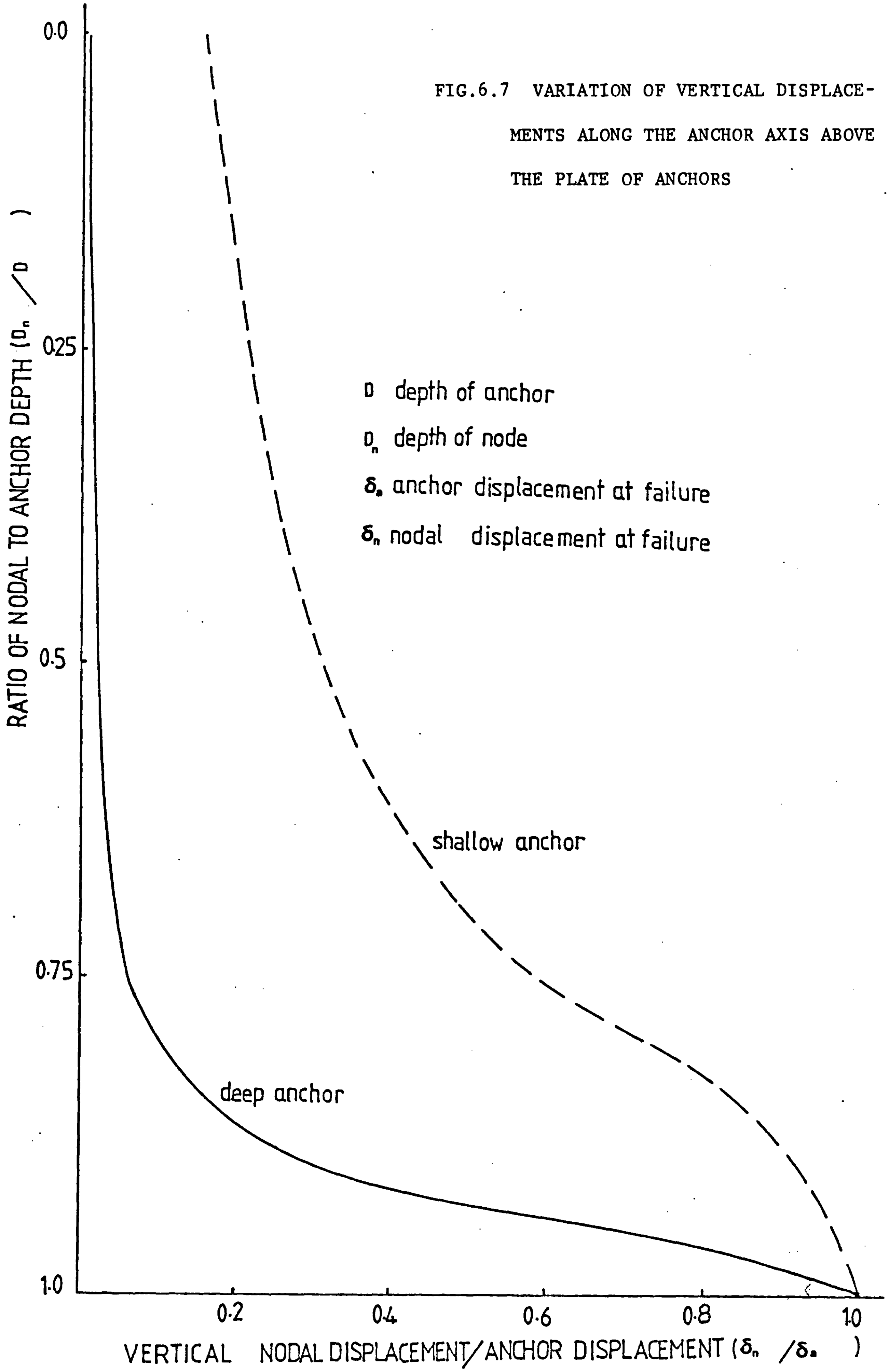

FIG.6.7 VARIATION OF VERTICAL DISPLACEMENTS ALONG THE ANCHOR AXIS ABOVE THE PLATE OF ANCHORS

FIG.6.8 SURFACE DISPLACEMENTS AT DIFFERENT STAGES OF LOADING.

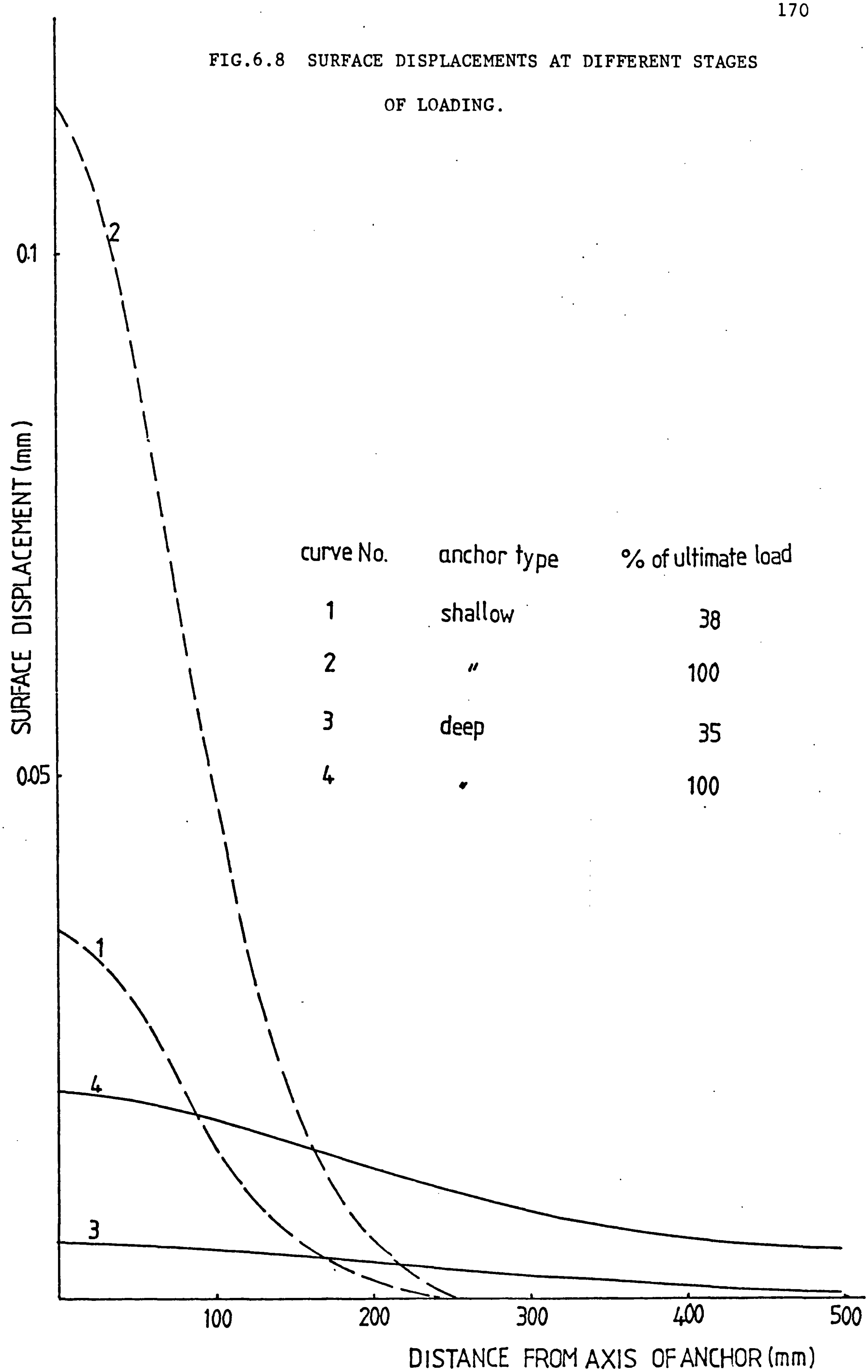

FIG.6.9 LOAD-DISPLACEMENT RELATIONSHIP OF SHALLOW ANCHOR

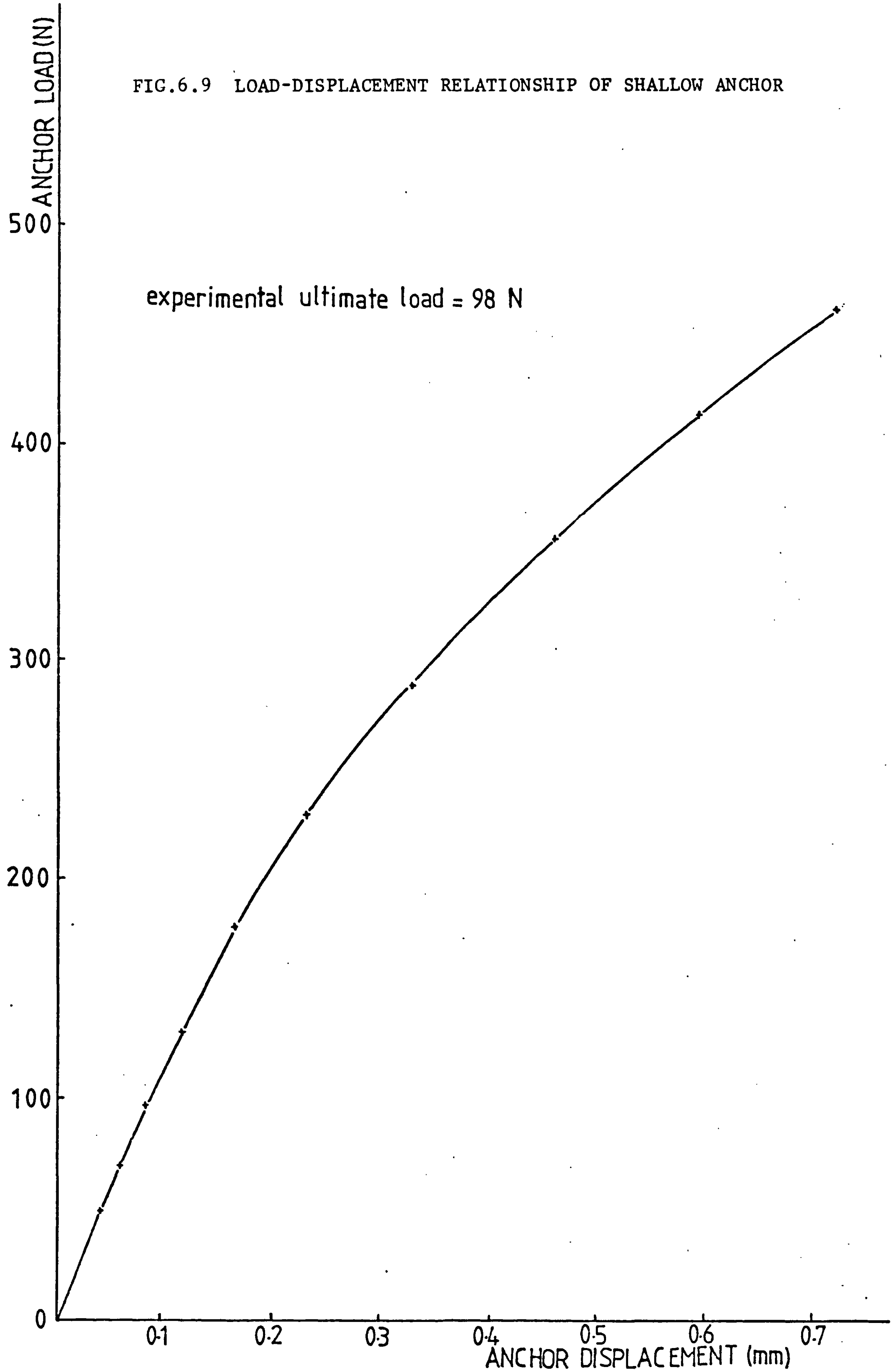

FIG.6.10 LOAD-DISPLACEMENT RELATIONSHIP OF DEEP ANCHOR

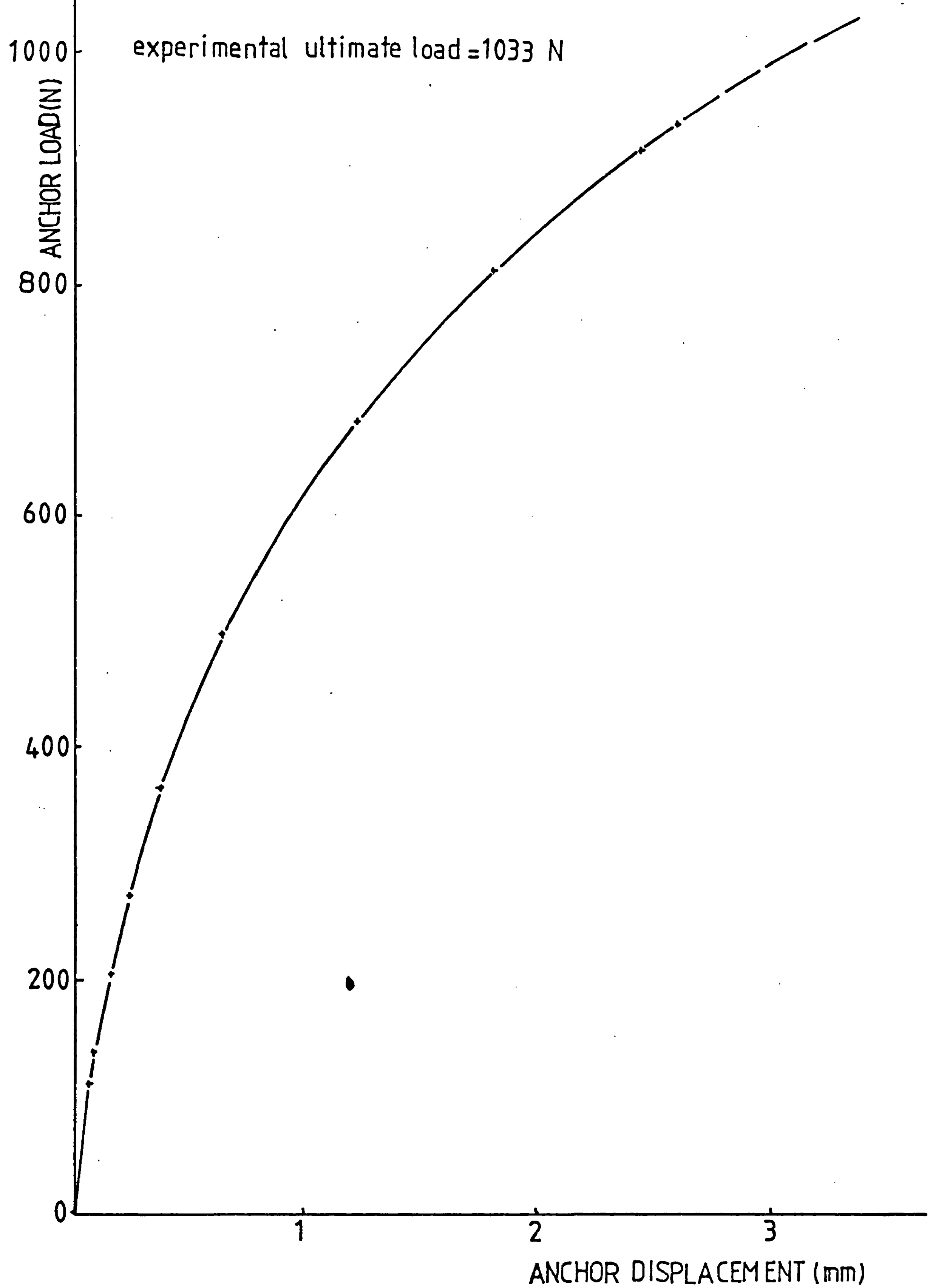

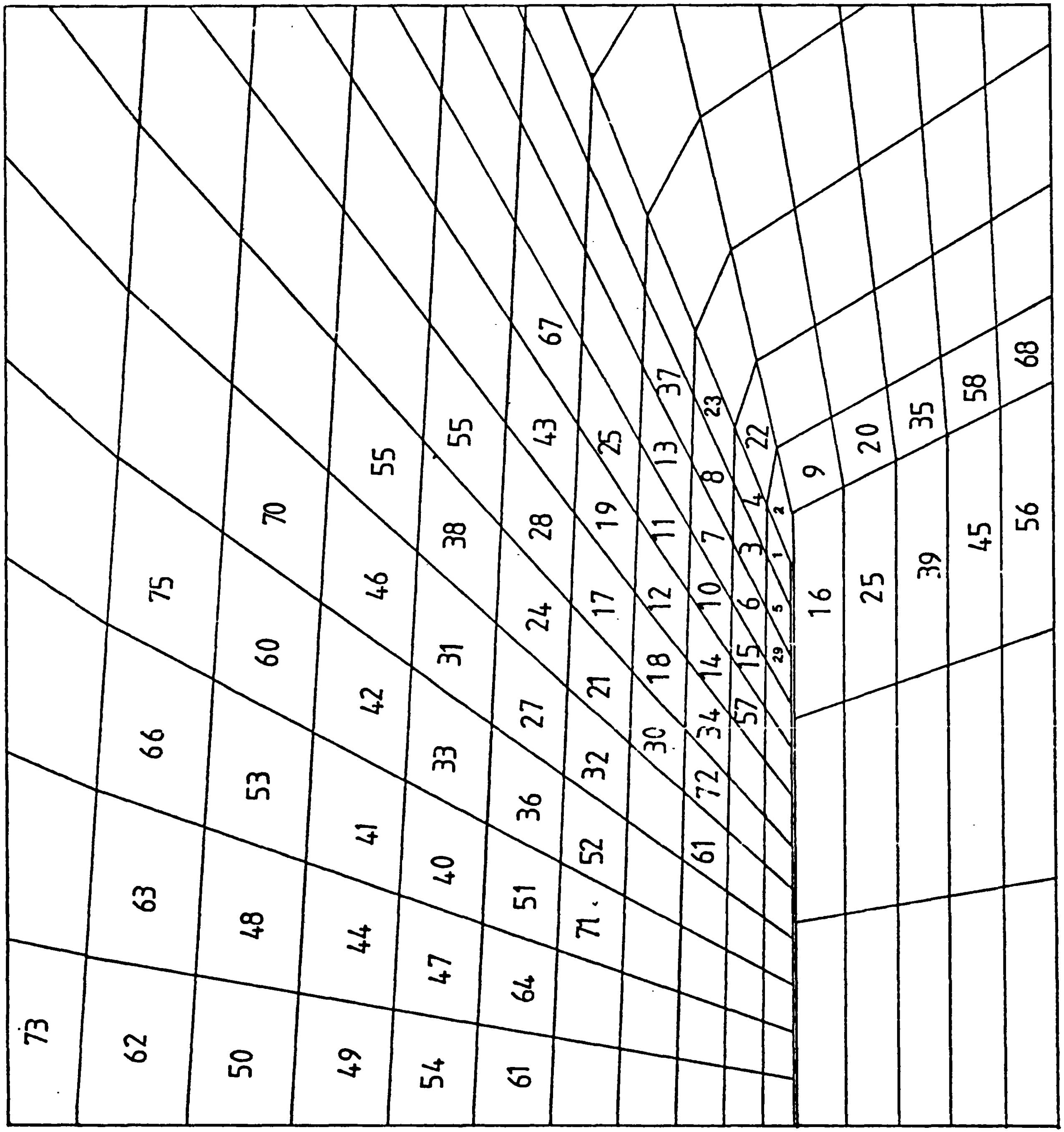

FIG.6.11 SHALLOW ANCHOR PLATE REGION ENLARGED ILLUSTRATING THE ORDER OF YIELDING OF ELEMENTS

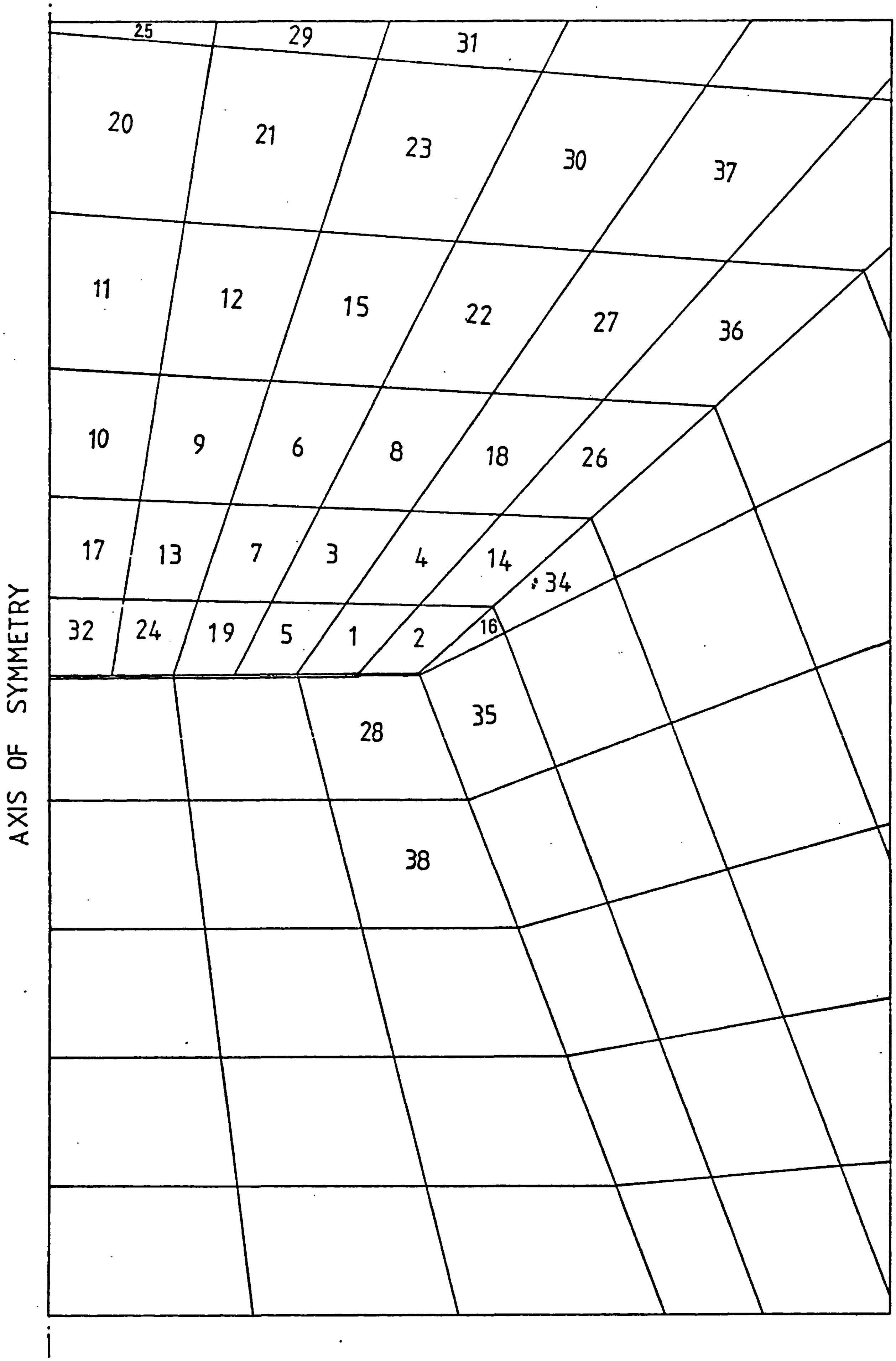

FIG.6.12 DEEP ANCHOR PLATE REGION ENLARGED ILLUSTRATING THE ORDER OF YIELDING OF ELEMENTS.

FIG.6.13 VARIATION OF MAJOR AND MINOR PRINCIPAL STRESS ALONG A'B' (SHALLOW ANCHOR)

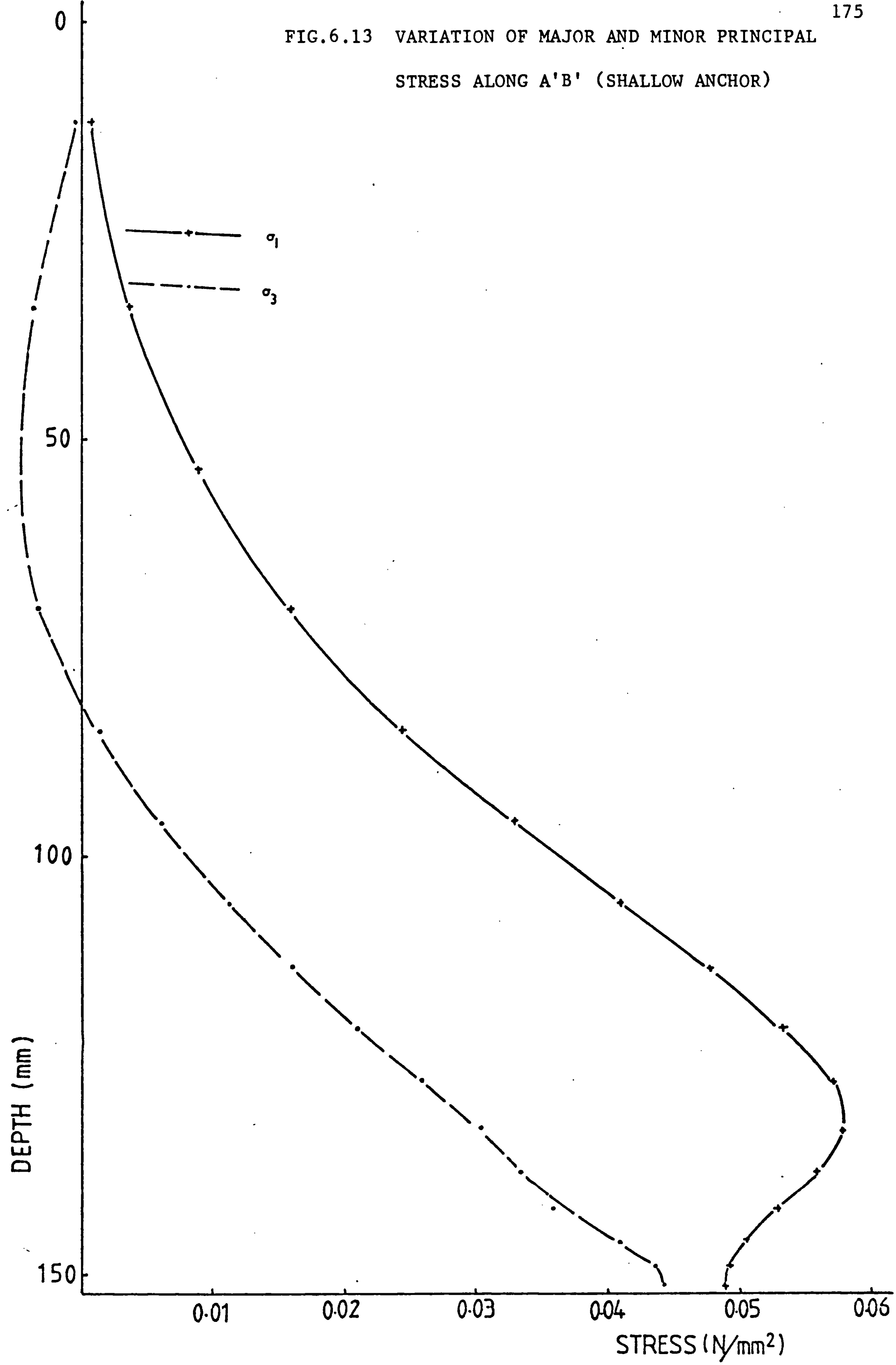

FIG.6.14 VARIATION OF MAJOR AND MINOR PRINCIPAL STRESS ALONG C'D' (DEEP ANCHOR)

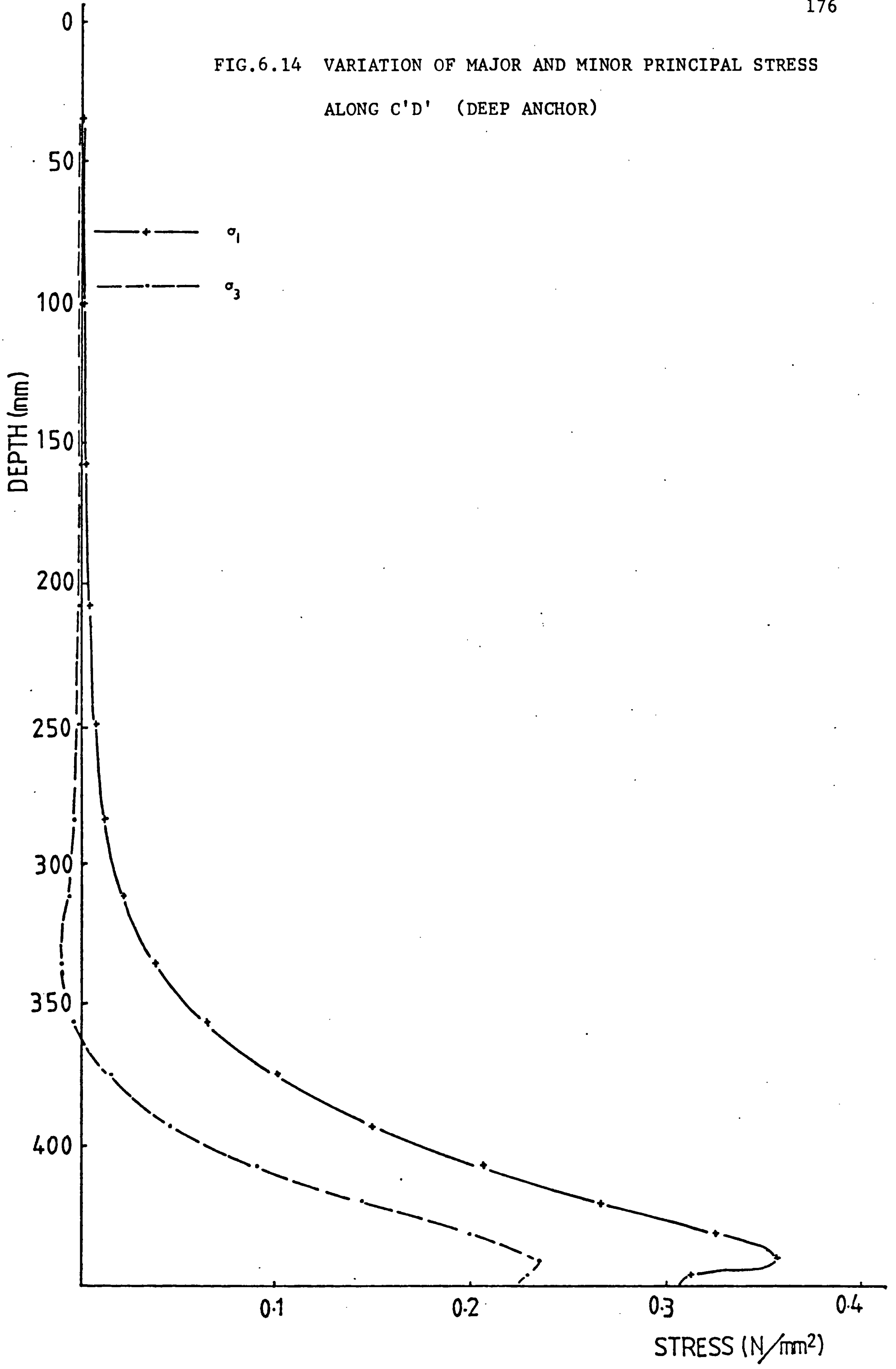

FIG.6.15 VARIATION OF NORMAL VERTICAL AND RADIAL STRESSES ALONG A'B' (SHALLOW ANCHOR)

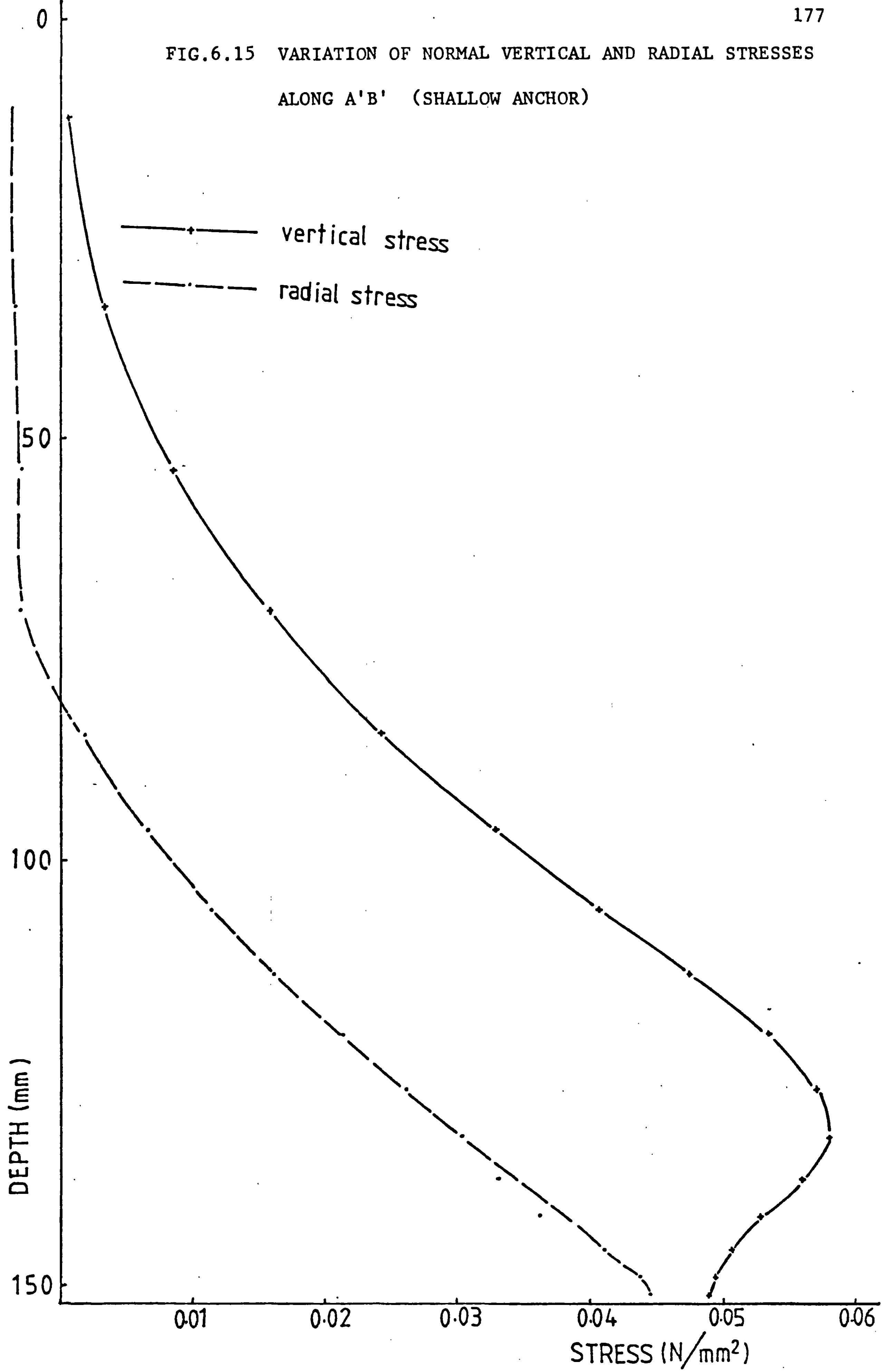

FIG.6.16 VARIATION OF SHEAR ON z-r PLANE AND MAXIMUM SHEAR STRESSES ALONG A'B' (SHALLOW ANCHOR)

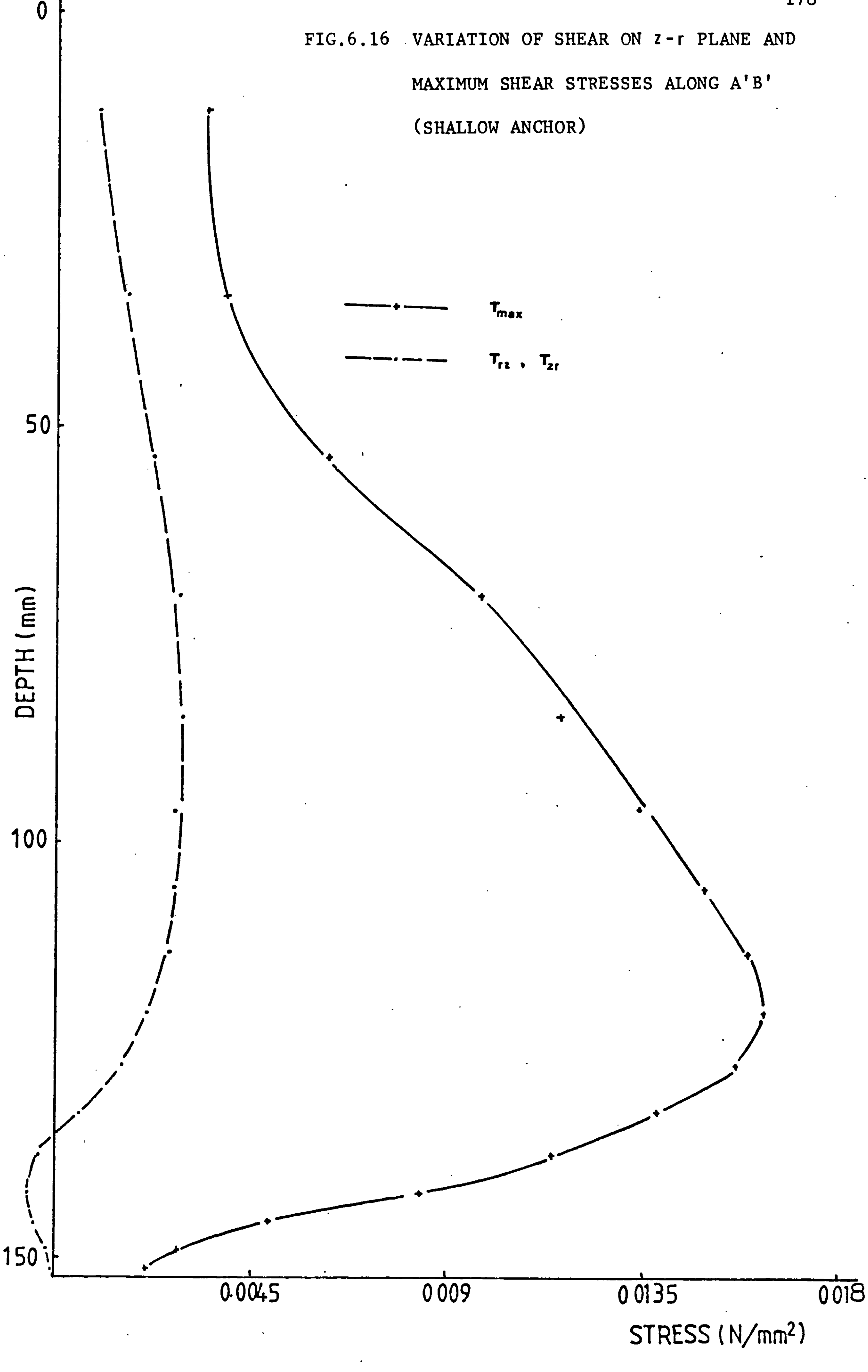

FIG.6.17 VARIATION OF NORMAL VERTICAL AND RADIAL STRESSES ALONG C'D' (DEEP ANCHOR)

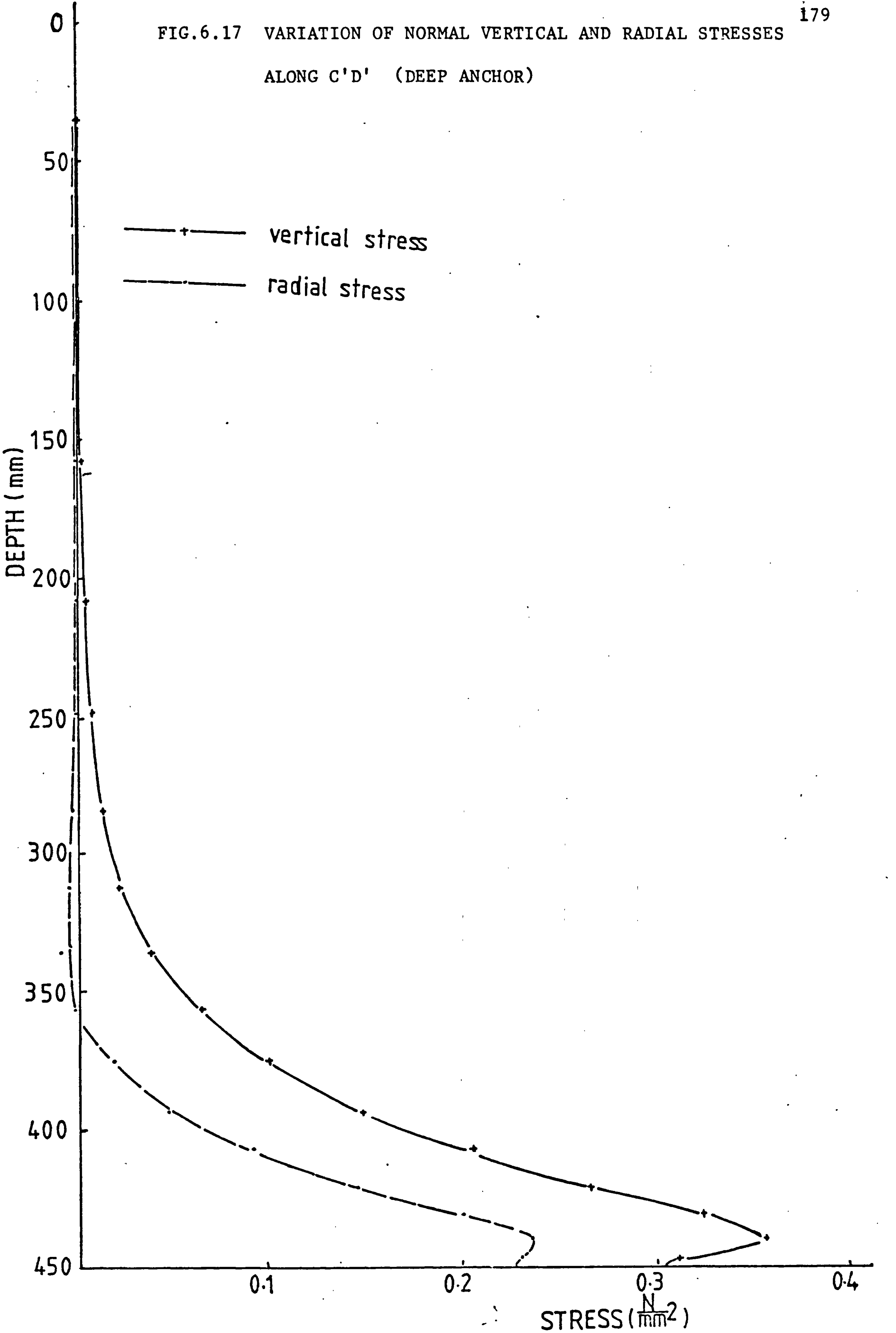

FIG.6.18 VARIATION OF SHEAR ON r-z OR z-r PLANE AND MAXIMUM SHEAR STRESSES ALONG C'D'(DEEP ANCHOR)

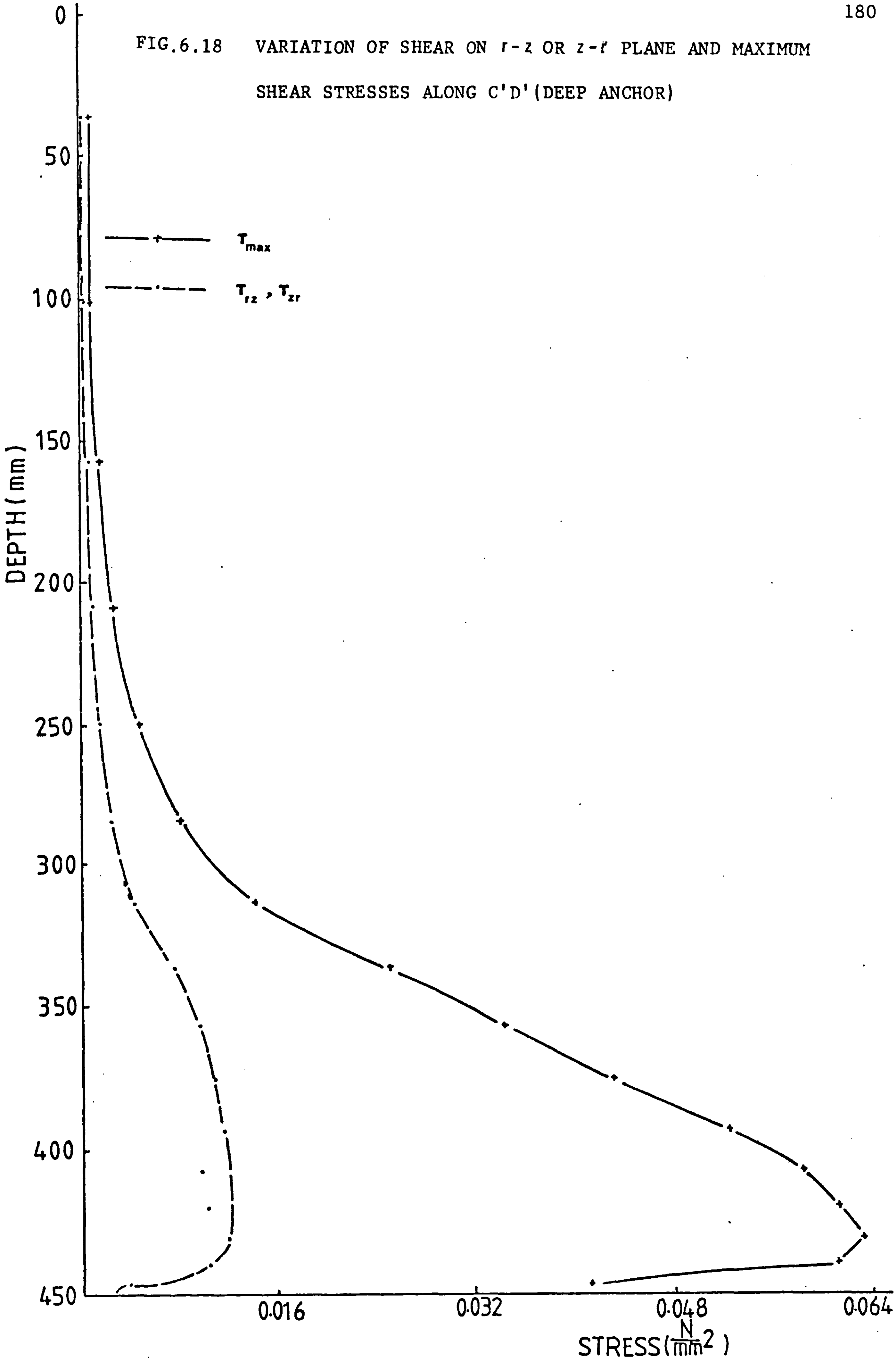

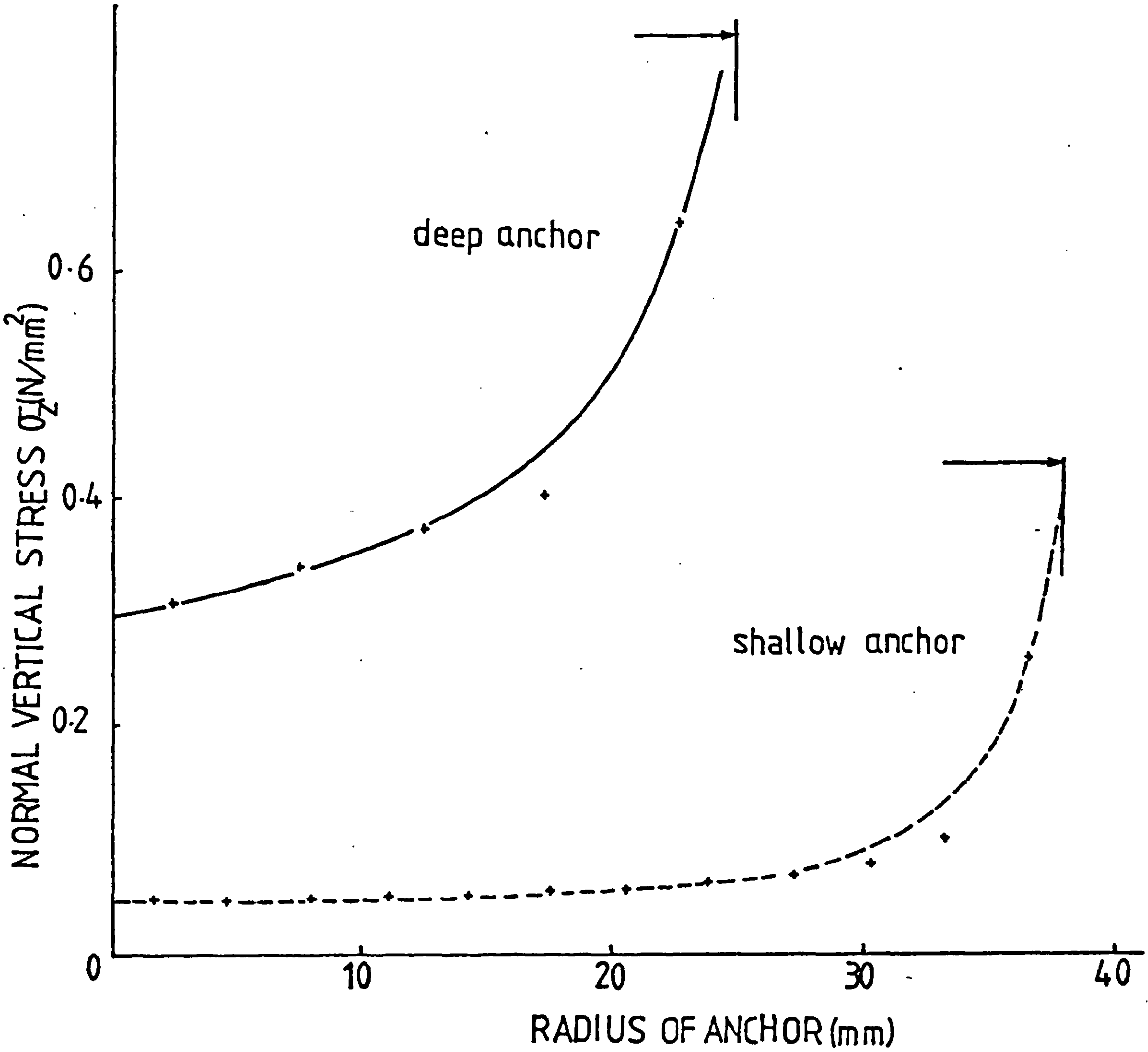

FIG.6.19 VARIATION OF VERTICAL COMPRESSIVE STRESSES ON THE ANCHOR PLATES.

CHAPTER 7

DISCUSSION AND COMPARISON OF RESULTS

CHAPTER 7

DISCUSSION AND COMPARISON OF RESULTS

7.1 INTRODUCTION:-

In this chapter a discussion of the present experimental results is presented followed by a comparison of these results with previous theories and experimental work. Comparison of the present and previous experimental results with the proposed approximate method for predicting the ultimate uplift resistance of circular plate anchors is made. The order of the discussion will be as follows:-

a/ Results of the internal and surface displacements reported in Chapter 5 and from the finite element analysis in Chapter 6.

b/ Relationship of load-displacement of the anchor as a function of the various parameters.

c/ The variation of ultimate anchor load with different parameters.

d/ The distribution of stresses and displacements predicted by the finite element method.

e/ Comparison of the present experimental results with previous theories and with the proposed approximate method.

f/ Comparison of the approximate method with previous experimental work.

g/ Design curves and examples using the approximate method.

The headings for these sections denote only the primary subjects for discussion in each section but do not exclude the discussion of subjects from other sections when they are considered to be relevant. Table 7.1 summarises the information obtained from the model testing and the finite element analysis and also the data which can be obtained from both methods.

7.2 INTERNAL AND SURFACE DISPLACEMENTS:-

In this section the results of internal and surface displacements obtained from photographic and model tests leading to a prediction of the formation of the failure surface will be discussed.

7.2.1 INTERNAL DISPLACEMENTS OF VERTICAL SHALLOW ANCHORS:-

Fig (7.1) shows the surface failure of one of the photographic tests for a depth to diameter ratio of the anchor of $\frac{D}{B} = 2$. The failure surface is generally slightly curved outwards as it approaches the soil surface, a fact which is also observed in the typical photographs shown in Figs (5.13, 5.14). The failure surface is near vertical at the top edge of the plate anchor and meets the free sand surface at an angle greater than 45^{o} to the horizontal. These findings confirm those observed by El-Rayes (1965) and Carr (1970) using time exposure photographs. These findings disagree with the assumed value of $(45 - \frac{\phi}{2})^{o}$ of Balla (1961), Vesic (1965) and Matsuo (1967).

Therefore the assumption of a straight line for a meridian section of the failure surface is a reasonable approximation to obtain the simple solution illustrated in the approximate method in Chapter 3.

7.2.2 INTERNAL DISPLACEMENTS OF VERTICAL DEEP ANCHORS:-

The mode of general shear failure continues to reach the sand surface as the depth of embedment increases. After a certain $\frac{D}{B}$ ratio the zone of failure does not reach the surface of the sand but is limited to a height H above the plate anchor. The ratio $\frac{H}{B}$ is the critical depth ratio differentiating between shallow and deep modes of failure. For a certain density of the sand $\frac{H}{B}$ appears to remain constant for further increase in the depth of embedment D. It is believed by the author that the sand immediately above the vertical anchor is displaced vertically upwards. The amount of displacement diminishes at higher levels above the anchor plate by an amount depending on the compressibility of the sand. The extent of the sand displacement is higher for less compressible sand e.g. dense sand, and reaches the surface for shallow anchors, however it is limited below the surface for deep anchors. This behaviour is taken into consideration in the approximate method.

Carr (1970) reported that his photographic work indicated that the sand above the deep anchor plate was lifted in a similar manner to that of a shallow anchor. From some of the photographs reported by Carr (1970) the author identified the failure surfaces shown in Fig (7.2 a,b,c) for shallow anchors and in Fig (7.2 d) for deep anchor .

McMullan (1974) reported that the displacement zone increased in area as the anchor plate displaced from zero reaching a maximum corresponding approximately to the ultimate load. This area was then approximately constant for further anchor displacement.

7.2.3 INTERNAL DISPLACEMENTS OF INCLINED ANCHORS:-

The failure surface developed for inclined anchors is more complicated than that for vertical anchors due to the lack of symmetry. Gillon (1970) used time exposure photographs to establish the failure surface of a strip anchor in shallow conditions. Fig (7.3) shows the observed failure profile by Gillon at three different angles of inclinations $\psi = 30^o, 45^o, 60^o$ from the vertical. It was observed from the experimental work on inclined anchors that there was an increase in the area of the shear failure surfaces and the upward yielding zone was not symmetrical about the anchor axis but deflected slightly upwards. These observations are in agreement with Kananyan (1966) who also reported that for pullout anchors the displacement of the anchor did not occur rigorously in the direction of the acting force but with a deflection upward.

McMullan (1974) carried out photographic and stereo-photogrammetric tests on vertical and inclined deep anchors for $\frac{D}{B} = 14$ with $\psi = 20^{o}$ and 40^{o}. As the anchor was inclined the displacement zone was displaced towards the trailing side of the anchor. Even for deep anchors symmetry of the failure region about the anchor axis did not exist as compared to that of a vertical anchor. The area of the failure surfaces varied with the inclination indicating the variation of ultimate uplift resistance with inclination.

This indicates that the general and local shear failures observed for vertical shallow and deep anchor exist also for inclined anchors. Due to the nonsymmetry of the failure zone and the complexity involved in any rigorous solution, symmetry is assumed in the proposed approximate method but with a consideration of the increase in the failure surface area.

7.2.4 SURFACE DISPLACEMENTS:-

Typical surface heave profiles from the author's tests are given in Fig (7.4) for vertical anchors embedded in dense, medium, and loose sand at different stages of loading. Generally, surface displacements increase as anchor load and displacement increase and as the density of the sand increases.

The surface heave profiles at failure for some tests are shown in Fig (7.5) and are plotted as the ratio of surface heave to anchor displacement $\frac{\delta s}{\delta au}$. For shallow anchors the heave ratios near the anchor axis are greatest, but reduce rapidly with distance from the anchor axis. With increase in depth the surface heave spreads further from the anchor axis but the maximum value is reduced. This decrease is expected and for large $\frac{D}{B}$ ratios uniform heave occurred, finally leading to deep anchor failure where no surface heave occurs.

Fig (7.6) shows the ratio of the surface displacement at the axis of the shallow anchor at ultimate load to the anchor displacement, $\frac{\delta c}{\delta au}$, plotted against $\frac{D}{B}$. High values of $\frac{\delta c}{\delta au}$ are obtained for low $\frac{D}{B}$ ratios and these decrease for increasing $\frac{D}{B}$ ratios and the higher values are obtained for dense sand.

These findings confirm the effect of low compressibility in dense sand in producing high displacement ratios at the sand surface and vice versa.

7.2.5 COMMENTS:-

From both the internal and surface displacements the following comments can be made:-

a/ The extent of sand movement above the anchor plate and hence the critical depth ratio $\frac{H}{B}$ where transition from shallow to deep anchor behaviour occurs are functions of sand relative density, anchor dimensions and inclination.

b/ The surface deformation increases with the relative density of the sand and the ratios of surface displacement to anchor displacement are greatest for shallow anchors, but reduce rapidly with distance from the anchor axis. For deep anchors the surface heave ratios spread further from the anchor axis but the maximum value is reduced.

c/ Based on the information obtained the simplified assumptions incorporated in the approximate method concerning the straight section of the failure surface and the compressibility of the sand are justified.

7.3 RELATIONSHIP BETWEEN UPLIFT RESISTANCE AND ANCHOR DISPLACEMENT:-

The load-displacement curves of plate anchors will be discussed in this section. The influence of different factors affecting the problem will be presented. Variations of sand density, depth and diameter of the anchor and its inclination from the vertical were the parameters studied in the present investigation. Only representative examples of the uplift load-displacement curves will be discussed due to the large number of model tests carried out by the author. The post-failure section of the curves can be examined since displacement controlled tests have been adopted in the present investigation.

7.3.1 EFFECT OF DENSITY:-

Dense, medium dense and loose sands were tested with densities, $\gamma = 1730, 1618, 1548\ kg/m^3$, these corresponded to relative densities of 85.2, 50.2, 25.4%, and covered most possible states of sand in the field. Vertical anchors (i.e. $\psi = 0^o$) with $\frac{D}{B} = 4, 15$ representing shallow and deep anchor respectively are chosen for discussion.

In Fig (5.17a) the shallow anchor case is illustrated where for all densities of sand the failure surface reaches the surface. A noticeable uplift load reduction takes place after the peak value has been attained especially in dense sand. This reduction can be explained as a result of dilatancy of the shearing sand causing a reduction in the shear strength along the failure surface and loosening of the sand in the failure zone. As the density of the sand decreases this reduction in load decreases and for loose sand little or no decrease in strength takes place. The relative position of the density to the critical density (i.e. where no volume change takes place during shearing of the sand), appears to have an influence on the shape of the anchor load-deflection curve. For loose sand which is below the critical density a decrease in volume occurs resulting in no reduction of load past the peak. However after considerable anchor displacement of shallow anchor in loose sand a slight reduction in load was recorded. This is explained as a result of both flowing of sand in the cavity created below the anchor and the considerable reduction of the depth of embedment on which the ultimate load of a shallow anchor depends significantly.

Fig (5.17b) represents the deep anchor with $\frac{D}{B} = 15$. For all the relative densities the load increases with the anchor displacement and reaches an ultimate value which is maintained nearly constant for further anchor displacements. The anchor displacement ratios at failure for $\frac{D}{B} = 15$ are higher than for $\frac{D}{B} = 4$.

7.3.2 EFFECT OF $\frac{D}{B}$:-

The extent of the reduction in shear strength of the dense sand on the failure surface can be illustrated in Fig (7.7). Curve 1 shows the behaviour of a shallow anchor of B = 50.8 mm and $\frac{D}{B} = 6$, while Curve 2 is for a deep anchor at the same depth but with B = 25.4 mm and $\frac{D}{B} = 12$. The ultimate resistance of the shallow, large diameter, anchor decreases after the peak to a value below that of the small diameter anchor which exhibits a deep failure mechanism. It was observed from the anchor load displacement curves obtained from the experimental results that for all the relative densities, deep anchors experience no reduction in mobilized uplift resistance after failure.

This may be explained as an effect of overburden soil above the failure zone which is adding resistance to the mobilized strength on the failure surface. The anchor displacement will not reduce the initial depth of embedment of the deep anchor significantly, however as mentioned in Section 7.3.1, this effect will be more pronounced in the case of shallow anchor. In addition the mobilized shear strength on the failure surface of shallow anchors depends to a greater degree on depth than for deep anchors.

7.3.3 EFFECT OF INCLINATION:-

Fig (5.16) shows that for a shallow anchor in dense sand the load reduces after the peak, while for a deep anchor the load increases with displacement without reduction similar to the vertical anchor. The anchor displacement at ultimate load increases with increase of the angle of inclination ψ. Although the depth of embedment is taken as the vertical depth D, the corresponding anchor depth in the direction of loading is $\frac{D}{\cos\psi}$ and the anchor displacement is that in the direction of loading. In comparison to the vertical anchor case, the inclined anchor with a higher value of depth of embedment (i.e. $\frac{D}{\cos\psi}$) shows the behaviour of deeper anchor. This explains the increase of anchor displacement corresponding to the ultimate load as ψ increases as well as the decrease in the critical $\frac{H}{B}$ ratio.

7.3.4 EFFECT OF γ, $\frac{D}{B}$, ψ AT INTERMEDIATE STAGES:-

Figs (5.19, 5.20) show the increasing value of anchor displacement at ultimate load and at 90% of the ultimate load with $\frac{D}{B}$ and the angle of inclination while it reduces with density.

The rate of development of anchor displacement $\frac{\delta a90\%}{\delta au}$ is found to be a function of $\frac{D}{B}$, density and ψ as shown in Fig (5.21). The ratio of $\frac{\delta a90\%}{\delta au}$ decreases as $\frac{D}{B}$ increases. This is explained by the steep anchor load displacement curve for shallow anchors and the increase of load without reduction associated with deep anchors. High values of $\frac{\delta a90\%}{\delta au}$ are observed for dense sand which indicates a high rate of mobilization of uplift resistance. This ratio reduces as ψ increases which is consistent with the development of high displacement at ultimate load.

From Figs (5.19, 5.20) correlation can be obtained between the ultimate load and anchor displacement as a function of $\frac{D}{B}$, ψ and the sand density at ultimate and prefailure loads.

7.3.5 COMMENTS:-

a/ Noticeable reduction was observed in the anchor load after the peak for shallow anchors embedded in dense sand due to the dilatancy of the sand, however in deep anchors, due to the effect of overburden sand, no reduction of load was exhibited.

b/ The anchor displacement at ultimate load increases with the angle of inclination.

c/ Correlation can be obtained between the anchor displacement at ultimate load and intermediate stages and the parameters $\frac{D}{B}$, ψ and the sand density.

7.4 VALUES OF ULTIMATE UPLIFT LOAD:-

7.4.1 EFFECT OF DENSITY:-

Fig (5.22) illustrates the relative density effect demonstrated by the formation of three distinct curves corresponding to each density. At $\frac{D}{B} = 25$ the value of $\frac{pu}{\gamma g D}$ for $D_r = 85\%$ (dense sand) is 10 and 3 times higher than that of $D_r = 25$ and 50% respectively. This indicates that higher ultimate loads can be obtained by compacting the sand above the anchor plate during the backfilling rather than by increasing the anchor dimensions.

7.4.2 EFFECT OF $\frac{D}{B}$:-

Fig (7.8) shows that the ultimate uplift load increases with the depth of anchor at an increasing rate, however the curves of the different densities of sand (D_r = 85.2, 50.2, 25.4%) become linear at greater depth depending on the respective density. These limits indicate the transfer to the deep failure mode. For greater depths the anchor load drops below the linear relationship. This can be explained as a result of reduction in the angle of internal friction due to the increase in anchor pressure.

For a given depth of embedment of a shallow anchor it was considered by the uplift theories that the shape of a failure surface is independent of the anchor plate diameter. The results of Table 5.1 support this argument which was also reported by Carr (1970). This will also be compared with the approximate method in Section 7.6.3.

Fig (7.9) shows that, for a given anchor depth, an increase in anchor plate diameter is found to reduce the average anchor plate pressure. However it was observed that for a constant $\frac{D}{B}$ ratio the anchor plate pressure is directly proportional to the anchor diameter.

Fig (5.22) shows the dimensionless ratio $\frac{pu}{\gamma gD}$ plotted against $\frac{D}{B}$ for different densities. For shallow anchors $\frac{pu}{\gamma gD}$ value increases with $\frac{D}{B}$ at an increasing rate until a change to a convex curve occurs at $\frac{D}{B}$ ratios of around 4.3, 7.8 and 10.5 corresponding to relative densities of 25.4, 50.2 and 85.2% respectively. These values correspond to the critical depth ratios $\frac{H}{B}$ observed by the surface transducers in the model tests which are the starting ratios for deep anchor behaviour. Then the rate of increase decreases as $\frac{D}{B}$ increases reaching a constant value at a very high $\frac{D}{B}$ ratio in a similar way to ultimate bearing capacity.

7.4.3 EFFECT OF INCLINATION:-

From the surface displacement transducers readings in the model tests it was found that the critical $\frac{H}{B}$ ratio (i.e. the limit ratio between shallow and deep anchor behaviour) decreases as ψ increases. This confirms the findings of Trofimenkov and Mariupolskii (1965) and the explanation was mentioned in Section 7.3.3.

Figs (5.23, 5.24) show the effect of anchor inclinations of $\psi = 22.5^{\circ}$ and 45° respectively on the ultimate uplift resistance. These figures show that the ultimate load increases with ψ. Large differences between the ultimate loads of inclined and corresponding vertical anchors were noticed at low $\frac{D}{B}$ ratios and high relative densities. As $\frac{D}{B}$ increases these differences gradually reduce. At a certain $\frac{D}{B}$ ratio the ultimate load of the inclined anchor is equal to that of the corresponding vertical anchor and for higher $\frac{D}{B}$ ratios it falls below it.

The $\frac{D}{B}$ ratio at which the curve of $\frac{pu}{\gamma gD}$ for an inclined anchor intersects with that of a vertical anchor increases with ψ and relative density.

In the present tests this intersection occurred only for loose sand (D_r = 25.4%) at both inclinations and for medium dense sand (D_r = 50.2%) only for $\psi = 22.5^o$. This intersection is assumed to occur for medium dense sand ($\psi = 45^o$) and for dense sand ($\psi = 22.5^o, 45^o$) at higher $\frac{D}{B}$ ratios than that covered in the model tests.

The findings reported by Larnach (1972, 1973) and McMullan (1974) that the anchor ultimate load occurs at $\psi = 20^o$ and 18^o respectively were not observed in this investigation.

These findings can be explained by the fact that the failure surface of a shallow inclined anchor has a larger sand volume being displaced in comparison with the corresponding vertical anchor, thus giving a higher ultimate load. However, due to the reduction in the critical $\frac{H}{B}$ ratio from that of the vertical anchor, the effect on the ultimate load is a gradual reduction and these findings can explain the difference of opinion regarding whether or not the ultimate load increases with the anchor inclination reported in Chapter 2, section 2.6.3.

7.5 DISCUSSION OF THE FINITE ELEMENT ANALYSIS RESULTS:-

7.5.1 GENERAL:-

In this section the results obtained by the author from the model tests and the finite element analysis will be discussed and compared. Although the results obtained from the finite element analysis are presented in a quantitative form, they are intended only to be a guide to the way in which a sand will behave at different stages of an uplift resistance test rather than a prediction of the precise values of the stresses and displacements which will occur. This is mainly due to the various assumptions and approximations included in the program and the properties of the material.

Two cases, namely shallow and deep anchors, will be considered and the results will be grouped into three sections.

a/ Nodal displacements.

b/ Values of ultimate uplift resistance and anchor load-displacement relationship.

c/ Magnitude and distribution of stresses.

7.5.2. NODAL DISPLACEMENTS:-

In Fig (6.5) the deformed mesh of a shallow anchor at the ultimate, which was considered to be the anchor load at 0.72 mm displacement, shows large vertical and small radial displacements. These displacements decrease as the distance from the anchor plate increases and result in a general shear failure as observed in the experimental model tests. The values of displacements directly above the anchor plate are high, creating large strains especially in the elements on the rim of the anchor, resulting in the starting of yield from this region. The propagation of yield will be discussed in section 7.5.4.

As the anchor displaces vertically a cavity is created below the anchor plate which was observed in the model tests. This is achieved in the finite element program by considering the elements on the top surface of the anchor plate to have nodes attached to it and the elements below the anchor plate to form a free surface. However in the model tests sand flows into the cavity from the sides of the anchor plate to fill part of the cavity.

In Fig (6.6) the deformed mesh of the deep anchor at ultimate load corresponding to 2.55 mm displacement shows similar trends of nodal displacements to the shallow anchor but only a localized type of failure occurred. The region above the anchor and around its rim suffers large deformations while that near the soil surface experiences very small or negligible deformations. This observation is found to be in accordance with the experimental results of local shear failure associated with the deep anchor.

Detailed information about the internal displacements of the region above the anchor axis for shallow and deep anchors respectively are shown in Figs (6.7, 6.8) and will be discussed in the following two sections.

7.5.2.1. INTERNAL DISPLACEMENTS:-

Accurate measurements of displacements in the vicinity of anchor plate models are difficult to obtain. Very few experimental techniques are available for recording soil movements in laboratory scale models (Carr & Hanna 1971). However these displacements can be obtained theoretically using the finite element method.

From Fig (6.7), for the shallow anchor, the vertical displacements at ultimate load have maximum values equal to the anchor displacement at the anchor plate level. These displacements decrease gradually to 16% of the anchor displacement at the soil surface (i.e. node 341). This shows that the soil directly above the anchor plate is compressed to a greater extent than the successive layers above. However, due to the soil compressibility, the displacement reached the sand surface in the shallow anchor (i.e. general shear failure). This is in agreement with the behaviour observed in the present experimental tests.

The deep anchor in Fig (6.7) shows similar trends to those observed in the shallow anchor, but these displacements attenuate very rapidly in the vertical direction. On reaching the sand surface (i.e. node 239) the ratio of the surface nodal displacement to that of the plate anchor is reduced to 0.8%, which for all practical purposes can be considered as negligible. Although a large displacement has been experienced by the plate anchor itself (i.e. 2.55 mm), the nodal displacements decrease with height. This would indicate that the failure surface is limited to a certain distance above the anchor plate and does not reach the sand surface as observed in the experimental model tests.

7.5.2.2 SURFACE DISPLACEMENTS:-

Fig (6.8) illustrates the profile of surface displacements for both shallow and deep anchors, each at two stages of loading. Curve 1 represents the profile of a shallow anchor at 38% of the ultimate load. At ultimate load (i.e. curve 2) the vertical surface displacement is a maximum at the axis of the anchor and attenuates very rapidly in the radial direction. At large radial distances from the axis curves 1 and 2 decrease below the surface profile of the deep anchor (i.e. curves 3 and 4). For both curves 3 and 4 which represent the profile of 35% and 100% of the ultimate load respectively, a local type of failure is indicated. These findings are similar to those found in the model test results presented in section 7.2.5 and Fig (7.5a).

In general the trends predicted by the finite element method concerning the nodal displacements, internal and surface deformations are in reasonable agreement with those observed from the laboratory model tests.

7.5.3 ULTIMATE LOAD AND LOAD DISPLACEMENT RELATIONSHIP:-

Fig (6.9) shows the load-deflection curve of a shallow anchor. It was found that the load increased with displacement and at failure it reached a value of 460 N corresponding to 0.72 mm anchor displacement. From the model tests the respective values were found to be 98 N and 2.2 mm which shows that, from the finite element analysis higher loads are obtained at lower displacement. Reducing the ultimate loads by both methods to a non-dimensional form $\frac{pu}{\gamma gD}$, values of 39 and 8.3 were obtained for the finite element and the experimental tests respectively.

Concerning the deep anchor in Fig (6.10) the ultimate load predicted was 930 N for an anchor displacement of 2.55 mm and the corresponding experimental values are 1033 N and 9 mm. The respective dimensionless ratios $\frac{pu}{\gamma gD}$ are 62.1 and 68.9

These differences between the finite element prediction and the experimental results can be attributed to the following:-

a/ In Fig (6.4) the stresses corresponding to strains higher than points E and F were taken by extrapolating the last segments CE and DF. This represents a strain hardening which is contrary to the strain softening seen in the experimental stress strain curve. Due to the inability of the finite element program to simulate strain softening behaviour high stresses are associated with yielding elements subjected to large deformations especially near the anchor rim. This resulted in predicting higher anchor ultimate loads by the finite element analysis.

b/ From the laboratory triaxial tests the minimum confining pressure which the author could obtain to simulate the stress state at the model plate anchor level was higher than that corresponding to the experimental model tests. Consequently a high level of stress was created leading to higher prediction of ultimate uplift resistance in the finite element analysis.

c/ Since sands have no tensile strength, the assumption in the finite element analysis that the material possesses equal tensile and comprehensive strength can contribute also to prediction of higher anchor ultimate loads.

7.5.4. ORDER OF YIELDING OF ELEMENTS AND FAILURE SURFACE :-

The order in which the elements yielded plastically for the shallow anchor case is shown in Fig (6.11). The first element to yield is the critical element at the rim of the anchor plate followed by the surrounding elements, and for further anchor displacements the yielding spreads further to the elements above the anchor as well as towards the anchor axis. This region represents the region of high shear stress.

At early stages the region of yielded elements forms a continuous medium between the anchor and the soil surface leaving an elastic wedge which was reported by many investigators (Carr, 1970; McMullan, 1974). This plastic region creeps to the soil surface at anchor failure indicating a general shear failure.

It was noticed also that the elements below the anchor plate rim yielded illustrating a region of tensile stresses.

The order in which the elements yielded in the deep anchor is shown in Fig (6.12). The yielding was similar to that of shallow anchor, however the vertical extent of the yielded elements above the anchor plate is comparatively low in spite of the fact that the ratio of anchor displacements of deep to shallow anchor at failure is more than 3. This suggests that local shear failure develops and in general it is in accordance with the experimental observations. Due to the large anchor displacement in the deep anchor case all the elements directly above the anchor plate yielded plastically.

From the yielding of elements of both shallow and deep anchors the failure surface can be approximated as an inverted truncated cone which reaches the sand surface in the former case. This assumption was considered in the approximate method of analysis proposed by the author in Chapter 3.

7.5.5 VARIATION OF STRESSES:-

Due to the symmetry of the anchor, the circumferential normal stress σ_θ is an intermediate principal stress. All the remaining stresses can be represented on the r-z cross section through the anchor axis.

7.5.5.1 PRINCIPAL STRESSES:-

It was observed that the directions of the major principal stresses were mainly vertical reflecting the direction of the anchor and nodal displacements. Fig (6.13) shows that the magnitudes of the major principal stresses which are compressive increase slightly over the anchor plate then decrease rapidly with increasing distance above the anchor plate reaching finally very low values at the soil surface. The minor principal stresses decrease even more rapidly and at midheight tend to be tensile stresses, however at the soil surface the stresses reduced to zero. The shape of the distribution of the principal stresses defines the extent to which the region above the plate anchor is stressed.

A similar distribution of principal stresses is noticed in the deep anchor case along C'D' in Fig (6.14). Higher stress values compared to the shallow anchor were obtained. The upper half region where low principal stresses prevail was only slightly affected by the anchor movement. This is supported by the distribution of vertical displacement in this region as discussed in section 7.5.2.1.

7.5.5.2 VARIATION OF NORMAL VERTICAL, RADIAL AND SHEAR STRESSES:-

Fig (6.15) shows distribution of normal vertical and radial stresses similar to that of the principal stresses in Fig (6.14). This is due to the symmetry of the anchor and consequently the nonexistence of shear stresses on the axis. The result of this is that on line A'B' near the axis shear stresses are very low and the values of the major principal and vertical stresses are close and the same relationship exists between the minor principal and the radial stresses. The circumferential stresses are identical to the intermediate principal stresses.

The pattern of the distribution of stresses showed the expected existence of a tensile region which extended from the soil to half the anchor depth. Fig (6.16) illustrates the distribution of the shear stresses in the r-z plane and the maximum shear stresses on line A'B' for a shallow anchor. The low values of shear stresses obtained near the anchor axis explain why the meshes along A'B' in Fig (6.2) suffer small deformations in contrast to the region above the anchor plate rim.

The maximum shear stresses have low values directly above the anchor plate. These stresses increase to a maximum value at a distance of 0.42 B and finally reduce as the surface is approached.

In the case of deep anchors, the distribution of vertical and radial stresses along C'D' in Fig (6.17) shows that similarity exists when compared with the distribution of principal stresses. The high compressive stresses directly above the anchor plate were completely dissipated when the soil surface was reached. The radial stress distribution is similar to that of the shallow anchor, but the tensile stress region extended from the soil surface to a distance of 2 B above the anchor plate.

Fig (6.18) illustrates that higher values of shear stresses and maximum shear stresses are obtained in comparison to the shallow anchor without negative stresses developing.

7.5.5.3 VARIATION OF VERTICAL NORMAL STRESSES ON ANCHOR PLATE:-

Fig (6.19) shows how the vertical compressive stress increases from the anchor axis towards the plate rim. The rate of increase is very rapid near the edge of the anchor plate and this resulted in high values of anchor load. The reason for this may be explained if we consider the analogy with the contact pressure under a rigid foundation. The distribution of the stresses on the anchor is similar to that of the foundation resting on a perfectly elastic material and vice versa for a material like sand. This case could not be simulated by the program.

7.5.6. COMMENTS:-

In general the results obtained from the finite element analysis depend on many factors. Among these factors are the capability of the program to represent the soil behaviour accurately and to satisfy the boundary conditions. The accuracy of the assumed soil parameters and whether they represent the conditions of the test is another important factor.

In this program Von-Mise's yield criteria was used as a failure criteria. In Von Mise's yield criteria the shear strength is not a function of the mean stress (i.e. the mean of the principal stresses). The shear strength on the shear failure in the sand mass depends on the normal pressure and this behaviour is better described by the Mohr Coulomb Criterion. The incorporation of the Mohr Coulomb Criterion instead of that of Von Mise's in the program and the assumption of the sand as a non-tension material are necessary. In addition to the above factors, the adoption of a more realistic stress strain curve would lead to better representation of the experimental tests and consequently the anchor behaviour during uplift loading.

7.6. COMPARISON OF RESULTS:-

7.6.1. PRESENT RESULTS AND PREVIOUS THEORIES:-

It is considered by the author that comparing the present model test results with the previous reported theories in Chapter 2 is important for further checking of the theories. The experimental results of the present investigation have been plotted in Figs (7.10, 7.11) for shallow and deep anchors along with the predicted values of ultimate loads of some of the theories reported in Chapter 2.

In Fig (7.10) the shallow anchor theories of Balla and Mariupolskii are plotted for three densities of sand corresponding to the experimental values tested (i.e. $\phi = 41.5^{\circ}$, 36.5°, 33.6° and D_r = 85.2, 50.2, 25.4% respectively). Balla's theory gives $\frac{pu}{\gamma g D}$ value at $\frac{D}{B} = 4$ for loose sand ($\phi = 33.6^{\circ}$) of the order of 91% of the value for dense sand ($\phi = 41.5^o$), however the experimental results gave 36%. This confirms the argument by Sutherland (1965) that Balla's theory is insensitive to changes in ϕ and therefore to sand density. This might be due to the narrow range of sand condition tested by Balla ($\phi = 36^o$ - 38^o) and so the great influence of varying the density was not observed. For dense sand ($\phi = 41.5^o$) the percentage of Balla's theoretical prediction to the present experimental value at $\frac{D}{B} = 4$ is 70% while that of the loose sand ($\phi = 33.6^o$) is 180%. This shows that Balla's theory underestimates the ultimate loads of dense sand and overestimates the loads for loose sand.

Mariupolskii's theory is plotted for shallow anchor range in Fig (7.10) and generally it was observed that low values of $\frac{pu}{\gamma gD}$ were predicted for the three densities at low $\frac{D}{B}$ ratios. Insensitivity to variation of angle of internal friction and density at low $\frac{D}{B}$ ratios occurred, but this is not the case as $\frac{D}{B}$ increases. As $\frac{D}{B}$ approaches 4 very high values of $\frac{pu}{\gamma gD}$ were predicted, even above the experimental results.

In Fig (7.13) for deep anchors Matsuo's anchor theory is shown to give higher values of ultimate load at small $\frac{D}{B}$ values. For $\frac{D}{B}$ values between 4 and 7 underestimation of ultimate load for dense sand and overestimation for loose sand occurred while for medium dense sand ($\phi = 36.5^o$, $D_r = 50.2\%$) reasonable agreement over a certain range exists.

Vesic's theory predicted ultimate loads for both shallow and deep anchors as in Fig (7.11). Very poor correlation exists between theory and experiments and all the theoretical values of $\frac{pu}{\gamma gD}$ for all the densities fall in the range between the experimental results of medium dense ($\phi = 36.5^o$) and loose sand ($\phi = 33.6^o$). This is an indication of the insensitivity to the variation of ϕ and D_r.

Meyerhof and Adams' theory is shown in Fig (7.11) for both shallow and deep anchor and is shown to be better than the other theories discussed. However, the theory overestimates the uplift load of loose sand and underestimates that of the dense sand. The results of the medium dense sand agree reasonably well with the theory for $\frac{D}{B}$ up to 6 beyond which the theoretical loads fall below the experimental values. The values of the critical $\frac{H}{B}$ ratio corresponding to ϕ equal to 41.5^o, 36.5^o, 33.6^o found experimentally were 10.5, 7.8, 4.3 respectively while according to Meyerhof and Adams (1968) the $\frac{H}{B}$ values correspond to 7.5, 5.6, 4.7 which shows a wide difference.

The above discussion would indicate the importance of the relative density and the compressibility of the sand for prediction of ultimate loads especially when considering different sands. This is also supported by the comparison of experiments of Baker and Kondner ($\phi = 42^o$) and that of Harvey and Burley ($\phi = 40^o$) shown in Chapter 2, Fig (2.13). It was believed that the high relative density but less frictional sand of Harvey and Burley offered greater uplift resistance than that of Baker and Kondner. The assumption of a surface failure depending only on the angle of internal friction is not accurate enough and so the effects of relative density and compressibility are necessary for any analysis of the problem. The assumption of many researchers that the failure surface reaches the soil surface at an angle of (45^o - $\frac{\phi^o}{2}$) to the horizontal is not confirmed by the photographs of the failure surface in Figs (5.13, 5.14, 7.1) which is also reported by Carr (1970) in his experimental work. Carr (1970) also reported the divergence of theories when compared with his experimental results as shown in Figs (7.12, 7.13).

7.6.2. COMPARISON OF EXPERIMENTAL RESULTS WITH THE APPROXIMATE METHOD:-

7.6.2.1 GENERAL:-

In Chapter 2 the reported theories have been shown to differ widely from each other with apparent discrepancies. Then in Section 7.5.1 the present experimental results have been plotted for both shallow and deep anchors as well as the experimental results reported by Carr (1970) against the theoretical predictions. It is concluded that none of the theories of uplift resistance is satisfactory for all sand types and states of density.

The approximate method which has been outlined in Chapter 3, and in which the additional parameters neglected by the previous theories have been considered, will be compared with the present and the previous experimental results reported. The comparison will cover all the ranges of sand densities, anchor $\frac{D}{B}$ ratios and inclinations.

7.6.2.2. CHARACTERISTICS OF SAND TESTED:-

Fig (7.14) shows the relationship between the critical $\frac{H}{B}$ ratios obtained experimentally and the angle of internal friction of the Leighton Buzzard sand used in the present investigation. $\frac{H}{B}$ is the critical depth to diameter ratio where transition from shallow to deep anchor behaviour starts. $\frac{H}{B}$ is a function of ϕ for a specific type of sand and varies from one type of sand to another. The angle of internal friction ϕ is also plotted against the relative density and the sand density as shown in Fig (7.14).

7.6.2.3. COMPARISON WITH VERTICAL, INCLINED, SHALLOW AND DEEP ANCHORS:-

In this section the ultimate loads predicted by the approximate method are compared with the experimental results obtained from the present model tests. The comparison covered shallow and deep cases of vertical and inclined anchors embedded in dense, medium dense and loose sand.

The approximate method assumes a truncated cone of failure subtending an angle α from the direction of loading. Comparing the failure surface from the photographs an assumed straight line failure surface is found to be a good approximation when trying to obtain a simple solution. The angle α is a function of ϕ , D_r and ψ for shallow and deep anchors. The parameter of relative density which was found to have a significant effect on the uplift resistance and neglected by the previous theories was considered in this method.

For deep anchors where the failure surface is limited at a distance below the surface, the effect of both overburden pressure and compressibility are considered. The effect of overburden pressure is the weight of the soil prism above the failure surface of height D-H, see Figs (3.4, 3.7). The effect of compressibility is considered by assuming the height H to be a function of ϕ and D_r. The effect of the surrounding soil above the failure surface which increases the uplift load depends on both the relative density and the angle of internal friction.

In general the parameters which are assumed by the author to be most important are taken into account in the approximate method. The equation of the ultimate load for the general inclined shallow anchor, where the vertical anchor is a special case (i.e. $\psi = 0^{o}$) is as follows:-

$$R_3 = \frac{\pi\gamma g}{24\cos^2\psi}\left(\cos^3\psi\left(\left(B + \frac{2D\tan\alpha}{\cos\psi}\right)^2 Q \left(D + \frac{B\cos\psi}{2\tan\alpha}\right) - \frac{B^3}{\tan\alpha}\right)\right.$$

$$\left. + 4D^2\tan\alpha(3B\cos\psi + 2D\tan\alpha)\right) + G_o\cos\psi \qquad (7.1)$$

where $Q = \cos\alpha \dfrac{(\cos(\psi - \alpha) + \cos(\psi + \alpha))}{\cos(\psi - \alpha)\cos(\psi + \alpha)}$ (7.2)

and for deep anchors

$$R_4 = \frac{\pi\gamma g}{24} \left(\cos\psi\left(\left(B + 2H\frac{\tan\alpha}{\cos\psi}\right)^2 Q\left(H + B\frac{\cos\psi}{2\tan\alpha}\right) - \frac{B^3}{\tan\alpha}\right) + 3\left(B+2H\frac{\tan\alpha}{\cos\psi}\right)^2\right.$$

$$Q(D-H)\cos\psi + \frac{4H\tan\alpha}{\cos^2\psi}(B\cos\psi(6D-3H) + H\tan\alpha(6D-4H)) + 12k_o\tan\bar{C}\phi\,(D-H)^2$$

$$\left.((B\cos\psi + 2H\tan\alpha)\left(3 + \frac{3Q}{2} - 2\sqrt{Q}\right)))\right) + G_o\cos\psi \qquad (7.3)$$

As mentioned earlier α is a function of ϕ, D_r and ψ.

$$\alpha = M\phi \qquad (7.4)$$

The values of M, $\bar{C}$ and $\frac{H}{B}$ are found empirically to be

$$M = 0.25\left(D_r\frac{(1+\cos^2\phi)}{2} + \frac{(1+\sin^2\phi)}{2}\right)(1+\cos\psi) \qquad (7.5)$$

$$\bar{C} = D_r\cos\phi \qquad (7.6)$$

$$\left(\frac{H}{B}\right)_\psi = \left(\frac{H}{B}\right)_{\psi=o}\frac{(1 + 0.4\cos\psi)}{1.4} \qquad (7.7)$$

See P. 218a.

According to the sand tested the densities at which model tests were carried out were 1730, 1618, 1548 kg/m^3 corresponding to $\phi = 41.5^\circ$, 36.5°, 33.6° and relative densities of 85.2, 50.2 and 25.4% respectively. The corresponding critical $\frac{H}{B}$ ratios are 10.5, 7.8, 4.3 for the vertical anchor. The term of the anchor body will not be included because it is known for any dimension of anchor.

Fig (7.15) shows the comparison between the ultimate load predicted by the approximate method and the experimental model test results of vertical anchors. It is shown that good correlation exists between them in both the shallow and deep anchor ranges. For dense, medium dense and loose sand good agreement is also found to exist for all the $\frac{D}{B}$ ratios tested. The method is found to be satisfactory for shallow as well as deep vertical anchors. The method is then tested against inclined anchors for $\psi = 22.5^{o}$ and 45^{o} as illustrated in Figs (7.16, 7.17) respectively. The comparison covers shallow and deep anchors as well as dense, medium dense and loose sand and a good correlation is found to exist for all $\frac{D}{B}$, density and inclination values.

It was concluded by the author that the approximate method gives good agreement with the present vertical and inclined anchor model test results covering shallow and deep anchors embedded in different densities of the sand.

The predicted ultimate loads by the approximate method were also plotted with the experimental results in the non-dimensional forms of $\frac{R}{B^3\gamma_g}$, against $\frac{D}{B}$ and $\frac{R}{B^2D\gamma}$ against $(\frac{D}{B})^2$ as reported by Baker and Kondner (1966) and are shown in Figs (7.18, 7.19). It is shown that in Fig (7.18 a,b,c) for shallow anchor ranges curves extend up to $\frac{H}{B}$ then become nearly straight lines in the deep anchor range. On the other hand in Fig (7.19 a,b,c) where $\frac{R}{B^2D\gamma_g}$ is plotted against $(\frac{D}{B})^2$ first straight lines exist in the shallow anchor range followed by curved lines in the deep range. These trends confirm those reported by Baker and Kondner (1966) showing the distinct limit between shallow and deep anchors and good correlations exist between the approximate method and the experiments.

7.6.2.4. COMPARISON OF SURFACE FAILURE:-

In section 7.6.2.3 comparison of ultimate loads was made between the approximate method and the model test results. In this section the surface failure dimensions on the sand surface were measured and compared with those predicted by the approximate method for shallow anchors. From Table 7.2, taking into account the approximate nature of the method, a comparison between the experimental and the approximate method predicted values of the surface failure dimensions B_{sj} and B_{sn} showed reasonable agreement. As the value of the angle of inclination ψ increases the dimensions predicted by the approximate method are slightly higher. This is explained by the dependence of the approximate method on the symmetry about the anchor axis.

The percentage of the contribution of the soil weight to the total ultimate uplift resistance is plotted for all densities and inclinations as shown in Fig (7.20). In the deep anchor case the contribution of the soil weight was taken as the weight of the soil inside the failure zone and the overburden soil.

It is shown that the relative contribution of the soil weight is highest at shallow depths and loose sand and decreases sharply in the shallow range, then decreases slowly in the deep range where loose sand contributes less than dense sand. The same trend is shown for inclined anchors, however a slight increase of the relative soil weight contribution is observed. This is an analogy to the bearing capacity factors and their relative contribution to the ultimate load. These findings are based on the predictions of the approximate method but could not be checked experimentally.

7.7. COMPARISON OF APPROXIMATE METHOD WITH OTHER TESTS:-

7.7.1. GENERAL:-

From Section 7.5 it was found that the approximate method is in good agreement with the author's test results. It was thought necessary by the author to compare the approximate method with other test results to check its general applicability for other types of sand.

This is also necessary to ensure that the agreement was not merely fortuitous for the sand used in the present investigation. The comparison is intended to cover shallow and deep anchors, both vertical and inclined. Model tests as well as field tests are compared for checking the dimensional similarity between the model and prototype.

7.7.2. COMPARISON WITH VERTICAL SHALLOW MODEL ANCHOR TESTS:-

The approximate method is plotted against the results of previous experimental results. The parameters necessary are the angle of internal friction ϕ, the relative density D_r and the critical ratio $\frac{H}{B}$ for each condition tested.

In Figs (7.21 a,b,c) experimental results carried out by El-Rayes (1965) at Glasgow University for three types of sand are plotted with the approximate method. In Fig (7.21a) Leighton Buzzard sand at four densities shows good correlation. Fig (7.21b) shows the results of local concreting sand at dense and loose states and Fig (7.21c) is plotted for Sizewell sand. These results agree well with the predications of the approximate method.

Balla (1961) and Mariupolskii (1965) model test results were plotted in Fig (7.22 a,b) and as shown the agreement is reasonable. The same agreement is shown in Fig (7.23a) where Sutherland (1965) model tests were plotted.

The approximate method is found to predict ultimate uplift resistances of shallow model anchors embedded in different types of sands at different densities with good accuracy.

7.7.3. COMPARISON WITH SHALLOW FIELD ANCHOR TESTS:-

The approximate method is assumed to predict ultimate loads for prototype scale anchors as well as model scale anchors. The field tests carried out at Sizewell nuclear power station and reported by Sutherland (1965) are plotted with the predictions of the approximate method as illustrated in Fig (7.23b). This agreement confirms the versatility of the approximate method in reasonably predicting the ultimate uplift resistance of both model and field shallow anchors.

7.7.4. COMPARISON WITH DEEP MODEL ANCHOR TESTS:-

Similar to shallow anchors the approximate method is compared with the results of some deep model anchor test results. For some of the results the critical $\frac{H}{B}$ was not reported, however from the plotting of $\frac{pu}{\gamma gD}$ against $\frac{D}{B}$ the $\frac{D}{B}$ ratio at which the behaviour of the curve changes indicates the change of mode of failure from shallow to deep. This $\frac{D}{B}$ ratio is taken by the author as the critical ratio $\frac{H}{B}$. In some papers the relative densities were not mentioned but from the description of the state of sand a reasonable value could be assumed. This information is used in the approximate method to predict the ultimate uplift resistance.

The results reported by Bemben and Kupferman (1975) for deep anchors embedded in two types of sand each at two different densities were plotted in Fig (7.24 a,b). The correlation with Sunderland sand is very good for both densities while for BBY sand the correlation for loose sand is good, however, the predicted values for dense sand are slightly higher than the experimental results.

The results reported by Harvey and Burley (1973) for vertical anchors are shown in Fig (7.25a) and good agreement is found. The results of Squivel and Diaz (1967) are plotted in Fig (7.25b) and better agreement is found with loose sand, however for dense sand slight underestimation is found with the prediction of the approximate method. The results reported by Baker and Kondner (1966) are plotted in Fig (7.26) and good agreement is found. Carr (1970) plotted his experimental results in Figs (7.12, 7.13) and compared them with the previous theories and the author plotted the predicted loads by the approximate method and was shown to give reasonable results with loose sand, however slight underestimation of loads occurs for dense sand. The explanation is that Carr's dense sand is subjected to dynamic overconsolidation by Kango hammer. Moreover Carr used a plate anchor of 25 mm thickness and 51 mm diameter which is considered as a very thick plate anchor which has considerable effect on the ultimate load. This effect is neglected as being very small for small thicknesses in the approximate method which is on the safe side.

7.7.5. COMPARISON WITH INCLINED SHALLOW, DEEP, MODEL AND FIELD ANCHOR TESTS:-

The results of inclined model tests reported by Harvey and Burley (1973) and the field tests reported by Kananyan (1966) are plotted in Fig (7.27) and compared with the approximate method. In Fig (7.27b) the ψ values tested by Kananyan (1966) were 0^{o}, 10^{o}, 20^{o}, 30^{o}, 40^{o}, 45^{o} and the predicted values show good agreement, however slight underestimation is observed. This is thought to be due to the existence of some cohesion ($c = 0.72$ psi) in the sand used by Kananyan (1966), while the predicted values were for purely cohesionless sand.

In Fig (7.27a) the results of Harvey and Burley (1973) are for $\psi = 0^{o}$, 15^{o}, 30^{o}, 45^{o}. It was noticed that the results for $\psi = 15^{o}$ and 30^{o} are lower than the vertical anchor of $\psi = 0^{o}$ of shallow depths. The theoretical values predicted by the approximate method and those predicted by Harvey and Burley (1973) inclined anchor theory were plotted for comparison with the experimental results. It was found that the approximate method shows more reasonable agreement with the experimental results.

It was considered by the author that the approximate method can predict to a reasonable degree the ultimate uplift resistance of model and prototype scale plate anchors, vertical and inclined, shallow and deep embedded in different types of sand and densities.

7.7.6. THE EFFECT OF INCLINATION:-

From the author's experimental results it was found that as ψ and γ increase the ultimate load increases. The effect of inclination in increasing the ultimate load is very slight at low ψ values and a loose sand state as shown in Fig (7.28a,b,c). The ultimate load of loose sand and $\psi = 22.5^{\circ}$ are very close to those of vertical ($\psi = 0^{\circ}$) but for $\psi = 45^{\circ}$ the increase is appreciable. As the density increases the effect of inclination is more significant.

This explains the difference of opinion between many investigators whether there is an increase of load as ψ increases as reported in sections 2.6.3 and 7.4.3.

It was observed from the experimental results that the critical $\frac{H}{B}$ value decreases as ψ increases which also confirms the findings of Trofimenkov and Mariupolskii (1965). Due to this reduction in the extent of the failure zone for deep anchors (i.e. reduction in $\frac{H}{B}$ value) the ultimate uplift resistance of inclined anchors tends to decrease the rate of load increase as $\frac{D}{B}$ increases falling below the ultimate load of a corresponding vertical anchor at high $\frac{D}{B}$ ratios.

The approximate method simulated these observations very closely as illustrated in Fig (7.28). The approximate method can predict ultimate loads of circular plate anchors for shallow and deep anchors embedded vertically in different types of sand and range of densities. The method also predicts ultimate loads of inclined anchors to a reasonable accuracy, however the range of inclination should not exceed 60°. This is due to the dependence of the soil resistance on the lateral deflection of the anchor.

7.8. DESIGN CURVES AND EXAMPLES:-

7.8.1. DESIGN CURVES:-

The design of any structure using anchors depends on two factors. The first factor is the maximum load which the anchor can resist assuming no failure in the anchor material. The other factor is the maximum displacement the anchored structure can tolerate and the safety factor can be based on either of the above criteria. Site investigation and pilot tests are necessary to provide the necessary information for design.

By stressing the anchor up to 70-80% of its ultimate load during construction, large initial anchor displacements can be induced and so will reduce the subsequent anchor displacements, Howat (1969).

Design tables shown in Appendix A were obtained for Leighton Buzzard sand using the approximate method. Design curves, obtained from these tables, and presented in Appendix B, show the plot of the dimensionless ratio $\frac{pu}{\gamma gD}$ against $\frac{D}{B}$ ratio ranging from 1 to 25. Three ranges of density (dense, medium dense and loose sand) are covered including anchor inclinations of 0°, 10°, 20°, 30°, 40° and 50°.

From Figs (5.19, 5.20) relationships can be obtained correlating the anchor displacements at 90% and 100% of the ultimate uplift resistance of the plate anchor.

The author believes that a better demonstration of the calculation of anchor ultimate load and displacement can be presented by some examples.

7.8.2. EXAMPLES OF DESIGN:-

In the design of anchors, as with any foundation problem, it is necessary to know some properties of the soil. These properties include the angle of internal friction ϕ, sand density γ, and the relative density D_r which can be obtained from penetration tests in boreholes and from laboratory tests on borehole samples of the soil. Other parameters are the anchor depth D, anchor diameter B, critical $\frac{H}{B}$ ratio of the soil and the anchor inclination from the vertical direction.

Ultimate loads are calculated, for the purpose of illustrating the design procedure, for anchors embedded in Leighton Buzzard sand in the following conditions.

a/ Vertical anchor ($\psi = 0^{o}$) embedded in dense sand.

b/ Inclined anchor ($\psi = 20^{o}$) embedded in medium dense sand.

c/ Inclined anchor ($\psi = 40^{o}$) embedded in loose sand.

a/ Vertical anchor ($\psi = 0^{o}$) embedded in dense sand:-

The following properties of the sand are assumed

$\phi = 40^{o}$, $D_r = 75\%$ and $\gamma = 1698\ kg/m^3$

1/ Shallow anchors:-

(i) Taking $\frac{D}{B} = 2$, B = 600 mm

From Table (A.1) $\frac{pu}{\gamma g D}$ corresponding to $\phi = 40^{o}$ and $\frac{D}{B} = 2$ is 7.45.

The ultimate load $R = \frac{pu}{\gamma g D} X \frac{\pi}{4} B^2 D\gamma g$.

$\therefore R_1 = 7.45 \times \frac{\pi}{4} \times (600)^2 \times 1200 \times \frac{1698 \times 9.807}{10^{12}} = 42$ KN

The value of R includes the shearing resistance on the failure surface and the weight of the soil inside the failure surfaces considering the anchor shaft filled with soil. The additional forces to be added are the anchor plate weight and the product of the volume of the anchor shaft and of the difference in weight between the density of the anchor shaft material and the soil.

Assuming the anchor shaft diameter and the anchor plate thickness to be 0.1 B for a reinforced concrete anchor, these additional forces were calculated. The percentage of the additional forces to R was found to be in the order of 1%. For design purposes, these additional forces were neglected and were considered to be on the safe side.

From Figs (5.19, 5.20), using interpolation, the ratios of anchor displacements to anchor diameter at ultimate load $\frac{\delta au}{B}$ and at 90% of the ultimate load $\frac{\delta a90\%}{B}$ are obtained.

$\frac{\delta au}{B} = 0.03$ and $\frac{\delta a90\%}{B} = 0.016$

$\therefore$ Anchor displacement at ultimate load $\delta au = 0.03 \times 600 = 18$ mm and anchor displacement at 90% of ultimate load $\delta a90\% = 0.016 \times 600 = 10$ mm.

(ii) Increasing B from 600 mm to 1200 mm, $\frac{D}{B} = 2$ and $\frac{pu}{\gamma g D} = 7.45$ we obtain

$R_1 = 337$ KN, $\delta au = 36$ mm $= a90\% = 20$ mm.

2/ Deep anchors:-

(i) $\frac{D}{B} = 12$, B = 600 mm and from Table A.1 or from Fig (B.1)

$\frac{pu}{\gamma g D} = 109.09$, the results are

R_2 = 3698 KN δau = 0.25 B = 150 mm, $\delta a90\%$ = 0.11 B = 66 mm

(ii) Increasing B from 600 mm to 1200 mm, $\frac{D}{B}$ = 12 and $\frac{pu}{\gamma gD}$ = 109.09 we obtain

R_2 = 29585 KN, δau = 300 mm, $\delta a90\%$ = 132 mm.

b/ Inclined anchor ($\psi = 20^o$) embedded in medium dense sand:-

The properties of medium dense sand are taken as $\phi = 37^o$, D_r = 54%, γ = 1628 kg/m^3.

The ultimate load acts in the direction of loading i.e. at 20^o from the vertical.

1/ Shallow anchor:-

Given $\frac{D}{B}$ = 2, B = 600 mm. From Table A.3 or Fig (B.9)

$\frac{pu}{\gamma gD}$ = 5.82 we obtain

R_3 = 32 KN, δau = 0.039B = 23 mm, $\delta a90\%$ = 0.02B = 12 mm.

2/ Deep anchor:-

$\frac{D}{B}$ = 12, B = 600 mm. From Table A.3 or Fig (B.9) $\frac{pu}{\gamma gD}$ = 62.48 we obtain

R_4 = 2031 KN, δau = 0.36B = 216 mm, $\delta a90\%$ = 0.18B = 108 mm.

c/ Inclined anchor ($\psi = 40^o$) embedded in loose sand:-

The properties of loose sand are taken as

$\phi = 34^o$, D_r = 29.3%, γ = 1559 kg/m^3

1/ Shallow anchor:-

$\frac{D}{B}$ = 2, B = 600 mm. From Table A.5 or Fig (B.17) $\frac{pu}{\gamma gD}$ = 4.71 we obtain

R_3 = 24.7 KN, δau = 0.11 B = 66 mm, $\delta a90\%$ = 0.06B = 36 mm.

2/ Deep anchor:-

These correlations were obtained from an examination of the results from the author's tests and those of other investigators. A total of 25 tests were analysed.

The expression given in equation 7.5 was obtained by a process of trial and error and Fig (7.14a) indicates the values of α (theoretical) resulting from the correlation compared with the α values (experimental) obtained from the 25 test results.

The correlation given in equation 7.6 was obtained by calculating the values of the theoretical ultimate loads using equation 7.3 and then subtracting from these values the component due to partial friction which embodies the factor $\bar{C}$ in equation 7.3. A theoretical ultimate load minus its partial friction component was then plotted and compared with the corresponding experimental curve, an example being shown in Fig (7.15). The difference between these two curves was then used to obtain the correlation given in equation 7.6. The validity of the correlation is shown in Fig (7.14b) where the theoretical values of $\bar{C}$ (obtained from the correlation) are plotted against the experimental $\bar{C}$ values from which the correlation was derived.

TABLE 7.1 MEASUREMENTS OBTAINED FROM MODEL TESTS AND FINITE ELEMENT ANALYSIS

CATEGORY	TYPE OF MEASUREMENT
Laboratory model tests only	Measurement of surface deformation at different stages of loading and internal displacements after model failure. Relationship between uplift resistance and anchor displacement at pre and post failure conditions for different anchor dimensions, inclinations and soil densities
Finite element analysis only	Magnitude, direction and distribution of stresses within the soil mass of vertical anchors. Order of yielding of elements. Detailed displacements of soil at the surface and within the mass of the soil at any stage of loading before failure.
Obtained from both methods	Relationship between uplift resistance and anchor displacements at pre failure conditions. Values of ultimate uplift resistance

TABLE 7.2 COMPARISON OF THE FAILURE SURFACE DIMENSIONS MEASURED AND THE APPROXIMATE METHOD

TEST NO.	ANGLE OF INCLIN	SAND DENSITY $\gamma kg/m^3$	ANCHOR DIMENSIONS			SURFACE FAILURE DIMENSIONS			
						EXPERIMENTAL		APPROX. METHOD	
			D (mm)	B (mm)	$\frac{D}{B}$	Bsj (mm)	Bsn (mm)	Bsj (mm)	Bsn (mm)
5	0°	1730	152.4	50.8	3	216		217.7	
6			203.2	50.8	4	254		273.6	
8			304.8	50.8	6	343		384.8	
18		1618	76.2	76.2	1	140		131.3	
20			152.4	76.2	2	203		186.4	
22			190.5	63.5	3	203		201.4	
39		1548	76.2	76.2	1	89		115.8	
72	22.5°	1730	76.2	76.2	1	178	152	184.7	162.6
73			152.4	76.2	2	305	254	287	252.2
74			190.5	63.5	3	355	305	307.3	283.3
75			203.2	50.8	4	305	254	334.9	288.5
83		1618	76.2	76.2	1	165	127	144.5	131.1
84			152.4	76.2	2	216	191	205.2	185.9
94		1548	76.2	76.2	1	152	127	128.5	117.3
95			152.4	76.2	2	229	178	173.7	158.8
105	45°	1730	76.2	76.2	1	216	152	311.4	174.5
106			152.4	76.2	2	254	229	487	272.8
107			190.5	63.5	3	254	229	552	309
109			254	50.8	5	305	254	675.4	378
116		1618	76.2	76.2	1	229	178	215.4	139.7
117			152.4	76.2	2	203	178	312.9	202.4
118			190.5	63.5	3	305	203	342.4	221
127		1548	76.2	76.2	1	216	152	184.2	123.7
128			152.4	76.2	2	254	178	254.8	171.5

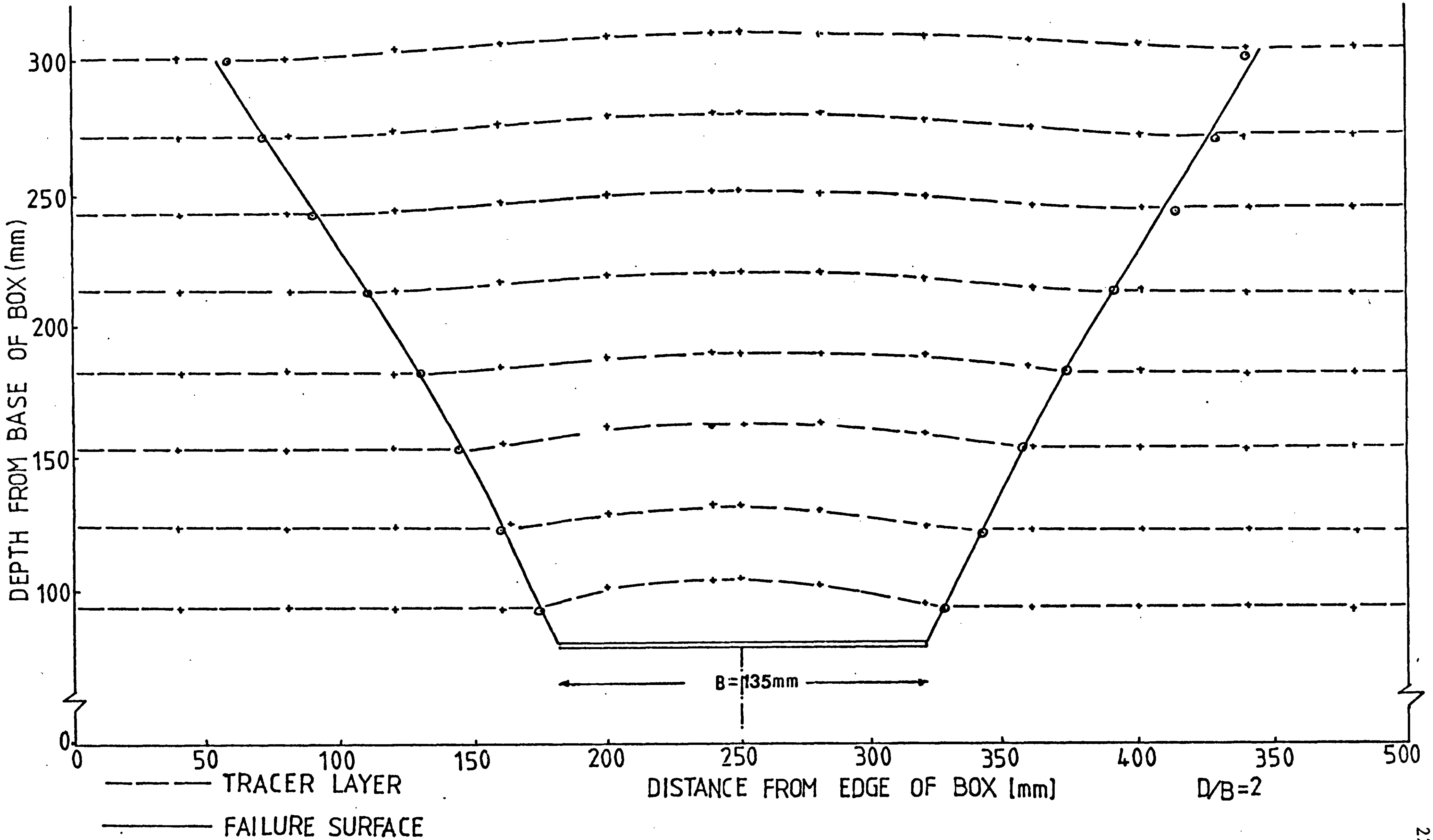

FIG.7.1 FINAL POSITION OF TRACER LAYERS

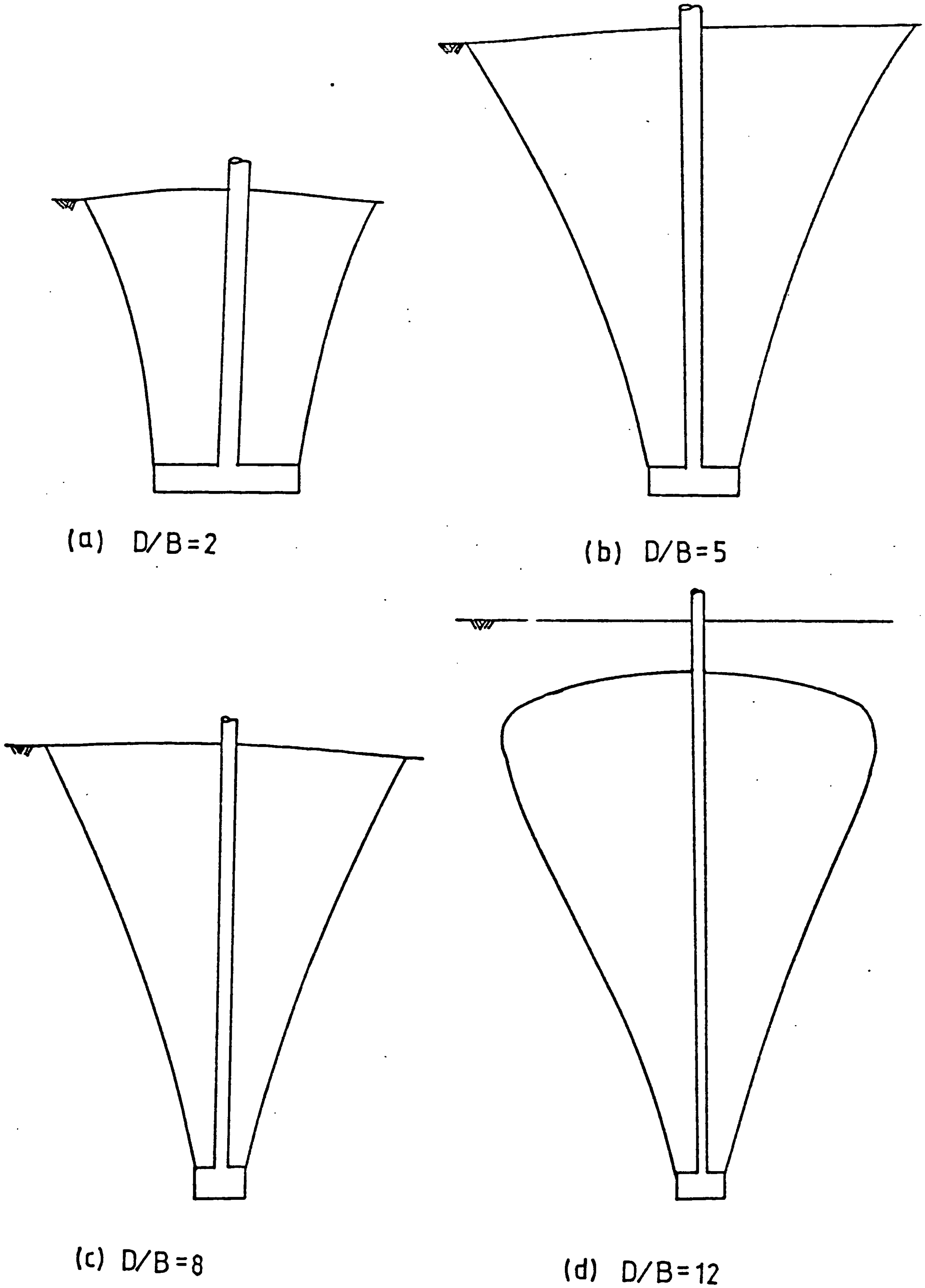

FIG.7.2 BOUNDARIES OF FAILURE SURFACE OBTAINED FROM PHOTOGRAPHIC TESTS

(AFTER CARR 1970)

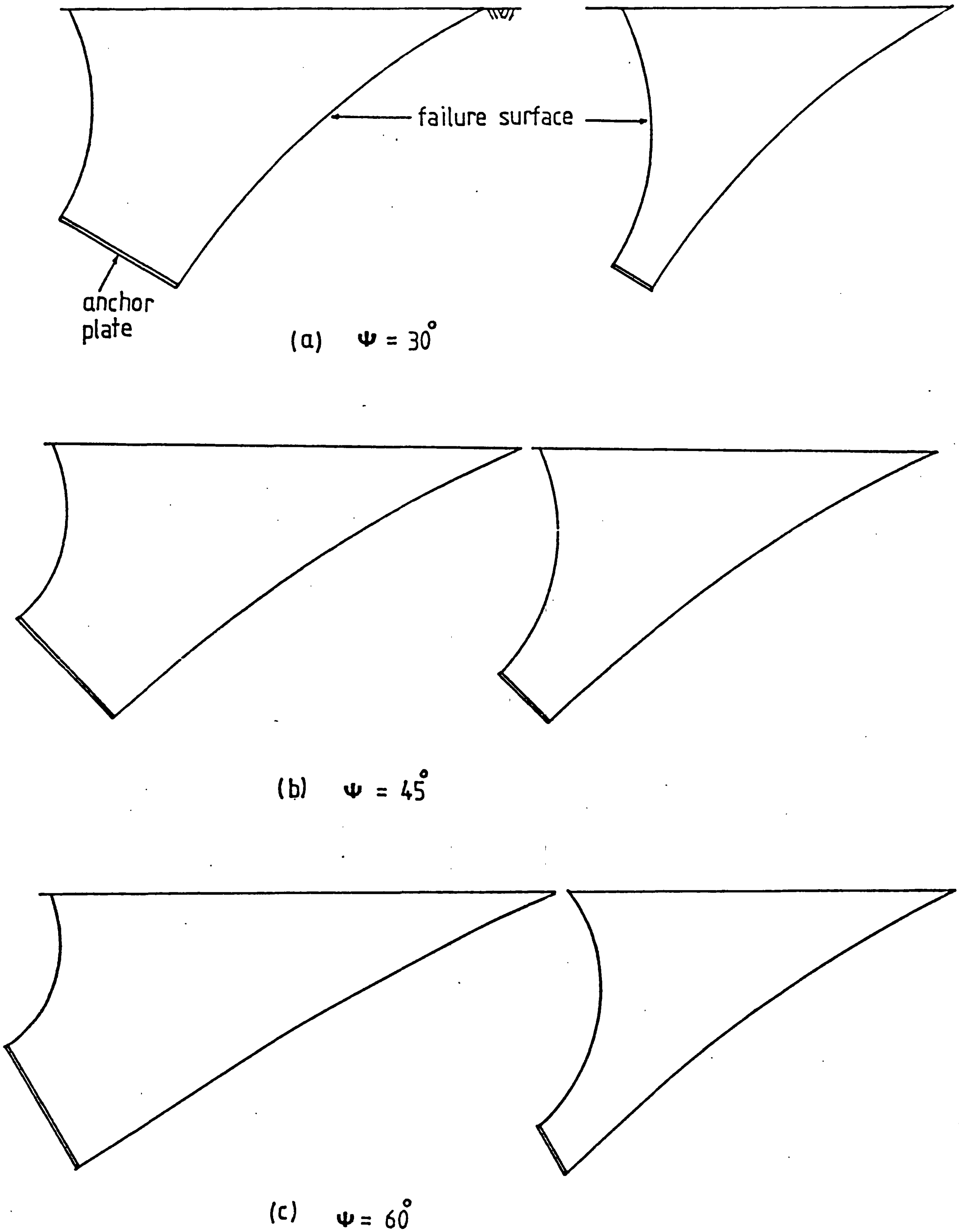

FIG 7.3 BOUNDARIES OF FAILURE SURFACES FOR INCLINED ANCHORS

(AFTER GILLON 1970)

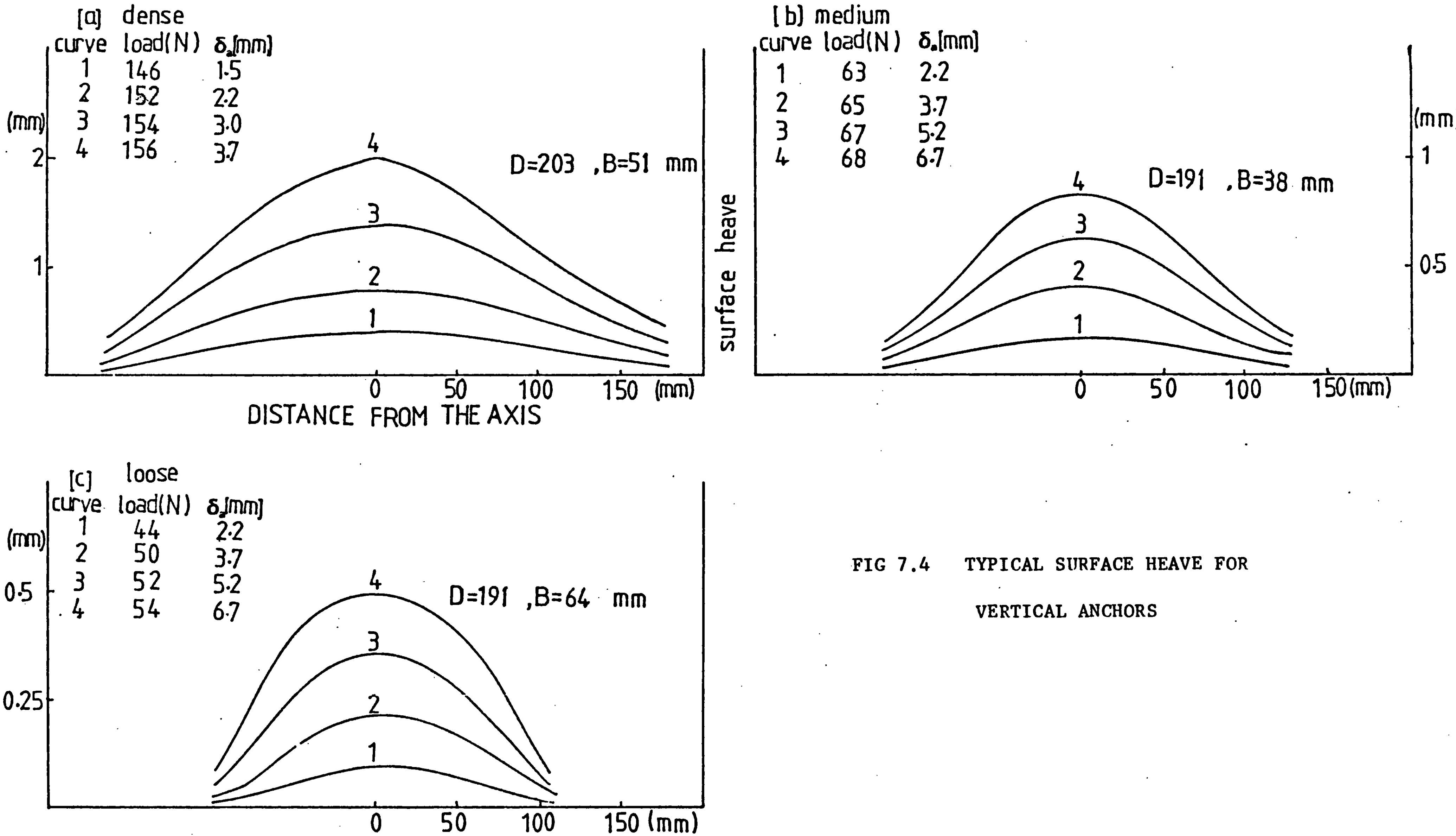

FIG 7.4 TYPICAL SURFACE HEAVE FOR VERTICAL ANCHORS

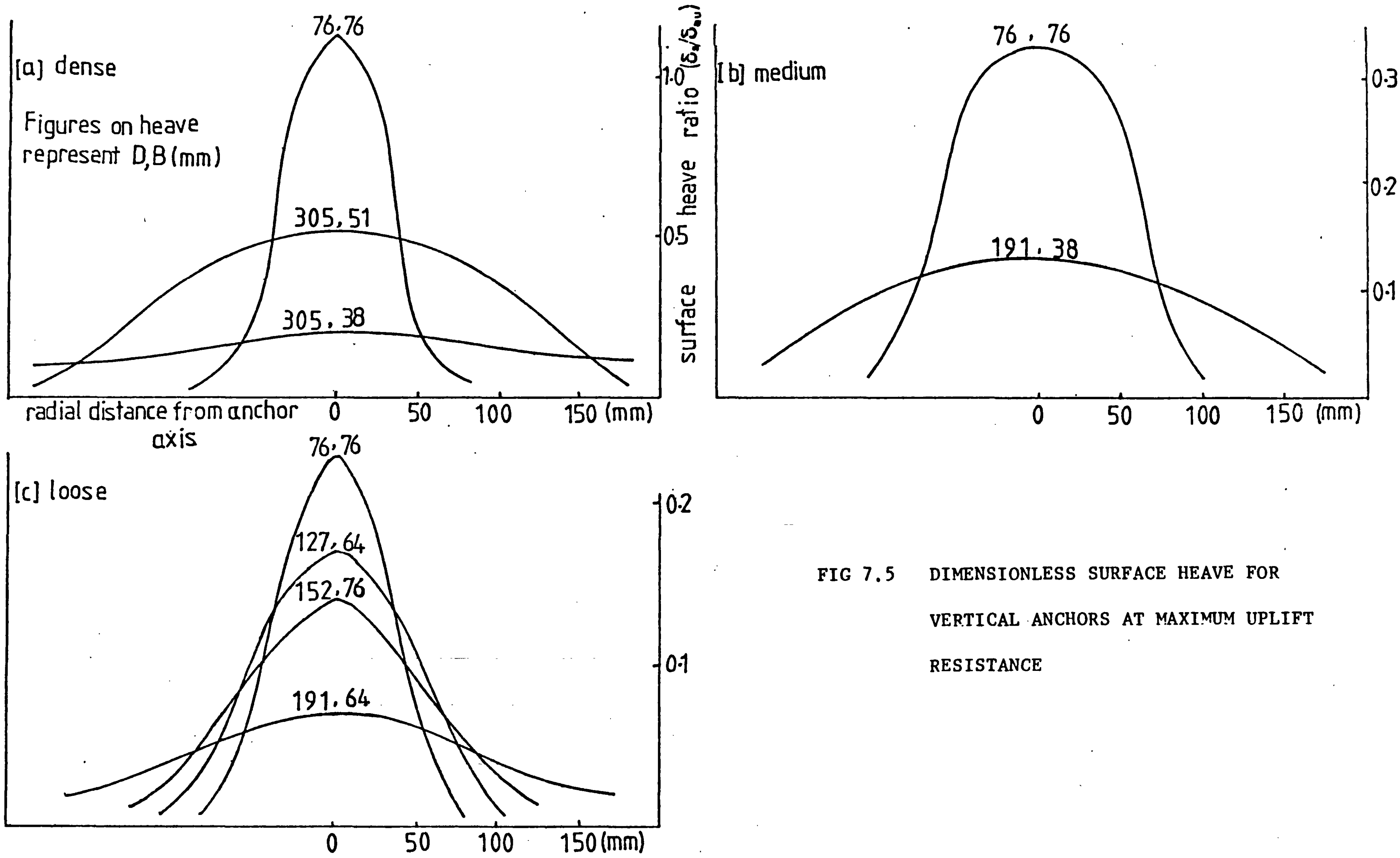

FIG 7.5 DIMENSIONLESS SURFACE HEAVE FOR VERTICAL ANCHORS AT MAXIMUM UPLIFT RESISTANCE

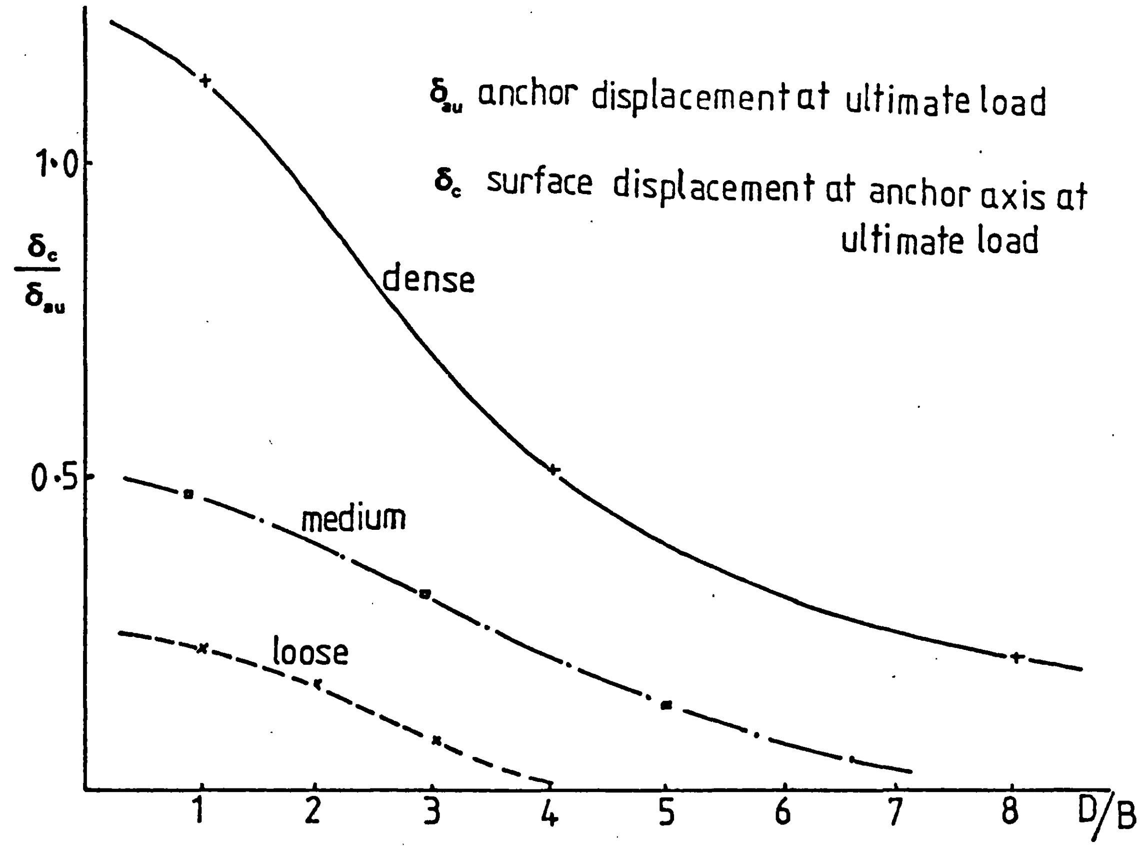

FIG 7.6 RATIO OF SURFACE DISPLACEMENT AT ANCHOR AXIS TO ANCHOR DISPLACEMENT AT ULTIMATE LOAD VERSUS D/B

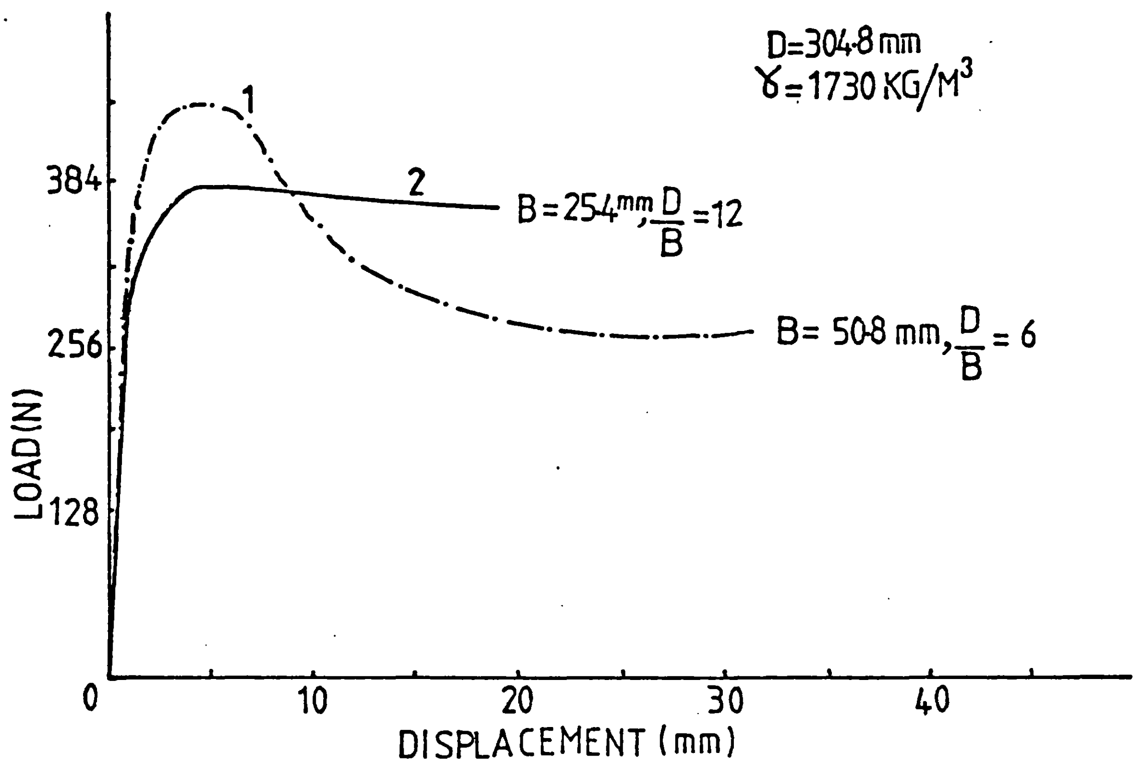

FIG 7.7 LOAD-DISPLACEMENT OF SHALLOW AND DEEP ANCHORS

FIG 7.8 RELATIONSHIP BETWEEN MAXIMUM UPLIFT LOAD AND ANCHOR DEPTH FOR DIFFERENT DENSITIES

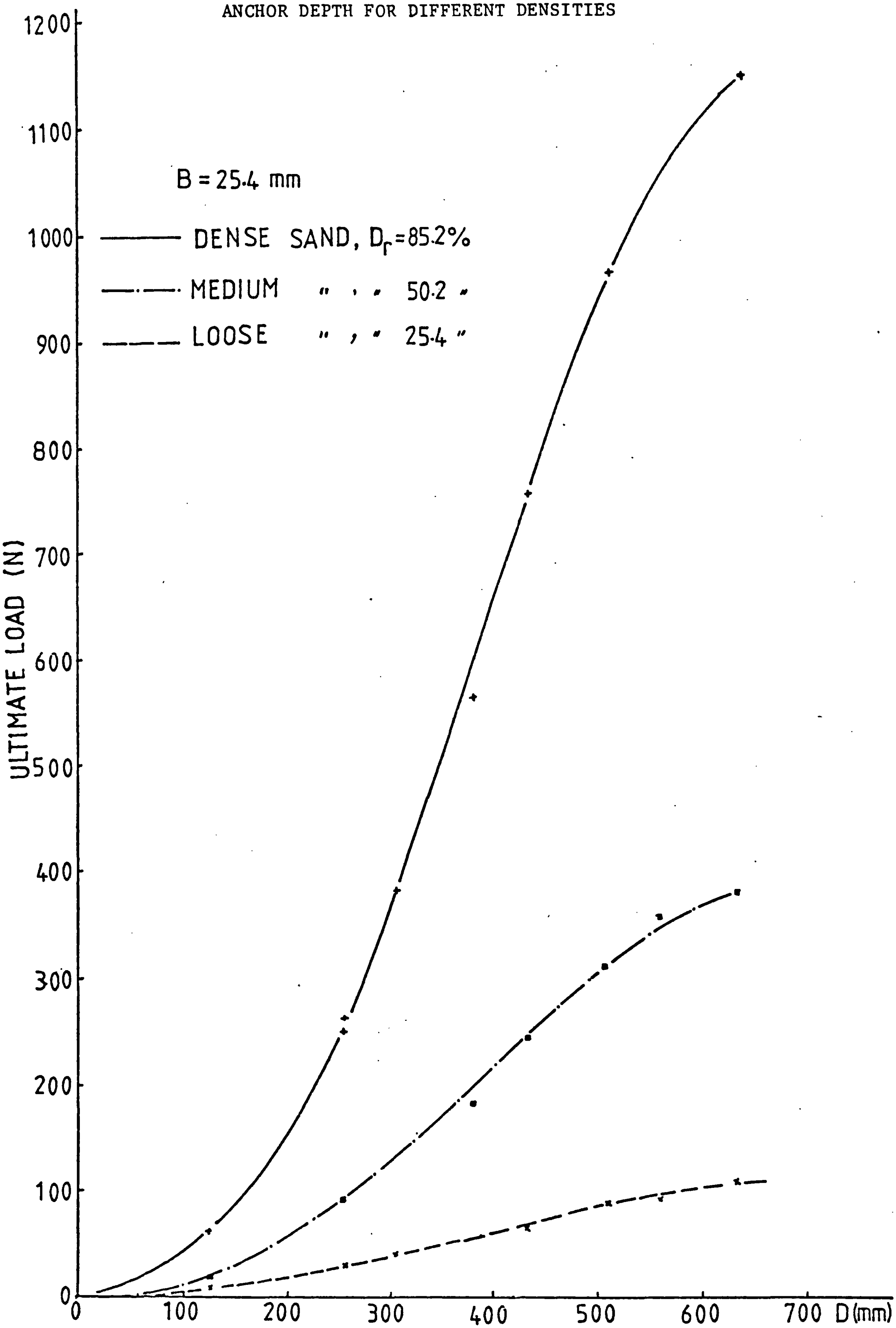

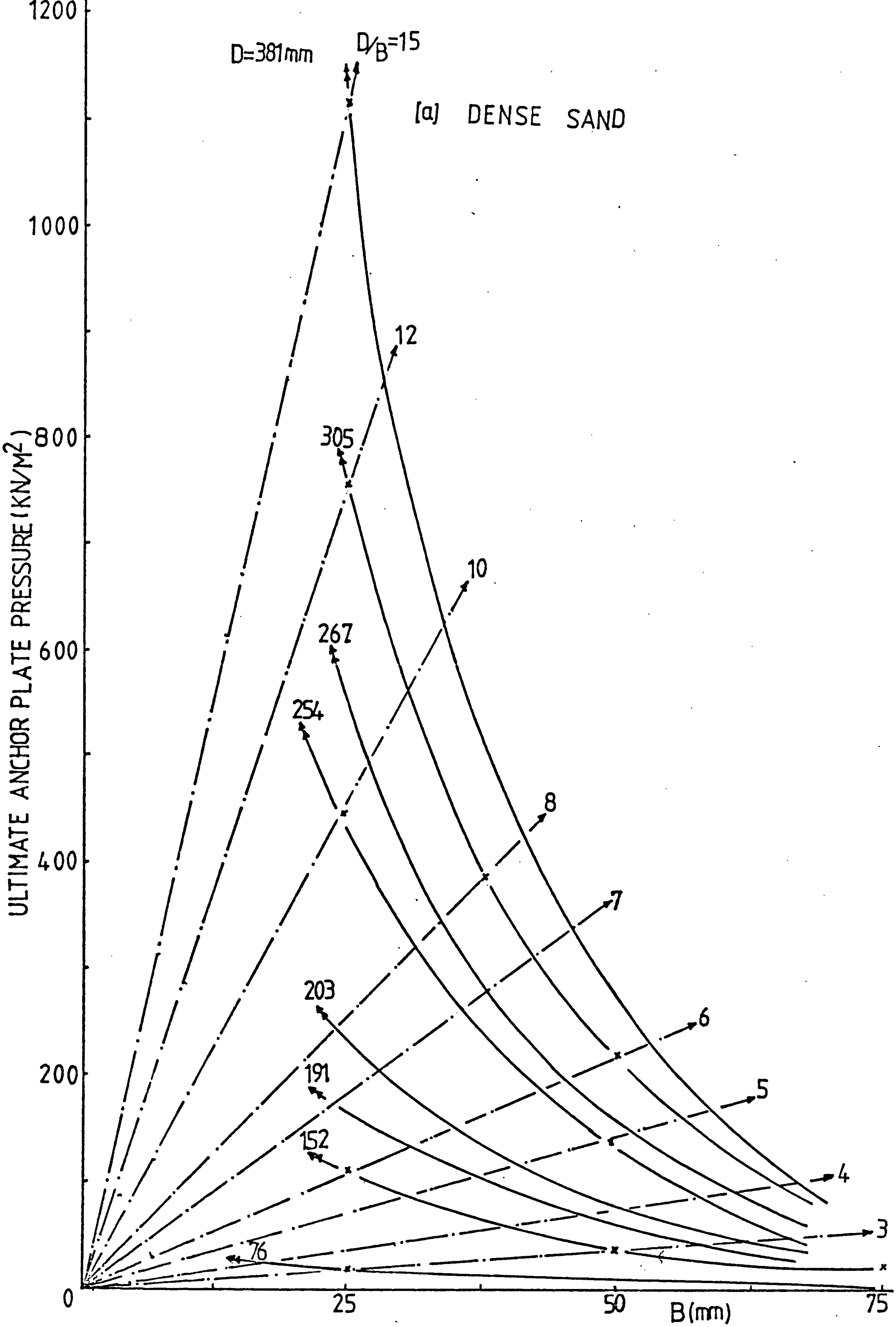
(a) DENSE SAND
D=381mm
D/B=15
12
305
10
267
254
8
7
203
6
191
5
152
4
3
76
ULTIMATE ANCHOR PLATE PRESSURE (KN/M²)
1200
1000
800
600
400
200
0
25
50
75
B(mm)

FIG 7.9 VARIATION OF ULTIMATE AVERAGE PRESSURE WITH DEPTH AND DIAMETER OF ANCHOR

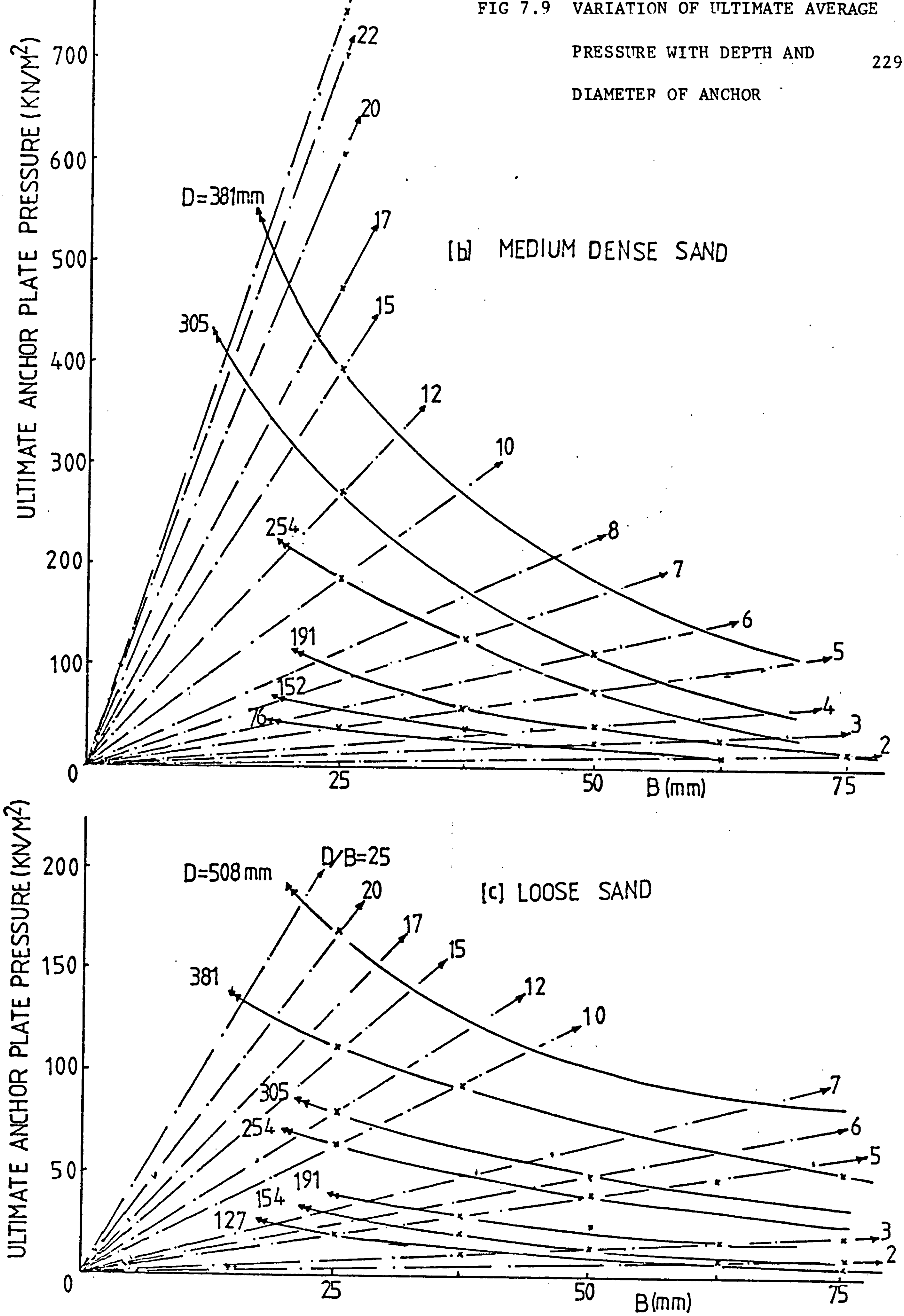

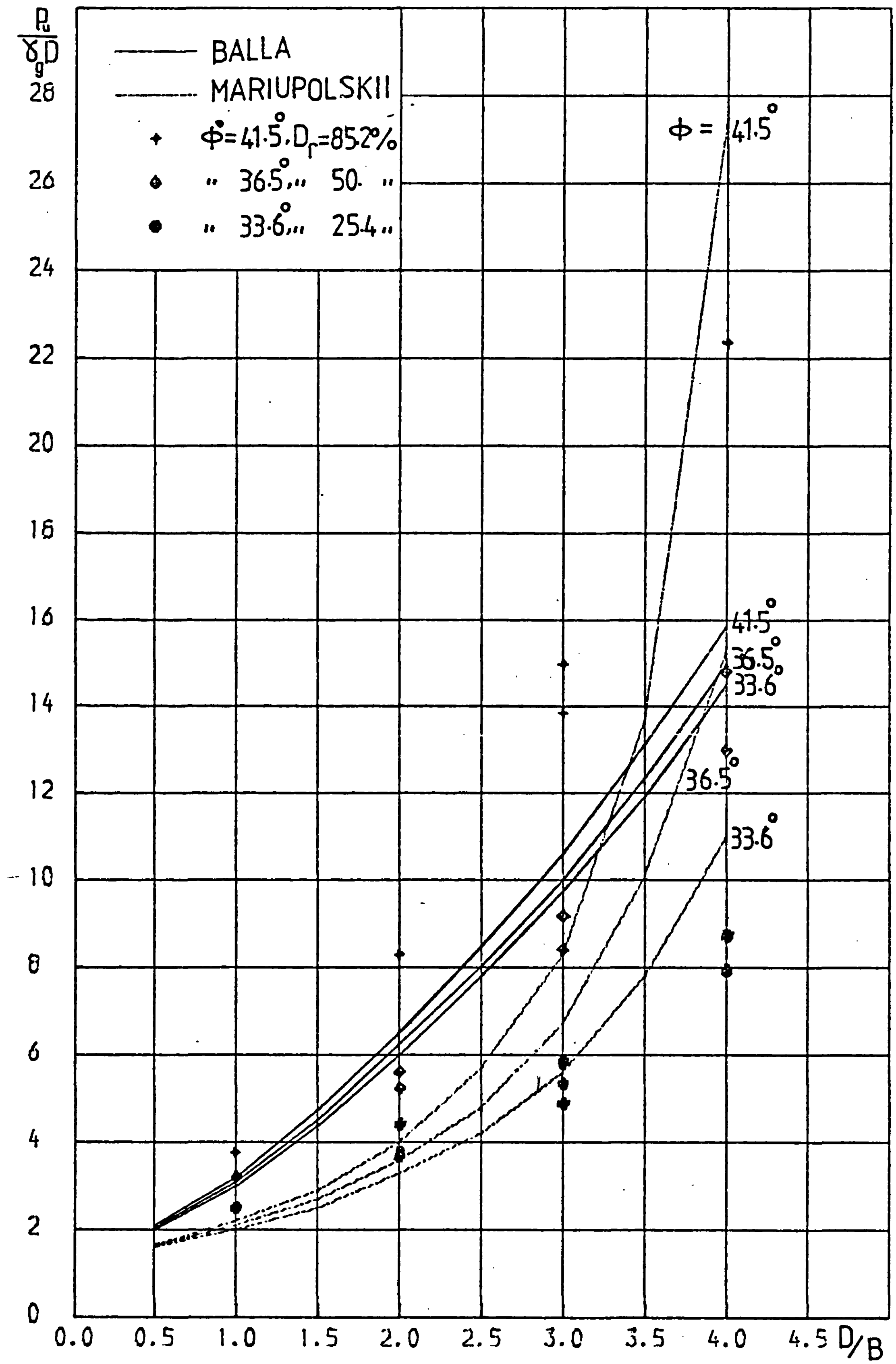

FIG 7.10 COMPARISON OF LOAD PREDICTION THEORIES WITH THE PRESENT SHALLOW MODEL TESTS

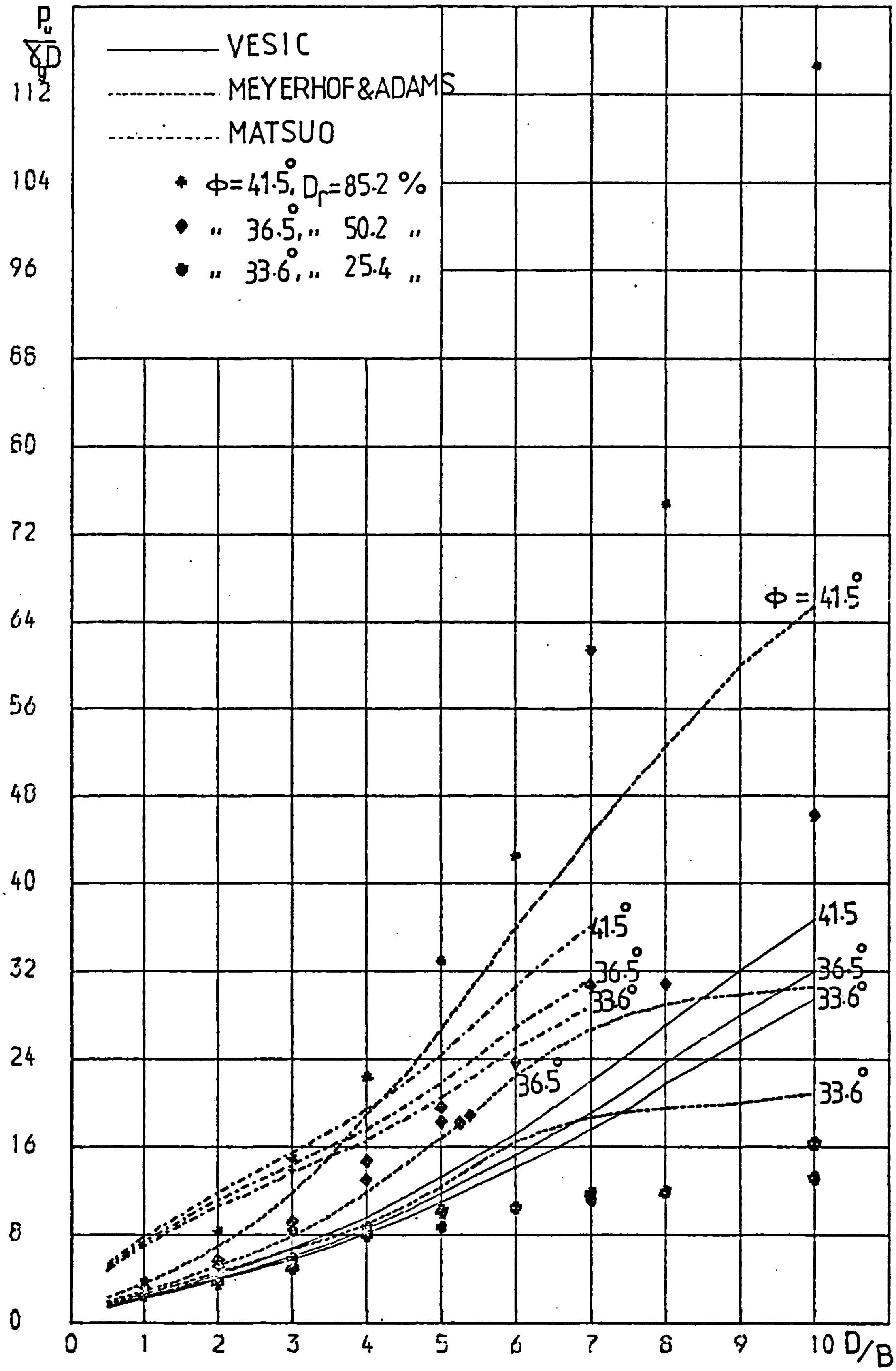

FIG 7.11 COMPARISON OF LOAD PREDICTION THEORIES WITH THE PRESENT DEEP MODEL TESTS

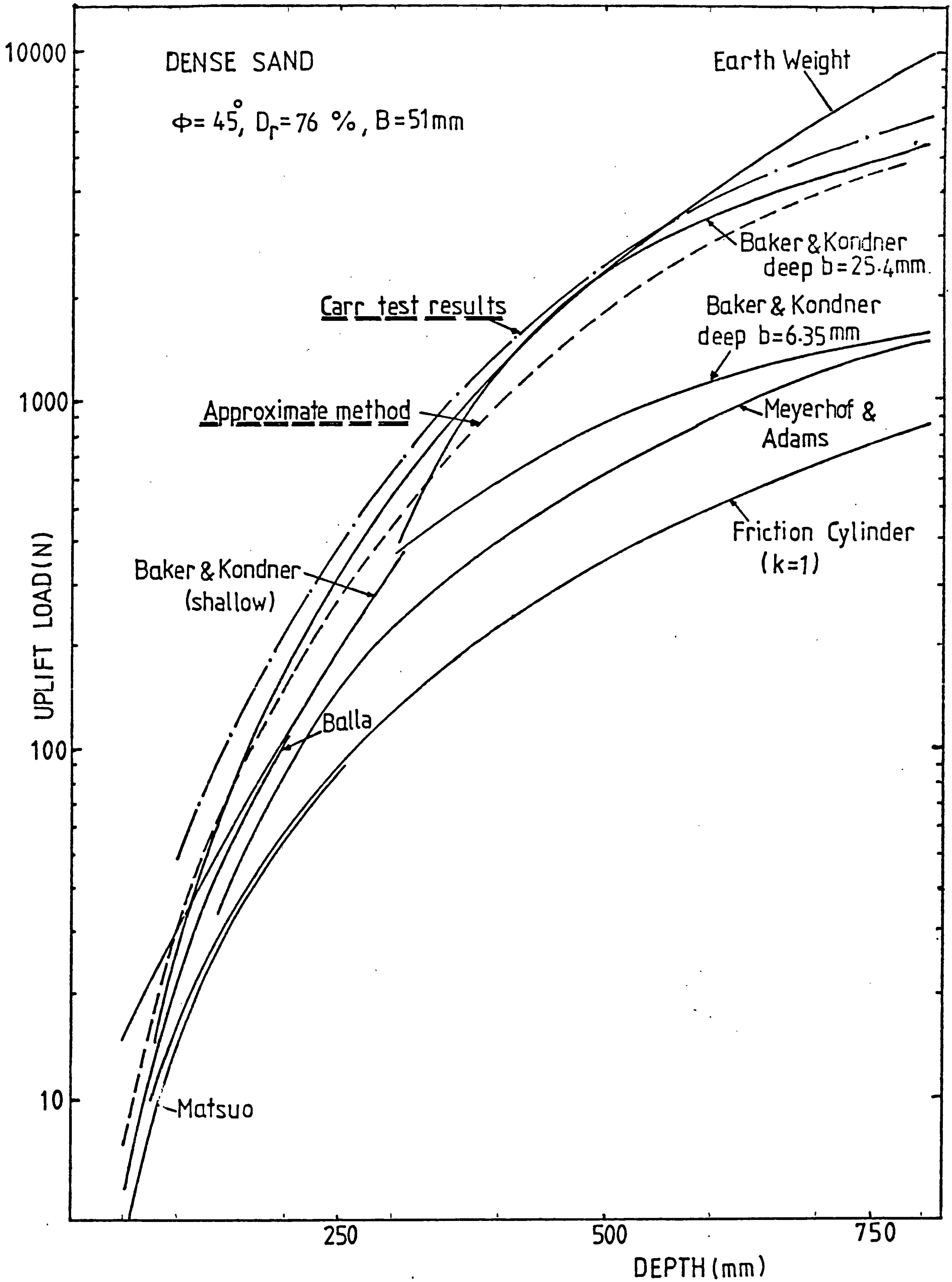

FIG 7.12 COMPARISON OF LOAD PREDICTION THEORIES WITH CARR TEST RESULTS (AFTEP CARR 1970)

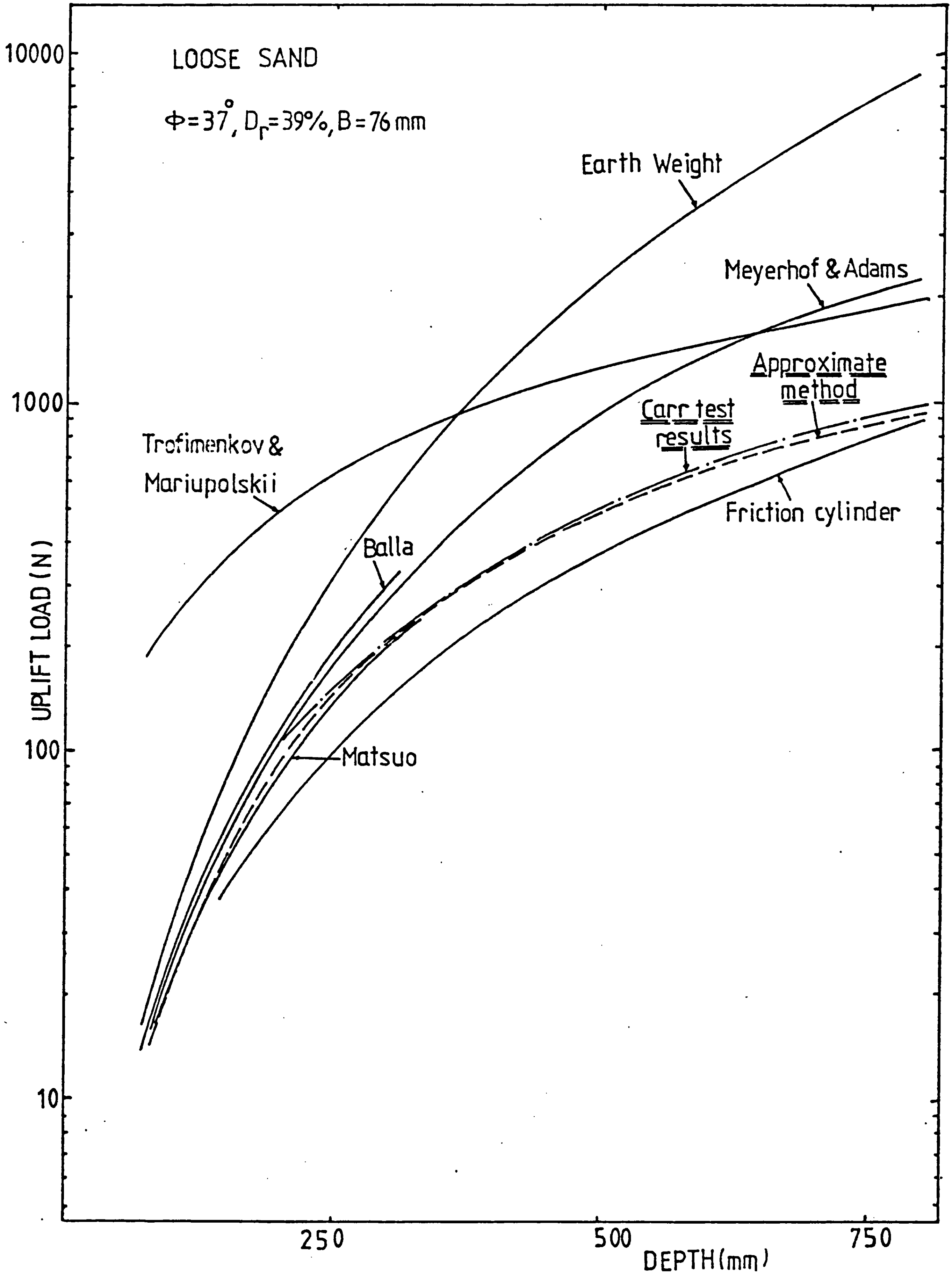

FIG 7.13 COMPARISON OF LOAD PREDICTION THEORIES WITH CARR TEST RESULTS

(AFTER CARR 1970)

FIG. 7.14 RELATIONSHIPS BETWEEN $\frac{H}{B}$, D_r AND DENSITY VERSUS ϕ^o

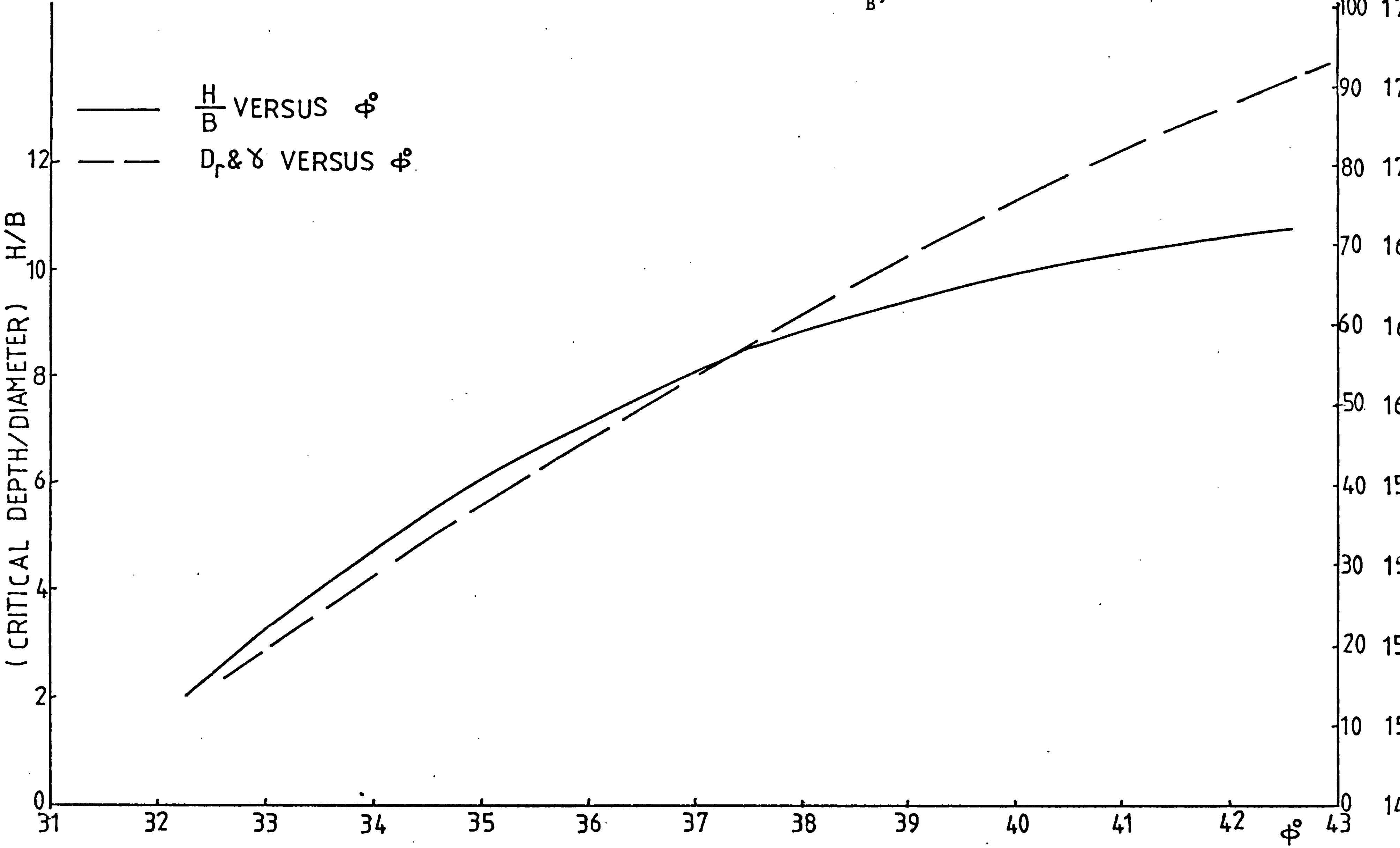

Fig.(7.14a) Comparison between the theoretical and experimental values of α.

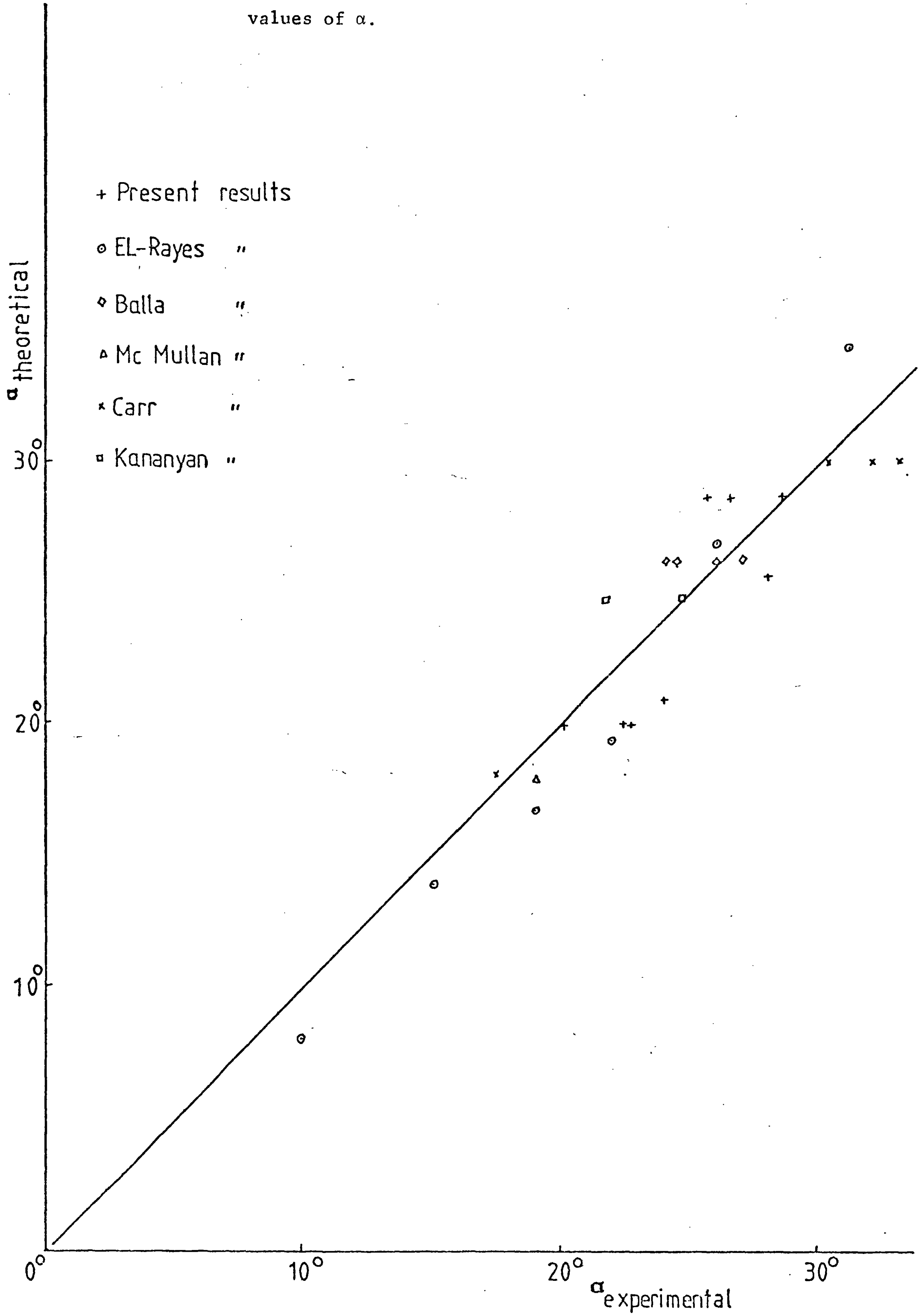

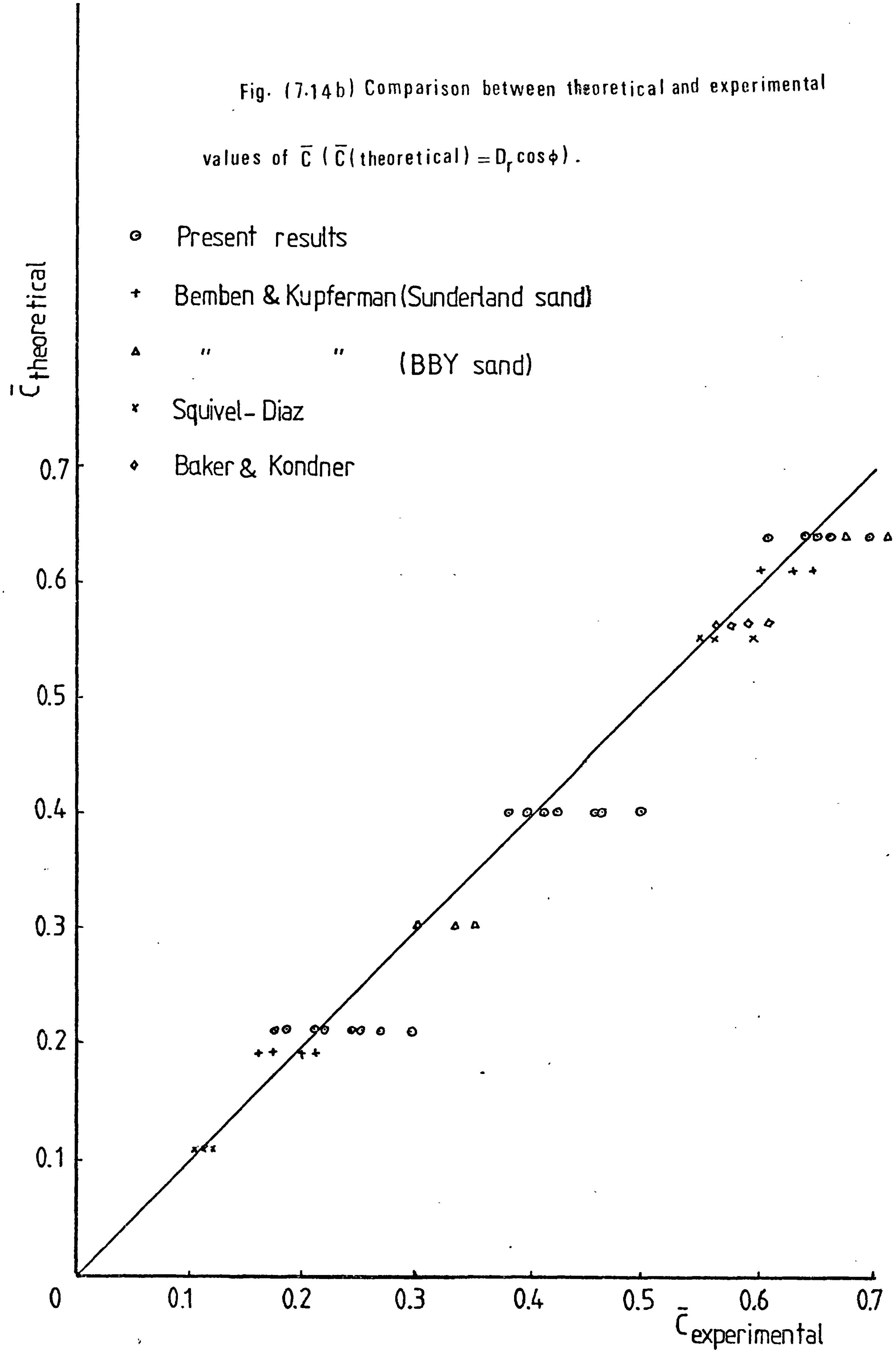

Fig. (7.14b) Comparison between theoretical and experimental values of $\bar{C}$ ($\bar{C}$(theoretical) $= D_r \cos\phi$).

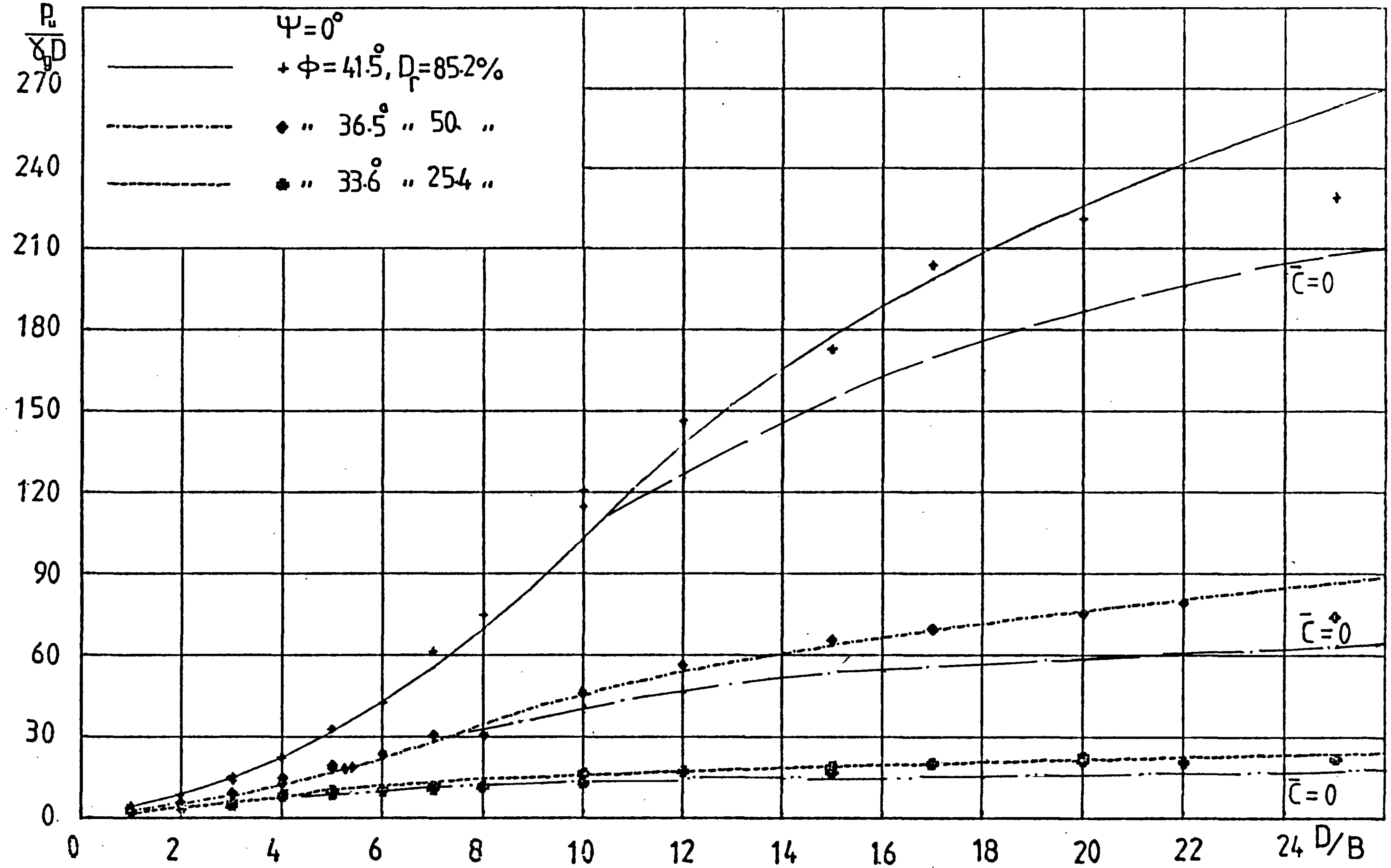

FIG 7.15 COMPARISON OF APPROXIMATE METHOD WITH PRESENT VERTICAL MODEL TEST RESULTS

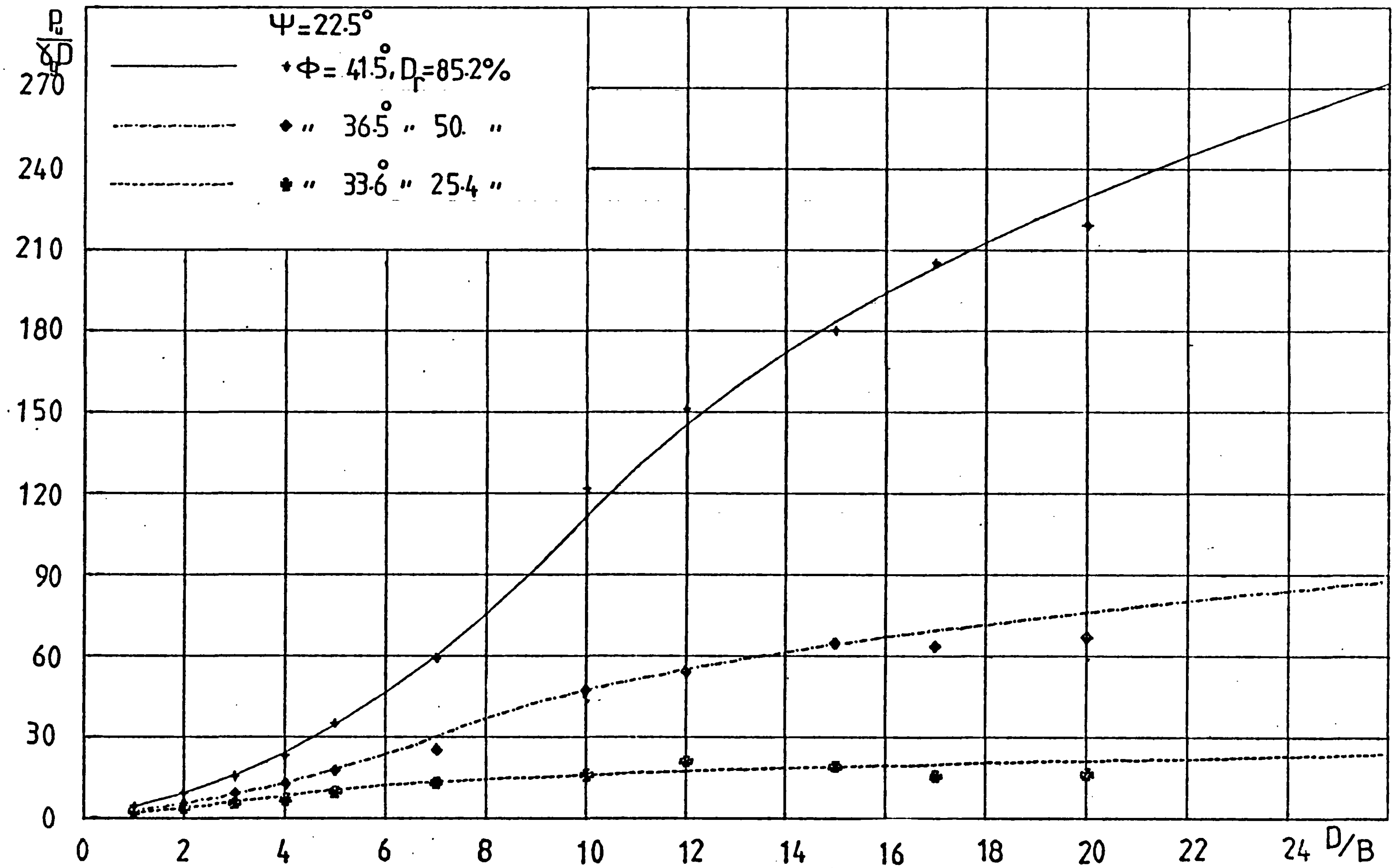

FIG 7.16 COMPARISON OF APPROXIMATE METHOD WITH PRESENT INCLINED MODEL TEST RESULTS

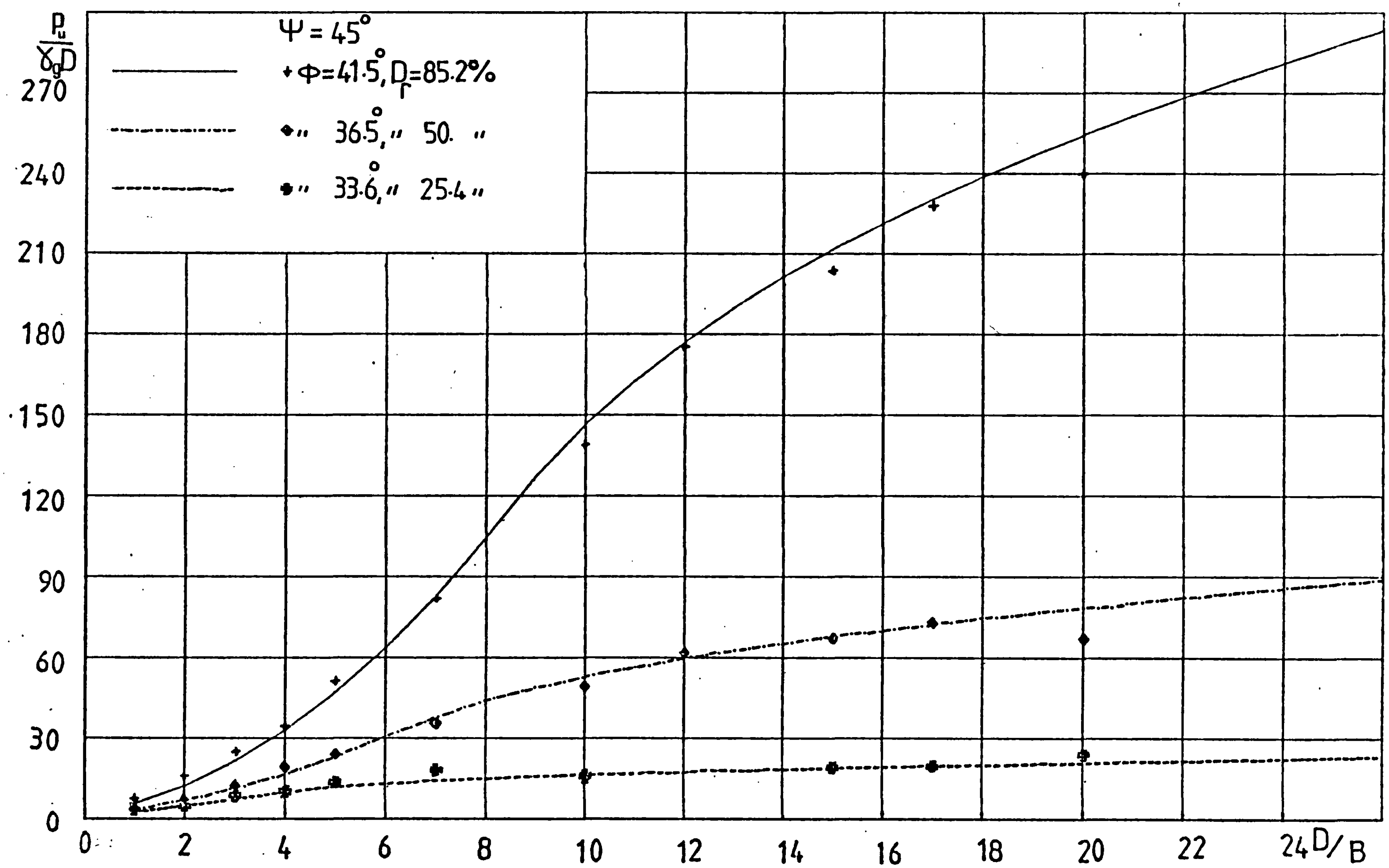

FIG 7.17 COMPARISON OF APPROXIMATE METHOD WITH PRESENT INCLINED MODEL TEST RESULTS

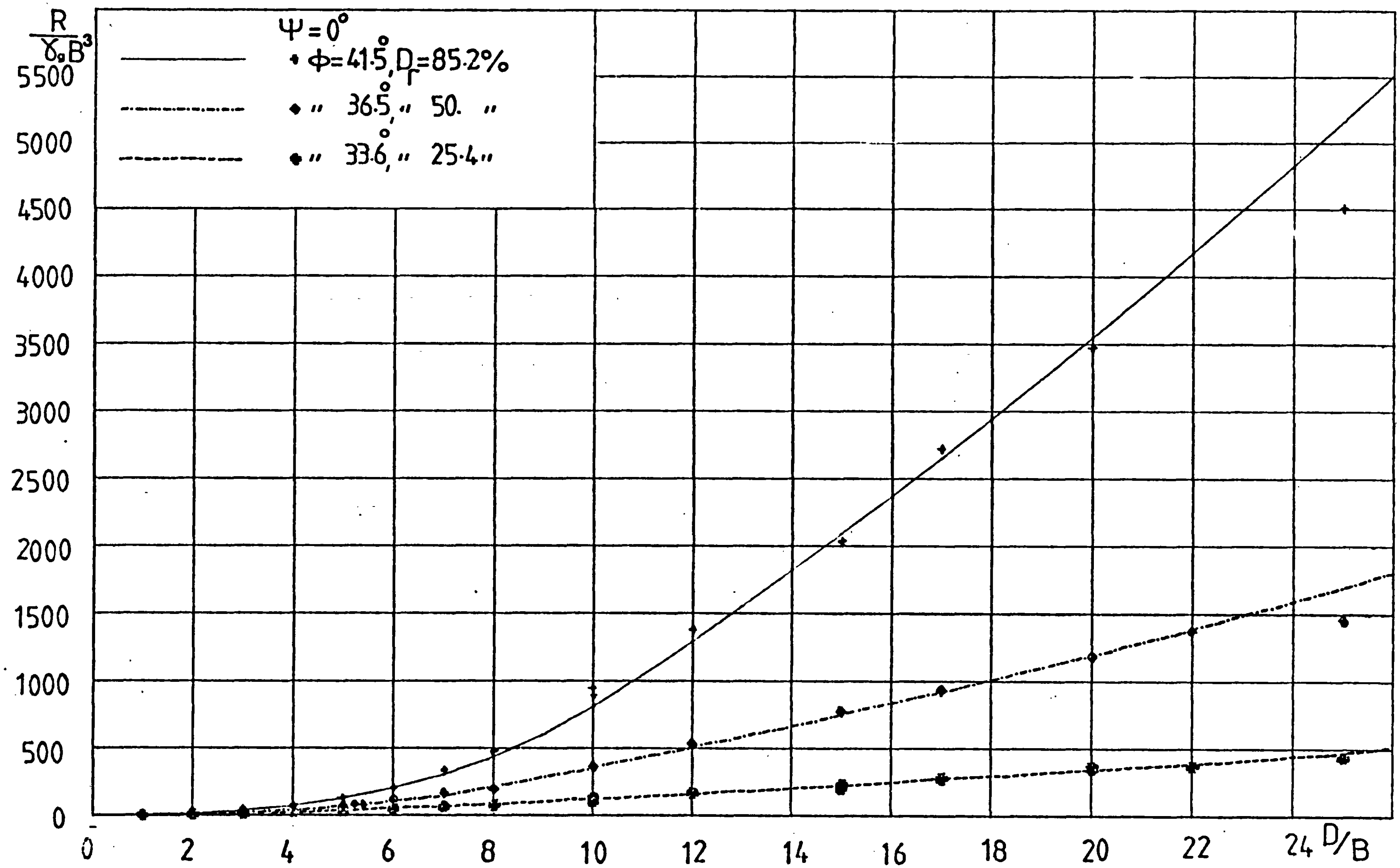

FIG 7.18a COMPARISON OF APPROXIMATE METHOD WITH PRESENT VERTICAL MODEL TEST RESULTS

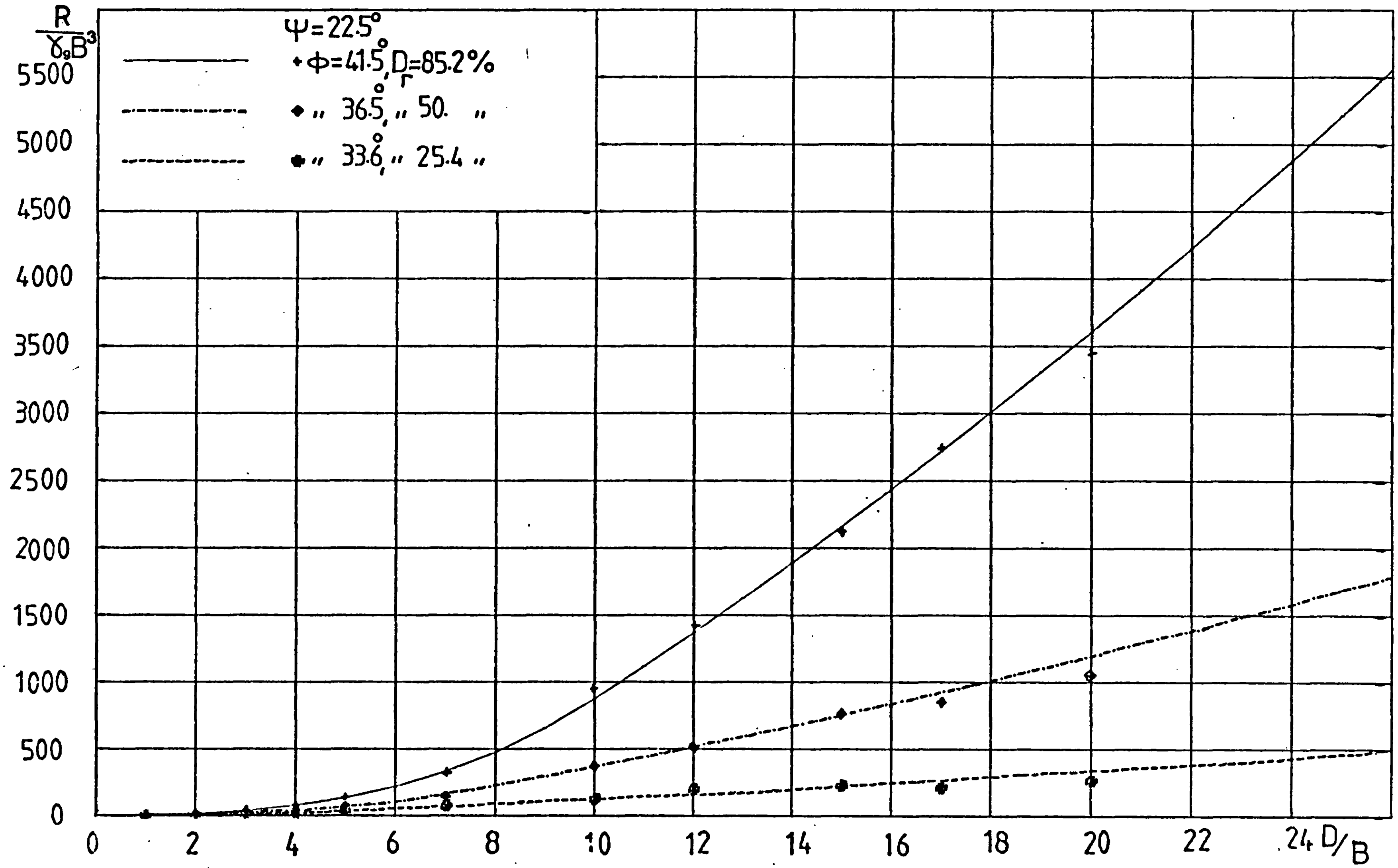

FIG 7.18b COMPARISON OF APPROXIMATE METHOD WITH PRESENT INCLINED MODEL TEST RESULTS

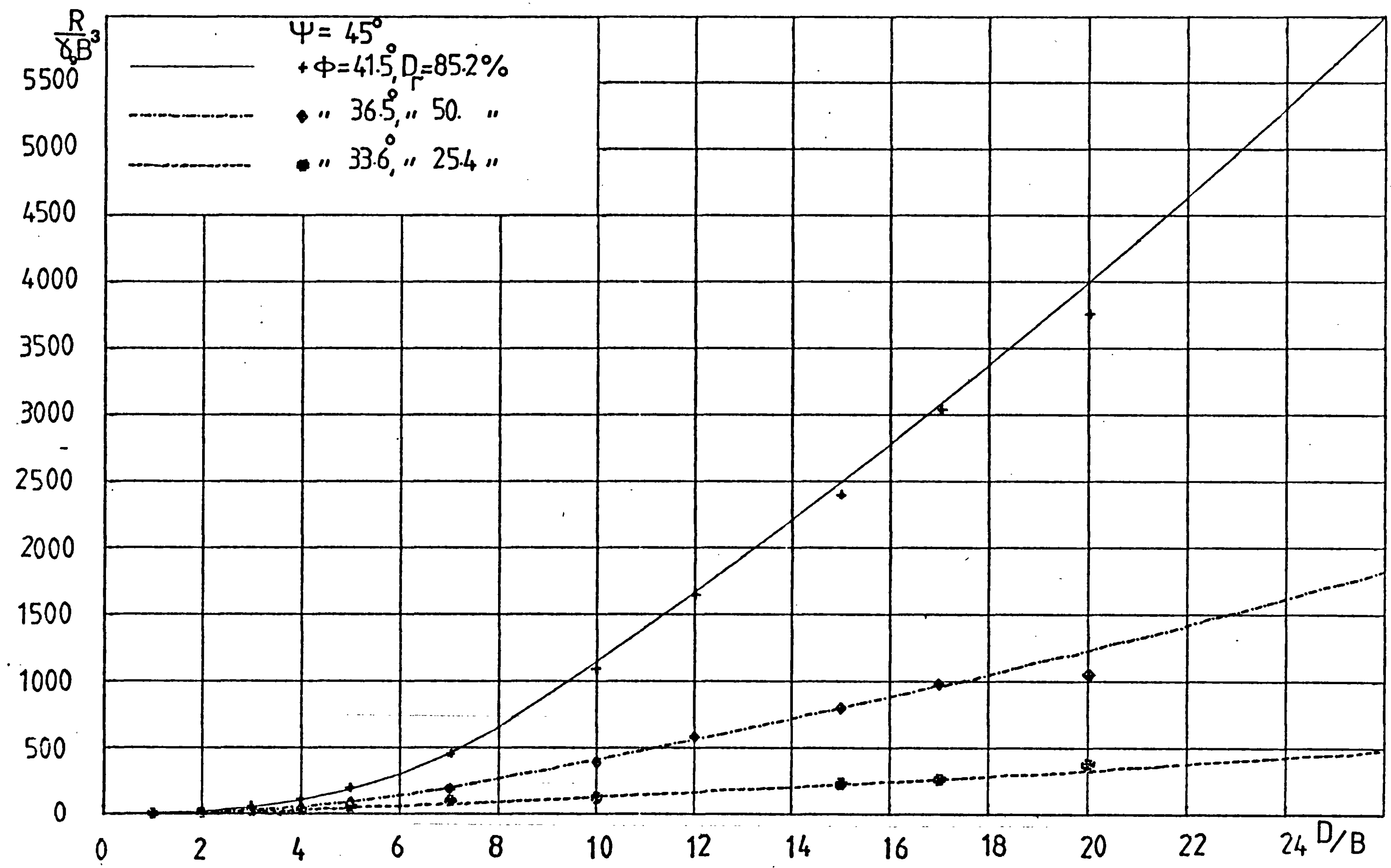

FIG 7.18c COMPARISON OF APPROXIMATE METHOD WITH PRESENT INCLINED MODEL TEST RESULTS

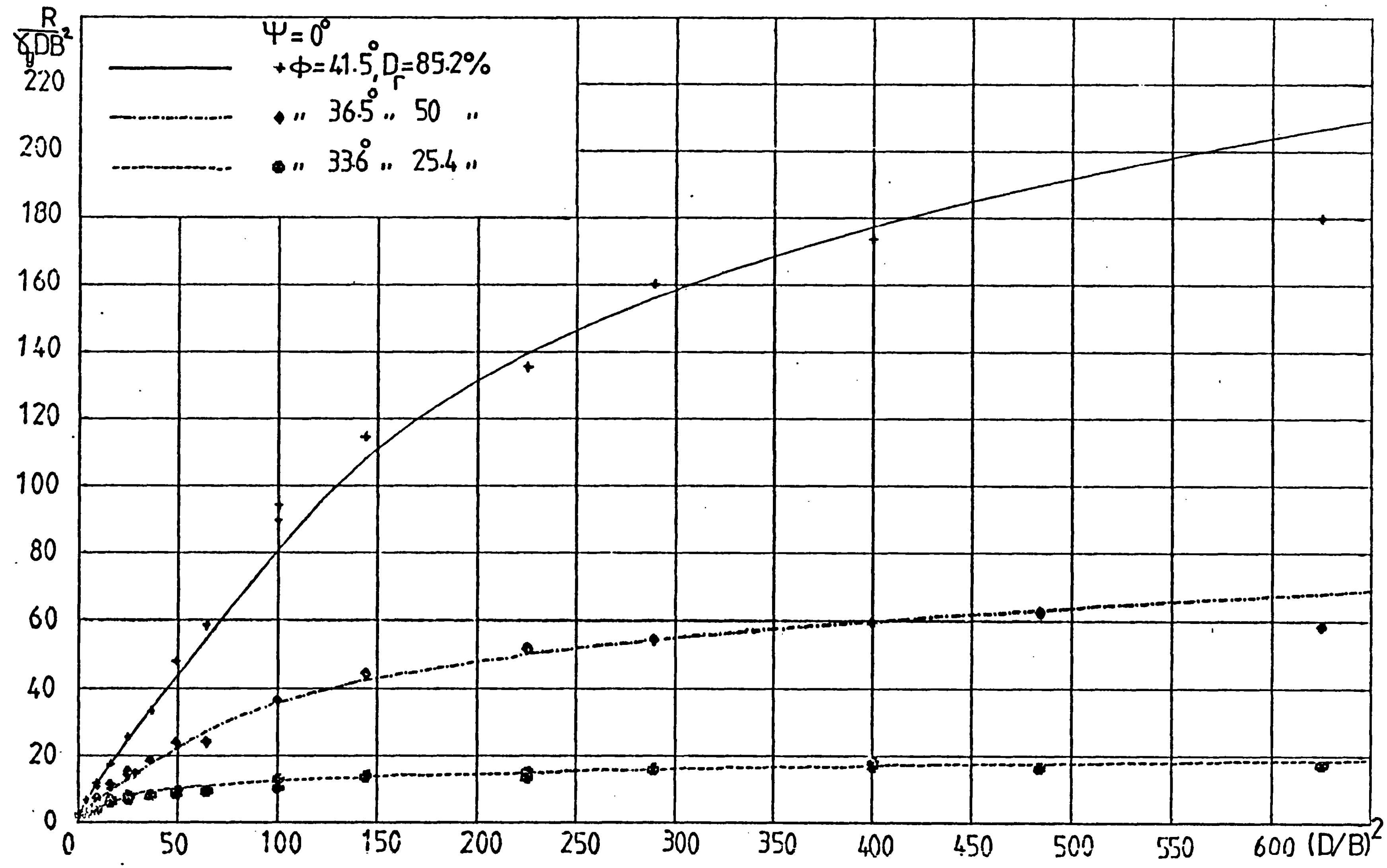

FIG 7.19a COMPARISON OF APPROXIMATE METHOD WITH PRESENT VERTICAL MODEL TEST RESULTS

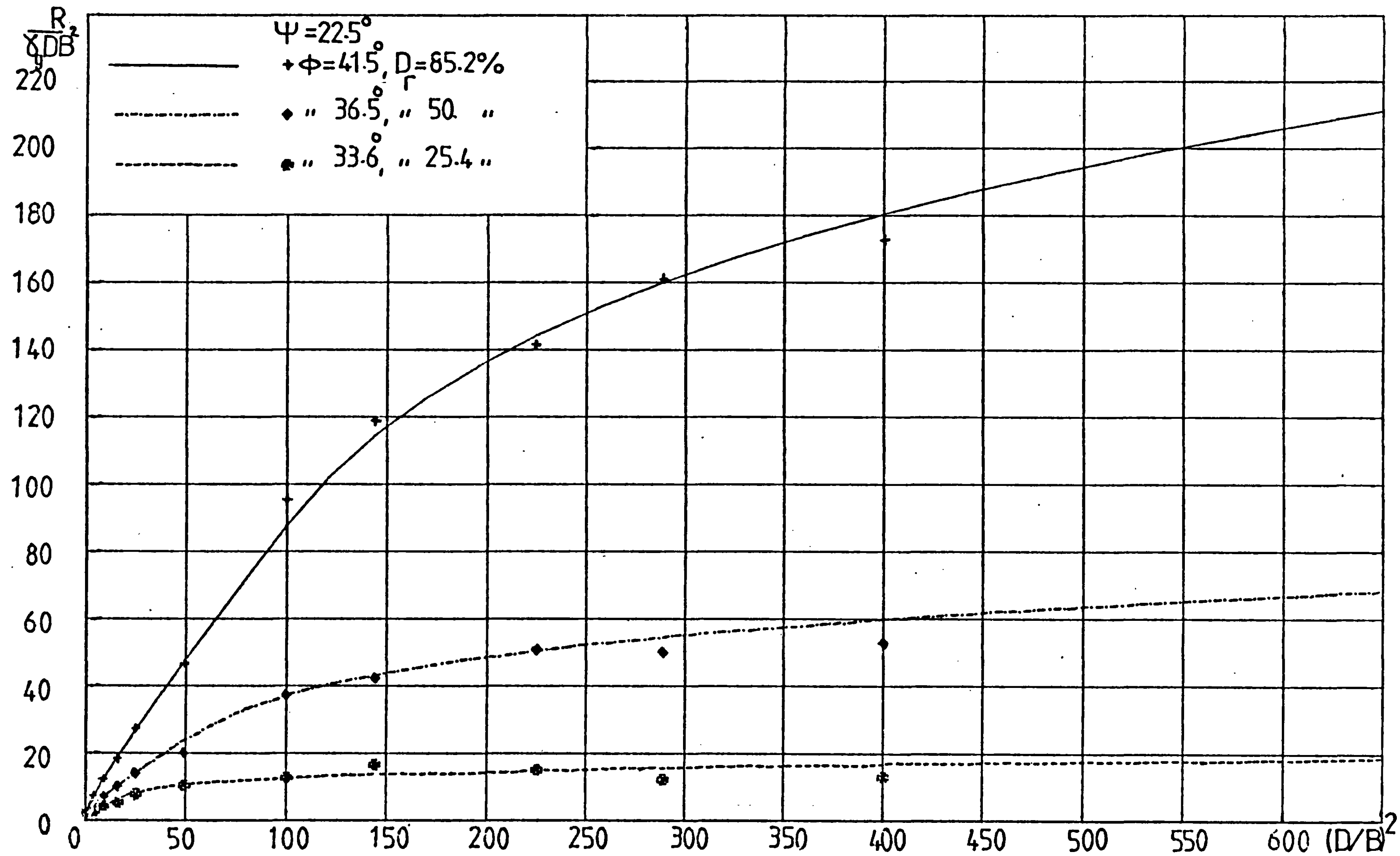

FIG 7.19b COMPARISON OF APPROXIMATE METHOD WITH PRESENT INCLINED MODEL TEST RESULTS

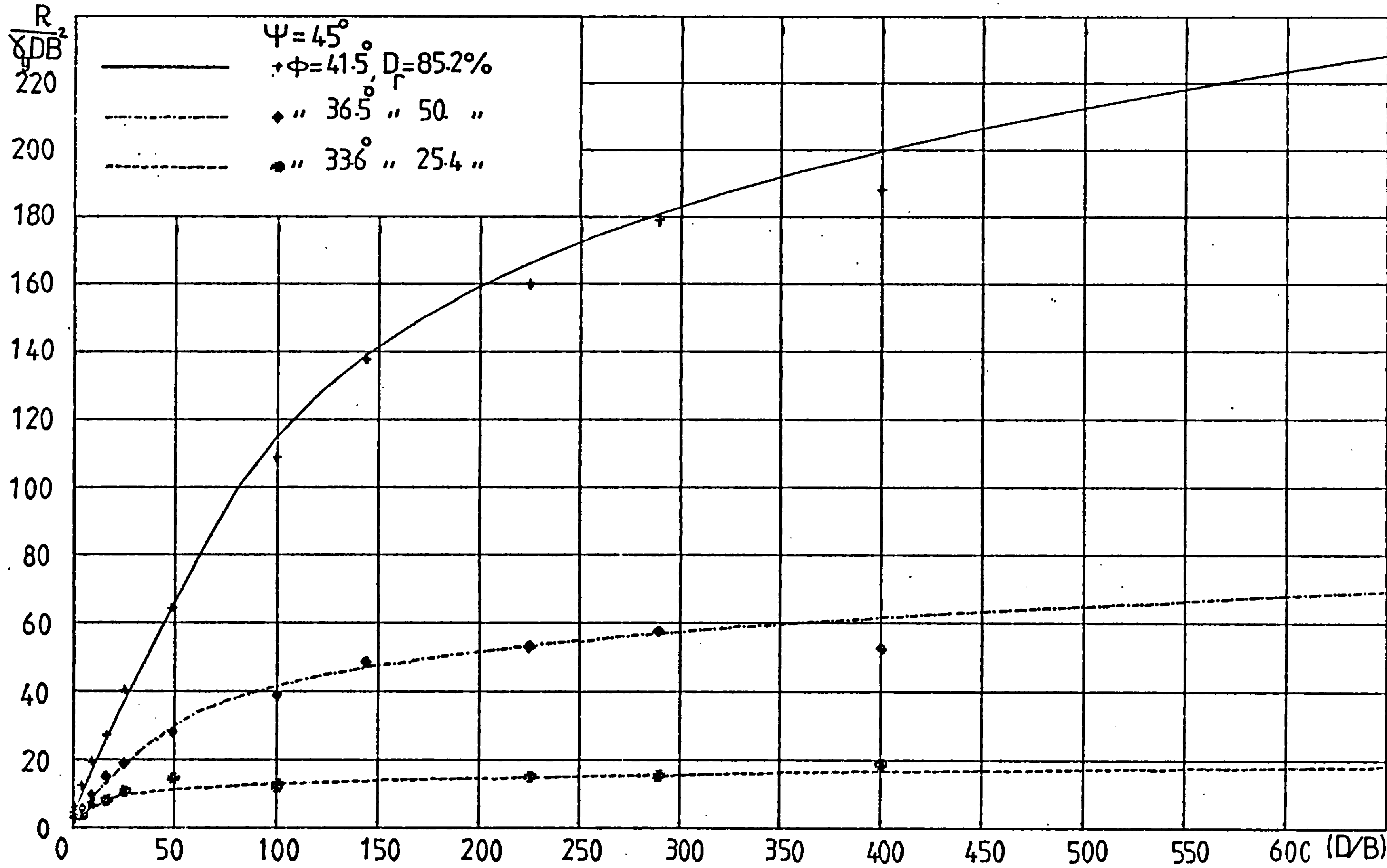

FIG 7.19c COMPARISON OF APPROXIMATE METHOD WITH PRESENT INCLINED MODEL TEST RESULTS

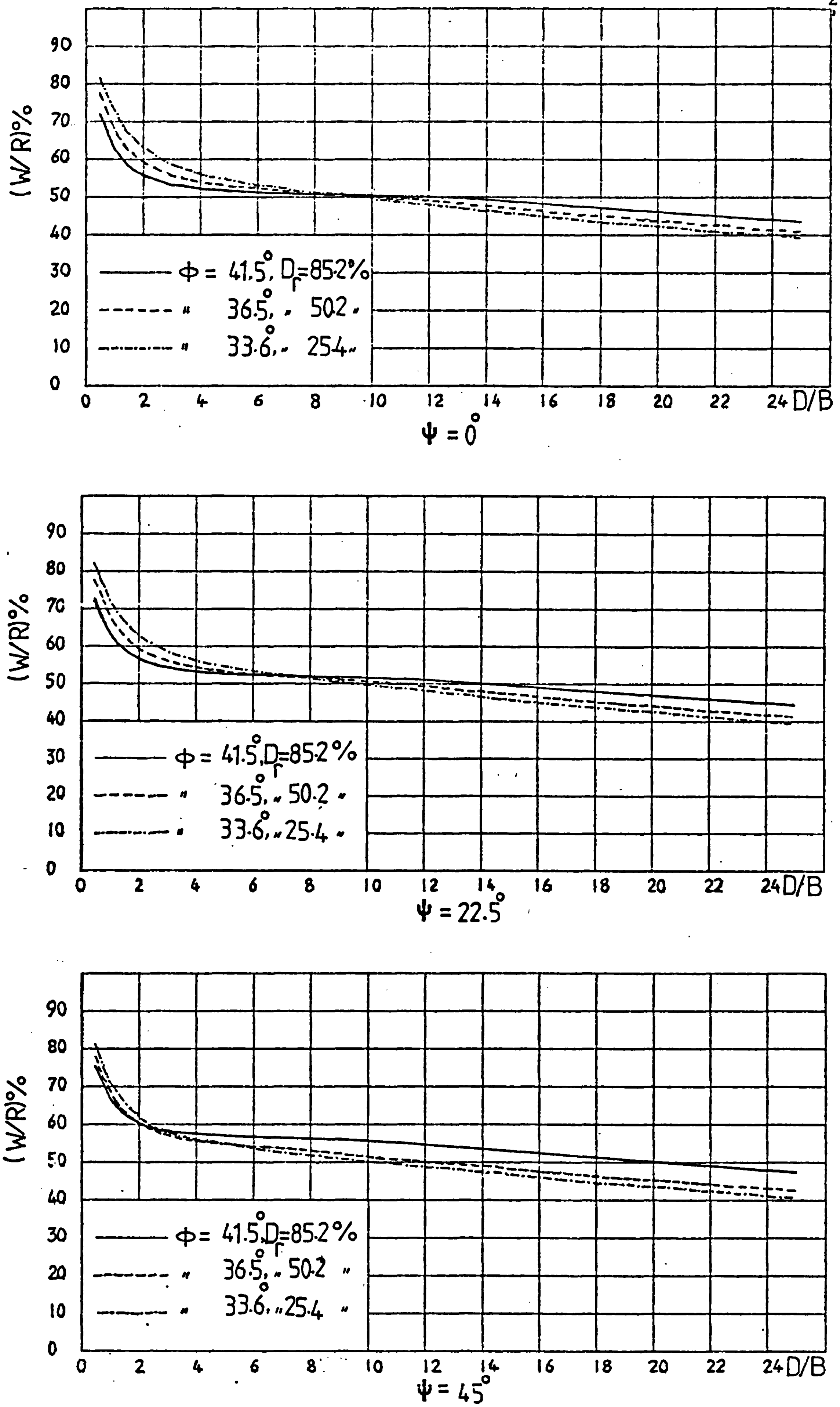

FIG 7.20 CONTRIBUTION OF SOIL WEIGHT TO ULTIMATE LOAD

PREDICTED BY THE APPROXIMATE METHOD

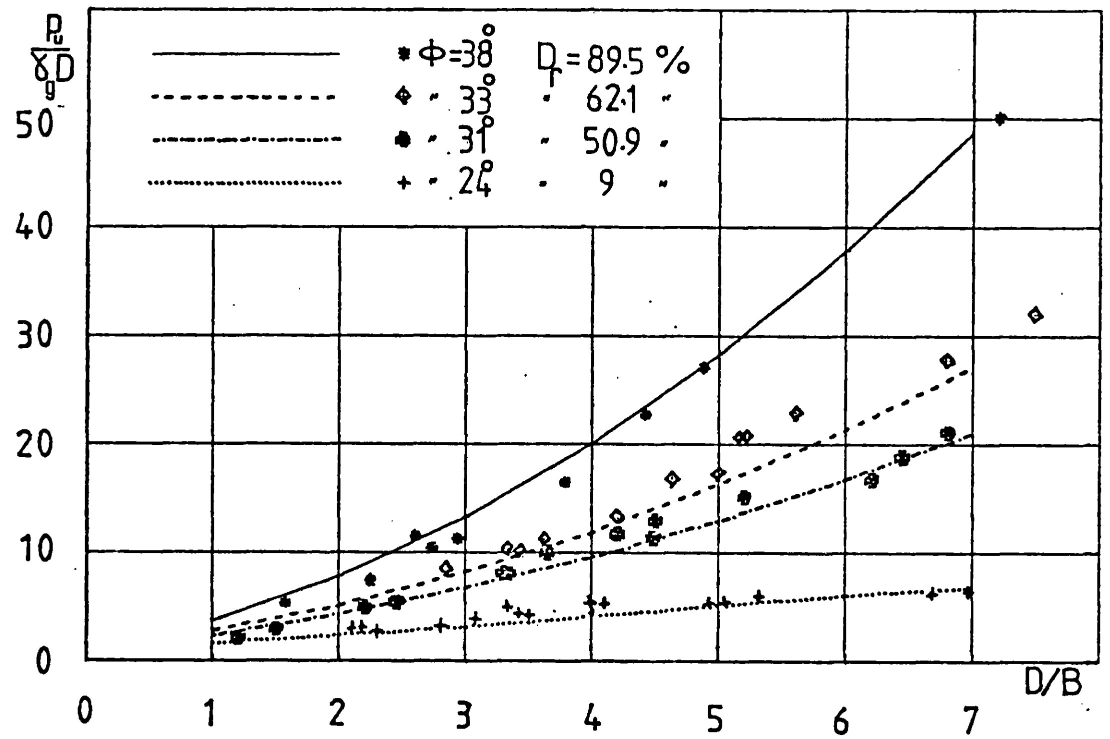

(a) EL-RAYES EXPERIMENTS (LEIGHTON BUZZARD)

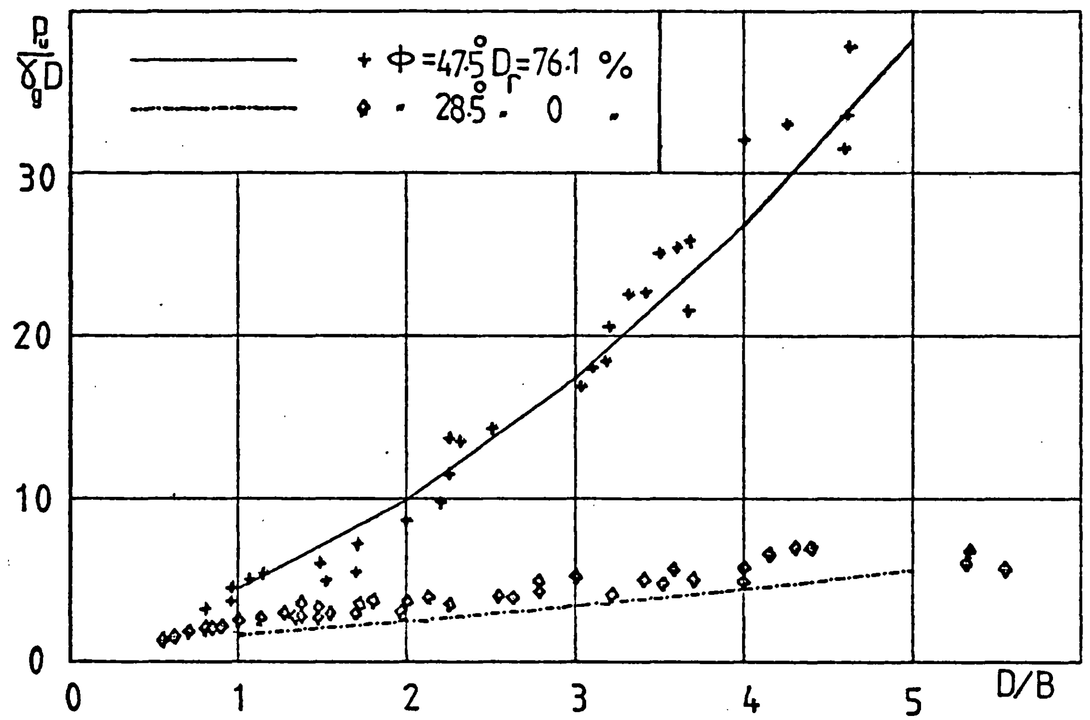

(b) EL-RAYES EXPERIMENTS (LOCAL CONCRETING)

FIG 7.21 COMPARISON OF APPPOXIMATE METHOD WITH EL-RAYES SHALLOW MODEL TEST PESULTS

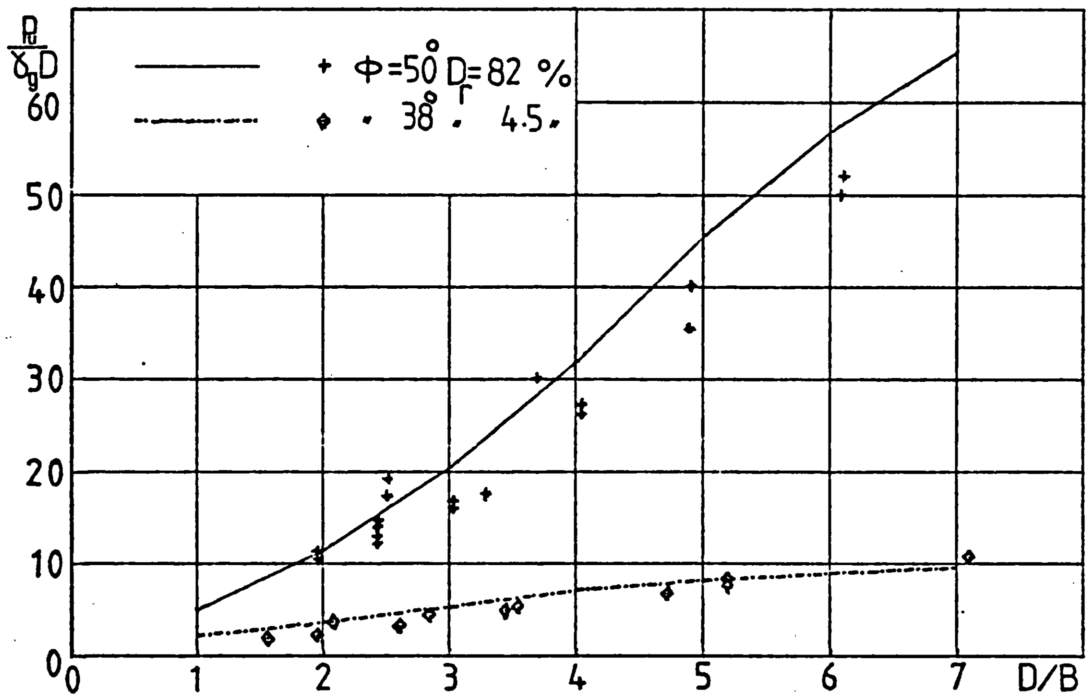

FIG 7.21c COMPARISON OF APPROXIMATE METHOD WITH EL-RAYES SHALLOW MODEL TEST RESULTS (SIZEWELL SAND)

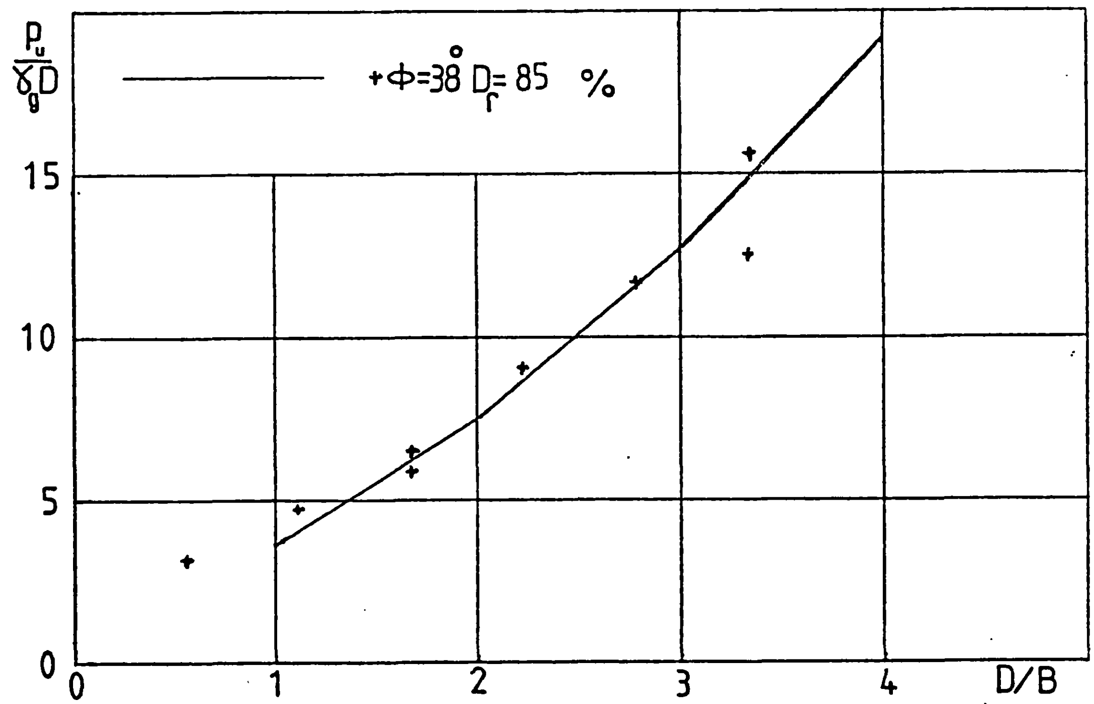

(a) BALLA MODEL TESTS

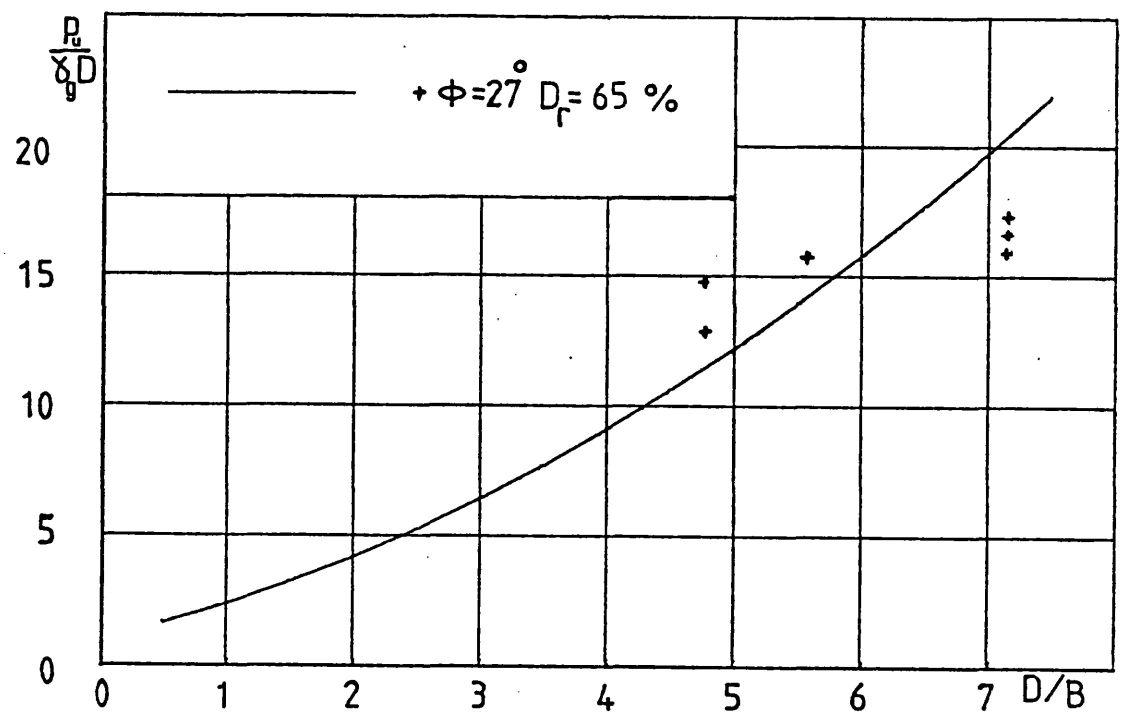

(b) MARIUPOLSKII MODEL TESTS

FIG 7.22 COMPARISON OF APPROXIMATE METHOD WITH BALLA AND MARIUPOLSKII SHALLOW MODEL TEST RESULTS

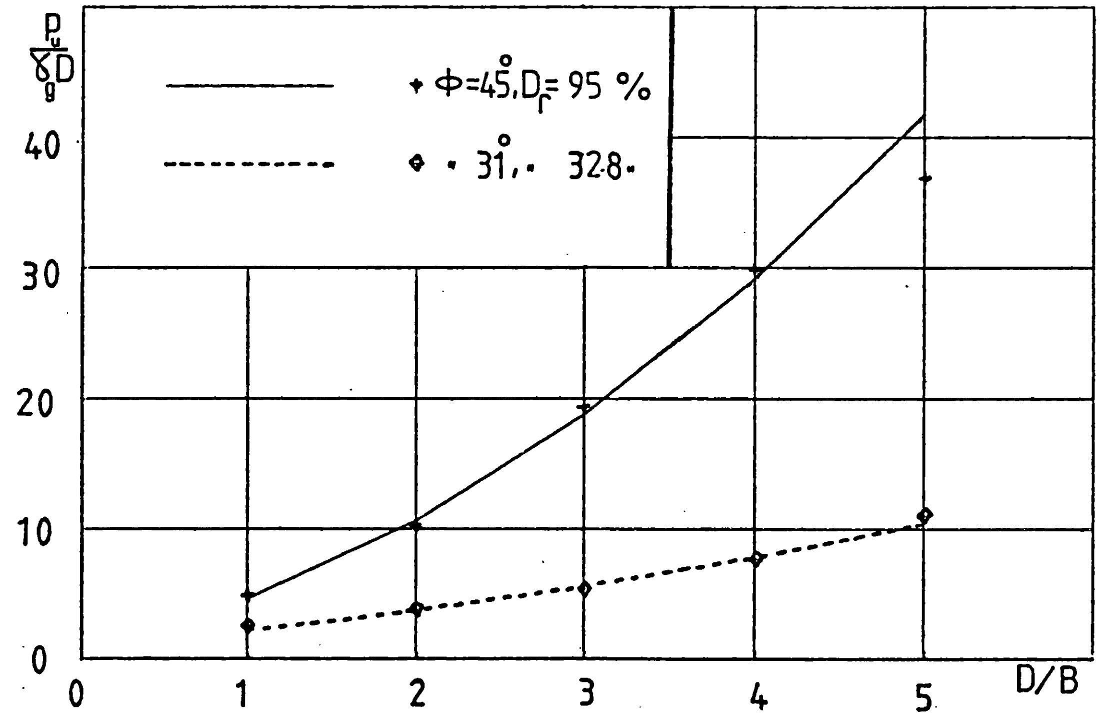

(a) SUTHERLAND (MODEL TESTS)

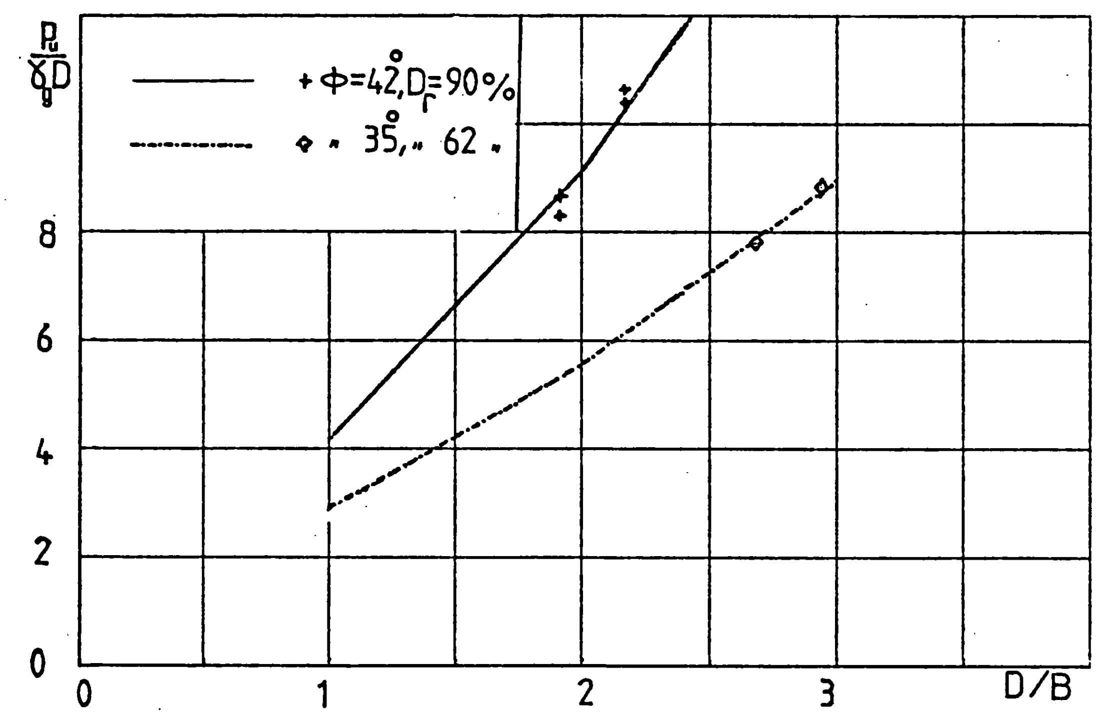

(b) SUTHERLAND FIELD TESTS

FIG 7.23 COMPARISON OF APPROXIMATE METHOD WITH SUTHERLAND SHALLOW MODEL AND FIELD TEST RESULTS

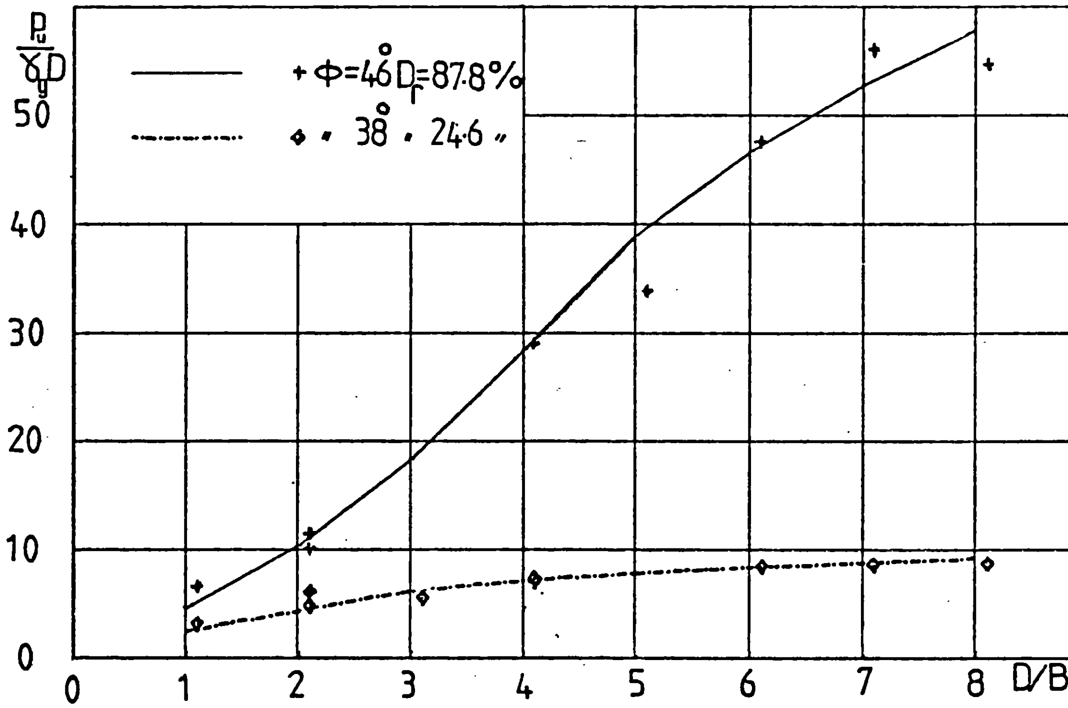

(a) BEMBEN AND KUPFERMAN (SUNDERLAND SAND)

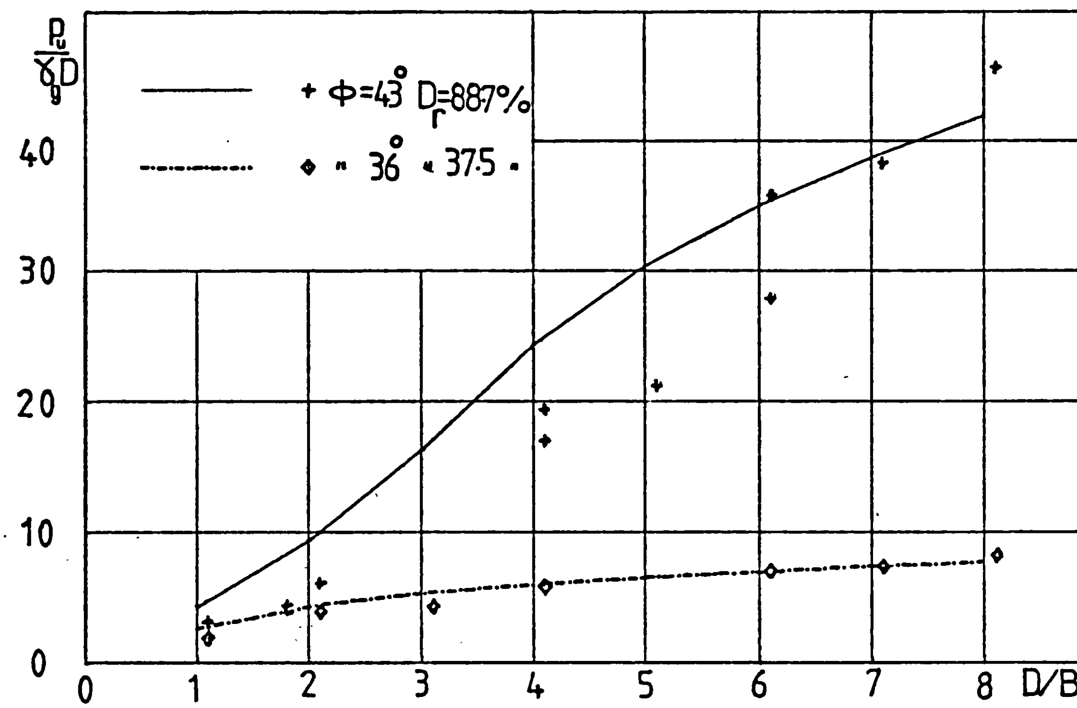

(b) BEMBEN AND KUPFERMAN (BBY SAND)

FIG 7.24 COMPARISON OF APPROXIMATE METHOD WITH BEMBEN AND KUPFERMAN DEEP MODEL TEST RESULTS

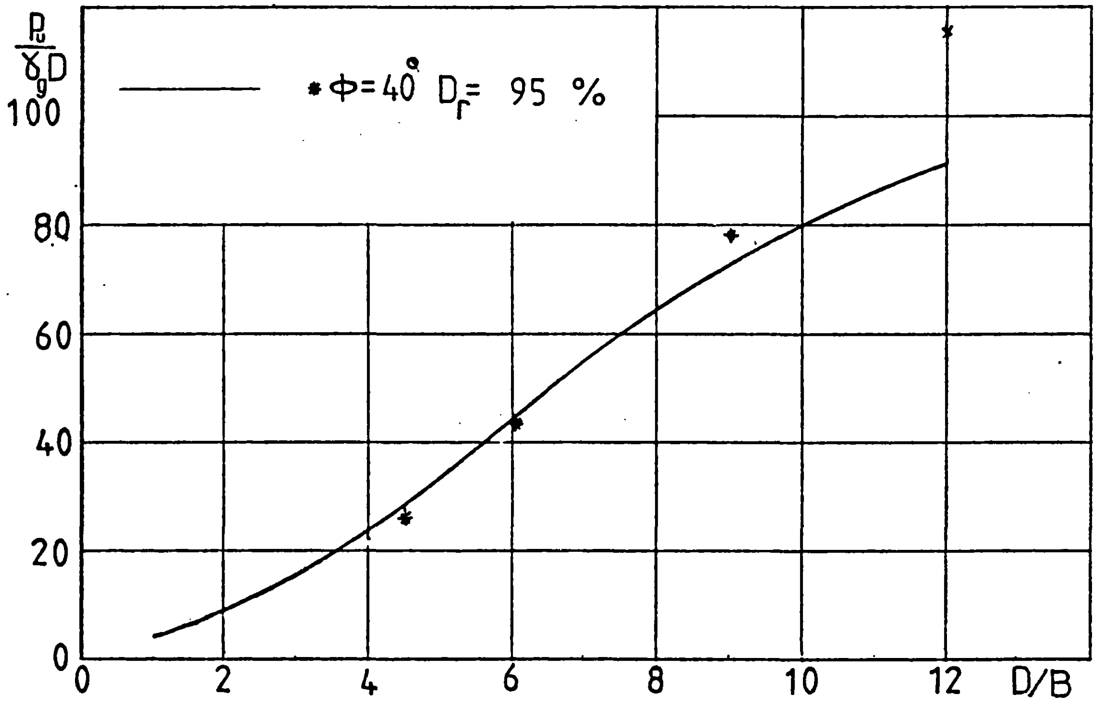

(a) HARVEY AND BURLEY (MODEL TESTS)

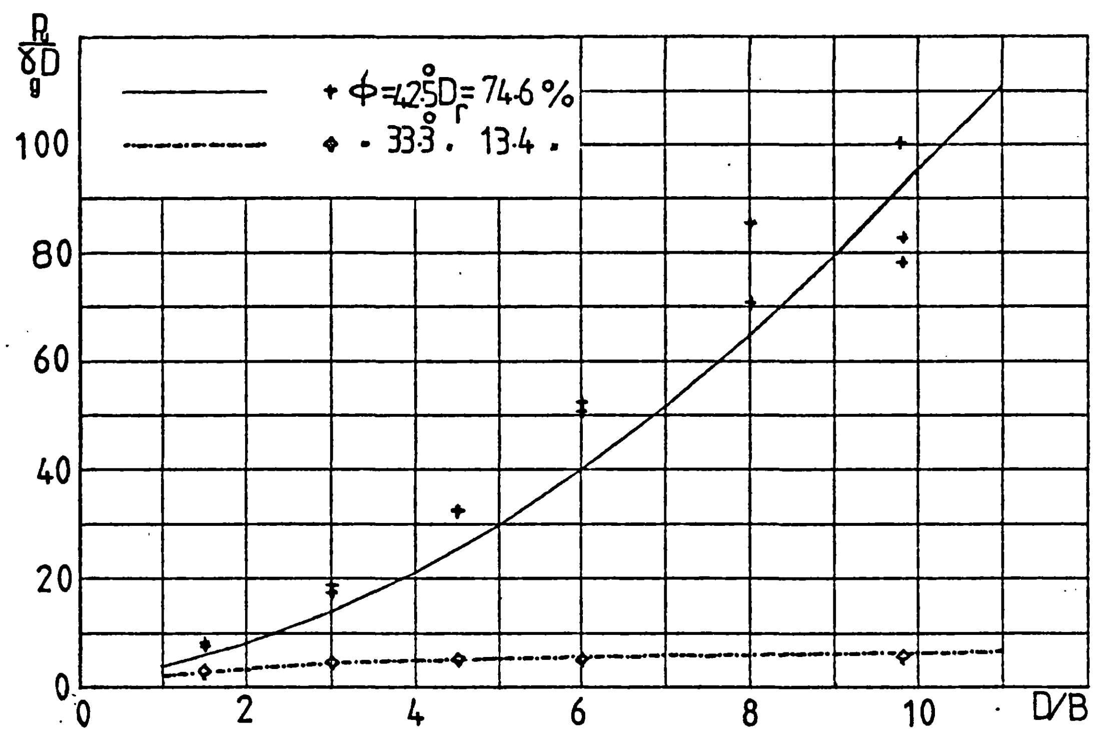

(b) SQUIVEL AND DIAZ (MODEL TESTS)

FIG 7.25 COMPARISON OF APPROXIMATE METHOD WITH HARVEY AND BURLEY, SQUIVEL AND DIAZ DEEP MODEL TEST RESULTS

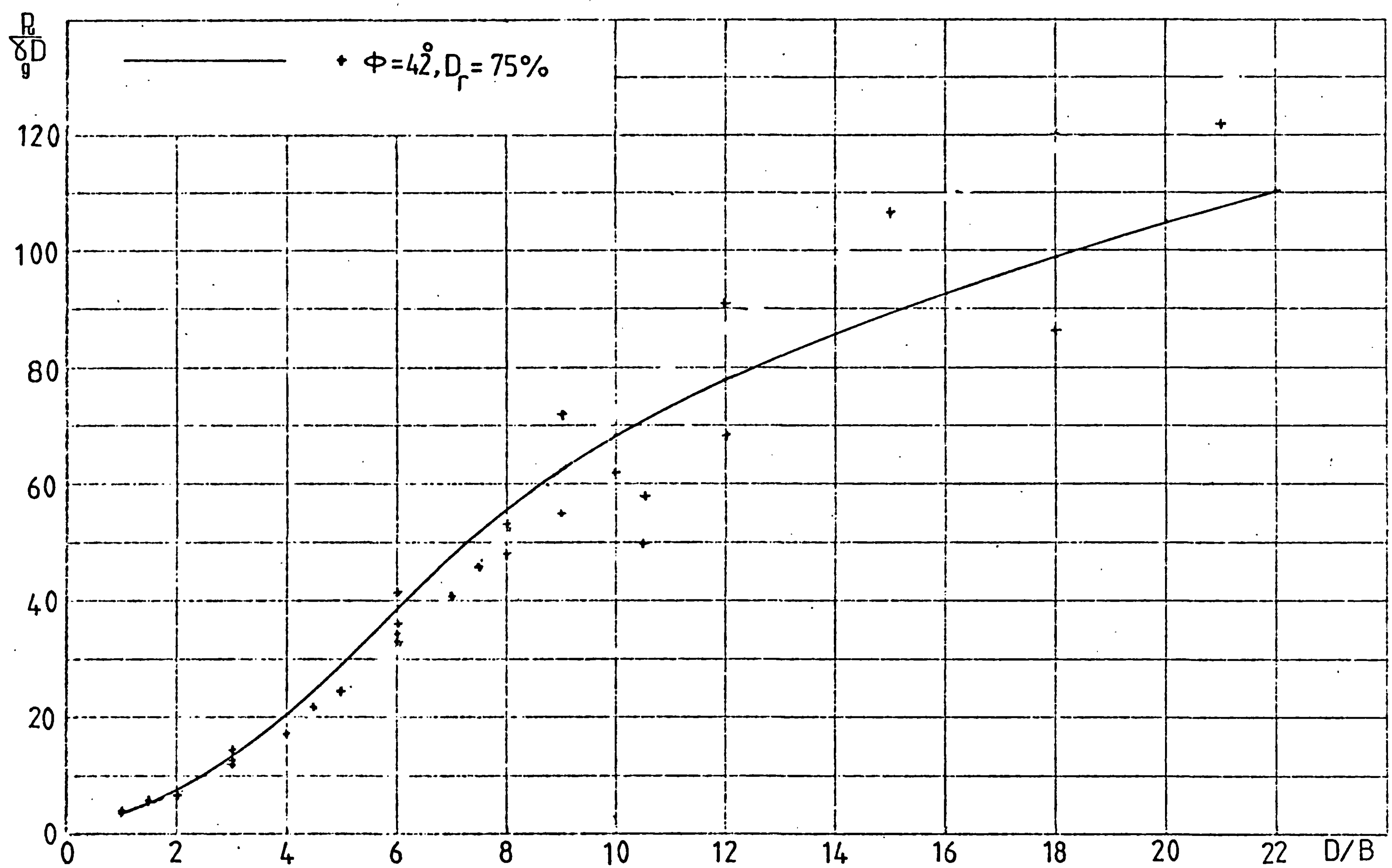

FIG. 7.26. COMPARISON OF APPROXIMATE METHOD WITH BAKER AND KONDNER DEEP MODEL TEST RESULTS

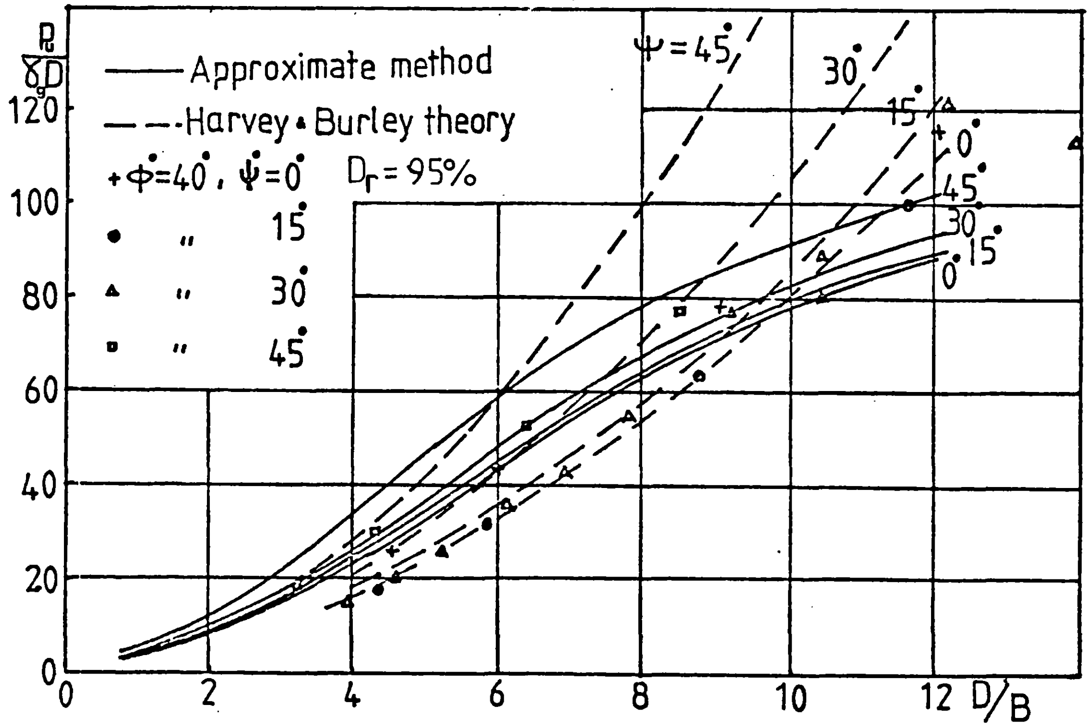

(a) HARVEY AND BURLEY (MODEL TESTS)

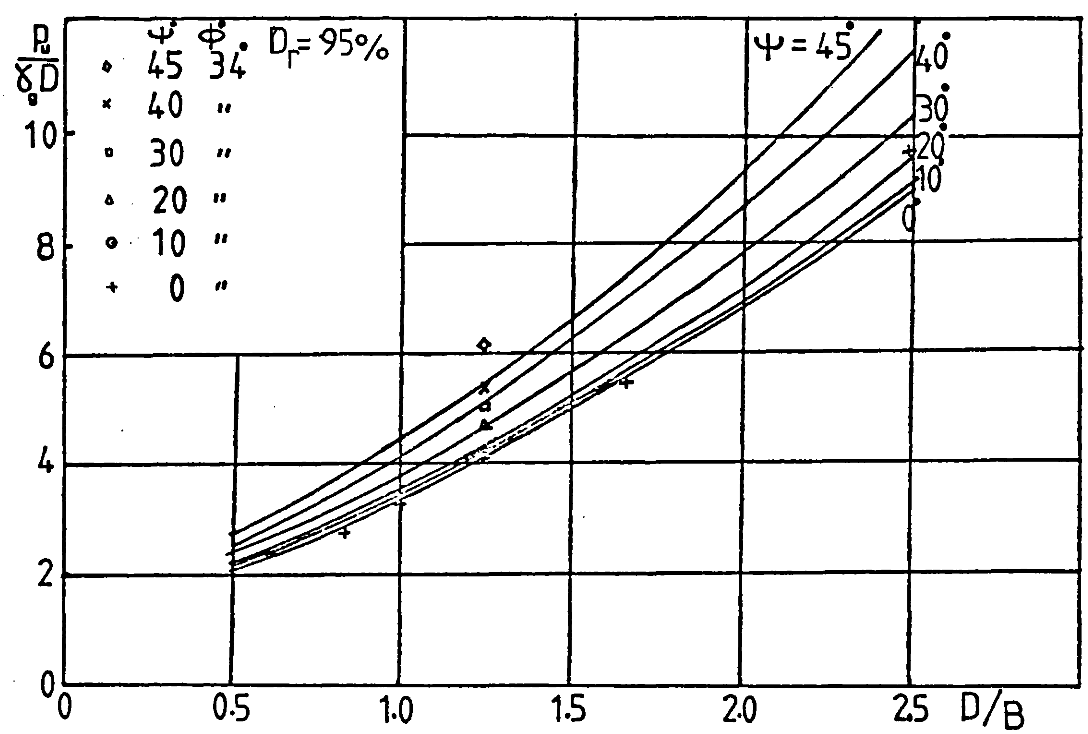

(b) KANANYAN FIELD TESTS

FIG 7.27 COMPARISON OF APPROXIMATE METHOD WITH HARVEY AND BURLEY DEEP MODEL AND KANANYAN FIELD INCLINED TEST RESULTS

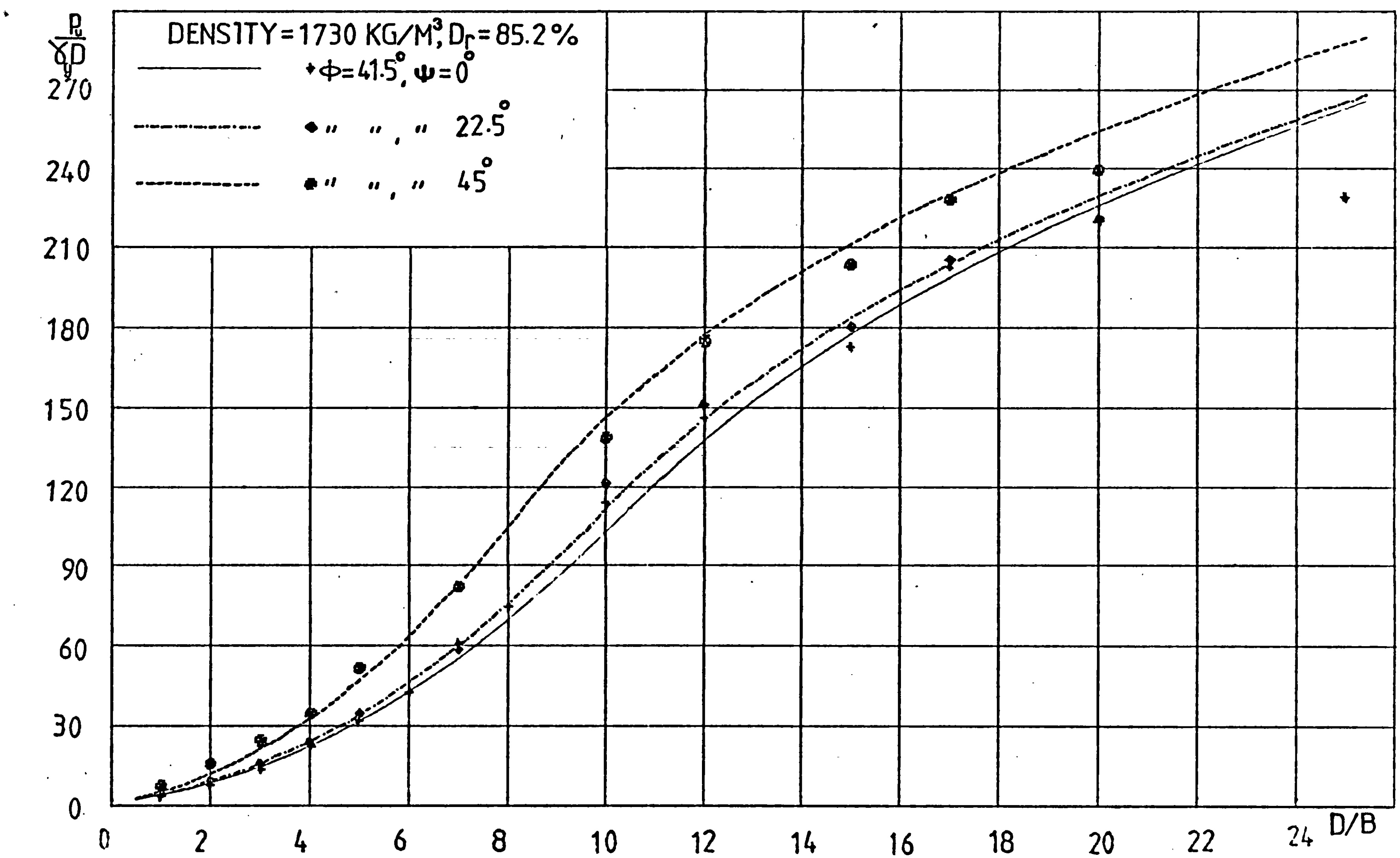

FIG 7.28a COMPARISON OF APPROXIMATE METHOD WITH THE VARYING INCLINATION OF PRESENT MODEL TESTS (DENSE SAND)

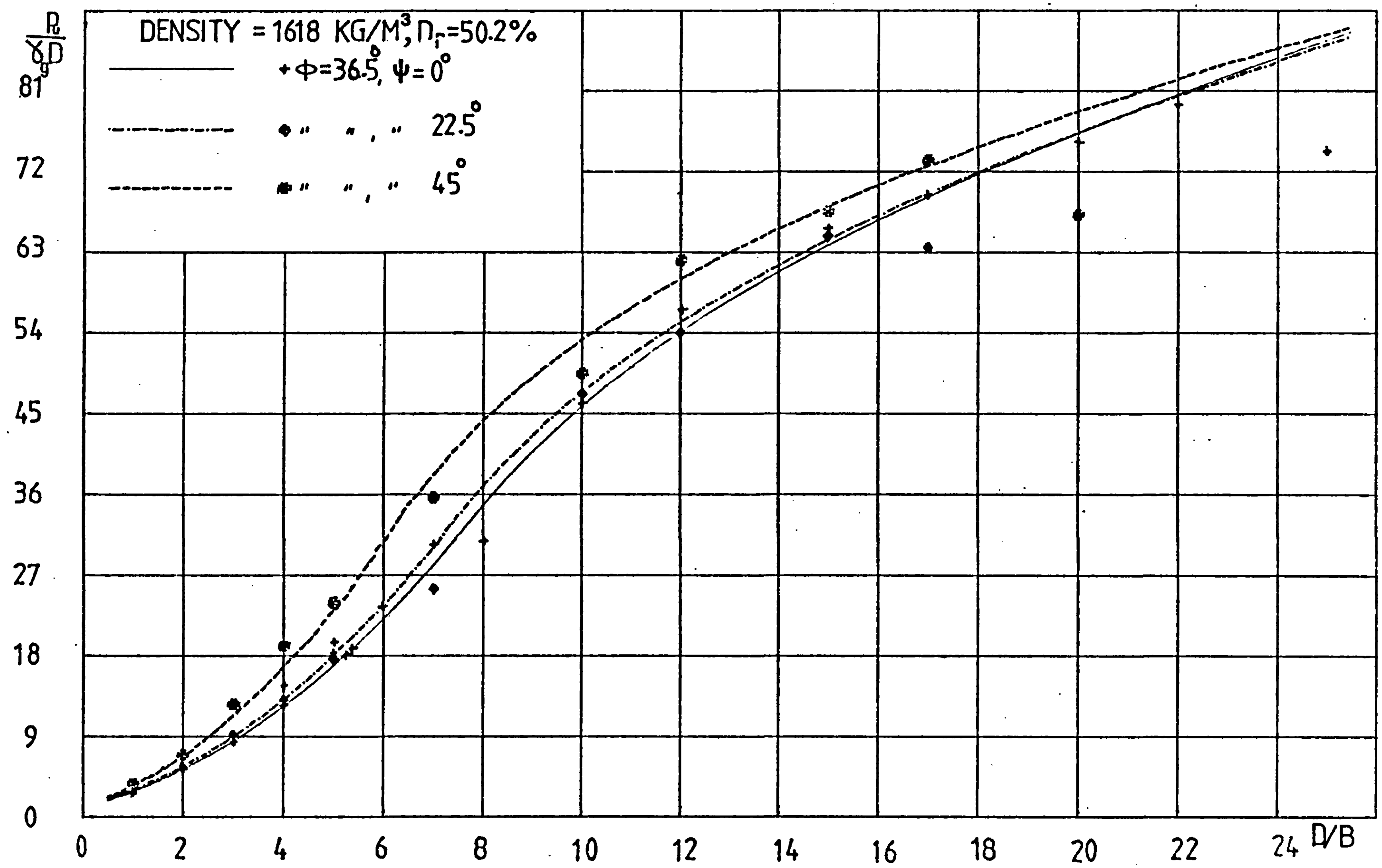

FIG 7.28b COMPARISON OF APPROXIMATE METHOD WITH THE VARYING INCLINATION OF PRESENT MODEL TESTS (MED. DENSE SAND)

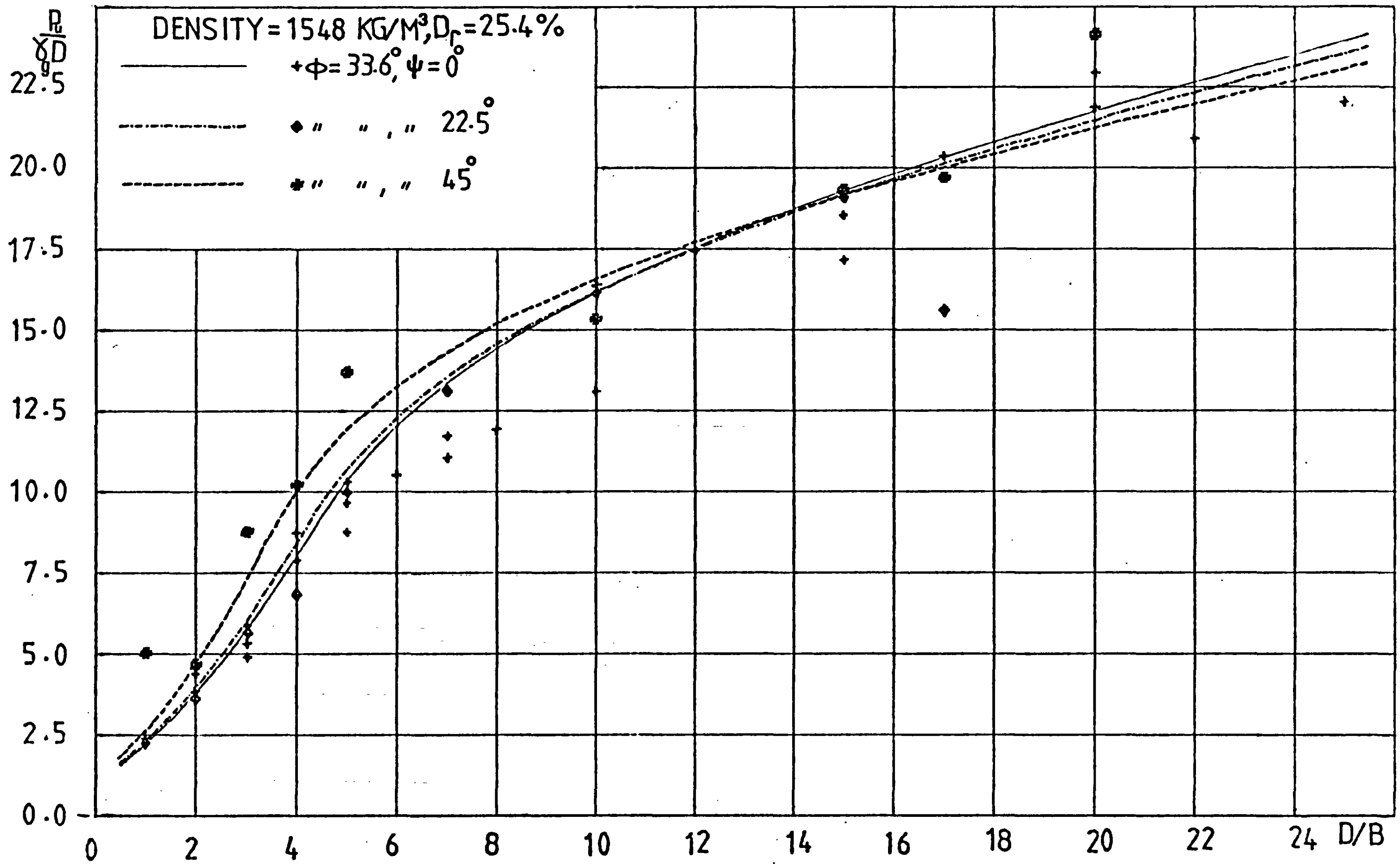

FIG 7.28c COMPARISON OF APPROXIMATE METHOD WITH THE VARYING INCLINATION OF PRESENT MODEL TESTS (LOOSE SAND)

CHAPTER 8

CONCLUSIONS AND SUGGESTIONS FOR FUTURE WORK

CHAPTER 8

CONCLUSIONS AND SUGGESTIONS FOR FUTURE WORK

This concluding chapter consists of two sections. The first section is the summary of conclusions from the previous chapters while the second presents the work in progress in the department and the author's suggestions for future work.

8.1. CONCLUSIONS:-

For each section of the work the summary of conclusions will be presented.

Based on the previous literature review on theoretical and experimental work applied to cohesionless soils and the proposed approximate method the following conclusions are reached.

1. Different theories were compared with each other and wide discrepancies are found to exist between them, and when compared to previous experimental results only fortuitous agreement occurred.
2. Different previous experimental results were compared with each other and an apparent anomaly is observed as discussed in Chapter 2, section 2.8 and illustrated in Figs (2.12, 2.13). However the author found that this is due to an inadequate description of the sand in terms of the angle of internal friction only. The relative density and the compressibility of the sand are other important parameters for shallow and deep vertical anchors in addition to the inclination factor for inclined anchors.
3. Depending on the previous and present experimental observations an approximate method is developed to predict the ultimate uplift resistance of circular plate anchors loaded normally in vertical or inclined directions when embedded in cohesionless soil. The method

assumed a simplified failure surface and the sand parameters neglected by previous investigators are considered. Using plastic equilibrium methods the ultimate loads are calculated for shallow, deep anchors in vertical and inclined positions embedded in different sand densities.

As a result of reviewing the factors affecting the deposition of uniform beds of sand and the apparatus constructed the following are concluded.

1. Techniques of adjusting the density of sand after deposition are avoided due to the creation of overconsolidation and anisotropy in the sand bed as a result of tamping or vibration.

2. Adjusting the sand density during deposition using traverse sand curtain and sand raining methods were adopted. However the former method is found to be more complicated and the variation in density is not sensitive beyond certain height of deposition. The latter method is very simple in construction and operation with reasonable degree of accuracy achieved. The apparatus is designed to allow testing of pushout, pullout displacement controlled tests for vertical and inclined anchors. From the load tests the anchor and surface displacements and the uplift loads can be measured electronically at different stages of loading. The photographic tests can provide the profile of failure surface in a three-dimensional axisymmetric test .

Based on the laboratory model tests in which the anchor depth, diameter, inclination and the sand density are varied are concluded with respect to:

a/ Nodal displacements.

1. From the photographic tests of shallow anchors the profile of failure surface is observed and found to be an outwardly curved surface extending from the anchor at an angle from the vertical and

meets the free sand surface at an angle greater than 45^{o} to the horizontal. This observation is confirmed by Carr (1970) and in disagreement with the assumed value of $(45 - \frac{\phi}{2})$ by some investigators.

2. From the surface displacement measurements of the load test two distinct failure mechanisms are observed, namely general and local shear failure corresponding to shallow and deep anchor cases with the critical $\frac{H}{B}$ ratio differentiating between them.

3. The surface failure is that where maximum relative differential movements occur and for simplification of the problem it is assumed to be a straight line in the meridian section through the anchor axis.

4. Due to the effect of compressibility, which is a function of the sand relative density, the amount of vertical movement of sand above the anchor decreases reaching the sand surface for shallow anchors and diminishes below the sand surface for deep anchors.

5. Similar trends to that shown for vertical shallow and deep anchors are observed for inclined anchors; however the failure surfaces are not symmetrical about the anchor axis. It was also observed that the critical $\frac{H}{B}$ ratio decreases with inclination.

6. Circular and elliptical failure surfaces are observed for shallow vertical and inclined anchors respectively.

7. The ratio of the surface displacements near the anchor axis for shallow vertical axis are the greatest. However the extent of the influence of the anchor plate is limited. For further increase of depth the surface heave spreads further from the anchor axis but with reduction in the maximum value. The displacements increase with density of sand.

b/ Load-displacement relationships

1. For shallow anchors, a noticeable uplift resistance reduction

to a residual value takes place after its peak value especially in dense sand. This is attributed to dilatancy of the shearing sand causing a reduction in shear strength along the failure surfaces.

2. For deep anchors, load increases with anchor displacement reaching an ultimate load which is maintained nearly constant for further displacement.

3. The anchor displacements at ultimate load increase with $\frac{D}{B}$ ratio resulting in large displacement for deep anchors; however these displacements decrease with increase of density yielding higher uplift loads.

4. The effect of depth of embedment on the development of shear strength is significant for shallow than that of deep anchors.

5. For inclined anchors, similar trends were observed and the anchor displacement at ultimate load increase with inclination from the vertical.

c/ Values of ultimate uplift load

1. The maximum uplift load is significantly dependent on the relative density or degree of compaction and the sand density. These factors, by governing the compressibility and shearing strength of the sand, controlled the mode of failure and determined the critical $\frac{H}{B}$ ratio. This ratio varied for vertical anchors in Leighton Buzzard sand from 4.25 to 10.5 for D_r = 25.44% and 85.12% respectively.

2. The ultimate loads increase with D and B or $\frac{D}{B}$ and the rate of increase is higher at shallow anchor range.

3. There is an increase of ultimate load with inclination for shallow anchors over that at vertical position which is noticeable for high values of density and inclination. This difference decreases as the density and inclination decrease. This is also the case for high $\frac{D}{B}$

ratio due to the reduction of critical $\frac{H}{B}$ ratio with inclination and so exhibiting deep anchor case earlier than the vertical anchor. At even higher $\frac{D}{B}$ ratios and depending on density and inclination the ultimate load falls below that of corresponding vertical anchor.

4. For a constant depth of embedment an increase in anchor diameter results in reduction of average ultimate pressure on anchor plate. However for constant $\frac{D}{B}$ this ultimate pressure is directly proportional to the anchor diameter.

5. From the non-dimensional analysis of test results of different anchor dimensions and soil properties, the concept of dimensional similarity is found to exist.

6. To obtain higher ultimate loads compacting the sand can be the most economical than increasing the anchor dimensions or inclinations.

With reference to the results of the finite element analysis these conclusions are obtained.

1. The nodal displacements predicted at anchor ultimate load represent the same trends reported in the model tests.

2. The qualitative distribution of stresses within the soil mass is in reasonable agreement with that expected.

3. The anchor load-displacement relationships obtained are higher than the experimental results due to the following:

(i) The idealized assumptions of the soil properties and the stress-strain relationships which are representing accurately the stress-strain state in the model tests.

(ii) Use of failure criterion which can not adequately simulate the behaviour of cohesionless soils.

Depending on the comparison of previous theories with the present experimental results and that of the proposed approximate method with the present and previous experimental results the following were concluded.

1. The approximate method compared to the author's test results showed good agreement for both shallow and deep cases of vertical and inclined anchors.

2. The approximate method showed good correlation with shallow and deep model tests as well as field tests results in vertical and inclined positions.

3. The method can simulate the behaviour observed in the model tests for various parameters tested. The percentage contribution of soil weight to the ultimate uplift resistance can be calculated and the method can explain the apparent discrepancy in the previous test results.

4. The approximate method is simple and hand calculation can be used to the ultimate loads.

5. With the versatility of the method, it was concluded that until a more comprehensive and adequate theory is developed the approximate method can be used to predict the ultimate loads of plate anchor. If the anchor dimensions, inclination and the sand properties of density, angle of internal friction and relative density are provided for the shallow anchor, and in addition the critical $\frac{H}{B}$ ratio for deep anchor, the ultimate loads can be obtained for any type of sand.

In reference to the prediction of ultimate loads provided with the appropriate parameters using the approximate method it can be summarised that:

1. A more appropriate method for presenting the ultimate loads is the design tables and charts. For the particular sand used in this investigation the results are produced for shallow, deep anchors at

different inclinations embedded in different densities.

2. Anchor displacements at ultimate loads can be predicted from the experimental results reported. According to the type of structure and soil and the permissible anchor displacement, the working load can be determined using the proper factor of safety.

8.2. WORK IN PROGRESS AND SUGGESTIONS FOR FUTURE STUDY

The present investigation forms part of a study into the uses of anchors being carried out in the department. Other work in progress includes

1. Experimental study of the behaviour of shallow and deep anchors subjected to static and cyclic loading of different amplitudes, storm loading and mean load. Studies of random wave effects and of initial tension and compression loading.

2. Groups of deep anchors embedded in close proximity in dense sand to act as single shallow foundation are chosen to develop a porosity or shape factor for a group. Group configuration based on an equilateral triangle will be stressed to working load levels rather than ultimate loads.

3. Many problems are involved in model scale testing of clay soils by controlling the material in each test and the preparation of soil strata of known history. The main objective of the tests is to examine the behaviour of plate anchors embedded in remoulded re-consolidated kaolin, the anchor being subjected to static and cyclic loads. In the static tests the parameters which will be studied will be the rate of loading, shear strength, $\frac{D}{B}$ and overconsolidation ratio to investigate the effect on the ultimate pullout capacity of the anchor. The cyclic test would examine the effect of a sinesoidal load cycle

with varying periods of different mean load level, and different load amplitudes on the resulting anchor movements.

The various anchor and soil parameters indicate the wide scope for further research. The following topics are considered to be worthy for experimental and theoretical investigation.

1. More testing is needed to find relationships between anchor loads and displacements. This is due to the fact that the extent of anchor displacement can be a failure criterion. Establishment of relationships for critical $\frac{H}{B}$ ratio of different soils.

2. The plate anchor is a simplified type of anchor and the study of other shapes of anchor geometry used in practice is necessary.

3. The load applied in this investigation is normal to the anchor plate and an investigation into more realistic types of unsymmetrical loading is needed.

4. Due to the installation of anchors in practice, soil disturbance occurs and the extent of this factor on the uplift load is worth investigation.

5. Extension of the work to simulate marine conditions using soils possessing cohesion and internal friction.

6. The extension of the finite element analysis using the indochronic constitutive relationships to model soil behaviour even during strain softening of single, group, vertical or inclined anchors and comparison with experimental results.

There are many other fields of work associated with anchors to be studied, e.g. prestress, creep underconstant load which have not been raised in this investigation. The further work under these headings is considered essential before a truly comprehensive understanding of anchor behaviour can be achieved.

REFERENCES

Abu-Taleb, M.G.A. (1974), "The behaviour of anchors in sand", Ph.D. Thesis, University of Sheffield.

Adams, J.I. and Hayes, D.C. (1967), "The uplift capacity of shallow foundations", Ontario Hydro Research Quarterly 19, 1.

Alyanak, I. (1961), "Vibration of sands with special reference to the minimum porosity test for sands", Proc. Midland Soil Mech. and Found. Engg. Soc., Vol. 4, pp 37-72.

Ashbee, R.A. (1969), "A uniaxial analysis for use in uplift foundation calculations", Central Electricity Research Laboratories, Lab. Report No. RD/L/R 1608.

Baker, W.H. and Kondner, R.L. (1966), "Pullout load capacity of a circular earth anchor buried in sand", National Academy of Sciences, Highway Research Record 108, pp 1-10.

Balla, A. (1961), "The resistance to breaking out of mushroom foundations for pylons", Proc. 5th Int. Conf. Soil Mech. and Found. Engg., Paris, Vol. 1, pp 569-576.

Bemben, S.M. and Kupferman, M. (1975), "The vertical holding capacity of marine anchor flukes subjected to static and cyclic loading", Proc. 7th Offshore Techn. Conf., Dallas, Vol. 1, pp 363-374.

Buckingham, E. (1914), "On similar systems; illustrations of the use of dimensional equations", Physical Review, Vol. 4, pp 345-376.

Burland, J.B. and Roscoe, K.H. (1969), "Local strains and pore pressures in a normally consolidated clay layer during one-dimensional consolidation", Geotechnique, Vol. 19, No. 3, pp 335-356.

Butterfield, R. and Andrawes, K.Z. (1968), "Wedge penetration into soils", Report No. CE/23/68, 67, University of Southampton, Dept. of Civil Engg.

Butterfield, R. and Andrawes, K.Z. (1970)a, "An air activated sand spreader for forming uniform sand beds", Geotechnique, Vol. 20, pp 97-100.

Butterfield, R. and Andrawes, K.Z. (1970)b, "A stereo-photogrammetric method for measuring displacement fields", Geotechnique, Vol. 20, No. 3, pp 308-314.

Carr, R.W. (1970), "An experimental investigation of plate anchors in sand", Ph.D. Thesis, University of Sheffield.

Carr, R.W. and Hanna, T.H. (1971), "Sand movement measurements near anchor plates", Proc. A.S.C.E., Soil Mech. & Found. Div., Vol. 97, SM5, pp 833-840.

Davie, J.R. (1973), "Behaviour of cohesive soils under uplift forces", Ph.D. Thesis, University of Glasgow.

Dzhioev, L.N. (1970), "Method of determining the bearing capacity of anchor foundations in rockfree soils", Hydrotechnical Construction, N.Y., No. 10, pp 924-927.

El-Rayes, M.K. (1965), "Behaviour of cohesionless soils under uplift forces", Ph.D. Thesis, University of Glasgow.

Esquivel-Diaz, R.F. (1967), "Pullout resistance of deeply buried anchors in sand", M.Sc. Thesis, Duke University, Durham, North Carolina, U.S.A.

Feda, J. (1961), "Research on the bearing capacity of loose soil", Proc. 5th Int. Conf. Soil Mech. & Found. Engg., Paris, Vol. 1, pp 635-642.

Gillon, M.D. (1970), "The ultimate resistance of deadman anchors subject to inclined load", M.Eng. Thesis, University of Canterbury, New Zealand.

Graton, L.C. and Fraser, H.J. (1935), "Systematic packing of spheres with particular relation to porosity and permeability", Journal of Geology, Vol. 43, pp 785-909.

Hanna, T.H. (1973), "The influence of anchor inclination on pullout resistance of clays", Canadian Geotechnical Jnl., Vol. 10, 5, pp 664-669.

Hanna, T.H. (1976), "A guide to design and construction of ground anchors", C.I.R.I.A.

Hanna, T.H., Sparks, R. and Yilmaz, M. (1972), "Anchor behaviour in sand", Proc. A.S.C.E. Soil Mech. & Found. Div., Vol. 98, SM 11, pp 1187-1208.

Hansen, Bent (1961), "The bearing capacity of sand tested by loading circular plates", Proc. 5th Int. Conf. Soil Mech. & Found. Engg. Vol. 1, pp 659-664.

Harvey, R.C. and Burley, E. (1973), "Behaviour of shallow inclined anchorages in cohesionless sand", Ground Engineering, Vol. 6, No. 5, pp 48-55.

Heikkila, K. and Laine, J. (1964), "Uplift resistance of guy anchor plate". Int. Conf. on Large Elect. System (C.I.G.R.E.), Paris, Paper 217.

Howat, M.D. (1969), "The behaviour of earth anchorages in sand", M.Sc. Thesis, University of Bristol.

Hunter, S.C. and Gamblen, D. (1974), "The theory of a rigid circular disc ground anchor in an elastic soil either with adhesion or without adhesion", Jnl. Mech. Phys. Solids, Vol. 22, pp 371-399.

James, J.P. (1967), "Stress-displacement relationship for sand subjected to passive pressure", Ph.D. Thesis, Manchester University.

James, R.G. (1965), "Stress and strain fields in sand", Ph.D. Thesis, Cambridge University.

Jasiewicz, J. (1963), "Application of dimensional analysis methods to civil engineering problems", Civil Engg. & Public Works Review, Part 1, pp 1125-1128, Part 2, pp 1279-1280.

Kananyan, A.S. (1966), "Experimental investigation of the stability of bases of anchor foundations", Soil Mech. & Found. Engg., Vol. 3, No. 6, pp 387-392. Translated from: Osnovaniya, Fundamentyi Mekhanika Gruntov.

Khadilkar, B.S. and Gogate, A.V. (1970), "Theoretical and experimental investigations of strength of anchor foundations", Proc. 2nd S.E. Asian Regional Conf. Soil Mech. & Found. Engg., Singapore pp 439-449.

Khadilkar, B.S., Paradkar, A.K. and Golait, Y.S. (1971), "Study of rupture surface and ultimate resistance of anchor foundation", Proc. 4th Asian Regional Conf. on Soil Mech. & Found. Engg., Bankok, pp 121-127.

Kolbuszewski, J.J. (1948a), "An experimental study of the maximum and minimum porosities of sands", Proc. 2nd Int. Conf. Soil Mech. & Found. Engg., Rotterdam, Vol. 1, pp 158.165.

Kolbuszewski, J.J. (1948b), "General investigation of the fundamental factors controlling loose packing of sands", Proc. 2nd Int. Conf. Soil Mech. & Found. Engg., Rotterdam, Vol. 7, pp 47-49.

Kolbuszewski, J.J. (1958), "Fundamental factors affecting experimental procedures dealing with pressure distribution in sands", Proc. Brussels Conf. Earth Pressure Problems, Vol. 1, pp 71-83.

Kolbuszewski, J.J. (1961), "Fundamental approach to basic factors controlling the behaviour of sands", Proc. Midland Soil Mech. & Found. Engg. Society, Vol. 4, pp 9-18.

Kolbuszewski, J.J. (1963), "A contribution towards a universal specification of the limiting porosities of granular mass", Proc. Europ. Conf. Soil Mech. & Found. Engg. Wiesbaden, Vol. 1, pp 265-271.

Kolbuszewski, J.J. and Jones, R.H. (1961), "The preparation of sand samples for laboratory testing", Proc. Midland Soil Mech. & Found. Engg. Society, Vol. 4, pp 107-123.

Kupferman, M. (1974), "The behaviour of embedded marine anchor flukes subjected to static and cyclic loading", Ph.D. Thesis, University of Massachusetts, U.S.A.

Larnach, W.J. (1972), "The pullout resistance of inclined anchors installed singly and in groups in sand", Ground Engg., Vol. 5, No. 4, pp 14-17.

Larnach, W.J. (1973), "The behaviour of grouped inclined anchors in sand", Ground Engg., Vol. 6, No. 6, pp 34-41.

Littlejohn, G.S. and Bruce, D.A. (1975), "Rock anchors - state of the art. Part 1: Design. Part 2: Construction", Ground Engg., Vol. 8, No. 3, pp 25-32, No. 4, pp 41-48, No. 5, pp 34-45, No. 6, pp 36-45.

Luga, A., Vorobkov, L., Ten, I. and Trofimenkov, J. (1961), "Bearing piles and open cassions for foundations", 5th Int. Conf. Soil Mech. & Found. Engg., Paris, Vol. 2, pp 85-89.

Mariupolskii, L.G. (1965), "The bearing capacity of anchor foundations", Soil Mech. & Found. Engg., Vol. 2, 1, pp 26-32. Translated from Osnovaniya, Fundamentyi Mekhanika Gruntov.

Matsuo, M. (1967), "Study on the uplift resistance of footing (1)", Japanese Soc. Soil Mech. & Found. Engg., Soils and Foundations, Vol. 7, No. 4, pp 1-37.

Matsuo, M. (1968), "Study on the uplift resistance of footing", Japanese Soc. Soil Mech. & Found. Engg., Soils and Foundations, Vol. 8, No. 1, pp 18-48.

Meyerhof, G.G. (1951), "The ultimate bearing capacity of foundations", Geotechnique, Vol. 2, No. 4, pp 301-322.

Meyerhof, G.G. (1973), "Uplift resistance of inclined anchors and piles", Proc. 8th Int. Conf. Soil Mech. & Found. Engg., Moscow, Vol. 2.1, pp 167-172.

Meyerhof, G.G. and Adams, J.I. (1968), "The ultimate uplift capacity of foundations", Canadian Geotechnical Jnl., Vol. 5, No. 4, pp 225-244.

MacDonald, H.F. (1963), "Uplift resistance of caisson piles in sand", M.Sc. Thesis, Nova Scotia Technical College, Canada.

McMeeking, R.M. and Rice, J.R. (1975), "Finite element formulations for problems of large elastic-plastic deformations", I.J.S.S., Vol. 11, No. 5, pp 601-616.

McMullan, D.J. (1974), "The behaviour of inclined ground anchors in sand both singly and in groups". Ph.D. Thesis, University of Bristol.

Nagtegaal, J.C., Parks, D.M. and Rice, J.R. (1974), "On numerically accurate finite element solutions in the fully plastic range", Computer Methods in Applied Mechanics and Engineering, Vol. 4, pp 153-177.

New Civil Engineer (1974), "Numerous benefits from submerged structure", 21 Feb., p8.

Ovesen, N.K. (1962), "Cellular cofferdams,.calculation methods and model tests", The Danish Geotechnical Institute, Bulletin No. 14.

Rice, J.R. and Tracey, D.M. (1973), "Computational fracture mechanics" in numerical and computer methods in structural mechanics , Academic Press.

Rocha, M. (1957), "The possibility of solving soil mechanics problems by the use of models", Proc. 4th Int. Conf. Soil Mech. & Found. Engg., London, Vol. 1, pp 183-188.

Roscoe, K.H. (1968), "Soils and model tests", Jnl. Strain Analysis, Vol. 3, No. 1, pp 57-64.

Sahota, B.S. (1979), "The break-out behaviour of a suction anchor embedded in a granular soil", M.Phil. Thesis, Robert Gordon's Institute of Technology, Aberdeen.

Sherif, M.M. (1975), "Pressures exerted by soil on retaining structures", Ph.D. Thesis, University of Leeds.

Sutherland, H.B. (1965), "Model studies for shaft raising through cohesionless soils", Proc. 6th Int. Conf. Soil Mech. & Found. Engg., Montreal, Vol. 2, pp 410-413.

Terzaghi, K. (1956), "Theoretical soil mechanics", John Wiley.

Tracey, D.M. (1973), "On the fracture mechanics analysis of elastic-plastic materials using the finite element method", Ph.D. Thesis, Brown University, U.S.A.

Tran-Von-Nhiem (1971), "Ultimate uplift capacity of anchor piles", Proc. 4th Conf. Soil Mech. & Found. Engg., Budapest, pp 829-836.

Trofimenkov, J.G. and Mariupolskii, L.G. (1965), "Screw piles used for mast and tower foundations", Proc. 6th Int. Conf. Soil Mech. & Found. Engg., Montreal, Vol. 2, pp 328-332.

Uzuner, B.A. (1975), "Centrally and eccentrically loaded strip foundations on sand", Ph.D. Thesis, University of Strathclyde, Glasgow.

Vafaeian, M. (1977), "Inclined loading plane strain tests on strip footing on sand", Ph.D. Thesis, University of Strathclyde, Glasgow.

Vesic, A.S. (1963), "Bearing capacity of deep foundations in sand", National Academy of Sciences, Highway Research Record, 39, pp 112-153.

Vesic, A.S. (1965), "Createring by explosives as an earth pressure problem", Proc. 6th Int. Conf. Soil Mech. & Found. Engg., Montreal, Vol. 2, pp 427-431.

Vesic, A.S. (1971), "Breakout resistance of objects embedded in ocean bottom", Proc. A.S.C.E. Soil Mech. & Found. Div., Vol. 97, SM 9, pp 1183-1205.

Vesic, A.S. (1972), "Expansion of cavities in infinite soil mass", Proc. A.S.C.E. Soil Mech. & Found. Div., Vol. 98, SM 3, pp 265-290.

Von Soos, P. (1972), "Anchors for carrying heavy tensile loads into the soil", European Conf. Soil Mech. & Found. Engg., Madrid pp 555-563.

Whalker, B.P. and Whitaker, T. (1967), "An apparatus for forming uniform beds of sand for model foundation tests", Geotechnique, Vol. 17, No. 2, pp 161-167.

Yilmaz, M. (1971), "The behaviour of groups of anchors in sand", Ph.D. Thesis, University of Sheffield.

APPENDIX A

DESIGN TABLES

D/B \ φ°	43	42	41	40	39	38	37	36	35	34	33	32
1.0	4.43	4.14	3.86	3.59	3.35	3.12	2.90	2.70	2.50	2.30	2.10	1.78
2.0	9.84	9.00	8.20	7.45	6.78	6.15	5.58	5.03	4.51	4.00	3.49	2.02
3.0	17.23	15.59	14.03	12.59	11.29	10.10	9.02	8.00	7.03	6.11	5.19	2.12
4.0	26.60	23.90	21.35	18.99	16.90	14.97	13.23	11.61	10.06	8.61	6.77	2.18
5.0	37.95	33.93	30.15	26.67	23.58	20.76	18.21	15.85	13.61	11.52	7.81	2.22
6.0	51.28	45.69	40.45	35.63	31.35	27.47	23.96	20.73	17.67	14.07	8.57	2.26
7.0	66.59	59.18	52.23	45.85	40.21	35.09	30.48	26.24	21.81	16.03	9.18	2.30
8.0	83.89	74.39	65.49	57.35	50.15	43.63	37.77	31.94	25.16	17.61	9.68	2.33
9.0	103.16	91.32	80.25	70.12	61.18	53.05	45.06	36.71	27.94	18.95	10.12	2.36
10.0	124.41	109.98	96.49	84.14	72.79	61.84	51.23	40.77	30.32	20.12	10.51	2.39
11.0	147.64	130.13	113.28	97.46	83.01	69.41	56.59	44.31	32.42	21.16	10.87	2.42
12.0	169.93	148.63	128.08	109.09	91.96	76.07	61.32	47.46	34.31	22.10	11.20	2.45
13.0	189.60	164.99	141.20	119.44	99.94	82.04	65.58	50.30	36.02	22.98	11.51	2.48
14.0	207.20	179.65	153.01	128.77	107.17	87.46	69.46	52.92	37.61	23.79	11.81	2.51
15.0	223.14	192.97	163.75	137.28	113.78	92.44	73.05	55.34	39.10	24.56	12.10	2.54
16.0	237.75	205.20	173.63	145.14	119.90	97.06	76.39	57.62	40.50	25.29	12.37	2.56
17.0	251.25	216.52	182.81	152.45	125.62	101.38	79.53	59.76	41.83	25.99	12.64	2.59
18.0	263.83	227.09	191.40	159.30	130.99	105.47	82.51	61.80	43.10	26.67	12.90	2.62
19.0	275.63	237.03	199.49	165.78	136.08	109.34	85.34	63.76	44.32	27.33	13.15	2.64
20.0	286.77	246.42	207.16	171.93	140.92	113.04	88.06	65.64	45.50	27.96	13.40	2.67
21.0	297.35	255.36	214.47	177.81	145.56	116.60	90.67	67.45	46.65	28.58	13.65	2.70
22.0	307.43	263.90	221.47	183.44	150.01	120.02	93.20	69.21	47.76	29.19	13.89	2.72
23.0	317.10	272.09	228.19	188.87	154.31	123.32	95.64	70.92	48.85	29.79	14.13	2.75
24.0	326.39	279.98	234.68	194.11	158.47	126.53	98.02	72.59	49.91	30.37	14.36	2.78
25.0	335.36	287.60	240.96	199.19	162.52	129.66	100.35	74.22	50.96	30.95	14.60	2.80

TABLE A.1 DESIGN TABLES ($\psi = 0^{\circ}$)

D/B \ φ°	43	42	41	40	39	38	37	36	35	34	33	32
1.0	4.49	4.19	3.90	3.63	3.38	3.15	2.93	2.72	2.52	2.32	2.11	1.78
2.0	9.98	9.12	8.31	7.54	6.86	6.22	5.64	5.08	4.55	4.04	3.52	2.02
3.0	17.48	15.81	14.22	12.75	11.44	10.23	9.12	8.09	7.10	6.17	5.24	2.17
4.0	27.00	24.25	21.65	19.25	17.12	15.16	13.39	11.75	10.18	8.71	6.80	2.18
5.0	38.54	34.45	30.59	27.05	23.90	21.03	18.44	16.05	13.77	11.64	7.83	2.22
6.0	52.10	46.40	41.05	36.14	31.79	27.84	24.28	20.99	17.89	14.16	8.59	2.26
7.0	67.66	60.10	53.02	46.52	40.78	35.57	30.89	26.59	22.00	16.09	9.18	2.30
8.0	85.25	75.56	66.50	58.20	50.88	44.24	38.29	32.26	25.31	17.66	9.68	2.33
9.0	104.85	92.78	81.49	71.17	62.08	53.76	45.51	36.98	28.06	18.98	10.11	2.36
10.0	126.47	111.75	98.00	85.36	73.68	62.45	51.62	40.99	30.42	20.14	10.50	2.39
11.0	150.00	132.03	114.73	98.54	83.79	69.94	56.92	44.49	32.49	21.16	10.85	2.42
12.0	172.08	150.34	129.38	110.06	92.65	76.54	61.60	47.60	34.36	22.10	11.18	2.45
13.0	191.55	166.54	142.37	120.29	100.55	82.44	65.82	50.42	36.06	22.96	11.49	2.48
14.0	208.99	181.06	154.06	129.53	107.70	87.80	69.66	53.00	37.63	23.77	11.79	2.50
15.0	224.78	194.25	164.70	137.96	114.25	92.73	73.21	55.40	39.10	24.53	12.07	2.53
16.0	239.25	206.36	174.48	145.73	120.30	97.30	76.52	57.65	40.48	25.25	12.34	2.56
17.0	252.63	217.58	183.57	152.97	125.96	101.58	79.63	59.78	41.80	25.95	12.60	2.59
18.0	265.09	228.05	192.08	159.77	131.28	105.63	82.57	61.80	43.05	26.62	12.86	2.61
19.0	276.79	237.89	200.10	166.18	136.32	109.46	85.38	63.73	44.26	27.27	13.11	2.64
20.0	287.83	247.21	207.70	172.27	141.11	113.13	88.06	65.59	45.43	27.90	13.36	2.66
21.0	298.32	256.06	214.94	178.09	145.71	116.65	90.65	67.39	46.57	28.51	13.60	2.69
22.0	308.32	264.53	221.87	183.68	150.12	120.03	93.15	69.13	47.67	29.11	13.84	2.72
23.0	317.90	272.65	228.54	189.05	154.38	123.31	95.57	70.82	48.75	29.70	14.08	2.74
24.0	327.11	280.46	234.96	194.24	158.50	126.49	97.93	72.47	49.80	30.28	14.31	2.77
25.0	336.01	288.02	241.19	199.28	162.51	129.58	100.23	74.09	50.83	30.85	14.55	2.80

TABLE A.2 DESIGN TABLES ($\psi = 10^{o}$)

D/B \ φ°	43	42	41	40	39	38	37	36	35	34	33	32
1.0	4.68	4.36	4.05	3.76	3.49	3.25	3.01	2.79	2.58	2.37	2.15	1.80
2.0	10.43	9.52	8.65	7.84	7.11	6.44	5.82	5.24	4.68	4.15	3.61	2.02
3.0	18.32	16.53	14.84	13.28	11.89	10.62	9.45	8.37	7.33	6.36	5.39	2.12
4.0	28.33	25.40	22.63	20.09	17.84	15.77	13.91	12.18	10.54	9.00	6.90	2.17
5.0	40.48	36.11	32.02	28.27	24.94	21.92	19.19	16.67	14.29	11.99	7.89	2.22
6.0	54.76	48.69	43.01	37.80	33.21	29.04	25.29	21.84	18.58	14.43	8.62	2.26
7.0	71.17	63.11	55.59	48.71	42.64	37.14	32.21	27.69	22.58	16.29	9.20	2.29
8.0	89.71	79.39	69.76	60.97	53.23	46.22	39.91	33.22	25.78	17.81	9.68	2.32
9.0	110.38	97.52	85.53	74.60	64.98	55.90	46.90	37.78	28.43	19.09	10.10	2.35
10.0	133.18	117.51	102.86	89.07	76.38	64.32	52.82	41.66	30.71	20.20	10.47	2.38
11.0	157.28	137.84	119.18	101.85	86.17	71.57	57.95	45.05	32.72	21.19	10.81	2.41
12.0	178.74	155.64	133.40	113.03	94.77	77.97	62.48	48.06	34.53	22.10	11.13	2.44
13.0	197.69	171.38	146.02	122.96	102.43	83.69	66.57	50.79	36.17	22.94	11.43	2.47
14.0	214.65	185.50	157.37	131.93	109.37	88.89	70.29	53.30	37.69	23.72	11.72	2.49
15.0	230.03	198.34	167.71	140.12	115.73	93.67	73.73	55.62	39.12	24.45	11.99	2.52
16.0	244.12	210.12	177.23	147.68	121.61	98.11	76.94	57.81	40.46	25.16	12.26	2.55
17.0	257.15	221.04	186.07	154.71	127.11	102.27	79.96	59.87	41.74	25.83	12.51	2.57
18.0	269.30	231.24	194.35	161.32	132.28	106.19	82.82	61.83	42.96	26.48	12.76	2.60
19.0	280.71	240.83	202.16	167.56	137.17	109.92	85.54	63.70	44.13	27.11	13.01	2.62
20.0	291.49	249.90	209.56	173.49	141.84	113.48	88.15	65.51	45.27	27.72	13.25	2.65
21.0	301.72	258.54	216.61	179.15	146.30	116.90	90.67	67.25	46.37	28.32	13.48	2.67
22.0	311.48	266.79	223.36	184.58	150.59	120.19	93.10	68.95	47.44	28.90	13.72	2.70
23.0	320.84	274.71	229.86	189.82	154.74	123.38	95.45	70.59	48.48	29.48	13.95	2.73
24.0	329.84	282.34	236.13	194.88	158.75	126.47	97.74	72.19	49.51	30.04	14.17	2.75
25.0	338.53	289.72	242.19	199.78	162.65	129.48	99.98	73.76	50.51	30.59	14.40	2.78

TABLE A.3 DESIGN TABLES ($\psi = 20^o$)

D/B \ φ°	43	42	21	40	39	38	37	36	35	34	33	32
1.0	5.07	4.69	4.34	4.01	3.71	3.43	3.17	2.93	2.69	2.46	2.23	1.82
2.0	11.33	10.29	9.31	8.41	7.60	6.86	6.18	5.54	4.93	4.35	3.77	2.03
3.0	19.97	17.95	16.05	14.32	12.77	11.36	10.09	8.91	7.78	6.72	5.65	2.12
4.0	30.98	27.66	24.56	21.73	19.23	16.95	14.90	13.01	11.22	9.55	7.08	2.17
5.0	44.34	39.41	34.83	30.64	26.96	23.62	20.62	17.87	15.27	12.60	8.01	2.21
6.0	60.07	53.22	46.85	41.06	35.96	31.36	27.24	23.46	19.79	14.89	8.69	2.25
7.0	78.16	69.07	60.64	52.97	46.25	40.18	34.76	29.62	23.57	16.65	9.24	2.28
8.0	98.62	86.98	76.19	66.39	57.81	50.07	42.66	34.86	26.59	18.08	9.69	2.31
9.0	121.44	106.93	93.49	81.30	70.23	59.58	49.30	39.19	29.11	19.29	10.09	2.34
10.0	146.57	128.60	111.47	95.53	81.08	67.58	54.92	42.87	31.27	20.35	10.44	2.37
11.0	170.30	148.19	127.06	107.72	90.41	74.48	59.79	46.08	33.18	21.29	10.77	2.40
12.0	190.90	165.23	140.66	118.38	98.60	80.57	64.11	48.95	34.89	22.15	11.07	2.42
13.0	209.10	180.32	152.73	127.88	105.91	86.02	67.99	51.54	36.45	22.95	11.36	2.45
14.0	225.41	193.88	163.61	136.45	112.54	90.98	71.54	53.93	37.90	23.69	11.63	2.48
15.0	240.22	206.20	173.52	144.28	118.61	95.54	74.82	56.15	39.26	24.39	11.89	2.50
16.0	253.79	217.53	182.65	151.52	124.23	99.78	77.88	58.22	40.53	25.06	12.14	2.53
17.0	266.36	228.03	191.14	158.26	129.49	103.75	80.76	60.19	41.75	25.70	12.39	2.55
18.0	278.08	237.85	199.09	164.59	134.44	107.50	83.49	62.06	42.91	26.32	12.63	2.58
19.0	289.10	247.09	206.59	170.58	139.13	111.07	86.10	63.85	44.03	26.92	12.86	2.60
20.0	299.51	255.84	213.70	176.27	143.60	114.48	88.59	65.57	45.12	27.51	13.09	2.63
21.0	309.41	264.17	220.49	181.71	147.88	117.75	91.00	67.24	46.17	28.08	13.32	2.65
22.0	318.86	272.13	227.00	186.93	152.00	120.90	93.32	68.86	47.19	28.63	13.54	2.68
23.0	327.92	279.78	233.25	191.96	155.97	123.96	95.57	70.43	48.19	29.18	13.76	2.70
24.0	336.64	287.15	239.29	196.83	159.83	126.92	97.77	71.96	49.17	29.72	13.98	2.72
25.0	345.07	294.28	245.15	201.55	163.57	129.80	99.91	73.46	50.13	30.25	14.19	2.75

TABLE A.4 DESIGN TABLES ($\psi = 30^{o}$)

D/B \ ϕ^{o}	43	42	41	40	39	38	37	36	35	34	33	32
1.0	5.77	5.29	4.85	4.44	4.08	3.75	3.44	3.16	2.88	2.62	2.36	1.86
2.0	13.02	11.72	10.52	9.43	8.46	7.59	6.80	6.07	5.37	4.71	4.05	2.05
3.0	23.09	20.58	18.27	16.18	14.35	12.69	11.21	9.84	8.55	7.34	6.03	2.12
4.0	35.97	31.86	28.09	24.69	21.72	19.05	16.67	14.48	12.42	10.52	7.35	2.18
5.0	51.65	45.57	39.98	34.96	30.59	26.66	23.17	19.98	16.99	13.49	8.20	2.21
6.0	70.15	61.69	53.94	46.98	40.93	35.52	30.71	26.33	21.57	15.61	8.84	2.25
7.0	91.44	80.22	69.96	60.76	52.77	45.63	39.23	32.49	25.08	17.24	9.34	2.28
8.0	115.54	101.18	88.06	76.29	66.04	56.28	46.80	37.38	27.89	18.57	9.77	2.31
9.0	142.45	124.51	107.72	92.20	78.22	65.20	53.02	41.41	30.24	19.70	10.13	2.33
10.0	169.13	146.42	125.03	105.65	88.45	72.72	58.28	44.86	32.26	20.69	10.47	2.36
11.0	191.91	165.12	139.85	117.19	97.25	79.22	62.86	47.87	34.04	21.57	10.77	2.39
12.0	211.71	181.42	152.79	127.30	104.99	84.95	66.91	50.56	35.64	22.37	11.05	2.41
13.0	229.24	195.87	164.30	136.31	111.91	90.09	70.57	52.99	37.11	23.11	11.32	2.44
14.0	244.98	208.87	174.68	144.46	118.18	94.77	73.91	55.24	38.47	23.81	11.58	2.46
15.0	259.28	220.71	184.15	151.91	123.94	99.09	77.01	57.32	39.74	24.47	11.82	2.48
16.0	272.42	231.61	192.89	158.81	129.28	103.10	79.90	59.28	40.94	25.10	12.06	2.51
17.0	284.60	241.72	201.02	165.24	134.27	106.86	82.62	61.13	42.09	25.70	12.29	2.53
18.0	295.98	251.19	208.65	171.28	138.98	110.42	85.20	62.90	43.18	26.29	12.52	2.56
19.0	306.68	260.12	215.86	177.01	143.45	113.80	87.66	64.59	44.24	26.85	12.74	2.58
20.0	316.81	268.57	222.70	182.45	147.71	117.04	90.03	66.22	45.26	27.40	12.95	2.60
21.0	326.46	276.64	229.23	187.66	151.79	120.15	92.30	67.79	46.25	27.94	13.17	2.63
22.0	335.68	284.36	235.50	192.66	155.72	123.15	94.51	69.32	47.22	28.47	13.38	2.65
23.0	344.53	291.78	241.53	197.49	159.52	126.06	96.65	70.81	48.16	28.98	13.59	2.67
24.0	353.06	298.94	247.36	202.16	163.21	128.88	98.73	72.27	49.09	29.49	13.79	2.70
25.0	361.30	305.87	253.02	206.70	166.79	131.63	100.77	73.69	50.00	29.99	13.99	2.72

TABLE A.5 DESIGN TABLES ($\psi = 40^{o}$)

D/B \ φ°	43	42	41	40	39	38	37	36	35	34	33	32
1.0	7.22	6.49	5.83	5.26	4.76	4.32	3.93	3.56	3.22	2.90	2.57	1.92
2.0	16.53	14.60	12.88	11.38	10.09	8.94	7.93	7.01	6.14	5.33	4.54	2.08
3.0	29.63	25.92	22.65	19.78	17.33	15.17	13.26	11.54	9.93	8.45	6.59	2.15
4.0	46.48	40.44	35.10	30.44	26.47	22.98	19.92	17.15	14.59	12.09	7.78	2.20
5.0	67.08	58.13	50.24	43.35	37.51	32.37	27.88	23.85	19.94	14.82	8.56	2.23
6.0	91.44	79.01	68.06	58.53	50.44	43.35	37.17	31.09	24.21	16.77	9.14	2.26
7.0	119.54	103.07	88.57	75.95	65.27	55.53	46.13	36.82	27.46	18.27	9.61	2.29
8.0	151.39	130.31	111.37	94.39	79.46	65.81	53.22	41.37	30.07	19.50	10.00	2.32
9.0	183.23	156.06	131.43	109.77	91.02	74.22	59.05	45.14	32.25	20.55	10.34	2.34
10.0	209.87	177.57	148.21	122.68	100.76	81.32	64.00	48.36	34.13	21.46	10.65	2.37
11.0	232.63	195.98	162.61	133.78	109.15	87.48	68.31	51.18	35.79	22.28	10.93	2.39
12.0	252.49	212.07	175.23	143.53	116.55	92.92	72.13	53.70	37.29	23.03	11.19	2.42
13.0	270.12	226.37	186.47	152.23	123.18	97.81	75.59	56.00	38.66	23.72	11.44	2.44
14.0	286.00	239.28	196.64	160.12	129.20	102.27	78.76	58.11	39.94	24.37	11.68	2.46
15.0	300.47	251.06	205.94	167.36	134.74	106.39	81.69	60.08	41.13	24.99	11.91	2.49
16.0	313.80	261.93	214.54	174.07	139.89	110.23	84.44	61.93	42.26	25.58	12.13	2.51
17.0	326.19	272.05	222.56	180.34	144.71	113.83	87.03	63.68	43.34	26.15	12.35	2.53
18.0	337.80	281.54	230.10	186.24	149.26	117.25	89.49	65.36	44.37	26.70	12.56	2.55
19.0	348.75	290.51	237.23	191.84	153.59	120.50	91.84	66.96	45.37	27.23	12.77	2.58
20.0	359.14	299.03	244.02	197.17	157.72	123.61	94.10	68.51	46.34	27.75	12.97	2.60
21.0	369.05	307.16	250.51	202.28	161.69	126.61	96.28	70.01	47.28	28.26	13.17	2.62
22.0	378.54	314.97	256.75	207.20	165.51	129.50	98.39	71.47	48.19	28.75	13.37	2.64
23.0	387.68	322.48	262.77	211.95	169.21	132.31	100.44	72.88	49.09	29.24	13.57	2.66
24.0	396.49	329.75	268.59	216.56	172.81	135.04	102.44	74.27	49.96	29.72	13.76	2.69
25.0	405.03	336.79	274.24	221.03	176.30	137.70	104.39	75.63	50.83	30.19	13.95	2.71

TABLE A.6 DESIGN TABLES ($\psi = 50^{\circ}$)

APPENDIX B

DESIGN CURVES

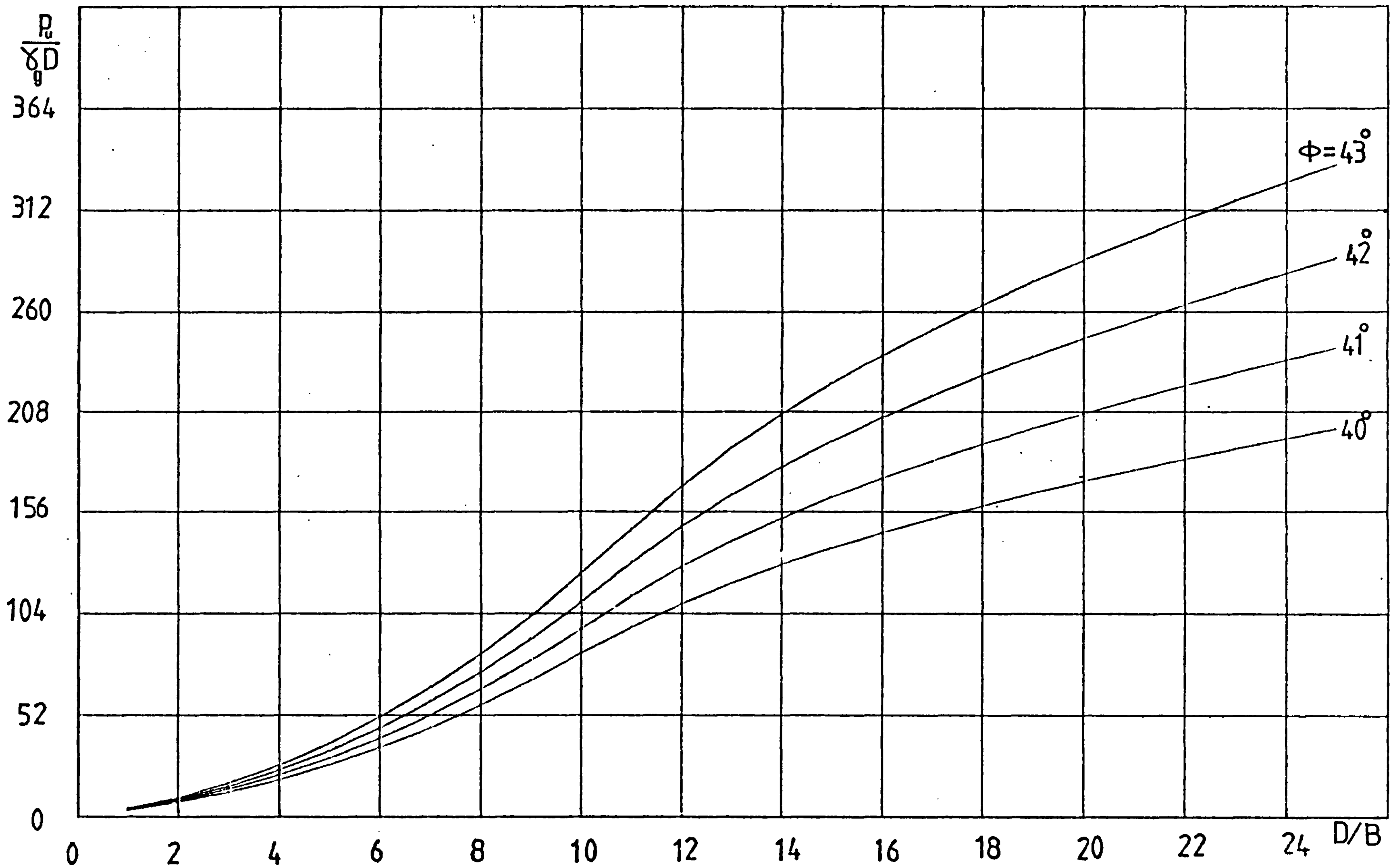

FIG B.1 DESIGN CURVES FOR DENSE SAND ($\psi = 0^\circ$)

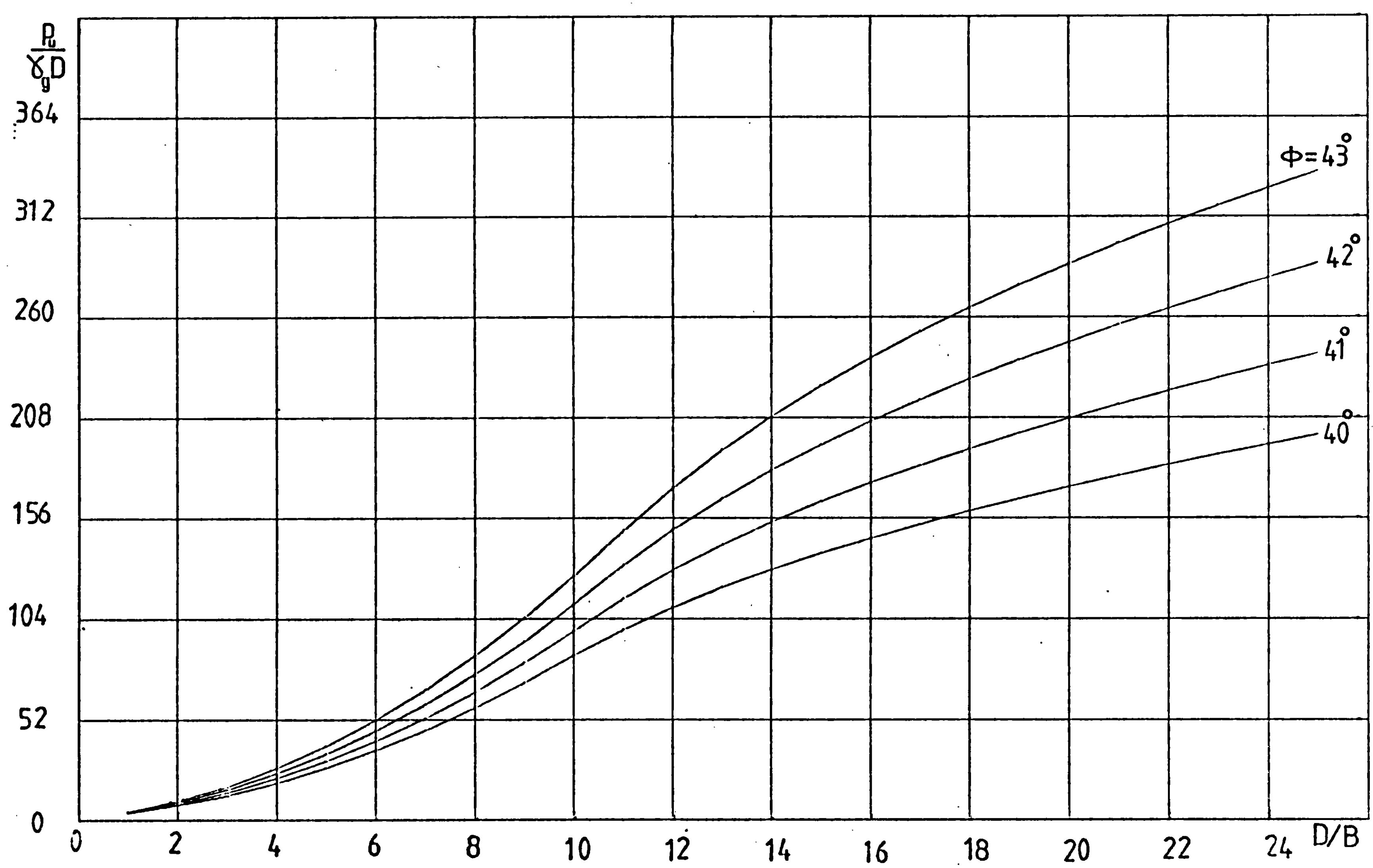

FIG B.2 DESIGN CURVES FOR DENSE SAND ($\psi = 10^{0}$)

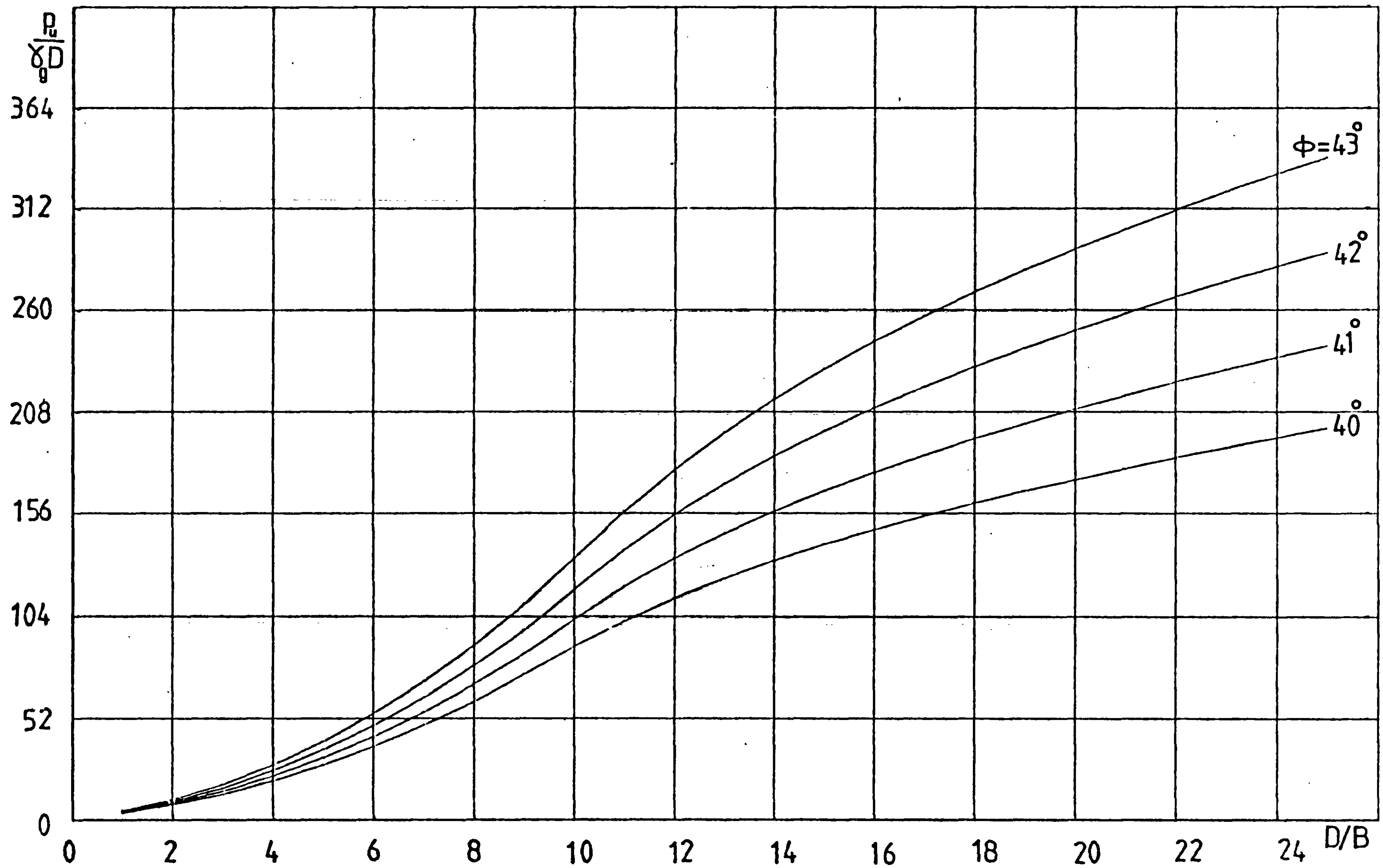

FIG B.3 DESIGN CURVES FOR DENSE SAND ($\psi = 20^\circ$)

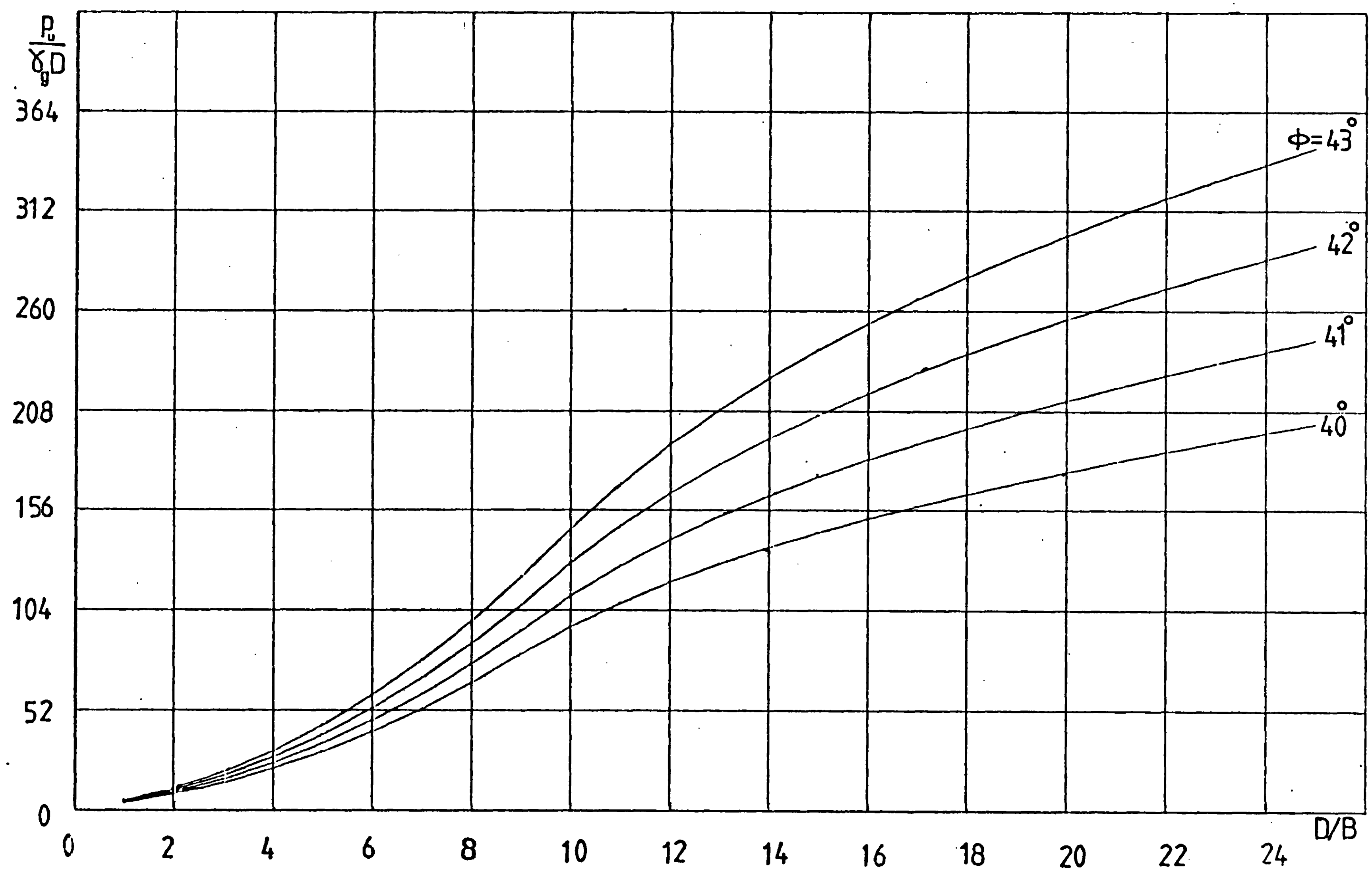

FIG B.4 DESIGN CURVES FOR DENSE SAND ($\psi = 30^{o}$)

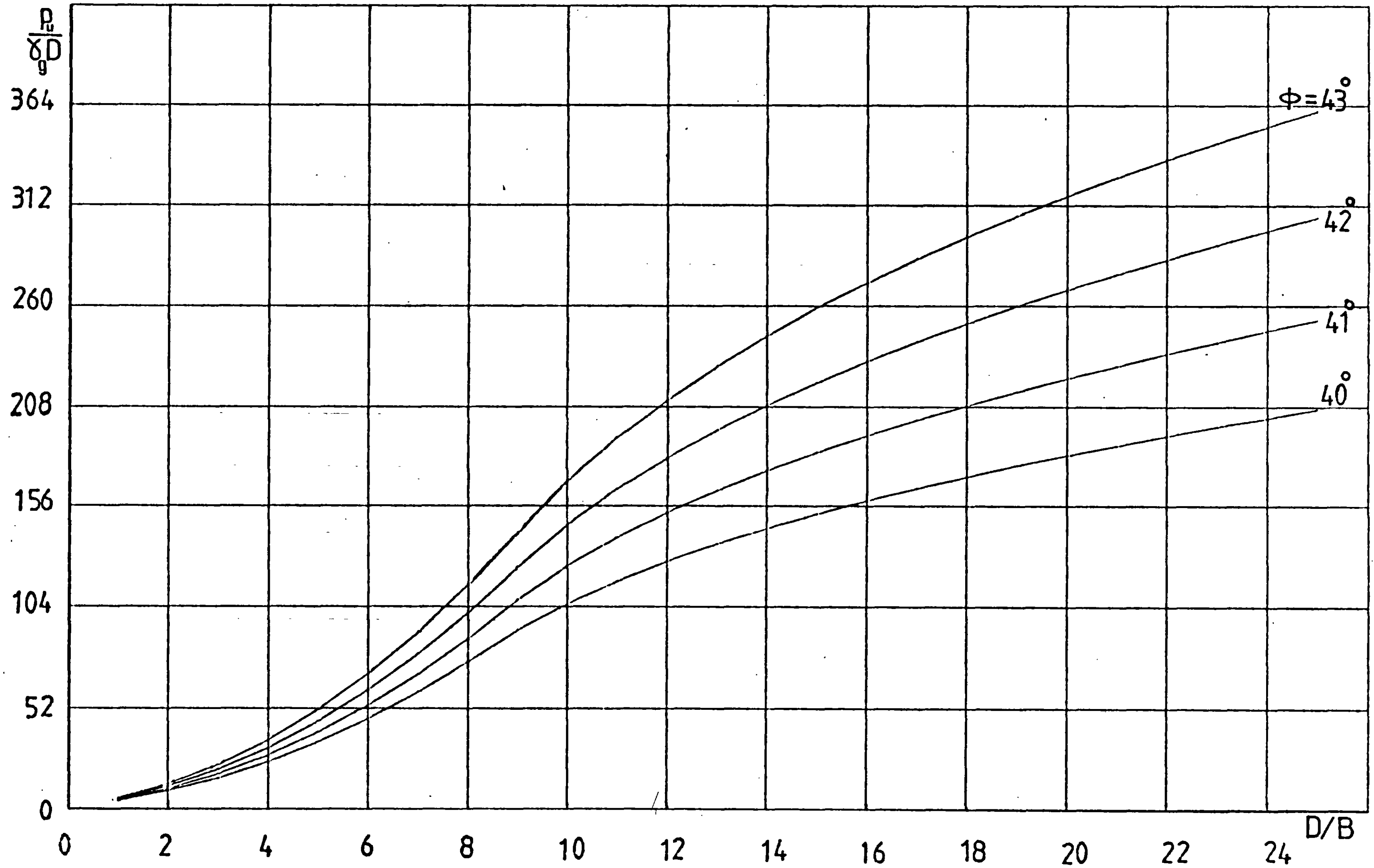

FIG B.5 DESIGN CURVES FOR DENSE SAND ($\psi = 40^\circ$)

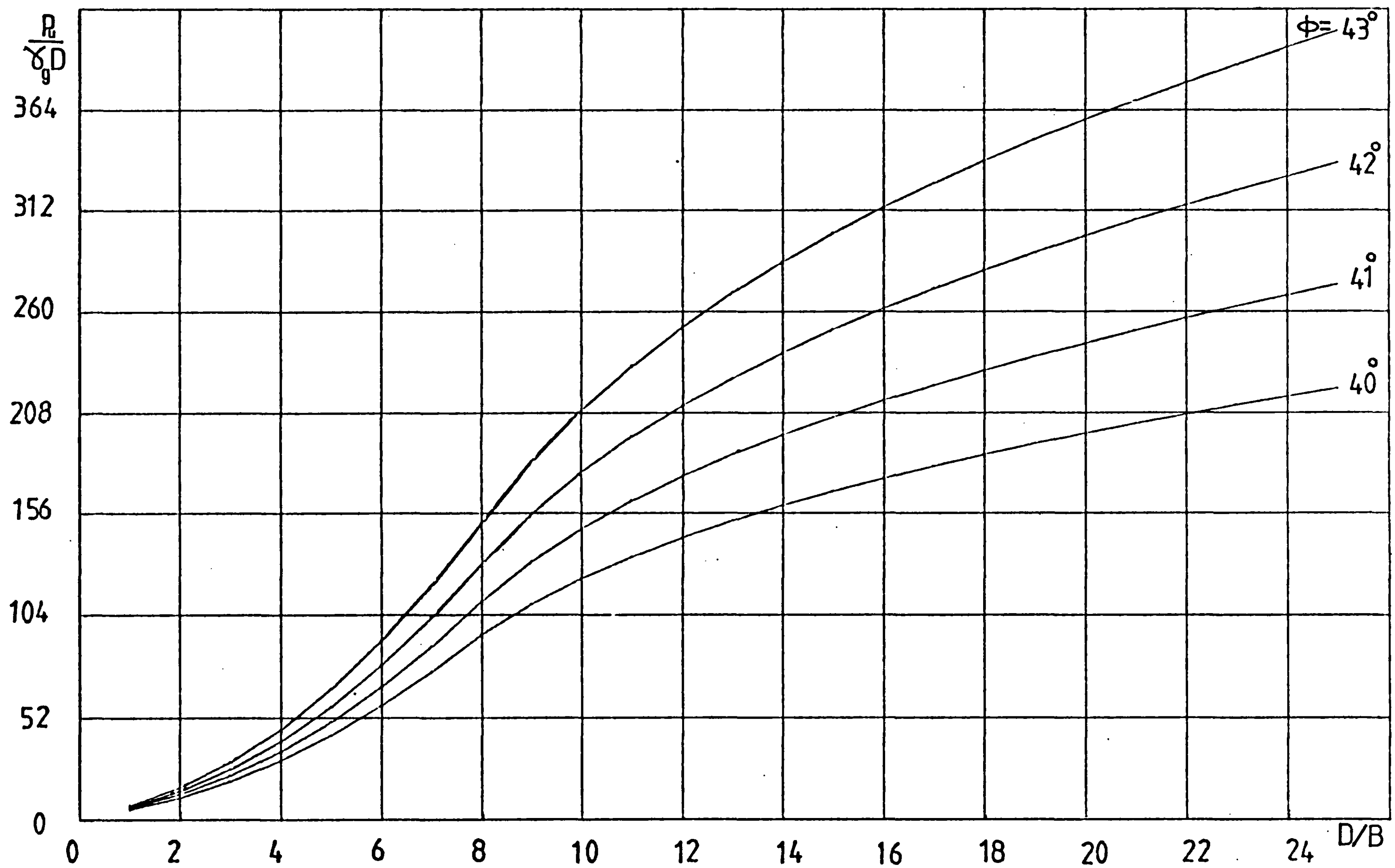

FIG B.6 DESIGN CURVES FOR DENSE SAND ($\psi = 50^{o}$)

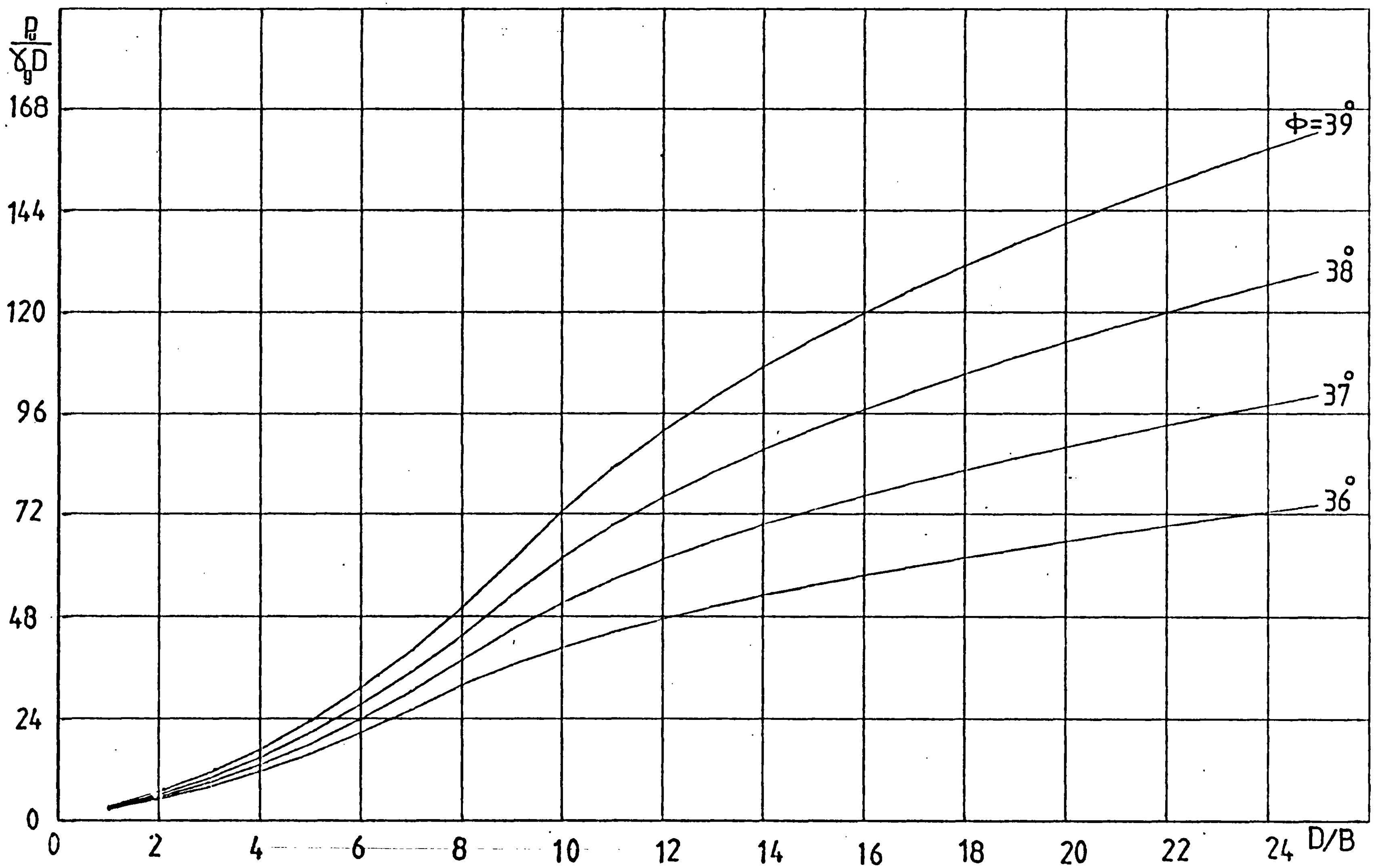

FIG B.7 DESIGN CURVES FOR MEDIUM DENSE SAND ($\psi = 0^\circ$)

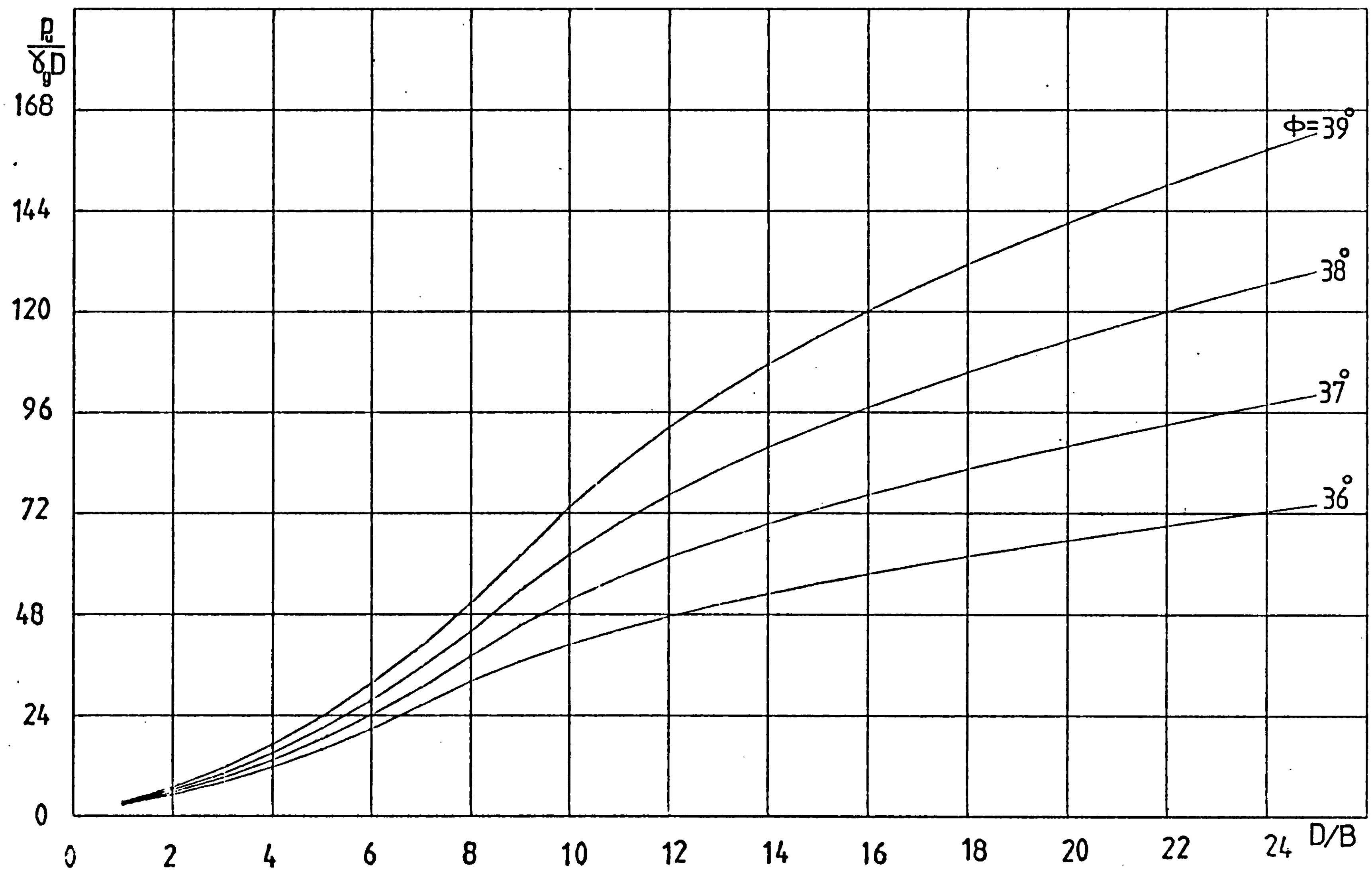

FIG B.8 DESIGN CURVES FOR MEDIUM DENSE SAND ($\psi = 10^{o}$)

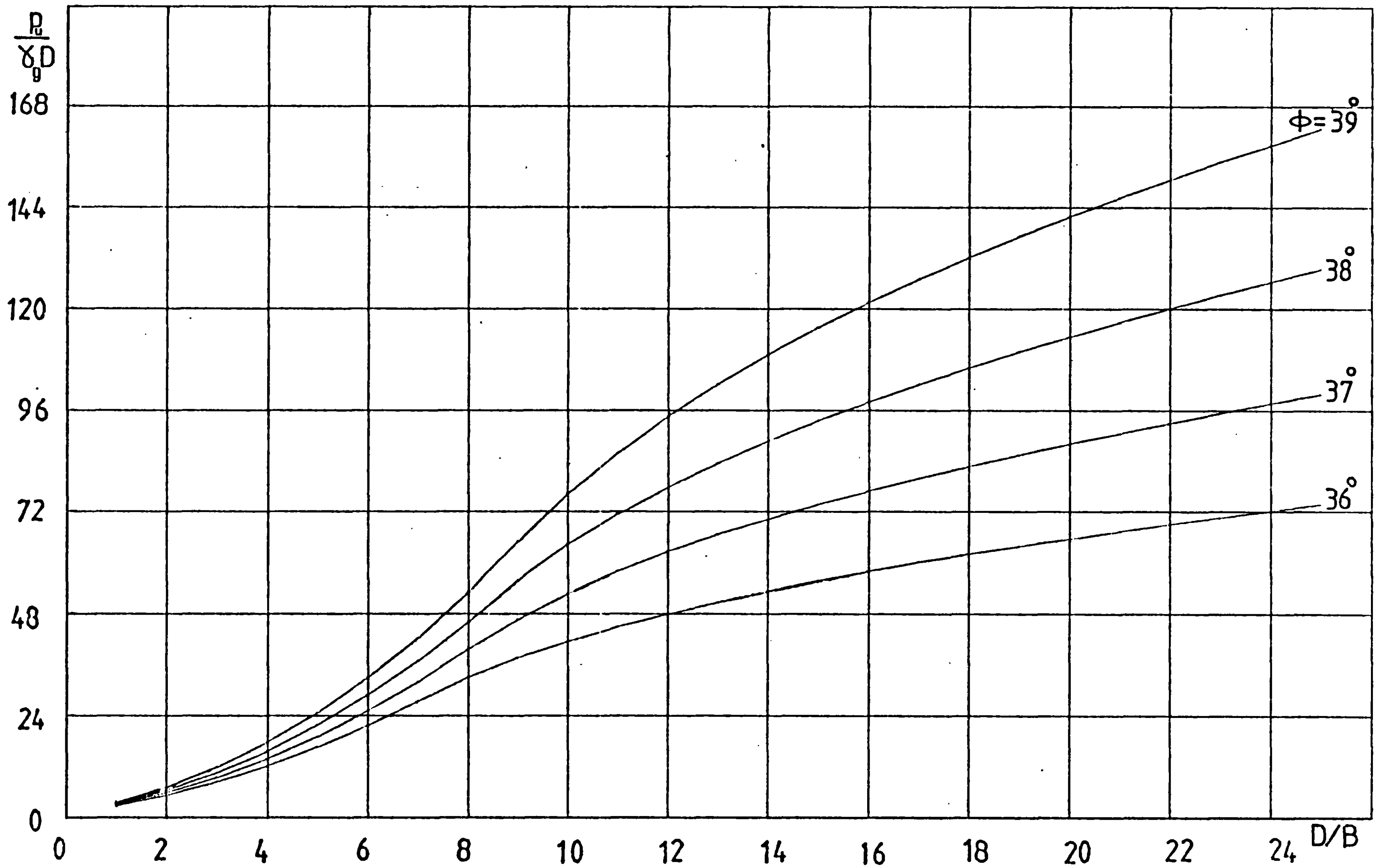

FIG B.9 DESIGN CURVES FOR MEDIUM DENSE SAND ($\psi = 20^o$)

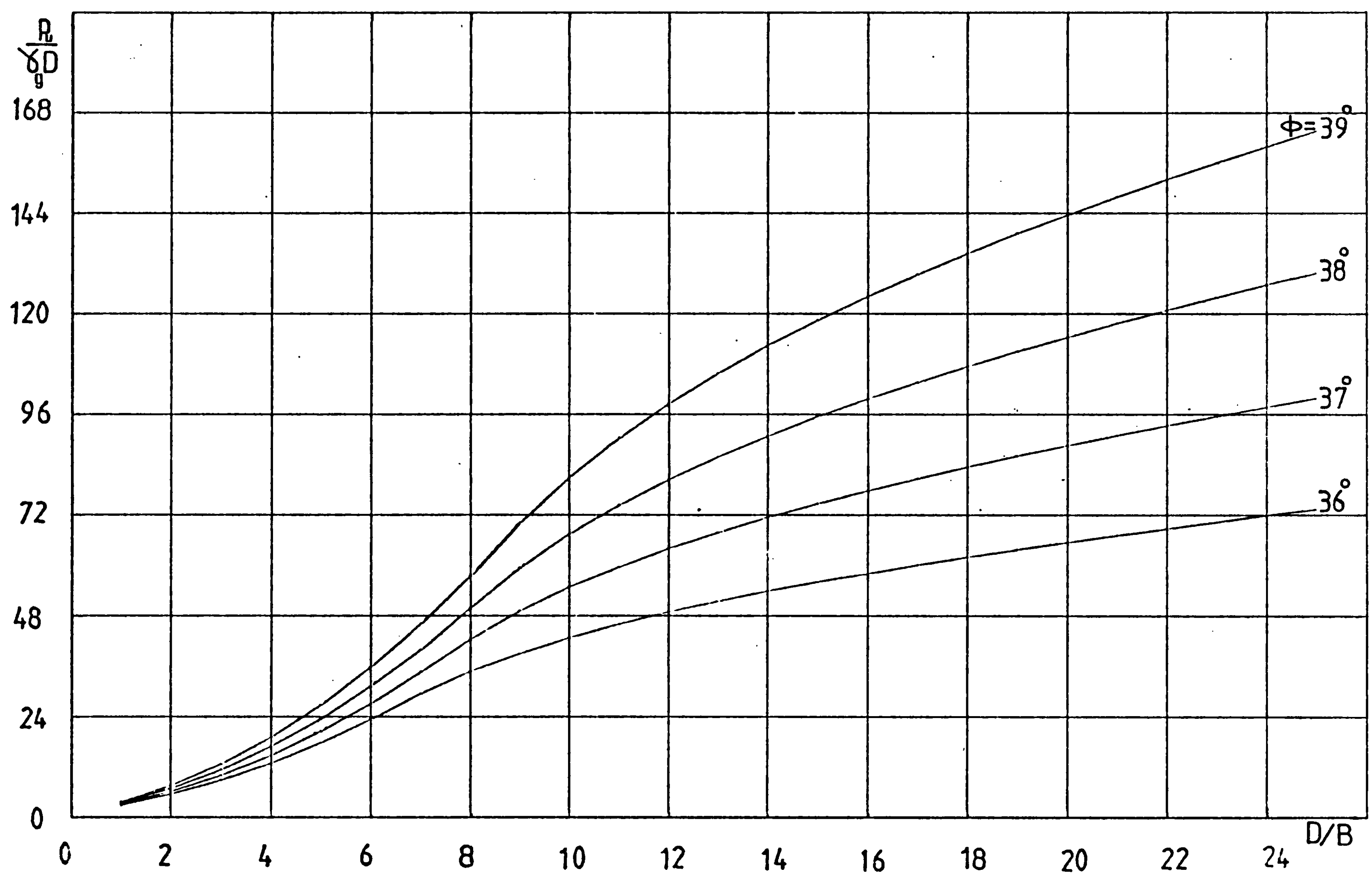

FIG B.10 DESIGN CURVES FOR MEDIUM DENSE SAND ($\psi = 30^o$)

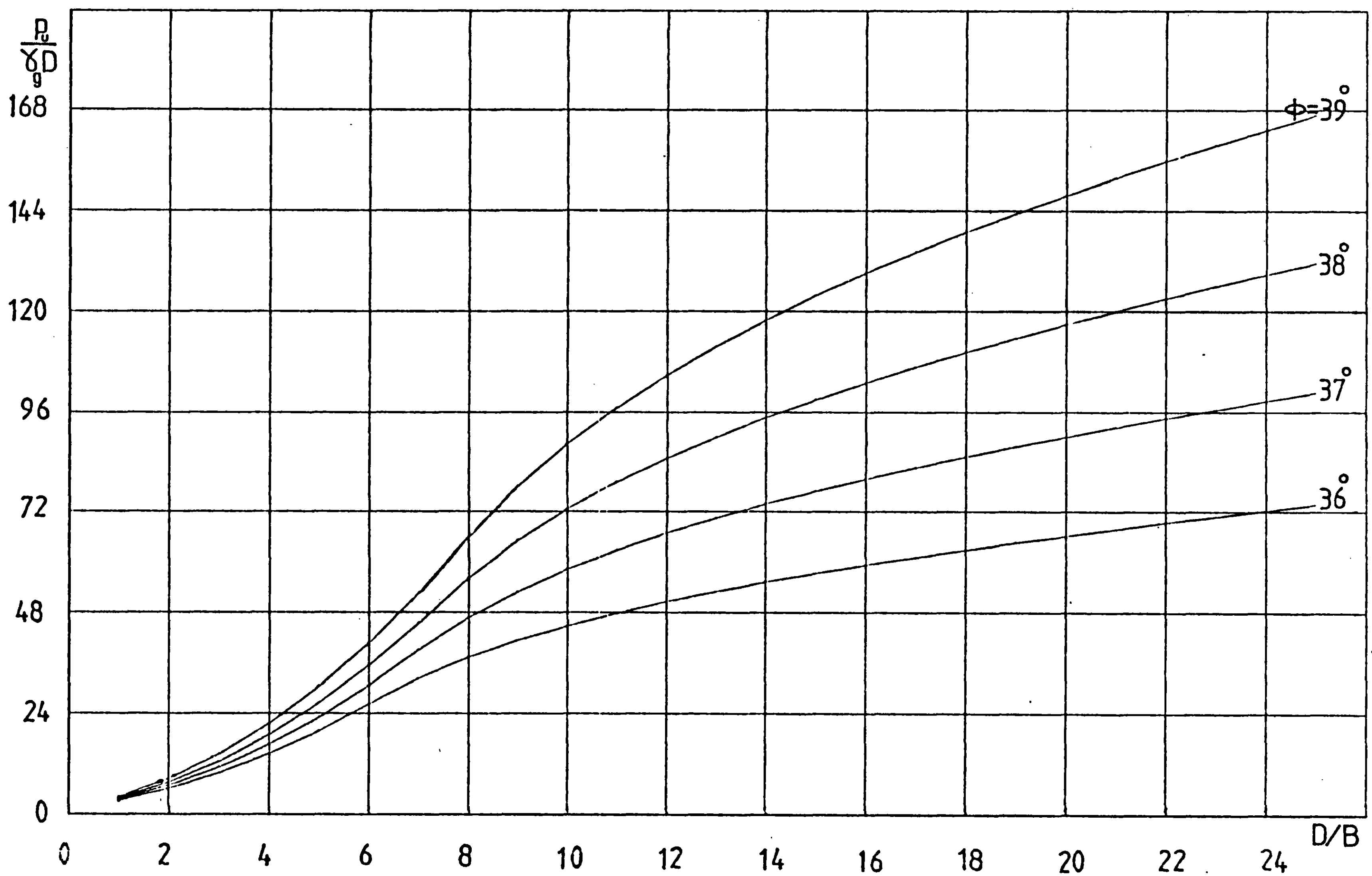

FIG B.11 DESIGN CURVES FOR MEDIUM DENSE SAND ($\psi = 40°$)

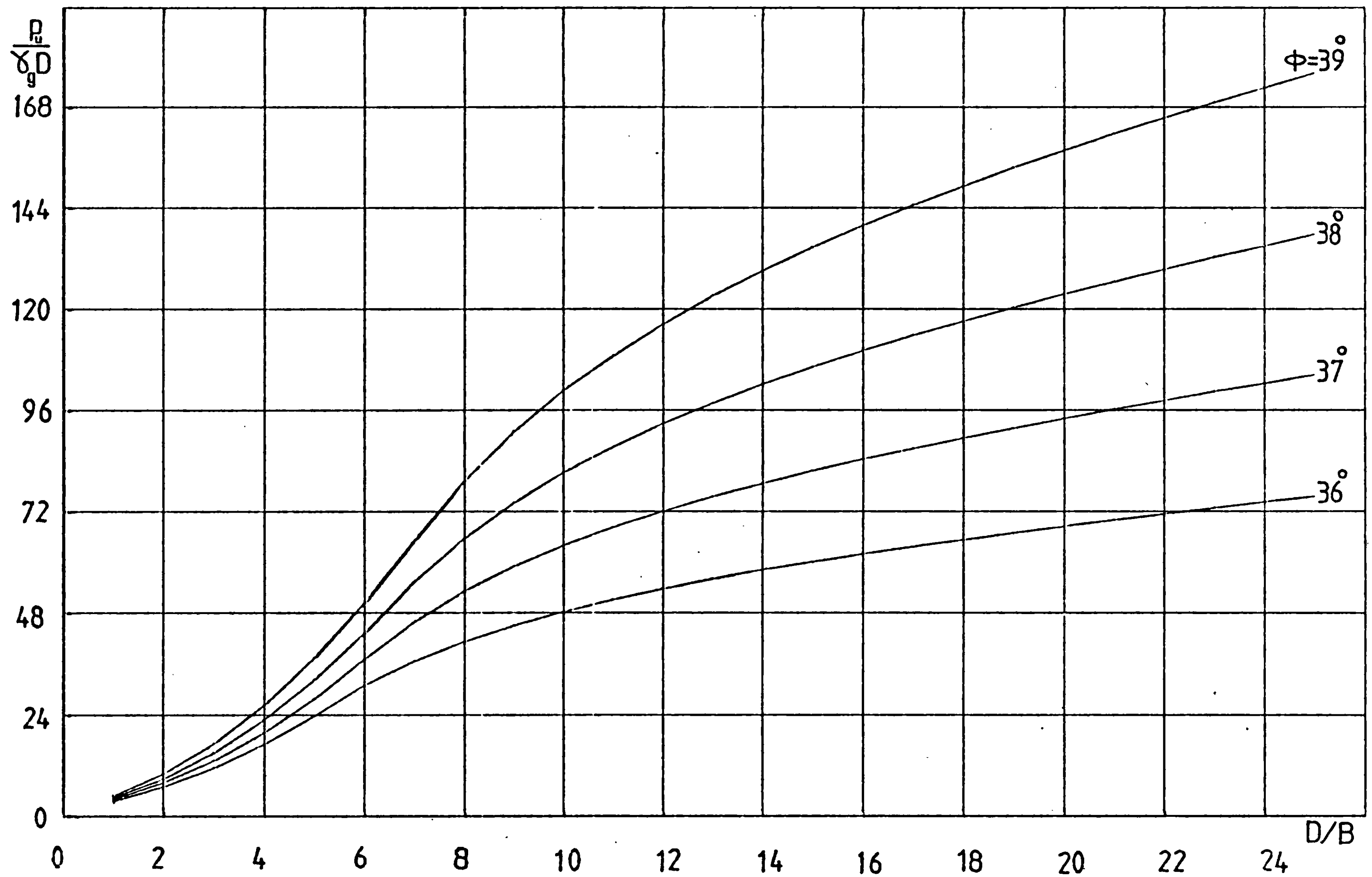

FIG B.12 DESIGN CURVES FOR MEDIUM DENSE SAND ($\psi = 50°$)

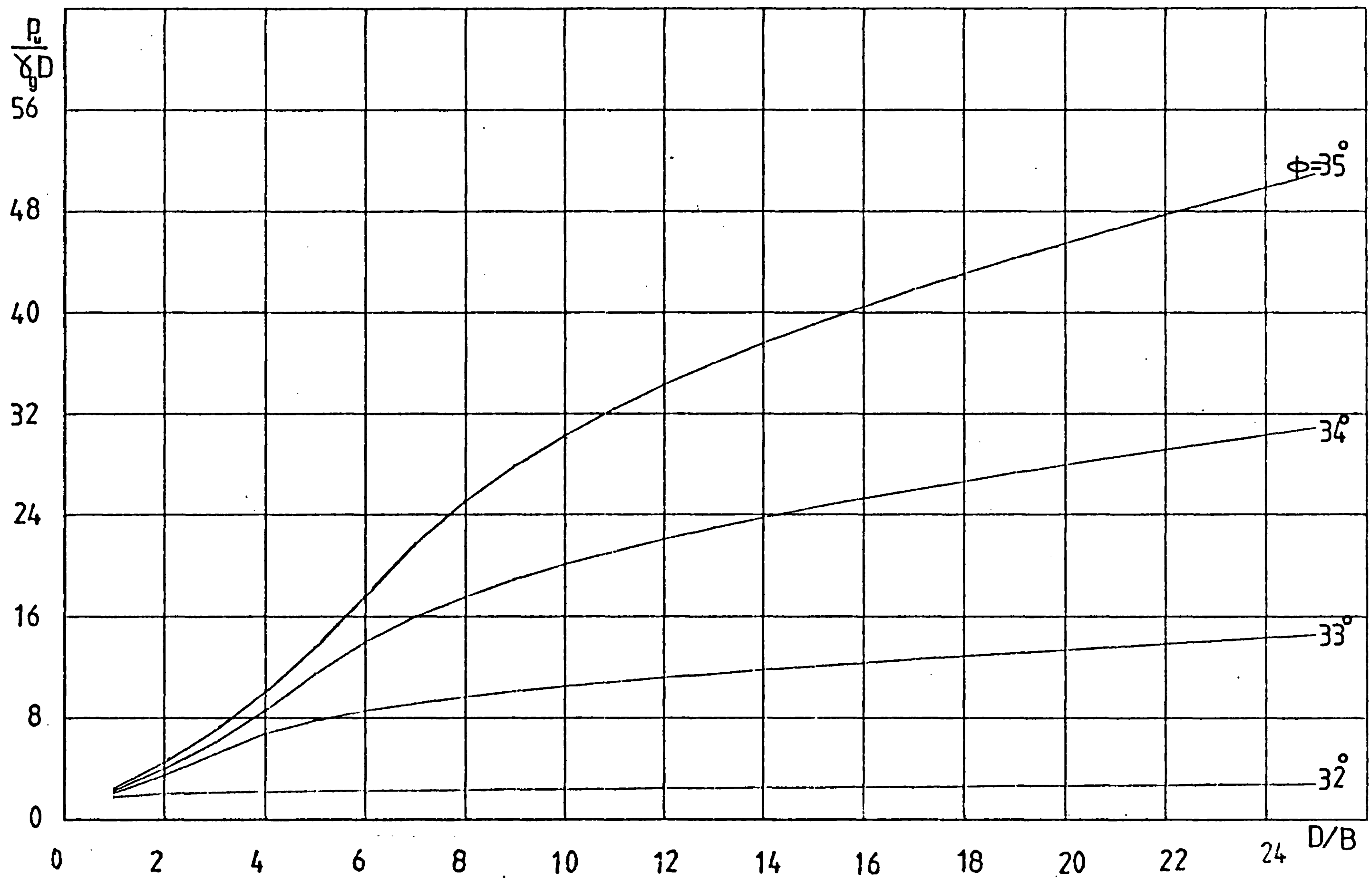

FIG B.13 DESIGN CURVES FOR LOOSE SAND ($\psi = 0^\circ$)

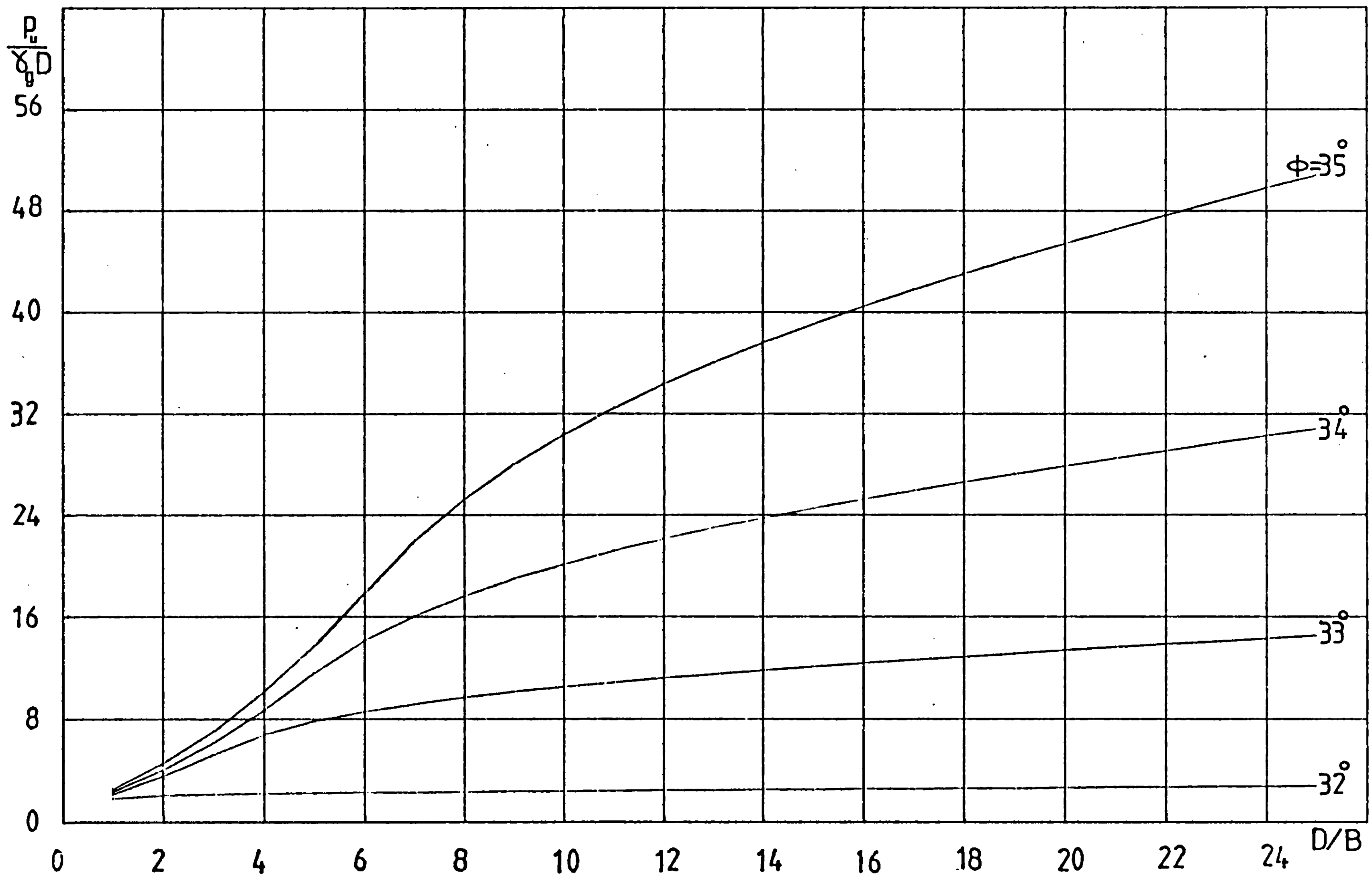

FIG B.14 DESIGN CURVES FOR LOOSE SAND ($\psi = 10^o$)

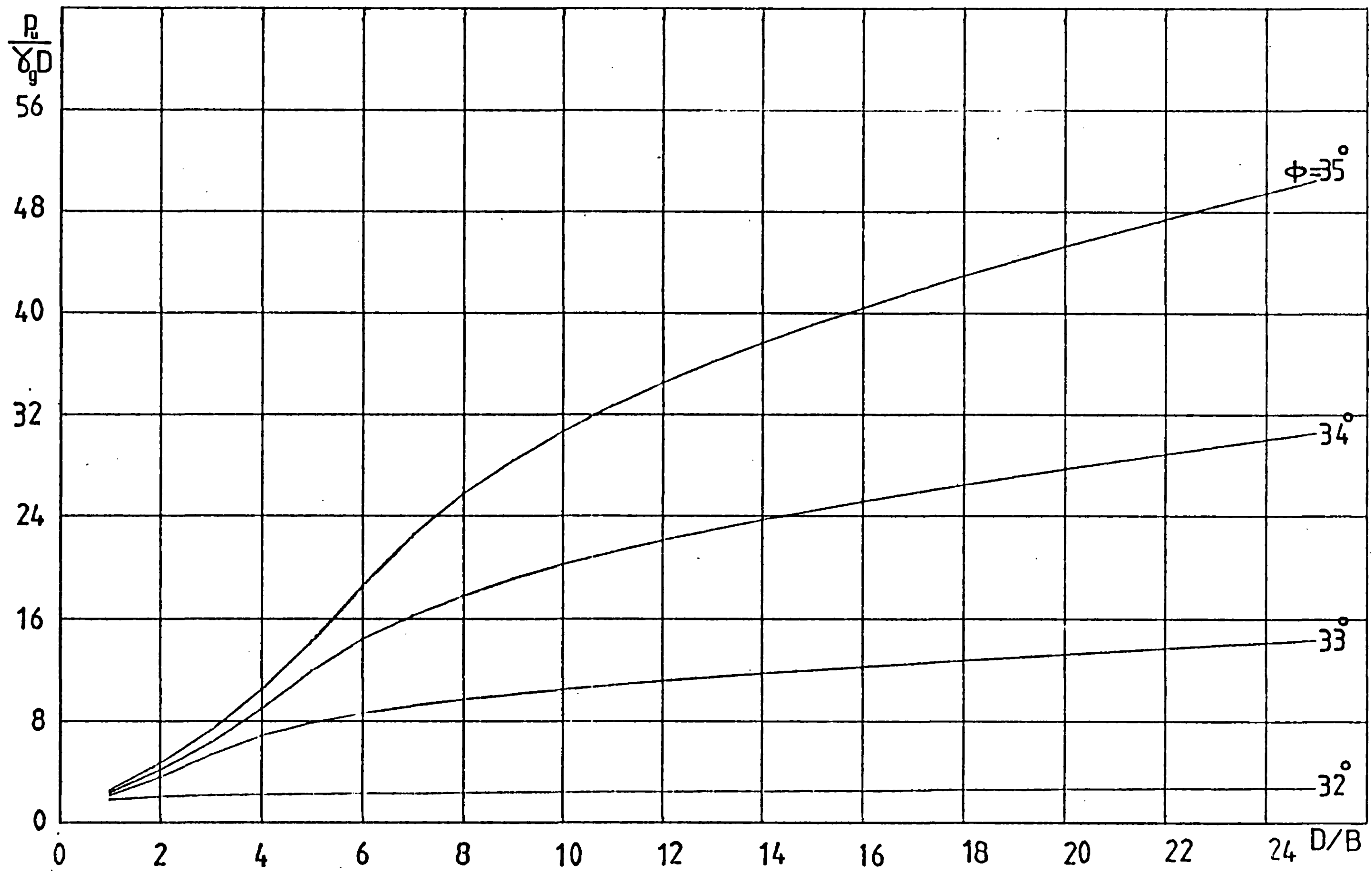

FIG B.15 DESIGN CURVES FOR LOOSE SAND ($\psi = 20^{o}$)

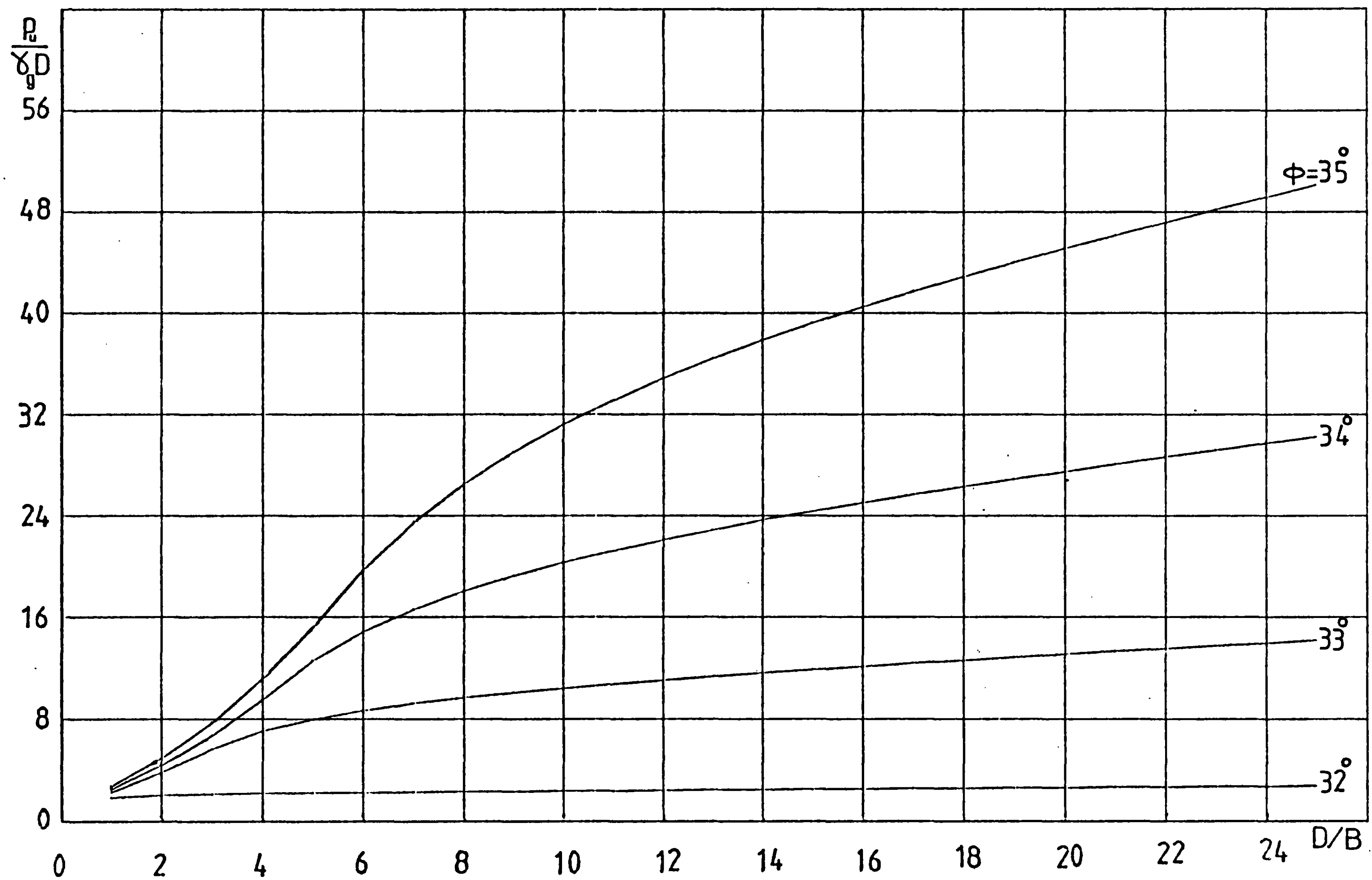

FIG B.16 DESIGN CURVES FOR LOOSE SAND (ψ = 30°)

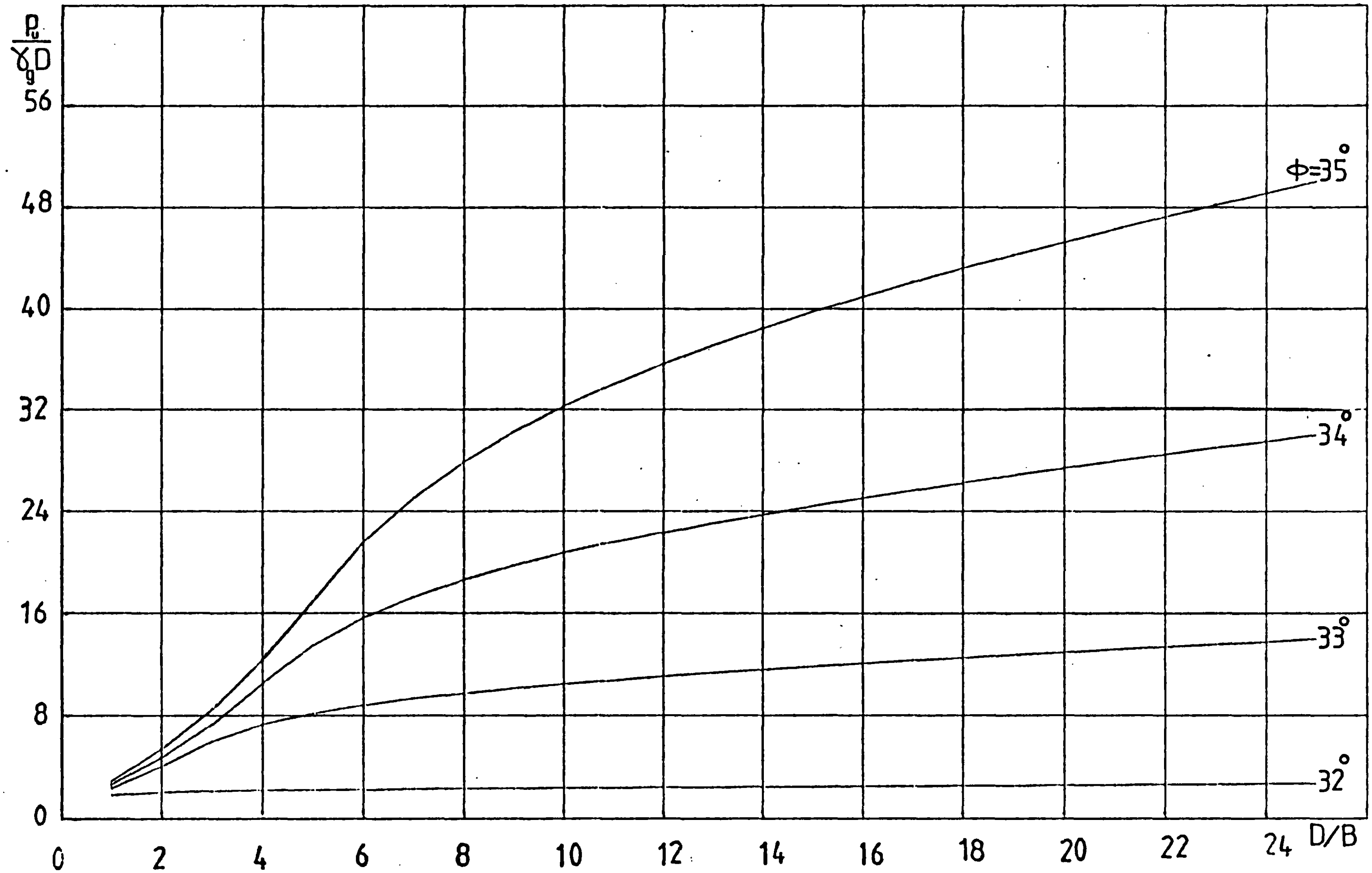

IG B.17 DESIGN CURVES FOR LOOSE SAND ($\psi = 40^\circ$)

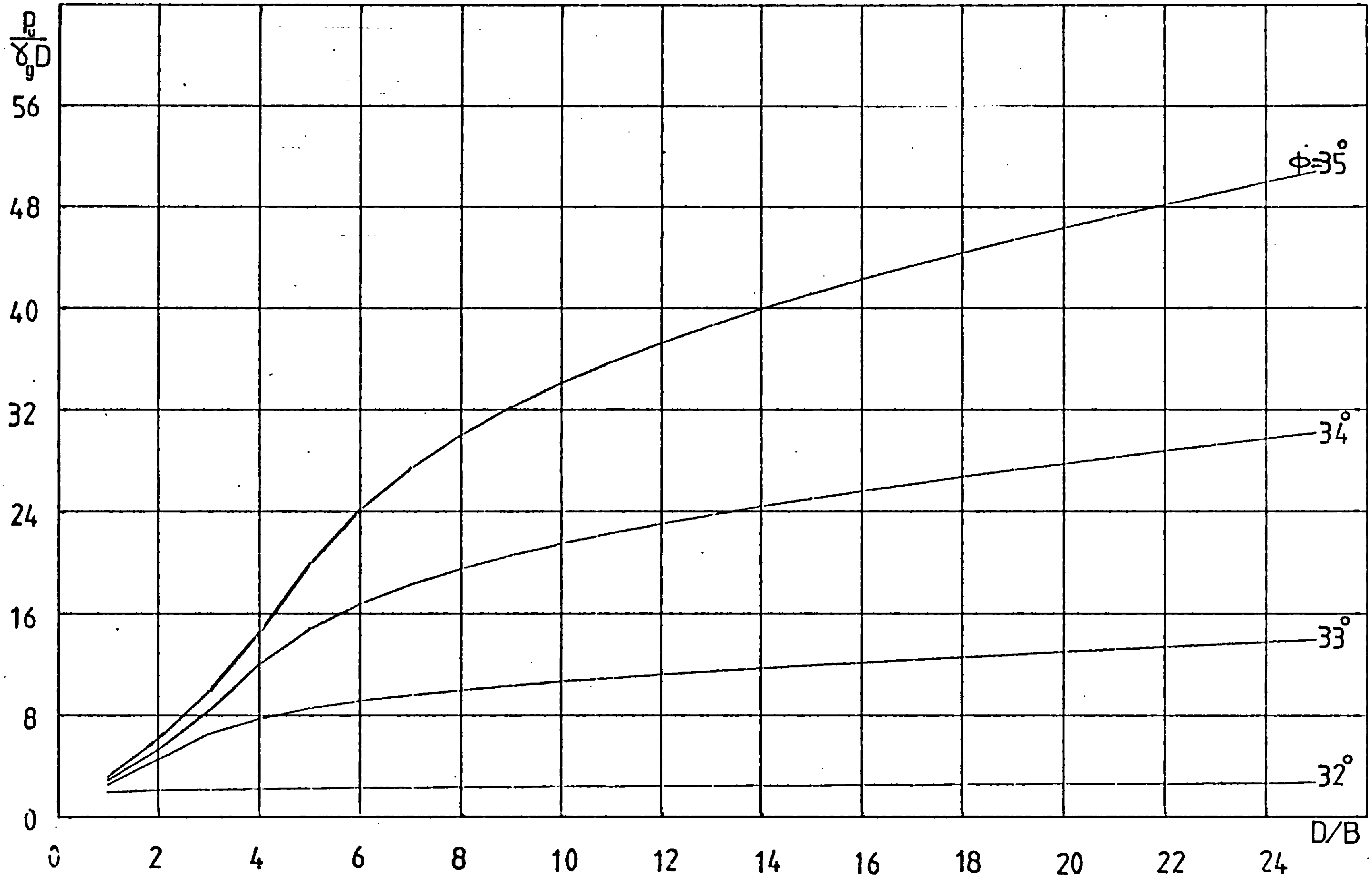

FIG B.18 DESIGN CURVES FOR LOOSE SAND ($\psi = 50^\circ$)